
[All ETDs from UAB](#)

[UAB Theses & Dissertations](#)

2021

Characterizing The Role Of Necroptosis Of Airway Epithelial Cells In The Immune Response To Respiratory Pathogens

Ashleigh Nichole Riegler
University of Alabama at Birmingham

Follow this and additional works at: <https://digitalcommons.library.uab.edu/etd-collection>

 Part of the [Medical Sciences Commons](#)

Recommended Citation

Riegler, Ashleigh Nichole, "Characterizing The Role Of Necroptosis Of Airway Epithelial Cells In The Immune Response To Respiratory Pathogens" (2021). *All ETDs from UAB*. 904.
<https://digitalcommons.library.uab.edu/etd-collection/904>

This content has been accepted for inclusion by an authorized administrator of the UAB Digital Commons, and is provided as a free open access item. All inquiries regarding this item or the UAB Digital Commons should be directed to the [UAB Libraries Office of Scholarly Communication](#).

CHARACTERIZING THE ROLE OF NECROPTOSIS OF AIRWAY EPITHELIAL
CELLS IN THE IMMUNE RESPONSE TO RESPIRATORY PATHOGENS

by

ASHLEIGH N. RIEGLER

CARLOS J. ORIHUELA, COMMITTEE CHAIR
ANDRE BALLESTEROS-TATO
MICHAEL J. GRAY
CRAIG L. MAYNARD
WILLIAM E. SWORDS

A DISSERTATION

Submitted to the graduate faculty of The University of Alabama at Birmingham,
in partial fulfillment of the requirements for the degree of
Doctor of Philosophy

BIRMINGHAM, ALABAMA

2021

CHARACTERIZING THE ROLE OF NECROPTOSIS OF AIRWAY EPITHELIAL
CELLS IN THE IMMUNE RESPONSE TO RESPIRATORY PATHOGENS

ASHLEIGH N. RIEGLER

GRADUATE BIOMEDICAL SCIENCES

ABSTRACT

Necroptosis, a programmed form of lytic cell death, is initiated by various viral and bacterial pathogens through irreparable ion dysregulation and energy depletion. This cellular damage results in the activation of the cellular kinases RIPK1 and RIPK3, consecutively, and the activation and membrane targeting of MLKL, the latter responsible for lysis. Here we have demonstrated that necroptosis of airway epithelial cells is key in the development of the adaptive immune response to asymptomatic colonization by *Streptococcus pneumoniae* (*Spn*). Briefly, necroptotic deficient animals or wildtype animals colonized with *Spn* lacking the necroptosis-triggering pneumolysin toxin, failed to recruit CD11c⁺ leukocytes to the sites where *Spn* were present, had dampened pathogen-specific serum IgG responses, were delayed in bacterial clearance, and were more susceptible to subsequent lethal re-challenge. Further, we examined the role of necroptosis in the generation of an adaptive immune response to influenza A (Flu), a viral pathogen also shown to induce necroptosis of airway epithelial cells. Infection of wildtype and necroptosis deficient (i.e. MLKL KO and RIPK3 KO) mice with Flu strain A/Puerto Rico/8/1934 indicated an MLKL-independent role for RIPK3 activation in the immune response to Flu. RIPK3 KO mice experienced the most severe weight loss, and significantly increased Flu specific CD8 T cell lung infiltrate at day 15 post-infection. *In vitro* analyses

and analysis of airway lavage from these Flu infected mice indicated that NF κ B-dependent release of IL-8 in the absence of RIPK3 was responsible for the increased pathology. These results collectively suggest fundamental differences in the role for necroptosis in the development of adaptive immunity against viral versus bacterial pathogens. Future studies are focused on determining the contribution of necroptosis to the intracellular signaling in response to respiratory bacterial and viral pathogens.

DEDICATION

I dedicate this work to my sister, Emmaleigh.

Your unconditional support and love have gotten me through some of the hardest times I have faced in my life and during my PhD. You are my very best friend and I love you “with all of the muches in the world”.

ACKNOWLEDGMENTS

I am very grateful to have done my graduate work the University of Alabama at Birmingham. The tremendous collaborative atmosphere has been invaluable in my time as a graduate student. Because of this collaboration, I have many people to thank for their part in my successes. First, I would like to thank my advisor, Dr. Carlos Orihuela, for allowing me to become part of his lab family and for supporting me over the years. I am grateful for his guidance and patience. His incredible ability to motivate and to maintain organization have been immensely helpful in my progression as a scientist and will remain invaluable tools that I hope to learn from and take with me in my future career. Carlos has not only been exceptionally skilled at problem solving and supporting my progress in a scientific sense, his care for those in his lab extends far beyond the bench. As I faced some of the toughest struggles of my personal life while I was in Carlos' lab, I am forever grateful to have had such a supportive and caring mentor during the hard days. I am proud to become a branch of the Orihuela research family tree. I would also like to thank my thesis committee members, Dr. Andre Ballesteros-Tato, Dr. Michael J Gray, Dr. Craig L Maynard, and Dr. W. Edward Swords, for their contributions. Over the years each has offered fantastic scientific guidance, many insightful suggestions, and has demonstrated a sincere interest not only in my scientific work but in me as a person and my future career. I am fortunate to have such a group of intelligent scientists and supportive individuals on my committee. While not members of my committee, I cannot go without thanking Dr. Kevin S Harrod and Jennifer Tipper. Their technical and scientific guidance when

transitioning to virology was instrumental in so many of my experiments. I would like to thank the UAB Immunologic Diseases and Basic Immunology training grant, including Dr. Harry Schroeder, Dr. Laurie Harrington, Dr. Ada Elgavish, and the rest of the T32 committee. I would like to recognize the members of the Briles lab who have all been extremely helpful and have contributed to my progress and understanding over the years. I would also like to acknowledge the members of the Ballesteros-Tato lab, specifically Dr. Andre Ballesteros-Tato and Meagan Jenkins. Meagan has given her time to teach me several techniques to aid in experiments, and both Andre and Meagan deserve a huge thanks for their patience in my slow understanding of the intricacies of proper immunology techniques. I would like to thank the former graduate student, Dr. Anukul Shenoy for sharing his enthusiasm for science with me, even when it seemed intimidating; and the former post-doctoral researchers, Dr. Norberto Gonzalez-Juarbe and Dr. Terry J. Brissac for being incredible resources of knowledge, for being supportive through the struggles, for being patient with me as I learned, and for always challenging me to think beyond my hypothesis. Thank you to the current and past Orihuela lab members, Katherine Kruckow, Dr. Sarah Beno, Dr. Christina Morra, Dr. Ninecia Scott, Dr. Hansol Im, Dr. Eriel Gutierrez-Martinez, Jennifer Luck, Robert Buckner, Xiuhong Song, Jessica Lane, and to the many others who spent time working in the lab. I am grateful for the technical help you have shared, for your support when I needed it, for putting up with me on the days that I was really stressed out, and for always being excited to talk to me about scientific problems or data. I would like to express my thanks to all of the current and past staff of the UAB Graduate Biomedical Sciences, Microbiology department and theme, and Graduate School offices for helping with the mountains of paperwork throughout the years, being a support line when I needed one, always advocating for the students, and for doing their jobs as to

make the life of a UAB GBS- Microbiology graduate student easier. I would like to acknowledge the many research mice who contribute to science daily and without whom I would not have been able to contribute to the understanding of the complexity of the immune system and this work would not have been possible. Finally, I would like to thank my friends and family for their continuous support and encouragement. Those I have met in graduate school that I consider friends are too numerous to name. I will never forget the experiences we've shared and hope to stay in touch as we all continue on to wherever our next steps may be. Many of these friends have been there for me when the challenges of graduate school seemed too great to overcome and for that I now consider them part of my family. To my family, I would like to express the deepest gratitude. You have all provided support and encouragement that helped drive me through the hard times. Thanks for listening to my problems and providing perspective. I would not be who am I today without you all.

TABLE OF CONTENTS

| | <i>Page</i> |
|---|-------------|
| ABSTRACT | ii |
| DEDICATION | iv |
| ACKNOWLEDGMENTS..... | v |
| LIST OF FIGURES | x |
| LIST OF ABBREVIATIONS..... | xiv |
| CHAPTER | |
| 1 EUKARYOTIC CELL DEATH AND AIRWAY INFECTIONS..... | 1 |
| Introduction | 1 |
| Bacterial CAP and <i>Streptococcus pneumoniae</i> | 3 |
| Viral pneumonia | 5 |
| How respiratory pathogens interact with host cells..... | 6 |
| Types of eukaryotic cell death (Necroptosis)..... | 8 |
| Main research goal..... | 14 |
| 2 NECROPTOTIC CELL DEATH PROMOTES ADAPTIVE IMMUNITY AGAINST COLONIZING PNEUMOCOCCI | 16 |
| 3 NECROPTOSIS INHIBITION PREVENTS LONG-TERM CARDIAC DAMAGE DURING PNEUMOCOCCAL PNEUMONIA AND INVASIVE DISEASE..... | 57 |
| 4 INFLUENZA-INDUCED OXIDATIVE STRESS SENSITIZES LUNG CELLS TO BACTERIAL TOXIN-MEDIATED NECROPTOSIS | 95 |
| 5 RIPK3 SUPPRESSES NFKB ACTIVATION DURING INFLUENZA A INFECTION OF AIRWAY EPITHELIAL CELLS TO REDUCE DISEASE PATHOLOGY..... | 141 |

| | |
|---|-----|
| 6 DISCUSSION, CONCLUSIONS, AND FUTURE DIRECTIONS | 187 |
| General discussion | 187 |
| Necroptosis during <i>Spn</i> colonization | 189 |
| IPD and necroptosis | 191 |
| The impact of necroptosis on IAV/ <i>Spn</i> co-infection | 193 |
| RIPK3 signaling during IAV pneumonia..... | 197 |
| Future directions | 202 |
| Summary | 203 |
| LIST OF GENERAL REFERENCES..... | 209 |
| APPENDIX..... | 227 |
| Animal research approval..... | 227 |

LIST OF FIGURES

| <i>Figure</i> | | <i>Page</i> |
|---|---|-------------|
| EUKARYOTIC CELL DEATH AND AIRWAY INFECTIONS | | |
| 1 | Summary of programmed cell death | 9 |
| 2 | General schematic of receptor-mediated necroptosis..... | 11 |
| 3 | Diagram of virus-induced necroptosis..... | 13 |
| 4 | General depiction of PFT-mediated necroptosis..... | 14 |
| NECROPTOTIC CELL DEATH PROMOTES ADAPTIVE IMMUNITY AGAINST COLONIZING PNEUMOCOCCI | | |
| 5 | Cell damage occurs during asymptomatic colonization by <i>Spn</i> | 27 |
| 6 | Necroptosis during <i>Spn</i> colonization is PFT dependent..... | 29 |
| 7 | Necroptosis during <i>Spn</i> colonization is pneumolysin dependent..... | 31 |
| 8 | Localized PFT-induced necroptosis affects the innate immune response to colonizing <i>Spn</i> | 33 |
| 9 | Inhibition of Ply-mediated necroptosis decreases the rate of <i>Spn</i> clearance..... | 34 |
| 10 | Necroptosis initiates protective, adaptive immunity against colonizing <i>Spn</i> | 36 |
| SUPPLEMENTAL FIGURES | | |
| 1 | Nasopharyngeal colonization model..... | 50 |
| 2 | Amount of apoptosis during <i>Spn</i> colonization is negligible..... | 51 |

| | | |
|---|--|----|
| 3 | Reduction in FaDu cytotoxicity is not due to <i>Spn</i> growth differences during treatment..... | 52 |
| 4 | Reduction in MLKL KO mice is not a genotype defect..... | 52 |
| 5 | Protection against secondary lethal challenge is not due to anti-pneumolysin antibody..... | 53 |

SUPPLEMENTAL TABLES

| | | |
|---|-----------------------------|----|
| 1 | Reagents and Resources..... | 54 |
|---|-----------------------------|----|

NECROPTOSIS INHIBITION PREVENTS LONG-TERM CARDIAC DAMAGE DURING PNEUMOCOCCAL PNEUMONIA AND INVASIVE DISEASE

| | | |
|---|--|----|
| 1 | Pneumolysin is required for <i>Spn</i> cardiac damage..... | 64 |
| 2 | Pneumolysin kills cardiomyocytes via necroptosis <i>in vitro</i> | 67 |
| 3 | Pneumolysin inhibition reduces necroptosis activation <i>in vitro</i> | 68 |
| 4 | IPD results in long-term cardiac damage..... | 71 |
| 5 | Therapeutic inhibition of necroptosis protects against organ damage during IPD..... | 74 |
| 6 | Therapeutic Ponatinib treatment reduces lung and cardiac damage from pneumococcal pneumonia and IPD..... | 76 |
| 7 | Ponatinib protects against long-term cardiac dysfunction..... | 78 |

SUPPLEMENTAL FIGURES

| | | |
|---|---|----|
| 1 | Cardiac pro-inflammatory mediators are increased during IPD..... | 91 |
| 2 | Necroptosis is active during pneumococcal cardiac infection but does not influence bacterial burdens..... | 91 |
| 3 | TIGR4 infection can lead to pericarditis..... | 92 |
| 4 | Ponatinib treatment does not affect pneumococcal growth..... | 93 |

| | | |
|---|---|----|
| 5 | Therapeutic Ponatinib treatment reduces cardiac damage from pneumococcal pneumonia and IPD..... | 94 |
| 6 | Necroptosis inhibition by Ponatinib does not influence pneumococcal burdens..... | 94 |

INFLUENZA-INDUCED OXIDATIVE STRESS SENSITIZES LUNG CELLS TO BACTERIAL TOXIN-MEDIATED NECROPTOSIS

| | | |
|---|---|-----|
| 1 | IAV/ <i>Spn</i> co-infection leads to increased mortality and enhanced tissue necroptosis..... | 107 |
| 2 | IAV infection promotes PFT-mediated cell death..... | 109 |
| 3 | IAV-mediated oxidative stress potentiates pneumolysin-mediated necroptosis..... | 112 |
| 4 | IAV-mediated oxidative stress persists after virus clearance <i>in vivo</i> | 116 |
| 5 | Influenza infection potentiates pneumolysin induced necroptosis activation during secondary <i>S. pneumoniae</i> challenge..... | 117 |
| 6 | Therapeutic neutralization of ROS reduces necroptosis activation during secondary bacterial pneumonia..... | 119 |
| 7 | Inhibition of necroptosis reduces disease severity and tissue injury during secondary bacterial pneumonia..... | 121 |

RIPK3 SUPPRESSES NFKB ACTIVATION DURING INFLUENZA A INFECTION OF AIRWAY EPITHELIAL CELLS TO REDUCE DISEASE PATHOLOGY

| | | |
|---|---|-----|
| 1 | RIPK3 deficiency but not MLK deficiency increases susceptibility to IAV infection..... | 155 |
| 2 | RIPK3 deficiency but not MLKL deficiency increases disease pathology during IAV infection independent of viral titer..... | 156 |
| 3 | RIPK3 deficiency alters immune cellular recruitment during IAV infection..... | 159 |

| | | |
|---|--|-----|
| 4 | RIPK3 deficiency alters cellular cytokine response to IAV infection..... | 162 |
| 5 | RIPK3 moderates NFκB signaling during IAV infection..... | 164 |

SUPPLEMENTAL FIGURES

| | | |
|---|--|-----|
| 1 | RIPK3 deficiency alters immune cell population dynamics in the lung during IAV infection..... | 182 |
| 2 | Deficiency in necroptotic signaling proteins alters the adaptive immune response in the lung and draining lymph node during IAV infection..... | 183 |
| 3 | Construction of RIPK3 deficient cell line by CRISPR/cas9..... | 185 |

SUPPLEMENTAL TABLES

| | | |
|---|------------------------|-----|
| 1 | Key reagents/kits..... | 186 |
|---|------------------------|-----|

DISCUSSION, CONCLUSIONS, AND FUTURE DIRECTIONS

| | | |
|---|---|-----|
| 1 | Summary of the impact of necroptosis and associated tissue damage on the host during infection..... | 195 |
| 2 | General depiction of RIPK3 during IAV infection..... | 199 |
| 3 | The initiation and outcomes of necroptosis during infection by airway pathogens..... | 205 |
| 4 | The balance of necroptotic signaling on host outcome..... | 206 |

LIST OF ABBREVIATIONS

| | |
|-----------------|---|
| AEC | airway epithelial cells |
| APC | antigen-presenting cell |
| BAL/BALF | Bronchoalveolar lavage (fluid) |
| Cali'09 | influenza strain A/California/07/2009 |
| CAP | community-acquired pneumonia |
| CbpA | choline-binding protein A (<i>a.k.a.</i> PspC) |
| CML | chronic myeloid leukemia |
| COX | cyclooxygenase |
| DAI | DNA-dependent activator of IFN regulators (<i>a.k.a.</i> Zbp1 and DLM-1) |
| DAMP | damage-associated molecular pattern |
| DMEM | Dulbecco's Modified Eagle's Medium |
| dpi | days post-infection |
| Flu | influenza |
| G-CSF | granulocyte colony stimulating factor |
| hpi | hours post- infection |
| IAV | influenza A virus |
| IFN | interferon |
| IgA | immunoglobulin A |
| IgG | immunoglobulin G |
| IgM | immunoglobulin M |

| | |
|-----------------|---|
| IL | interleukin |
| IPD | invasive pneumococcal disease |
| KO | knockout |
| LDH | lactate dehydrogenase |
| LEC | lung epithelial cells |
| LR | laminin receptor |
| LytA | pneumococcal autolysin A |
| MACE | major adverse cardiac events |
| MLKL | mixed lineage kinase domain like pseudokinase |
| mLN | mediastinal lymph node |
| nHBE | normal human bronchial epithelial cells |
| NP | influenza nuclear protein |
| NSA | necrosulfonamide |
| NEC | necrostatin |
| NP | nucleoprotein (of influenza virus) |
| p38 MAPK | 38 mitogen-activated protein kinase signaling cascade |
| PB1 | polymerase B1 (of influenza virus) |
| PACE | pneumococcal pneumonia associated cardiac event |
| PAFR | platelet-activating factor receptor |
| PAMP | pathogen-associated molecular pattern |
| PCD | Programmed cell death |

| | |
|-------------------|--|
| PCV7 | 7-valent pneumococcal conjugate vaccine |
| PCV13 | 13-valent pneumococcal conjugate vaccine |
| pdmH1N1 | pandemic H1N1 influenza A/California/07/2009 |
| pIgR | polymeric immunoglobulin receptor |
| Ply | pneumolysin |
| PMN | polymorphonuclear cells |
| PR8 | influenza strain A/Puerto Rico/8/1934 |
| PRR | pattern recognition receptor |
| PspA | pneumococcal surface protein A |
| RIPK | receptor-interacting serine threonine kinase |
| ROS | reactive oxygen species |
| rPly | recombinant pneumolysin |
| <i>Spn</i> | <i>Streptococcus pneumoniae</i> |
| SpxB | pneumococcal pyruvate oxidase |
| Th cells | T-helper cells |
| THY | Todd- Hewitt Broth with 0.5% yeast extract |
| TLR | Toll-like receptor |
| TNF | tumor necrosis factor |
| WT | wildtype |

CHAPTER 1

EUKARYOTIC CELL DEATH AND AIRWAY INFECTIONS

Introduction

Airway infections often act as the bookends of human life. Respiratory infections are commonly the first infections which occur after birth and, for many, pneumonia is the illness associated with death. In the United States, respiratory infections are responsible for more days lost work or school time than any other category of acute illness (CDC, 2019). Worldwide, respiratory tract infections are the 3rd leading cause of death, according to the World Health Organization (WHO)(WHO, 2016). Severity and long-term health impact of respiratory tract infections are various and are largely associated with the type of infection. Respiratory tract infections are categorized according to their regional location, into upper respiratory tract infections (URIs) and lower respiratory tract infections (LRIs). URIs are infections which involve the nose, sinuses, pharynx, larynx, as well as the large airways and, in patients, present with cough without signs of pneumonia. URIs are often also associated with otitis, especially in children. URIs are among the top three outpatient diagnoses in the United States, accounting for an estimated 10 million outpatient appointments annually and nearly half of all adult antibiotic prescriptions in the United States (Fendrick, Monto, Nightengale, & Sarnes, 2003; Gonzales, Steiner, & Sande, 1997).

While URIs remain extremely prevalent in the human population, the majority of deaths attributed to respiratory tract infections are result of LRI. LRIs are infections of the bronchi, bronchioles, or alveoli (clinically presenting as pneumonia) (Dasaraju & Liu, 1996). According to the United States Center for Disease Control (CDC) in 2019, pneumonia is within the top ten causes of death in the United States (Kochanek, Xu, & Arias, 2020), and pose the most serious threat to health and mortality.

The WHO characterizes pneumonia as the leading cause of infectious death worldwide, and in the United States more than 1 million people are diagnosed and 50,000 people die of pneumonia annually (Prevention, 2020b). The most common type of infectious pneumonia resulting in hospitalization is community acquired, being transmitted and contracted outside of the hospital setting. Community acquired pneumonia (CAP) is one of the leading causes of hospital admission due to acute infection, accounting for approximately 1% of all medical admissions (Trotter, Stuart, George, & Miller, 2008). In the United States, nearly 5 million cases of CAP are diagnosed each year, 20% of cases resulting in hospitalization with a 12% to 40% mortality among those hospitalized (Grief & Loza, 2018). As of 2017, CAP is the leading cause of infectious death and eighth leading cause of overall death in the United States (Kochanek, Murphy, Xu, & Arias, 2019).

Respiratory infections, including CAP, are associated with various parasites, fungi, bacteria, and viral pathogens which elicit irritating and potentially damaging inflammation of host tissues during infection. Of the types of pathogens associated with respiratory tract infections, viral and bacterial pathogens result in the greatest number of respiratory tract infections and hospitalizations due to CAP, worldwide.

Bacterial CAP and Streptococcus pneumoniae

Among the numerous bacterial pathogens associated with respiratory tract infections and capable of causing CAP, *Streptococcus pneumoniae* (*Spn*) is the most common, responsible for 80% of all CAP cases. *Spn* is the leading cause of pneumonia mortality worldwide, and in 2016 accounted for more deaths than all other causes combined (Collaborators, 2018). Generally speaking, the attack rate, or number of respiratory infections compared to the estimated number of asymptomatic colonization cases, for the *Spn* is very low. However, because so many individuals are colonized, typically ranging from 5-20% of adults and 20-50% of children (Goldblatt & O'Brien, 2018; E. L. Smith et al., 2020; H. C. Smith, German, Ferreira, & Rylance, 2019), the disease burden for *Spn* remains enormous. Children under the age of 5 as well as individuals 65 years of age or older represent the majority of pneumococcal cases. In 2019, there were an estimated 502,600 non-bacteremic pneumococcal cases and 29,500 invasive pneumococcal disease (IPD) cases in adults 50 years and older and more than 14.5 million episodes of IPD in children younger than 5 years of age are recorded annually, accounting for ~800,000 deaths worldwide. Due to its prevalence, morbidity, and ability to quickly adapt to antibiotic intervention therapies, *Spn* is included as a serious threat on the 2019 *Antibiotic Resistance Threats in the United States* list by the CDC (Control, 2020).

Spn is a Gram-positive bacterium which asymptotically colonizes the nasopharynx of many individuals. In hosts with compromised immune systems and under certain environmental conditions, *Spn* can disperse from the nasopharynx into the lungs to cause pneumonia, the blood to cause sepsis, or the central nervous system to cause

meningitis, the latter three encompassing IPD (Austrian, 1981; Lynch & Zhanel, 2010). During infection, *Spn* has adapted many mechanisms to evade the host immune system as well as damage host cells and tissues.

One such mechanism which serves as the basis for the pneumococcal vaccines is the polysaccharide capsule. The pneumococcal capsule is a critical virulence determinant of *Spn*, serving to protect the bacteria from host complement deposition, surface protein-targeted immunoglobulin binding, as well as allowing for resistance to desiccation and oxidative stress during transmission (Paton & Trappetti, 2019). *Spn* are categorized into serotypes according to their polysaccharide capsule and, notably, there are a total of 100 structurally and serologically distinct *Spn* capsule types identified to date (Ganaie et al., 2020), 23 of which are included in the PPSV23 pneumococcal vaccine. The ever-adapting *Spn* continues to evade host immunity partially by means of its capsule.

Another virulence determinant which impacts host organ damage and invasiveness of *Spn*, as well as other bacterial pathogens, is the production of bacterial toxins. *Spn* produces and releases a pore-forming toxin (PFT), pneumolysin (ply), which is capable of binding to cholesterol in host cell membranes. As the PFT namesake implies, binding of pneumolysin to cholesterol eventually results in the formation of a small pore on the host cell surface, ultimately disrupting ion regulation and cellular signaling (Mitchell & Dalziel, 2014). Along with various other bacterial virulence factors (such as neuraminidases, hyaluronidases, enzymatic surface proteins, and hydrogen peroxide production by *spxB*), ply contributes significantly to the host damage and disease pathology observed during pneumococcal infection.

Viral pneumonia

In addition to bacterial causative agents of respiratory infections and CAP, viruses are the causative agent of a large population of diagnoses. While bacterial pathogens are the main cause of pneumonia, approximately 75% of CAP diagnoses, viral infections are common in the upper and middle respiratory tract (*e.g.* laryngitis, bronchitis, and bronchiolitis)(Yu, 2020). Viral respiratory tract infections are generally classified clinically by syndrome (*e.g.* bronchiolitis, croup, the common cold, or pneumonia) rather than causative virus which has made incidence tracking difficult. Some viral pathogens commonly cause characteristic clinical manifestations (*e.g.* respiratory syncytial virus [RSV] typically causes bronchiolitis and rhinovirus typically causes the common cold) which does allow some inferences to be made, however each virus is capable of causing many of the viral respiratory syndromes under certain conditions or in certain hosts. The advent of PCR has improved viral pathogen identification, especially in CAP patients. Of the many viruses which can cause respiratory tract infections, the most common are rhinoviruses, influenza viruses, parainfluenza viruses, and coronaviruses, as well as respiratory syncytial virus in children (Burk et al., 2016). Of these and pertinent to my work, influenza viruses cause some of the highest viral-associated costs and mortalities worldwide.

In the United States, the CDC estimates that influenza has resulted in 9-45 million illnesses, 140,000-810,000 hospitalizations, and 12,000-61,000 deaths annually since 2010(Prevention, 2020a). Much like *Spn*, severity of influenza respiratory illness varies widely with severe disease is more likely in older patients, immunocompromised

individuals, and infants. Influenza viruses are single-stranded RNA viruses belonging to the *Orthomyxoviridae* family of viruses. Influenza viruses are divided into four types: A, B, C, and D; with influenza A and B associated with the seasonal epidemics known as flu season, C associated with mild illness, and D primarily affecting cattle. Influenza A virus (IAV) can further be divided into subtypes based on two vital virus surface proteins: hemagglutinin (H) and neuraminidase (N) which influence the ability of the virus to interact with or infect host cells. IAV is the most common cause of the human flu and is estimated by the WHO to annually affect 1 billion individuals, resulting in 300,000 to 500,000 deaths in non-pandemic years (Clayville, 2011). Further, 4-8% of the United States population is diagnosed with IAV each year (Tokars, Olsen, & Reed, 2018). Thus, viral respiratory tract infections, especially IAV infections, have considerable impact on global human health. Interestingly, while morbidity associated with IAV infections may result directly from viral infection, more often it results from exacerbation of underlying cardiopulmonary conditions or bacterial superinfection. Notably and directly related to this work, one of the most commonly associated bacterial pathogens during IAV infection is *Spn* (Gill et al., 2010; Louie et al., 2009; Koenraad F. van der Sluijs, van der Poll, Lutter, Juffermans, & Schultz, 2010). The impact of this co-infection is further discussed in Chapter 4 of this dissertation.

How Respiratory pathogens interact with host cells

The respiratory tract serves the critical function of gas exchange and it is therefore crucial that the host response to airway pathogens is compatible with this function. Pathogens which have evolved to express a propensity for the respiratory system have

consequently developed various mechanisms to interact with host cells and counter the host responses. Pathogen sensing mechanisms expressed by the host cells include the pattern recognition receptors (PRRs), which are further characterized into the C-type lectin receptors (CLRs), toll-like receptors (TLRs), Nod-like receptors (NLRs), RIG-I-like receptors (RLRs), AIM2-like receptors (ALRs), and intracellular DNA sensors such as cGAS which are expressed on the surface of, in the endosomes, and within the cytosol of cells (Kawasaki & Kawai, 2014). These PRRs recognize various molecular patterns associated with cell damage (*i.e.* damage-associated molecular patterns; DAMPs) and infection (*i.e.* pathogen-associated molecular patterns; PAMPs). PAMPs include certain glycans expressed by various bacteria, like the *Spn* polysaccharide capsule or portions of the bacterial cell envelope (*e.g.* lipopolysaccharide (LPS) and peptidoglycan); specific pathogen-associated nucleic acid structures, like double-stranded RNA (dsRNA) and unmethylated triphosphate Cytosine-Guanine (CpG) DNA expressed by viral and bacterial pathogens; as well as select proteins, like bacterial flagellin (Mogensen, 2009). Sensing of pathogens and the damage to host cells which they elicit is the primary orchestrator of both the severity of infection as well as the protective immunity which is generated as result.

Including PRRs, respiratory pathogens interact with host cells by various mechanisms, dampening or eliciting immune responses, maintaining and damaging host cells, orchestrating transmission to a new host, and ultimately impacting disease pathology as well as mortality. These mechanism by which the host interacts with respiratory pathogens during infection is influenced by location (*e.g.* the region of the airway that is being infected), the host microbiota, as well as the host immune system, both the propensity to respond and the existing immunity. Due to its vital functioning in gas exchange and host

survival, the airway is highly developed to resist damaging infection. In addition to expressing the various PRRs, airway cells are specialized in the maintenance of structure of the mucosal barrier; secrete specialized substances, like mucins, surfactants, and lactoferrin, which trap or repel pathogens from disseminating throughout the airways, prevent capillary leakage, aid in opsonization, sequester airway iron from invading microbes; as well as mechanically inhibit dissemination (*e.g.* cilia) (Kell, Heyden, & Pretorius, 2020; Whitsett & Alenghat, 2015). Additionally, within the lower respiratory tract, resident macrophages (*i.e.* alveolar macrophages) patrol the airway for pathogens promptly elicit an immune response upon detection of infection (Hussell & Bell, 2014). Notably and related to this work, while airway cells are adapted to sense and respond to potential pathogens, this response may include the initiation of programmed cell death (Amarante-Mendes et al., 2018).

Types of Eukaryotic Cell Death (Necroptosis)

Eukaryotic cell death is a complex network of programmed and non-programmed cellular signals, with diverse functional output. Programmed cell death (PCD) pathways are conserved across the eukaryotic domain and so, the complex roles these pathways play in development, survival, and response to stimuli are vital to homeostasis. For decades the phrase “programmed cell death” was exclusively attributed to apoptosis. We now, however, know that programmed cell death is far more heterogeneous (Arya & White, 2015). PCD is now defined to include apoptosis, pyroptosis, autophagy, necroptosis, and a list of other cell-suicide mechanisms (General summary of the listed mechanisms shown in **Figure 1**). With this increased awareness of the astonishing complexity of programmed

cell death, the roles which these pathways play in homeostasis and response to infection become ever more multifaceted.

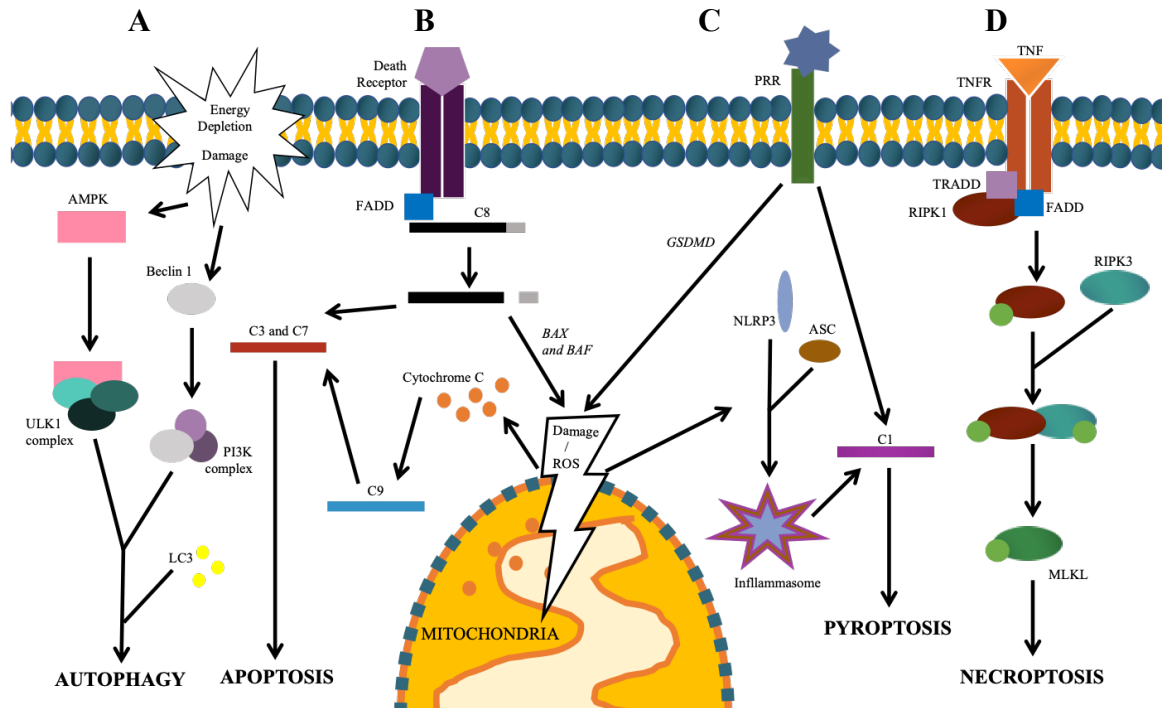


Figure 1. Summary of programmed cell death. Figure depicting the general pathways of eukaryotic cell death. **A)** Autophagy results from energy depletion or uncontrolled cell damage which result in the activation of the AMP-activated protein kinase (AMPK) which complexes with ULK1, as well as the accumulation of Beclin1 which subsequently complexes with PI3 kinase (PI3K) and other damage-associated cellular proteins, ultimately resulting in the maturation of LC3 (aka MAP1LC3B), the ubiquitination of cellular components, the engulfment of these components by autophagosomes, and finally cell death. **B)** Apoptosis is initiated by various mechanisms but most canonically either by extrinsic activation of a cellular death receptor which cleaves caspase 8 (“C”-8) or by the intrinsic sensing of mitochondrial damage through the release of cytochrome C (also further initiated by C8 activation through BAX and BAF). The Cytochrome C is sensed by C9. Both extrinsic and intrinsic pathways result in the activation of C3 and/or C7 which subsequently initiate the organized degradation of cellular components and packaging into apoptotic bodies, ultimately resulting in cell death. **C)** Proptosis is generally triggered by activation of a PRR or by cellular damage which subsequently activate C1. Typically, C1 complexes with NLRP3, ASC, and other cellular proteins to form the inflammasome, ultimately resulting in increased processing of cellular IL-1 β and cell death. **D)** Necroptosis is canonically carried out by activation of the TNFR1 which then complexes FADD, TRADD, and RIPK1, resulting in the activation of RIPK1 by phosphorylation. This activated RIPK1 then activates RIPK3 and together they activate MLKL. Activated MLKL then targets cell membranes, ultimately resulting in cell death. Phosphorylation indicated by green circles.

Classically, PCD referred to cellular signaling which was mediated by intracellular cysteine-aspartic proteases called caspases, and resulted in the neat packaging of cellular contents (*i.e.* apoptotic bodies), broadly identified as apoptosis. Apoptosis can be initiated through extracellular or intracellular stress stimuli, ultimately resulting in the activation or cleavage of cellular effector caspases 3, 6, and/or 7 which interact with other cellular proteins to initiate nuclear fragmentation, membrane blebbing, and packaging of cellular contents into apoptotic bodies for clearance by the innate immune cells (Elmore, 2007). Apoptosis has been shown to play a vital role in immune regulation and homeostasis, through the elimination of self-reactive immune cells to prevent autoimmunity, as a mechanism for cells to respond to noxious agents or damage, by selectively eliminating cells during organism development, as well as various other mechanisms (Elmore, 2007; Meier, Finch, & Evan, 2000).

One of the recently identified modes of PCD is necroptosis. Necroptosis or programmed necrosis is a classically caspase-independent cell death pathway originally described *in vitro* when stimulation of Fas ligand by tumor necrosis factor (TNF) occurred in the presence of the pan-caspase inhibitor Z-VAD-FMK (Degterev et al., 2008). It is since been shown that during classical necroptosis, activation of TNF receptor 1 (TNFR1) leads to the formation of a membrane bound complex (complex I) containing TNFR1, the adaptor protein TRADD, and the receptor interacting protein kinase (RIPK)1. Subsequently, the adaptor protein FADD is recruited to the cytoplasmic complex (complex II), leading to the activation of RIPK3 and its substrate the mixed lineage kinase-like (MLKL). MLKL then trans-locates to cellular membranes to induce their rupture or cause

the engagement of other unknown death mediators (Vandenabeele, Galluzzi, Vanden Berghe, & Kroemer, 2010) (**Figure 2**).

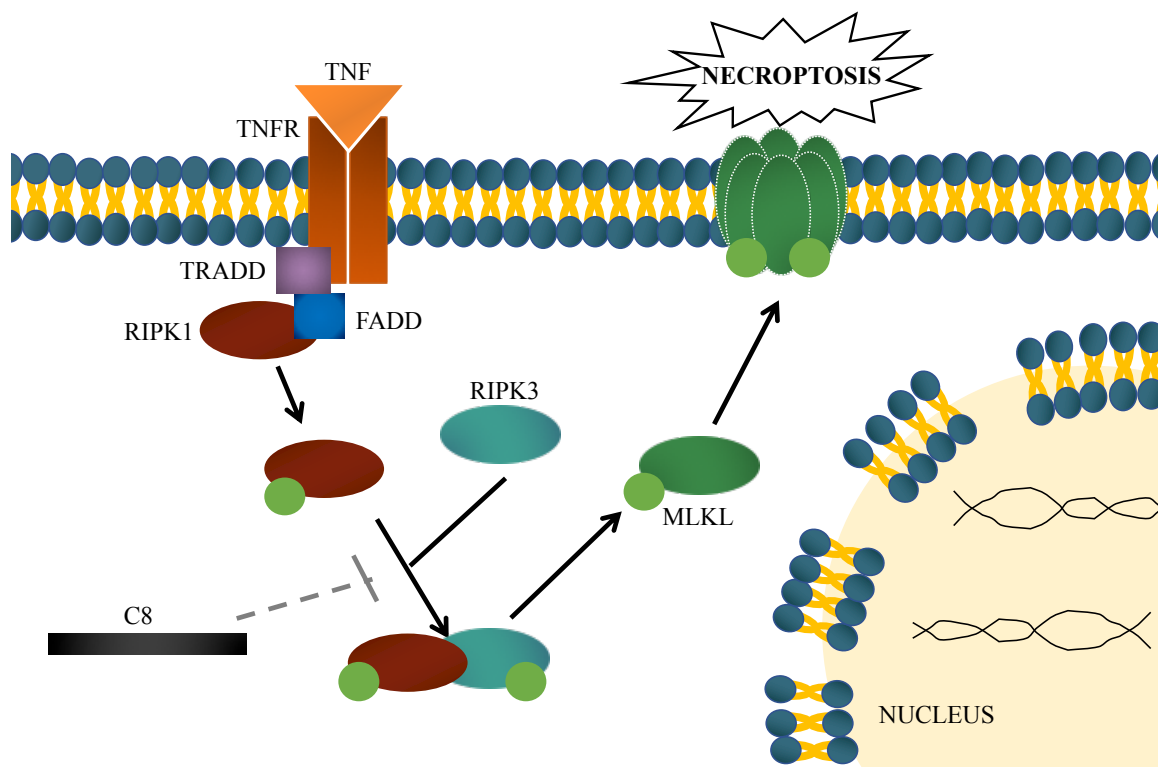


Figure 2. General schematic of receptor-mediated necroptosis. Diagram of receptor-mediated necroptosis during caspase 8 (C8) inhibition. Phosphorylation is indicated with green circles.

In addition to TNFR activation, toll like receptors 3 and 4 can trigger necroptosis in the presence of a pan-caspase inhibitor by recognition of LPS or dsRNA, respectively (X. Sun et al., 1999). These also act via the RIPK3-containing complex II. Notably and as chemically shown during its initial discovery, the necroptosis signaling cascade occurs when caspases are inhibited, particularly caspase 8 as its active presence acts to cleave RIPK1 and prevent further necroptotic signaling. Since necroptosis requires caspase inhibition, its physiological role during infection was at the time of its discovery was

uncertain. Recently, multiple studies have shown that viruses can encode proteins that inhibit caspase activation leading to cell sensitization to TNF-mediated necrosis (Chan et al., 2003; Q. Zhou et al., 1997). This suggests that necroptosis may serve as backup mechanism to fight viral infections. Of note, the physiological role of necroptosis infections is an emerging topic of research and is still not well defined.

While less inflammatory modes of PCD (e.g. apoptosis) are preferential to host cells when challenged, the necroptosis pathway is highly evolutionarily conserved (Dondelinger, Hulpiau, Saeys, Bertrand, & Vandenabeele, 2016). The general rationale behind this is that necroptosis is considered to be a protective mechanism by which cells abort viral replication (Nailwal & Chan, 2019). This pathway is initiated through the direct sensing of viral nucleic acids or protein interactions with DNA-dependent activator of interferon regulatory factors (DAI; a.k.a. Zbp or DLM-1), resulting in the activation of RIPK3 (Kuriakose et al., 2016; Nogusa et al., 2016; Thapa et al., 2016; T. Zhang et al., 2020) (**Figure 3**). Along such lines, mice deficient in necroptotic signaling proteins are more susceptible to various viral infections (e.g. Vaccinia viruses, Herpes Simplex viruses, and West Nile Virus)(Cho et al., 2009; Daniels et al., 2017; Z. Huang et al., 2015; Wang et al., 2014). Additionally, it has been shown that select viruses (e.g. Cytomegaloviruses) possess mechanisms to block necroptosis signaling during infection, to ensure the development of mature viral particles (Omoto et al., 2015; Upton, Kaiser, & Mocarski, 2010). Collectively, necroptosis is considered to be beneficial to host survival during viral infection.

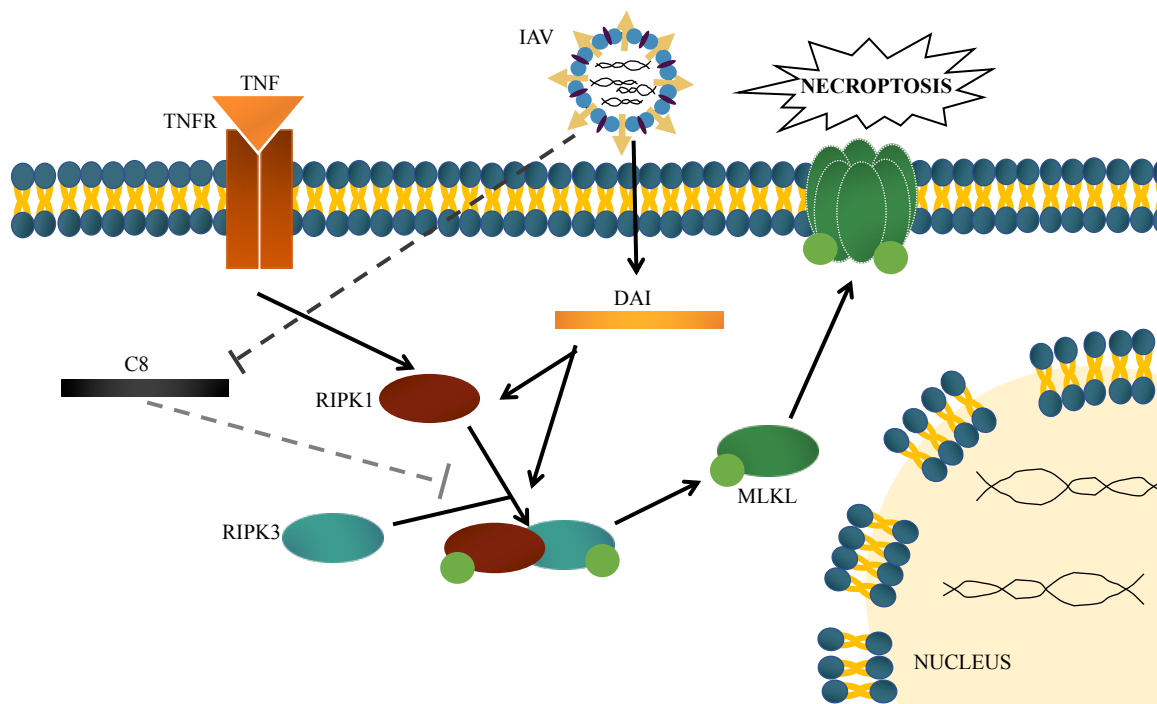


Figure 3. Diagram of virus-induced necroptosis. Diagram of necroptosis as triggered by DAI-sensing of viral infection. Phosphorylation is indicated by green circles.

Importantly and in stark contrast to the above, necroptosis has been demonstrated to largely be detrimental to the host during bacterial infection. Bacterial PFTs, like the pneumococcal ply, are capable of inducing necroptosis of various host cells through ion dysregulation, further increasing the severity of disease (**Figure 4**). For example, PFT-mediated necroptosis of airway epithelial cells and macrophages during bacterial pneumonia by *Spn*, *Serratia marcescens*, or *Staphylococcus aureus*, significantly increases pulmonary injury and mortality in mice (Gonzalez-Juarbe et al., 2018; Gonzalez-Juarbe et al., 2017a; Gonzalez-Juarbe et al., 2015; Kitur et al., 2015). Subsequently and in these models, treatment with necroptosis inhibitors protects against pulmonary injury. Our group has also shown that PFT-mediated necroptosis contributes to the severity of disseminated

bacterial infection, most notably during pneumococcal cardiac invasion (Gilley et al., 2016; Shenoy et al., 2017).

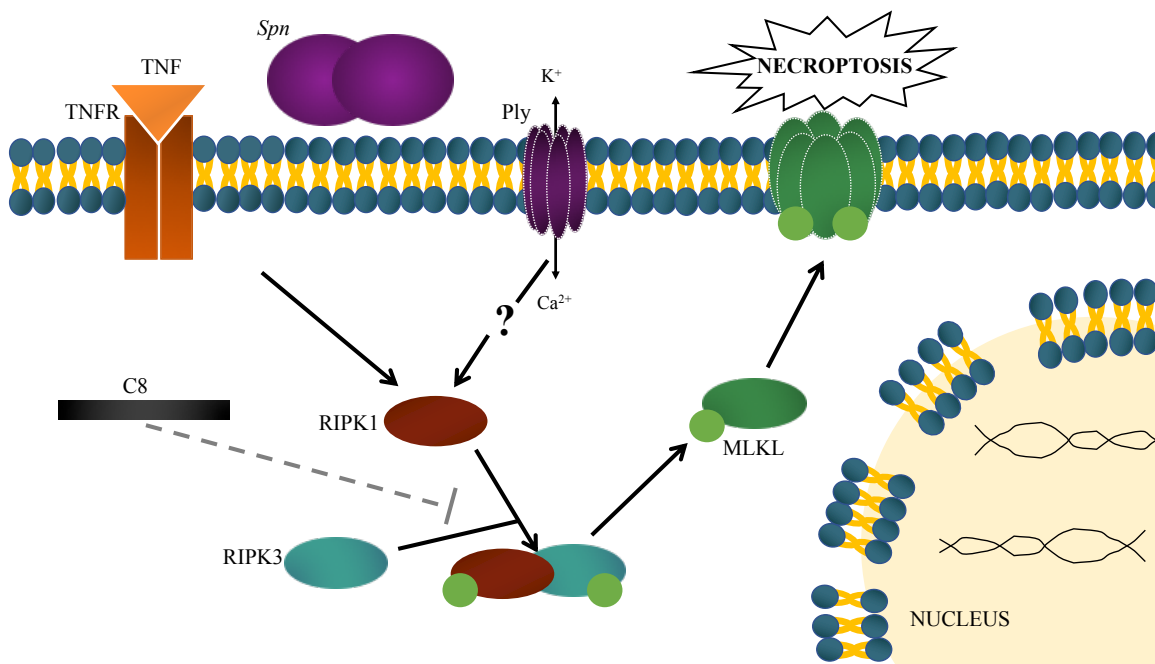


Figure 4. General depiction of PFT-mediated necroptosis. Diagram of PFT-mediated necroptosis modeled with ply of *Spn*. Phosphorylation is indicated with green circles

Main research goal

While a foundation of work has been published showing the role of necroptosis in the pathology of these diseases, little is known about the impact of this conserved PCD mechanism on the immune regulation during and in response to these infections. The goal of this proposal was to further characterize the role of necroptosis in the immune response to infections by airway pathogens, using *Streptococcus pneumoniae* and Influenza A virus as model systems. Here we sought to identify this role during bacterial and viral pneumonia, bacterial/viral co-infection, as well as during invasive pneumococcal disease. Understanding the natural mechanisms by which organisms elicit immunity to infections

can provide a foundation upon which we may further our development of therapeutics and prevention mechanisms for these diseases.

NECROPTOTIC CELL DEATH PROMOTES ADAPTIVE IMMUNITY AGAINST
COLONIZING PNEUMOCOCCI

by

ASHLEIGH N. RIEGLER, TERRY BRISSAC, NORBERTO GONZALEZ-JUARBE,
AND CARLOS J. ORIHUELA

Frontiers in Immunology

Copyright

2019

by

Ashleigh Riegler *et al.*

Used by permission

Format adapted and errata corrected for dissertation

PREFACE

Previously we have shown that pneumolysin, the PFT of *Streptococcus pneumoniae*, elicits necroptosis of various host cell types during pneumococcal pneumonia. It is known that asymptomatic colonization by *Spn* is a requisite precursor to disseminated pneumococcal infections, such as pneumonia. This colonization is accomplished primarily through the biofilm formation by *Spn*. Additionally, we have shown that biofilm *Spn* express and release more ply than *Spn* growing planktonically (like the main growth form observed during pneumonia). Whether this increased ply during colonization results in necroptosis of host cells or whether this impacts the host response to colonization was unknown. Here we used mouse and tissue culture models to identify whether *Spn* elicit necroptosis during asymptomatic colonization and whether this necroptosis alters the host innate and adaptive response, impacting the susceptibility to disseminated infection. This work adds to our understanding of the role of necroptosis during infections by *Spn* and identifies a new, beneficial role for this highly inflammatory cell death.

ABSTRACT

Pore-forming toxin (PFT) induced necroptosis exacerbates pulmonary injury during bacterial pneumonia. However, its role during asymptomatic nasopharyngeal colonization and toward the development of protective immunity was unknown. Using a mouse model of *Streptococcus pneumoniae* (*Spn*) asymptomatic colonization, we determined that nasopharyngeal epithelial cells (nEC) died of pneumolysin (Ply)-dependent necroptosis. Mice deficient in MLKL, the necroptosis effector, or challenged with Ply-deficient *Spn* showed less nEC sloughing, increased neutrophil infiltration, and altered IL-1 α , IL-33, CXCL2, IL-17 and IL-6 levels in nasal lavage fluid (NALF). Activated MLKL correlated with increased presence of CD11c⁺ antigen presenting cells in *Spn*-associated submucosa. Colonized MLKL KO mice and wildtype mice colonized with Ply-deficient produced less antibody against the *Spn* protein antigen PspA, were delayed in bacterial clearance, and were more susceptible to a lethal secondary *Spn* challenge. We conclude that PFT-induced necroptosis is instrumental in the natural development of protective immunity against opportunistic PFT-producing bacterial pathogens.

INTRODUCTION

Regulated cell death without loss of membrane integrity, such as apoptosis, is a vital aspect of organ development, immunity, physiological maintenance, and wound healing (Opferman and Korsmeyer, 2003; Elmore, 2007). In contrast, necrotic cell death, where organelle and cell membrane integrity are lost and cytoplasmic components are released, is generally considered to be detrimental, an unintended consequence of extreme physiological perturbation, irreversible mechanical damage, and/or catastrophic

energy depletion. Yet, we now know that death by necrosis, without simultaneous activation of the pyroptotic inflammasome, is in some instances regulated by the cell (Dorn, 2010; Chavez-Valdez et al., 2012; Chan et al., 2015). The latter suggests that a loss of cell integrity can be in some instances beneficial to the organism as a whole.

One form of programmed necrosis, called necroptosis, is canonically activated as result of death receptor ligation, *e.g.* tumor necrosis factor receptor 1, with concurrent caspase-8 inhibition (Kang et al., 2013; Walsh, 2014). This results in the activation of receptor-interacting serine/threonine protein-kinases (RIPK)-1 and RIPK-3, which then together activate mixed lineage kinase domain pseudokinase (MLKL) by phosphorylation. Activated MLKL (pMLKL) targets phosphatidylserine residues in cellular membranes leading to their dissolution (Dhuriya and Sharma, 2018). Importantly, cytosolic contents released from necroptotic cells serve as alarmins and signal to nearby cells of imminent danger or injury and trigger inflammation (Vandenabeele et al., 2010; Kaczmarek et al., 2013; Pasparakis and Vandenabeele, 2015). Necroptosis is known to occur following sterile injury, such as ischemia-reperfusion (Linkermann et al., 2013; Kim et al., 2018), during viral infection in cells that have blocked apoptosis (Orzalli and Kagan, 2017), and during infection with bacteria that produce pore-forming toxins (PFT). In the latter circumstance, PFT-induced membrane damage results in ion dysregulation and energy depletion, which activates RIPK1 in non-canonical fashion (Gonzalez-Juarbe et al., 2015; Kitur et al., 2015; Ahn and Prince, 2017; Gonzalez-Juarbe et al., 2017; Gonzalez-Juarbe et al., 2018). During pneumonia, bacterial PFTs induce necroptosis of alveolar macrophages and lung epithelial cells, exacerbate tissue injury, and contribute to reduced lung function. Common opportunistic respiratory pathogens including

Streptococcus pneumoniae (*Spn*), *Staphylococcus aureus*, and *Serratia marcescens* have been shown to induce PFT-mediated necroptosis of lung cells; with necroptosis deficiency or its inhibition reducing injury and improving survival (Gonzalez-Juarbe et al., 2015; Gonzalez-Juarbe et al., 2017).

Spn is the leading cause of community-acquired pneumonia and is responsible for ~1.4 million deaths annually (WHO, 2016; Sattar and Haseer Koya, 2018). For *Spn*, colonization of the nasopharynx is a prerequisite to the development of pneumonia and invasive disease (Bogaert et al., 2004). Within the nasopharynx, *Spn* forms biofilms (Marks et al., 2012; Blanchette-Cain et al., 2013), a growth phenotype that produces and releases more of its PFT, pneumolysin (Ply) (Shenoy et al., 2017). Natural immunity against *Spn* typically develops as result of repeated colonization events by different serotypes during early childhood. Broad protective immunity is achieved as result of obtaining a threshold of immune recognition against conserved proteins found on the bacterial surface (Wilson et al., 2017). This is in contrast to the protective antibody that is elicited by the current pneumococcal vaccines; which are composed of an unrelated protein conjugated to as many as 13 distinct *Spn* capsular polysaccharides (Centers for Disease and Prevention, 2010; WHO, 2011; Haber et al., 2016; Keller et al., 2016). Thus, vaccine-immunized individuals remain susceptible to the >80 non-vaccine serotypes of *Spn* unless they have developed the aforementioned broad protective immunity that arises as result of colonization. Taken together, the global health impact of *Spn* is tremendous and *Spn* serves as an excellent prototype to examine the effects of PFT-induced necroptosis on the innate and adaptive immune response in the airway.

Herein we explored the role of PFTs in the host-pathogen interactions which occur during *Spn* colonization and serve to prevent the development of disease. Our goals were to identify whether necroptosis was initiated by Ply during asymptomatic colonization, to characterize the influence of this form of cell death on the immune responses during primary infection, and to assess the role of PFT-induced necroptosis on the generation of broad protective immunity against bacterial antigens. Importantly, our findings provide meaningful insight into the host-pathogen interactions of nasopharyngeal colonizing, PFT-producing bacteria and indicate that cell death by necroptosis is a critical driver of host immunity.

MATERIALS AND METHODS

Mice. Animal experiments were carried out using male and female 6–12-week-old adult mice. Wildtype C57BL/6 were supplied from Jackson Labs (Sacramento, California) and *MLKL*^{-/-} mice in the C57BL/6 background were obtained from Dr. Warren Alexander (Murphy et al., 2013) and housed in the University of Alabama at Birmingham Animal Facilities. To achieve colonization, nasal aspiration was performed on each mouse as previously described with an inoculum of $\sim 1 \times 10^5$ CFU in 10 μ L saline (Blanchette-Cain et al., 2013). To model pneumonia, oropharyngeal aspiration with an inoculum of $\sim 1 \times 10^6$ CFU in 100 μ L saline was used as previously described (Gonzalez-Juarbe et al., 2017). Tissue samples were collected from mice at the indicated time points after inoculation. Nasal lavage (NALF) and collection of nasal turbinates, including nasal associated lymphoid tissue (NALT) were performed post-mortem as previously described (Blanchette-Cain et al., 2013).

Bacterial strains and culture. *S. pneumoniae* serotype 4 strain TIGR4 and serotype 2 strain D39, and previously described isogenic deletion (TIGR4 Δ *ply*) or functional (toxoid, TIGR4w433F) mutants were used in this study (Lizcano et al., 2010; Zafar et al., 2017). All strains were grown on tryptic soy agar supplemented with sheep's blood (Remel R01202) overnight or in tryptic soy broth supplemented with 0.5% yeast extract (THY) at 37°C in 5% CO₂. Bacteria in log phase growth (OD₆₂₀ ~0.5) were used for experiments.

Escherichia coli expressing recombinant Ply or PspA was grown in lysogeny broth (LB) supplemented with kanamycin (50 µg/mL) or ampicillin (100 µg/mL), to log phase (OD₆₂₁ ~0.3-0.5) and the HIS tagged recombinant proteins were purified by nickel column chromatography as previously described (Ren et al., 2003; Douce et al., 2010). All bacterial strains have been fully sequenced, recombinant protein expression was confirmed by immunoblot, and pneumolysin activity was confirmed by red blood cell hemolysis (Sanders et al., 2008).

Tissue staining for microscopy. For staining and microscopy, euthanized mice were decapitated and their heads placed in PBS with 1X protease phosphatase inhibitor cocktail on ice. Following removal of the exterior skin and flesh, dissected heads were decalcified for 4 hours using RDO Decalcification solution (Election Microscopy Sciences; 3:1 in water), neutralized following manufacturer's protocol, and embedded in OCT. Sectioned samples were prepared for staining by treating in acetone for 10 min at -

20°C then 70% ethanol for 5 min at 20°C. Following rehydration with PBS and permeabilization with PBS Triton-X (0.02%), samples were blocked with 5% BSA for 45 min at room temperature then probed for specified protein (1/1000) at 4°C overnight. Samples were washed 3 times for 5 min in PBS-T (PBS-0.05% Tween20). Samples were then incubated in corresponding fluorescent secondary antibody solution for 1 hour at room temperature. Blocking, probing, and detection were then repeated for additional, specified antigens. Following final detection and wash, nuclei were detected using NucBlue (Invitrogen) per manufacturer's instruction and mounted in Fluorsave (EMD Millipore).

Microscopy and image analysis. Images were captured using a Leica LMD6 with DFC3000G-1.3-megapixel monochrome camera or DFC450C-5-megapixel RGB CCD (Leica Biosystems, Buffalo Grove, IL). Wherever noted, tile scanned images were compiled using the Tile Scan stitching feature of the Leica Application Suite X (LAS X) (Leica Biosystems, Buffalo Grove, IL). Mean Fluorescent Intensity (MFI) calculated using ImageJ 1.51h (National Institutes of Health, USA).

Western blot analysis. Tissue homogenates in PBS were desalted using Amicon 10kDa spin columns (Millipore). Desalted homogenates were incubated for 30 min at 4°C in Protein lysis Buffer (50mM TrisHCl-150mM NaCl-1% Triton X100-1X HALT Protease Phosphatase Inhibitor Cocktail), centrifuged (14000rpm at 4°C) for 15 min, and concentrations of the resulting the resulting whole protein lysates were determined from the supernatant using a Bicinchoninic Acid assay kit (Sigma-Aldrich) according to the

manufacturer instructions. 10 μ g of total protein were loaded and separated on a 10% polyacrylamide gel (Biorad) before transfer on nitrocellulose membrane (Biorad). Membranes were blocked in 5% Non-dry fat milk and washed 3 times for 5 min in TBS-0.1%Tween20 (TBST). Membranes were incubated with anti-MLKL (1/1000), anti-pMLKL (1/1000), anti-caspase3/Cleaved caspase3 (1/2000) or anti-actin (1/10000), in 5%BSA overnight at 4°C with gentle agitation. Membranes were then washed 3 times for 10min in TBST and incubated with HRP-conjugated goat anti-rabbit (1/10000, Jackson). Membranes were washed 3 times for 10 min in TBST, once for 5 min with TBS and signal was detected using Clarity™ Western ECL and ChemiDoc XRS+ (Biorad). Protein expression was determined by densitometry using ImageJ.

Inhibitors, antibodies, and other chemicals. The MLKL inhibitor necrosulfonamide (NSA) was obtained from Tocris Bioscience (QL, United Kingdom). To inhibit caspases, the general caspase inhibitor Z-VAD-fmk was obtained from R&D Systems (Minneapolis, MN). The lipid oxidase inhibitor Liproxstatin-1, used to inhibit Ferroptosis, was obtained from Sigma (St Louis, MO). Cytopins were stained with PROTOCOL® HEMA 3® Stain set from Fisher Scientific (Kalamazoo, MI).

Cell Culture. FaDu (HTB-43) human pharyngeal epithelial cells were obtained from the American Type Culture Collection (Manassas, VA) and cultured in Gibco™ Minimum Essential Medium supplemented with 10% Fetal Bovine Serum (Atlanta Biologicals) and 1% Gibco™ Antibiotic-Antimycotic. Cultures were grown at 37°C in 5% CO₂. Cell infection experiments were carried out in 96-well plates seeded at 1 x 10⁴ cells/well and

infected 24-30 hours after seeding with *S. pneumoniae* at an MOI of 10 overnight (15 hours). For positive lysis controls, LDH Lysis Buffer from the Pierce LDH Cytotoxicity Assay Kit was added according to manufacturer's instructions to lysis control wells 20-30 min prior to sample collection.

Statistics. Statistical comparisons were calculated using GraphPad Prism 8 (La Jolla, CA). Comparisons between two cohorts at a single time point are calculated by Mann-Whitney U test. Comparisons between groups of >2 cohorts or groups given multiple treatments were calculated by ANOVA with Tukey's (one-way) or Sidak's (two-way) post-test or by Kruskal-Wallis H test with Dunn's multiple comparison post-test, as determined by the normality of data groups. Repeated measures are accounted for whenever applicable.

Study Approval. The aim of this study was to characterize the role of necroptosis in the innate and adaptive immune responses to colonizing *Streptococcus pneumoniae*. All animal studies were performed in compliance with the federal regulations set forth in the Animal Welfare Act, the recommendations in the National Institutes of Health Guide for the Care and Use of Laboratory Animals, and the University of Alabama at Birmingham Institutional Animal Use and Care Committee (IACUC). All protocols used in this study were approved by the IACUC at the University of Alabama at Birmingham (protocols #20479 and #21231). Power calculations from past studies were used to calculate the number of mice needed to ensure statistical power. Unless otherwise noted, all *in vitro* experiments are composed of a minimum of 3 biological replicates, with ≥ 3 technical

replicates each. All *in vivo* experiments were done with a minimum of 3 biological replicates. All results were confirmed with a minimum of two independent experiments.

RESULTS

Cell death occurs during asymptomatic colonization by *S. pneumoniae*.

Nasopharyngeal colonization was established in 6-8 week-old male and female mice by instillation of $\sim 10^5$ CFU of serotype 4 strain TIGR4 into the nares. This resulted in a colonization burden of $\sim 2 \times 10^5$ CFU/g nasoturbinate at 7-days post-inoculation and clearance of *Spn* by 21-days post-inoculation (**Supplemental Figure S1A**). Colonized mice appeared normal with no overt physical signs of distress (**Supplemental Figure 1B, C**). Despite this, nasal lavage fluid (NALF) collected 7-days post-inoculation showed greater nasopharyngeal epithelial cell (nEC) sloughing in colonized mice versus negative controls (**Figure 1A**). This corresponded with increased amounts of the cell damage markers lactate dehydrogenase (LDH; **Figure 1B**) and Interleukin (IL)-1 α (**Figure 1C**) in isolated NALF. Notably, IL-1 α is a pro-inflammatory cytokine that is only released when cells die of necrosis (Elkon, 2007). Consistent with previous publications (Joyce et al., 2009; Zafar et al., 2017), microscopic examination of nasal sections revealed pathological evidence of damage and inflammation in colonized mice, including large clusters of mucous and sloughed nECs in the lumen (**Figure 1D**); the latter being the most likely source of those detected in NALF.

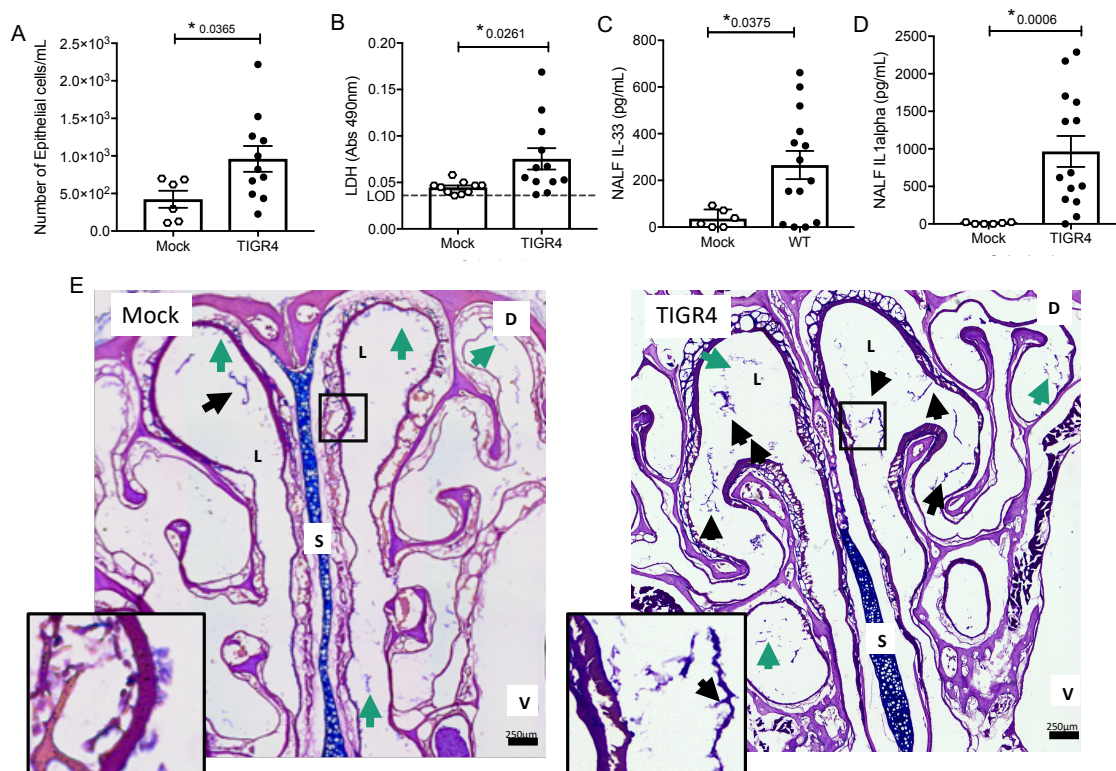


Figure 1. Cell damage occurs during asymptomatic colonization by *Spn*. Nasal lavage collected from wildtype C57BL/6 (WT) mice at day 7 post-inoculation with TIGR4 or PBS (Mock) analyzed for (A) nEC sloughing, quantified from HEMA stained Cytospin samples, (B) lactate dehydrogenase (LDH), dashed line indicating limit of detection, (C) IL-33, and (D) IL-1 α . Mean \pm SEM. Mann-Whitney U test used for comparisons (n=10-14). P values listed on graph; * indicates a value \leq 0.05. (E) Representative nasal section and zoomed inset from WT mouse either mock colonized or colonized with TIGR4, collected at day 7 post-inoculation and stained with Alcian/PAS. Lumen (L), septum (S), dorsal side (D), and ventral side (V) denoted. Arrows indicating luminal clusters of epithelial cells (black) and mucus (green). Inset source region denoted by black box outline. Images Tile Scan assembled at 10x magnification.

We examined the specific type of cell death that occurred during colonization, namely whether necroptosis was occurring. Nasal sections (**Figure 2A**) and nasal homogenates (**Figure 2B**) from colonized mice were positive for pMLKL, suggesting nECs were dying of necroptosis. Moreover, the same samples showed negligible amounts of cleaved caspase-3 (**Figure S2**). Further implicating necroptosis as the principal mode of nasopharyngeal epithelial cell death following *Spn* exposure, death of FaDu human pharyngeal cells infected with TIGR4 *in vitro* was reduced when cells were pre-treated with the necroptosis inhibitor necrosulfonamide (NSA). No protection against death was observed when FaDu cells had been pre-treated with the pan-caspase inhibitor Z-VAD-fmk (Z-VAD) or the ferroptosis inhibitor Liproxstatin-1 (Liprox) (**Figure 2C**). We next tested necroptosis deficient (MLKL KO) mice. Colonized MLKL KO mice showed decreased nEC sloughing (**Figure 2D**) as well as decreased LDH and IL-1 α levels in NALF (**Figure 2E, F**), when compared to colonized WT controls. We thereby conclude that necroptosis occurred within the nasopharynx during asymptomatic colonization with *Spn*, and the inability to activate this cell death mechanism resulted in lower amounts of alarmins released by dying cells.

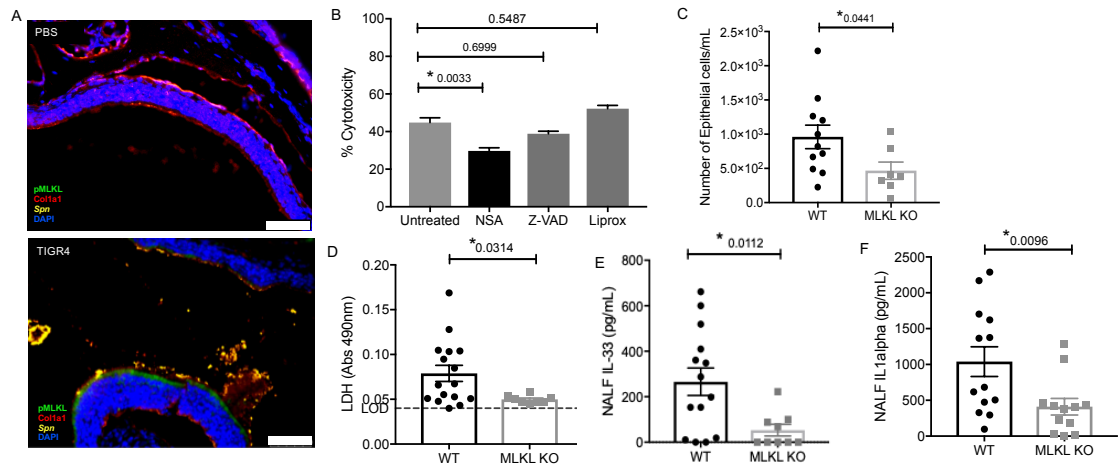


Figure 2. Necroptosis during *Spn* colonization is PFT dependent. (A) Representative IF images of nasal turbinates from WT mice collected at day 7 post-inoculation with TIGR4 or PBS stained for pMLKL (green), collagen-1a (red), Spn (yellow), and DAPI (Blue). Imaged at 40X Tile Scan. Scale bars indicate 50 μm. (B) FaDu cell death (%cytotoxicity) as measured by LDH release from cells pre-treated with normal media or media containing 10 μM of either the MLKL inhibitor Necrosulfonamide (NSA), the general caspase inhibitor ZVAD, or the ferroptosis inhibitor Liproxstatin-1 (Liprox), for 1 hour then challenged overnight (15 hours) with TIGR4 at an MOI of 10. One-way analysis of variance used for comparisons (Cytotoxicity $F=14.78$, $p<0.0001$; CFU $F=34.38$, $p<0.0001$) (See also Figure 5A). (C-F) NALF from WT and MLKL KO mice colonized with TIGR4 analyzed for (C) nEC sloughing, (D) LDH, dashed line indicates limit of detection, (E) IL-33, and (F) IL-1 α . LDH Absorbance at 490nm LOD normalized to absorbance of uninfected control NALF. Mean \pm SEM; Mann-Whitney U test for comparisons (N=10-14 animals per genotype). P values listed on graph; * indicates a value ≤ 0.05 . (See also Figures 4 and 5)

Necroptosis during *Spn* colonization is PFT-dependent. Given our findings, we examined whether the observed nEC necroptosis was initiated by *Spn*'s PFT. Infection of FaDu cells with Ply deficient *Spn* (TIGR4 Δ ply) resulted in less cell death compared to infection with wildtype *Spn* (TIGR4); moreover, pre-treatment of cells with NSA, Z-VAD-fmk, or Liprox did not further reduce damage caused by the Ply-deficient *Spn* (**Figure 3A**). Nasal sections and homogenates from WT mice colonized with TIGR4 Δ ply did not show activation of MLKL (*i.e.* positive pMLKL staining) in *Spn*-associated regions, unlike those colonized with wildtype TIGR4 (**Figure 2B, 3B**). Nor did TIGR4 Δ ply colonized WT mice have meaningful amounts of cleaved caspase-3 (**Figure S2B**); suggesting cell death was reduced overall. NALF from WT mice colonized with TIGR4 Δ ply were similar to that from MLKL KO mice colonized with TIGR4 with fewer sloughed nECs (**Figure 3C**) and drastically reduced levels of detectable LDH (**Figure 3D**) and IL-1 α (**Figure 3E**) when compared to NALF from WT mice colonized with TIGR4. Collectively, these data suggest that the necroptosis during colonization by *Spn* is Ply-dependent.

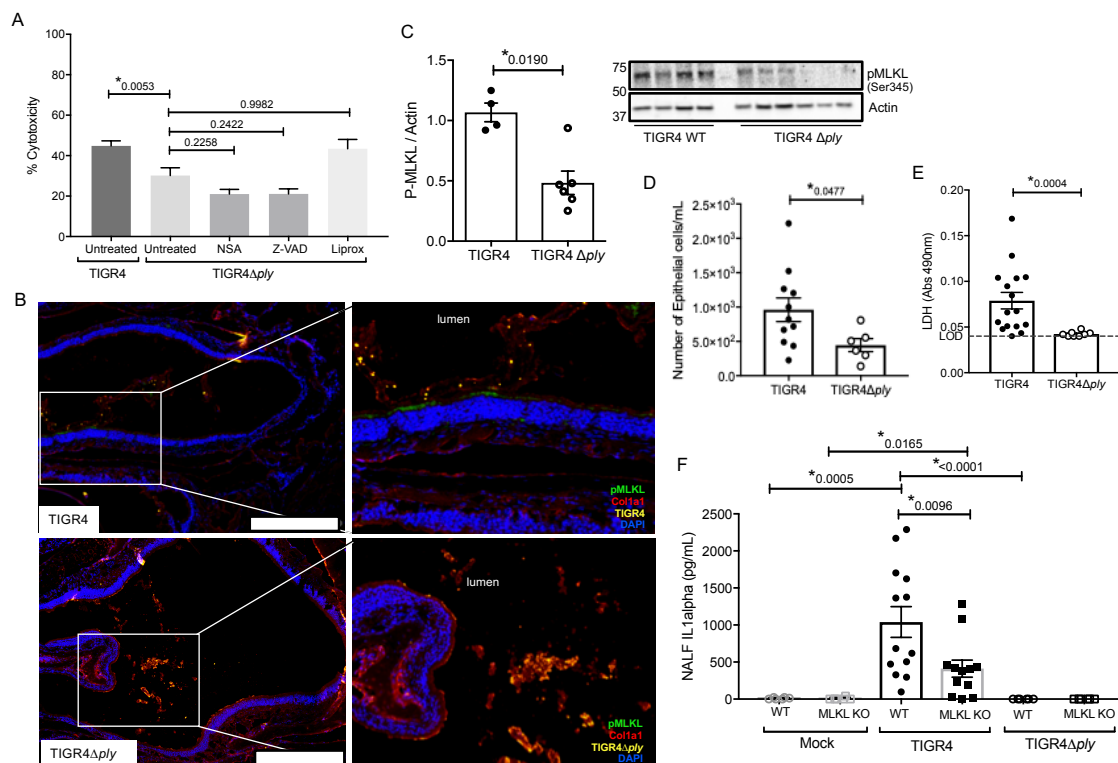


Figure 3. Necroptosis during *Spn* colonization is pneumolysin dependent. (A) FaDu pharyngeal cell death as measured by percent LDH release from cells pre-treated with normal media or media containing 10 μ M of either the MLKL inhibitor Necrosulfonamide (NSA), the general caspase inhibitor ZVAD, or the ferroptosis inhibitor Liproxstatin-1 (Liprox), for 1 hour then challenged overnight (15 hours) with TIGR4 or TIGR4 Δ ply at an MOI of 10. One-way analysis of variance (F=11.86, p<0.0001); P values listed on graph; * indicates a value \leq 0.05 (See also Figure S3B). (B) Representative immunofluorescent images of nasal turbinates from wildtype mice colonized with TIGR4 or TIGR4 Δ ply, at day 7 post inoculation with 10⁵ CFU. Turbinates fixed and stained for collagen-1a (red), *Spn* (yellow), pMLKL (green), and DAPI (Blue). Imaged at 40X magnification and Tile Scan assembled. White scale bars indicate 250 μ m. (C) Western blot and densitometry for pMLKL and actin in nasal homogenates from mice colonized with TIGR4 or TIGR4 Δ ply. Nasal lavage at 7-days post intra-nasal inoculation with TIGR4 or TIGR4 Δ ply analyzed for (D) nEC sloughing, (E) lactate dehydrogenase (LDH), and (F) IL-1 α . LDH Absorbance at 490nm LOD normalized to absorbance of uninfected control NALF. Mann-Whitney U test used for two-way comparisons and Kruskal-Wallis test with Dunn's post-test for multiple comparisons (Two infection experiments; total n=10-14 animals per genotype). P values listed on graph; * indicates a value \leq 0.05. (See also Supplemental Figures 2 and 3)

Necroptosis alters the innate immune response to colonizing *Spn* and decreases the duration of colonization. We sought to better characterize how necroptosis influenced the innate immune response to pneumococcal colonization. NALF collected from MLKL KO mice at 7-days post-inoculation contained more of chemokine ligand-2 (CXCL2) (**Figure 4A**), a known neutrophil chemoattractant (Niggli, 2003). NALF isolated from MLKL KO mice also had strikingly lower levels of the key colonization clearance cytokines IL-17 (**Figure 4B**) and IL-6 (**Figure 4C**). Despite having fewer sloughed nEC, TIGR4 colonized MLKL KO mice had more polymorphonuclear cells (PMNs) in their NALF (**Figure 4D**) 7-days post-inoculation than WT controls. In addition to the luminal cellular responses detected in NALF, we examined the submucosal immune cell population by fluorescent microscopy of nasal tissue sections. Fluorescent intensity for CD11c, an immune cell marker often associated with mature dendritic cells, positively correlated with that of pMLKL ($R^2=0.7413$, $P<0.0001$, $N=33$) (**Figure 4E**) in nasal sections from WT colonized mice. Conversely, pMLKL-associated fluorescence did not correlate with that of F4/80, a common macrophage marker ($R^2=0.08428$, $P=0.0958$), or Ly6G, a common neutrophil marker ($R^2= 0.0005553$, $P=0.8948$) (**Figure 4F, G**). Importantly, when colonized with TIGR4, WT mice cleared pneumococcal colonization faster than the MLKL KO mice (**Figure 5**). Thus, cell death by necroptosis during *Spn* colonization contributes toward greater amounts of pro-inflammatory cytokines previously associated with *Spn* clearance, reduced neutrophils, recruitment of potential antigen-presenting cells, and more rapid elimination of bacteria from the site of colonization.

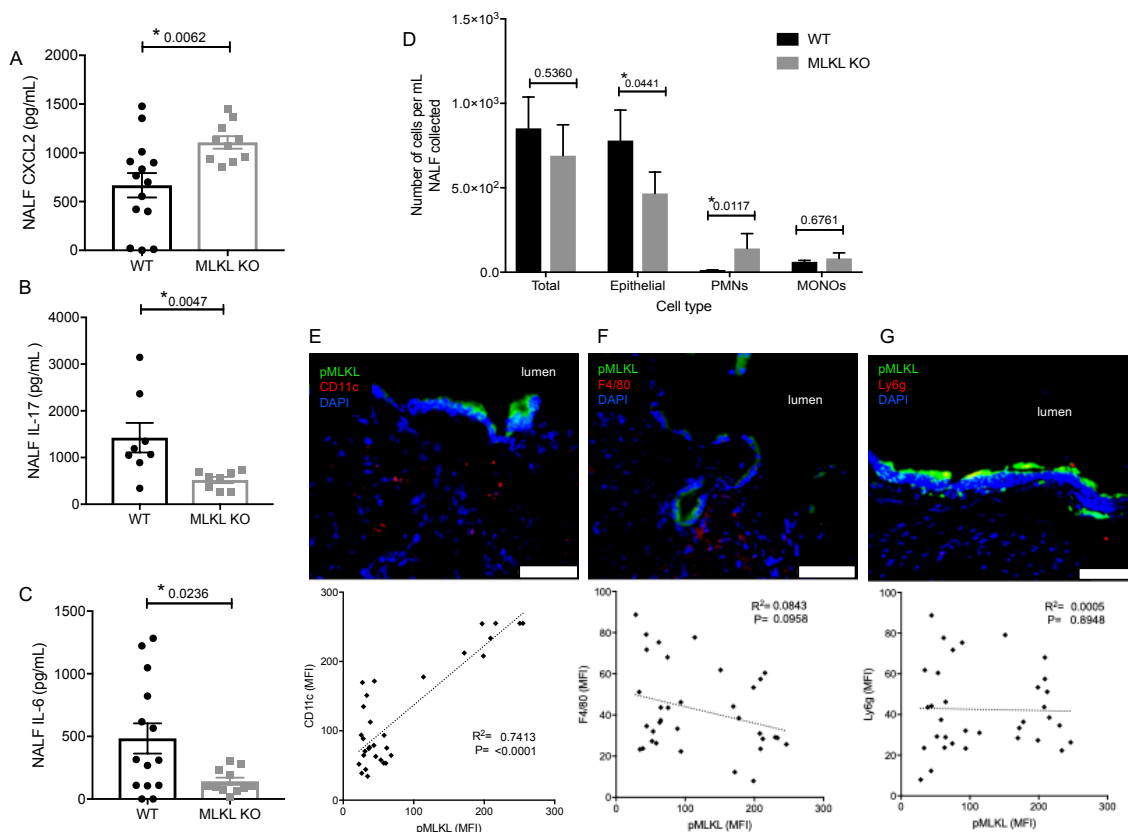


Figure 4. Localized PFT-induced necroptosis affects the innate immune response to colonizing *Spn*. Nasal lavage at day 7 post intra-nasal inoculation with 10^5 CFU TIGR4 analyzed for (A) CXCL2, (B) IL-17, and (C) IL-6. Mann-Whitney U test used for comparisons. $N=10-14$ animals per group; P values listed on graph; * indicates value ≤ 0.05 . (D) Quantification of epithelial cells, polymorphonuclear cells (PMNs), and mononuclear cells (MONOs) in NALF at day 7 post intra-nasal inoculation with TIGR4 as quantified by HEMA stained Cytospins. One-way analysis of variance ($F=14.85$, $p < 0.0001$); P values listed on graph; * indicates value ≤ 0.05 . (E-F) Representative immunofluorescently stained nasoturbinate section from wildtype mice colonized with TIGR4, at day 7 post inoculation, and correlation of pMLKL to cell-specific marker in stained sections. Sections stained for pMLKL (green), DAPI (blue), and (E) CD11c ($N=35$, $R^2 = 0.7413$, $P < 0.0001$), (F) F4/80 ($N=37$, $R^2 = 0.08428$, $P = 0.0958$), or (G) Ly6g ($N=35$, $R^2 = 0.00056$, $P = 0.8948$) in red. Imaged at 40X magnification and Tile Scan assembled. White scale bars indicate 50 μ m.

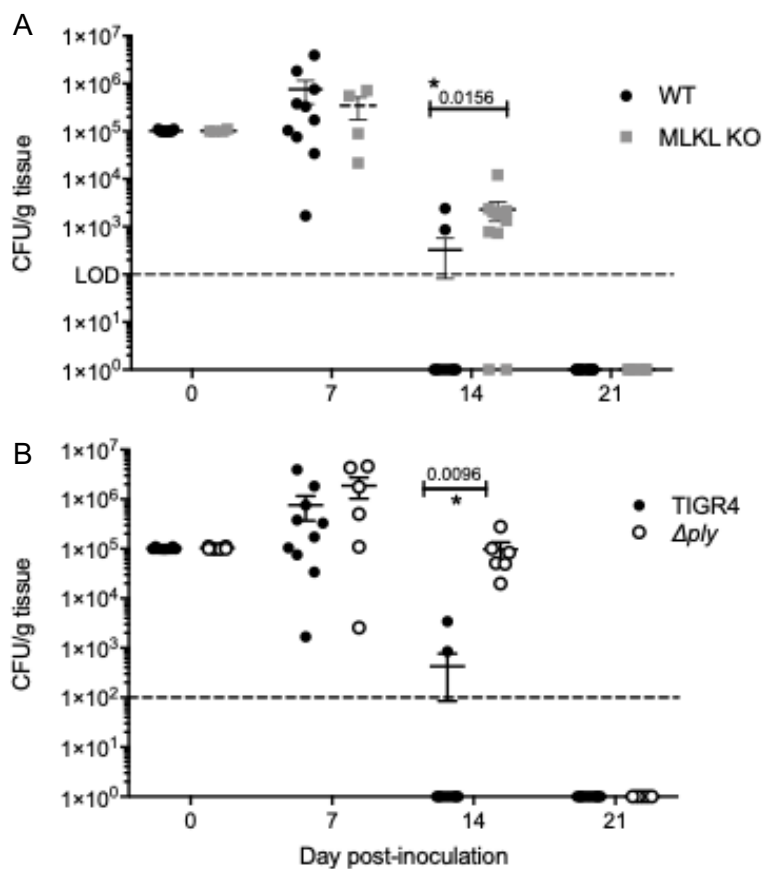


Figure 5. Inhibition of Ply-mediated necroptosis decreases the rate of *Spn* clearance. Number of *Spn* in nasal homogenates of (A) wildtype and MLKL KO mice colonized with TIGR4 and (B) wildtype mice colonized with TIGR4 or TIGR4 Δ ply collected at days 0, 7, 14, and 21 post-inoculation. Mean \pm SEM shown. N= 5-10 mice/group; two-way ANOVA with Sidak multiple comparisons, * = $P \leq 0.05$. Dashed line indicates limit of detection. Note that day 14 and 21 homogenates also plated in 100 μ L spread plates to confirm clearance (limit of detection 100 CFU/g tissue).

Nasopharyngeal Ply-mediated necroptosis promotes antibody production against *Spn* surface components. Development of antibody against *Spn* surface proteins is a key facet of naturally acquired protective immunity (McCool et al., 2002). Given the delay in *Spn* clearance and reduced number of CD11c⁺ cells, we tested whether Ply-mediated necroptosis influenced the production of anti-*Spn* antibodies during colonization. To do this we measured the production of antibody against pneumococcal surface protein A (PspA). Briefly, PspA is a highly-conserved pneumococcal antigen, against which antibodies are protective (McDaniel et al., 1991). Serum from WT mice colonized with TIGR4 had more anti-PspA IgG than MLKL KO mice colonized with the same. Similarly, WT mice colonized with TIGR4 had higher anti-PspA IgG than WT mice colonized with TIGR4 Δ *ply*. Along these lines, colonization of WT mice with an isogenic strain encoding the non-lytic Ply toxoid (TIGR4w433F) resulted in less anti-PspA IgG than WT mice colonized with TIGR4, implicating the necroptotic activity of the toxin as necessary for the immune-stimulatory effect of Ply (**Figure 6B**). Interestingly, these differences in antibody response were not observed in the T cell independent IgG response against type 4 capsular polysaccharide (**Figure 6C**), suggesting that necroptosis mediated inflammation in particular impacts antigen-presentation. The lack of an IgG response against PspA in colonized MLKL KO mice was not due to their inability to produce IgG or their ability to respond to mucosal protein challenge (**Figure S4**). Thus, Ply-mediated necroptosis positively influences the production of anti-pneumococcal antibody against T cell dependent antigens of colonizing *Spn*.

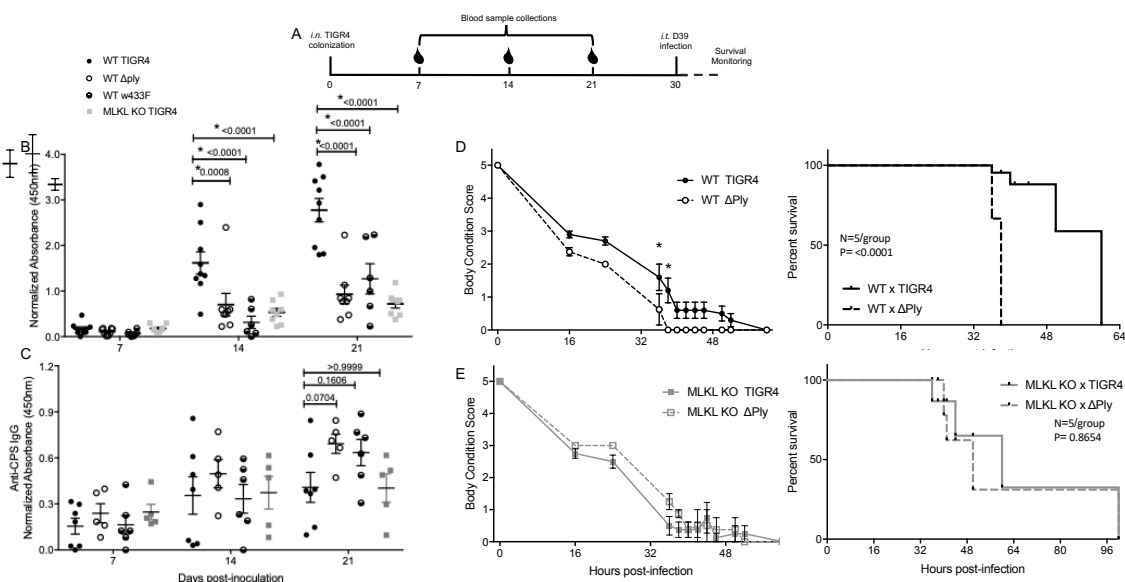


Figure 6. Necroptosis initiates protective, adaptive immunity against colonizing *Spn*.

(A) Representative diagram of challenge and sample collection from mice in secondary lethal infection model. Serum IgG against (B) PspA or (C) type 4 capsular polysaccharide from wildtype (WT) or MLKL KO mice colonized with TIGR4, TIGR4 Δ ply, or TIGR4w433F. Two-Way repeated measures ANOVA with Sidak's multiple comparisons test (Interaction $F=9.21$, $p=0.4380$; Time $F=59.31$, $p<0.0001$). $N=5-8$ mice/group. (D-E) WT and MLKL KO mice colonized with wildtype TIGR4 (solid) or TIGR4 Δ ply (dashed) and re-challenged intra-tracheally at day 30 post colonization inoculation with a lethal infectious dose of D39 (106). Body condition score and survival of (D) WT and (E) MLKL KO mice after intratracheal challenge. Body condition scores analyzed by Two-Way ANOVA with repeated measures (WT: Interaction $F=1.169$, $p=0.1030$; Time $F=88.67$, $p<0.0001$) (KO: Interaction $F=0.8801$, $p=0.3386$; Time $F=90.45$, $p<0.0001$). Comparisons of time points with p -value ≤ 0.05 indicated by asterisk. Survival analyzed by Mantel-Cox Log-rank test (WT: Chi square= 15.34, $p<0.0001$) (KO: Chi square= 0.2603, $p=0.6099$). P values listed on graphs * indicates value ≤ 0.05 . (See also Supplemental Figures 5). Mean \pm SEM plotted for all panels.

Necroptosis initiates the development of protective immunity. Finally, we tested whether Ply-mediated necroptosis impacted naturally-acquired protective immunity, *i.e.* survival during subsequent lethal intra-tracheal challenge with a different serotype of *Spn*. To do this we used the following schema (**Figure 6A**); note that 21-days after colonization with TIGR4, no bacteria were detectable within nasal homogenates of mice (**Figure 5**). All mice, regardless of background died following secondary lethal D39 serotype 2 challenge. However, mice that had initially been colonized with TIGR4 Δ *ply* succumbed more rapidly to infection versus those previously colonized with TIGR4 (**Figure 6D**). Moreover, MLKL KO mice first colonized with TIGR4 were equivalent in susceptibility to D39 as MLKL KO mice colonized with TIGR4 Δ *ply* (**Figure 6E**). This decreased mortality was not due to antibody against Ply, as shown by the increased susceptibility of WT mice colonized by TIGR4w433F and subsequently challenged with D39 (**Figure S5**). Note that a direct comparison between WT and MLKL KO mice was not made since we have already demonstrated that MLKL KO mice are protected against severe forms of *Spn* disease, such as the pneumonia modeled here in our secondary infection (Gonzalez-Juarbe et al., 2015; Gonzalez-Juarbe et al., 2017). All together, these data demonstrate that PFT-mediated necroptosis during colonization is a key initiator of protective immunity against subsequent challenge by *Spn* of a different serotype.

DISCUSSION

The strikingly detrimental effects of necroptosis on tissue injury are well documented (Linkermann et al., 2013; Zhou and Yuan, 2014). This includes within the lower respiratory tract during infection with diverse PFT-producing bacterial pathogens

(Gonzalez-Juarbe et al., 2015; Kitur et al., 2015; Gonzalez-Juarbe et al., 2017). Yet, necroptosis also plays a pivotal role in the control of intracellular pathogens which inhibit apoptotic signaling. For example, necroptosis aborts the replication of viruses that have blocked caspase activation (Pan et al., 2014; Nogusa et al., 2016; Orzalli and Kagan, 2017). In some instances, cell death by necroptosis may even serve to limit pathological inflammation through the divergence from other even more inflammatory forms of necrosis (Kitur et al., 2016). Along such lines, and at the onset of our study, whether necroptosis was beneficial or detrimental in regards to infectious outcomes against colonizing pathobionts in the nasopharynx was unknown. Our results herein demonstrate that despite the associated tissue damage, cell death by necroptosis is beneficial and serves as a key initiator of innate and adaptive immunity against the colonizing PFT-producing pathogen, in this instance *Spn*. The impact of these findings is broad and may further extend to the numerous other PFT-producing mucosal colonizers.

Much of the damage resultant from necroptosis is due exacerbated inflammation. Molecules that contain DAMPs and other alarmins, such as IL-1 α , are strong immune stimulants which interact with nearby cells to induce proinflammatory cytokine signaling, initiate recruitment of antigen presenting cells (APC), and serve to activate APCs (Land, 2015). Our observations that IL-1 α and the key clearance cytokine IL-17 were increased in lavage from *Spn* colonized WT mice, but not MLKL KO mice or WT mice colonized with *Spn* lacking Ply, as well as the observed correlation of pMLKL with submucosal CD11c⁺ cells suggest that Ply- induced necroptosis may be the mechanism by which these key cytokines which drive APC recruitment are released during colonization. In turn, the observed delay in *Spn* clearance seen in MLKL KO mice is most likely related

to the reduction of these cytokines, as the clearance of *Spn* from the murine nasopharynx is accelerated by IL-1 family cytokines and IL-17 signaling (Zhang et al., 2009; Cohen et al., 2011; Lemon et al., 2015). Notably, increased neutrophil infiltration has been reported for IL-1 α KO mice (Kafka et al., 2008). Thus, the increased levels of PMNs seen in NALF of MLKL KO mice is consistent with the decreased release of IL-1 α and the greater levels of CXCL2 that were observed.

The role of PFTs, specifically Ply, during colonization and disease is multifaceted and not fully understood. For example, Ply is important in the initial establishment of *Spn* nasopharyngeal colonization (Hotomi et al., 2016); however this effect diminishes over time and mutants lacking Ply colonize for longer (van Rossum et al., 2005; Matthias et al., 2008; Das et al., 2014). Necroptosis may also increase *Spn* transmission as it has been shown that Ply-dependent inflammation is key in the transmission of *Spn* to a new host (Zafar et al., 2017). Previous publications have shown that the Ply-induces cytokine and chemokine production which ultimately results in increased antigen delivery to lymphoid tissues and recruitment of APCs (Matthias et al., 2008; Kung et al., 2014). Our observations that MLKL KO mice and WT mice colonized with Ply mutant strains have reduced CD11c⁺ cell recruitment, diminished IgG response to *Spn* protein antigens, and delayed *Spn* clearance, is in agreement with these prior reports. Moreover, these data add the new understanding that programmed necrosis is a vital aspect of this process; *i.e.* facilitating the release of alarmins from nEC which help to activate the immune system.

Given the latter, these results suggest the ability to undergo necroptosis is one way the host immune system is able to recognize and respond differently to potential pathogens (*i.e.* those producing PFTs) versus non-threatening bacteria which colonize the

same niche. Necroptosis-facilitated recruitment of APCs and the associated enhanced generation of protective antibody would in turn reduce the likelihood of severe disease caused by subsequent versions of the same PFT-producing pathogen. Extrapolating from this, our results further suggest that necroptosis induced during viral infection may also facilitate the recruitment of APCs and the generation of an adaptive immune response to viral antigens. Thus, further studies on whether directed necroptosis and resulting alterations in the local inflammatory signaling can be used to trigger adaptive immunity are worth pursuing. Open questions include the specific role of established and newly identified alarmins such as IL-1 α and IL-33, in these processes.

A beneficial role for necroptosis during colonization is in stark contrast to that observed during severe bacterial diseases. Within the nasopharynx and during asymptomatic colonization, necroptosis serves to release factors that initiate a robust immune response and protect the host. These dual consequences reflect the double-edged sword which is the immune system. Further studies examining how the host utilizes necroptosis as an immune stimulus in response to asymptomatic viral infections, viral and bacterial co-infections, polymicrobial bacterial infections, and at other anatomical sites are warranted. In summary, our observations have important implications on our understanding of mucosal immunity and the co-evolution of the immune system with obligate mucosal pathogens like *Spn*.

ACKNOWLEDGMENTS

We thank Dr. Warren Alexander (Walter and Eliza Hall Institute of Medical Research Parkville, Victoria, Australia) for the gift of the MLKL KO mice and Dr. Douglas Green

(St. Jude Children's Research Hospital, Memphis, TN) for supplying our colony. We thank Drs. David Briles (The University of Alabama at Birmingham, Birmingham, AL) and Timothy Mitchell (University of Birmingham, Birmingham, United Kingdom) for the gift of the rPspA and rPly expression plasmids, respectively. We thank Dr. Jeffrey Weiser (New York University School of Medicine, New York, NY) for the gift of the pneumolysin toxoid strain TIGR4w433F. We thank the Pathology Core Laboratory at the University of Alabama at Birmingham for tissue embedding. We thank Anukul T. Shenoy, Sarah M. Beno, Katherine L. Kruckow, Kelley M. Bradley, and Shekwonya Evelyn Samuel for technical assistance throughout. **Funding:** A.N.R. was supported by National Institutes for Health (NIH) Immunologic Diseases and Basic Immunology training grant 2T32AI007051-41. C.J.O. was supported by NIH grants [AI114800](#) and [AG055144](#).

REFERENCES

- Ahn, D., and Prince, A. (2017). Participation of Necroptosis in the Host Response to Acute Bacterial Pneumonia. *J Innate Immun* 9(3), 262-270. doi: 10.1159/000455100.
- Blanchette-Cain, K., Hinojosa, C.A., Akula Suresh Babu, R., Lizcano, A., Gonzalez-Juarbe, N., Munoz-Almagro, C., et al. (2013). Streptococcus pneumoniae biofilm formation is strain dependent, multifactorial, and associated with reduced invasiveness and immunoreactivity during colonization. *MBio* 4(5), e00745-00713. doi: 10.1128/mBio.00745-13.
- Bogaert, D., De Groot, R., and Hermans, P.W. (2004). Streptococcus pneumoniae colonisation: the key to pneumococcal disease. *Lancet Infect Dis* 4(3), 144-154. doi: 10.1016/S1473-3099(04)00938-7.
- Centers for Disease, C., and Prevention (2010). Licensure of a 13-valent pneumococcal conjugate vaccine (PCV13) and recommendations for use among children - Advisory Committee on Immunization Practices (ACIP), 2010. *MMWR Morb Mortal Wkly Rep* 59(9), 258-261.
- Chan, F.K., Luz, N.F., and Moriwaki, K. (2015). Programmed necrosis in the cross talk of cell death and inflammation. *Annu Rev Immunol* 33, 79-106. doi: 10.1146/annurev-immunol-032414-112248.
- Chavez-Valdez, R., Martin, L.J., and Northington, F.J. (2012). Programmed Necrosis: A Prominent Mechanism of Cell Death following Neonatal Brain Injury. *Neurol Res Int* 2012, 257563. doi: 10.1155/2012/257563.

- Cohen, J.M., Khandavilli, S., Camberlein, E., Hyams, C., Baxendale, H.E., and Brown, J.S. (2011). Protective contributions against invasive *Streptococcus pneumoniae* pneumonia of antibody and Th17-cell responses to nasopharyngeal colonisation. *PLoS One* 6(10), e25558. doi: 10.1371/journal.pone.0025558.
- Das, R., LaRose, M.I., Hergott, C.B., Leng, L., Bucala, R., and Weiser, J.N. (2014). Macrophage migration inhibitory factor promotes clearance of pneumococcal colonization. *J Immunol* 193(2), 764-772. doi: 10.4049/jimmunol.1400133.
- Dhuriya, Y.K., and Sharma, D. (2018). Necroptosis: a regulated inflammatory mode of cell death. *J Neuroinflammation* 15(1), 199. doi: 10.1186/s12974-018-1235-0.
- Dorn, G.W., 2nd (2010). Mechanisms of non-apoptotic programmed cell death in diabetes and heart failure. *Cell Cycle* 9(17), 3442-3448. doi: 10.4161/cc.9.17.12944.
- Douce, G., Ross, K., Cowan, G., Ma, J., and Mitchell, T.J. (2010). Novel mucosal vaccines generated by genetic conjugation of heterologous proteins to pneumolysin (PLY) from *Streptococcus pneumoniae*. *Vaccine* 28(18), 3231-3237. doi: 10.1016/j.vaccine.2010.02.014.
- Elkon, K.B. (2007). IL-1[alpha] responds to necrotic cell death. *Nat Med* 13(7), 778-780.
- Elmore, S. (2007). Apoptosis: a review of programmed cell death. *Toxicol Pathol* 35(4), 495-516. doi: 10.1080/01926230701320337.
- Gonzalez-Juarbe, N., Bradley, K.M., Riegler, A.N., Reyes, L.F., Brissac, T., Park, S.S., et al. (2018). Bacterial Pore-Forming Toxins Promote the Activation of Caspases in Parallel to Necroptosis to Enhance Alarmin Release and Inflammation During Pneumonia. *Sci Rep* 8(1), 5846. doi: 10.1038/s41598-018-24210-8.

- Gonzalez-Juarbe, N., Bradley, K.M., Shenoy, A.T., Gilley, R.P., Reyes, L.F., Hinojosa, C.A., et al. (2017). Pore-forming toxin-mediated ion dysregulation leads to death receptor-independent necroptosis of lung epithelial cells during bacterial pneumonia. *Cell Death Differ.* doi: 10.1038/cdd.2017.49.
- Gonzalez-Juarbe, N., Gilley, R.P., Hinojosa, C.A., Bradley, K.M., Kamei, A., Gao, G., et al. (2015). Pore-Forming Toxins Induce Macrophage Necroptosis during Acute Bacterial Pneumonia. *PLoS Pathog* 11(12), e1005337. doi: 10.1371/journal.ppat.1005337.
- Haber, P., Arana, J., Pilishvili, T., Lewis, P., Moro, P.L., and Cano, M. (2016). Post-licensure surveillance of 13-valent pneumococcal conjugate vaccine (PCV13) in adults aged 19 years old in the United States, Vaccine Adverse Event Reporting System (VAERS), June 1, 2012-December 31, 2015. *Vaccine* 34(50), 6330-6334. doi: 10.1016/j.vaccine.2016.10.052.
- Hotomi, M., Yuasa, J., Briles, D.E., and Yamanaka, N. (2016). Pneumolysin plays a key role at the initial step of establishing pneumococcal nasal colonization. *Folia Microbiol (Praha)* 61(5), 375-383. doi: 10.1007/s12223-016-0445-z.
- Joyce, E.A., Popper, S.J., and Falkow, S. (2009). *Streptococcus pneumoniae* nasopharyngeal colonization induces type I interferons and interferon-induced gene expression. *BMC Genomics* 10, 404. doi: 10.1186/1471-2164-10-404.
- Kaczmarek, A., Vandenabeele, P., and Krysko, D.V. (2013). Necroptosis: the release of damage-associated molecular patterns and its physiological relevance. *Immunity* 38(2), 209-223. doi: 10.1016/j.immuni.2013.02.003.

- Kafka, D., Ling, E., Feldman, G., Benharroch, D., Voronov, E., Givon-Lavi, N., et al. (2008). Contribution of IL-1 to resistance to *Streptococcus pneumoniae* infection. *Int Immunol* 20(9), 1139-1146. doi: 10.1093/intimm/dxn071.
- Kang, T.B., Yang, S.H., Toth, B., Kovalenko, A., and Wallach, D. (2013). Caspase-8 blocks kinase RIPK3-mediated activation of the NLRP3 inflammasome. *Immunity* 38(1), 27-40. doi: 10.1016/j.immuni.2012.09.015.
- Keller, L.E., Robinson, D.A., and McDaniel, L.S. (2016). Nonencapsulated *Streptococcus pneumoniae*: Emergence and Pathogenesis. *MBio* 7(2), e01792. doi: 10.1128/mBio.01792-15.
- Kim, H., Zamel, R., Bai, X.H., Lu, C., Keshavjee, S., Keshavjee, S., et al. (2018). Ischemia Reperfusion Induces Death Receptor-Independent Necroptosis via Calpain-STAT3 Activation in a Lung Transplant Setting. *Am J Physiol Lung Cell Mol Physiol*. doi: 10.1152/ajplung.00069.2018.
- Kitur, K., Parker, D., Nieto, P., Ahn, D.S., Cohen, T.S., Chung, S., et al. (2015). Toxin-induced necroptosis is a major mechanism of *Staphylococcus aureus* lung damage. *PLoS Pathog* 11(4), e1004820. doi: 10.1371/journal.ppat.1004820.
- Kitur, K., Wachtel, S., Brown, A., Wickersham, M., Paulino, F., Penaloza, H.F., et al. (2016). Necroptosis Promotes *Staphylococcus aureus* Clearance by Inhibiting Excessive Inflammatory Signaling. *Cell Rep* 16(8), 2219-2230. doi: 10.1016/j.celrep.2016.07.039.
- Kung, E., Coward, W.R., Neill, D.R., Malak, H.A., Muhlemann, K., Kadioglu, A., et al. (2014). The pneumococcal polysaccharide capsule and pneumolysin differentially

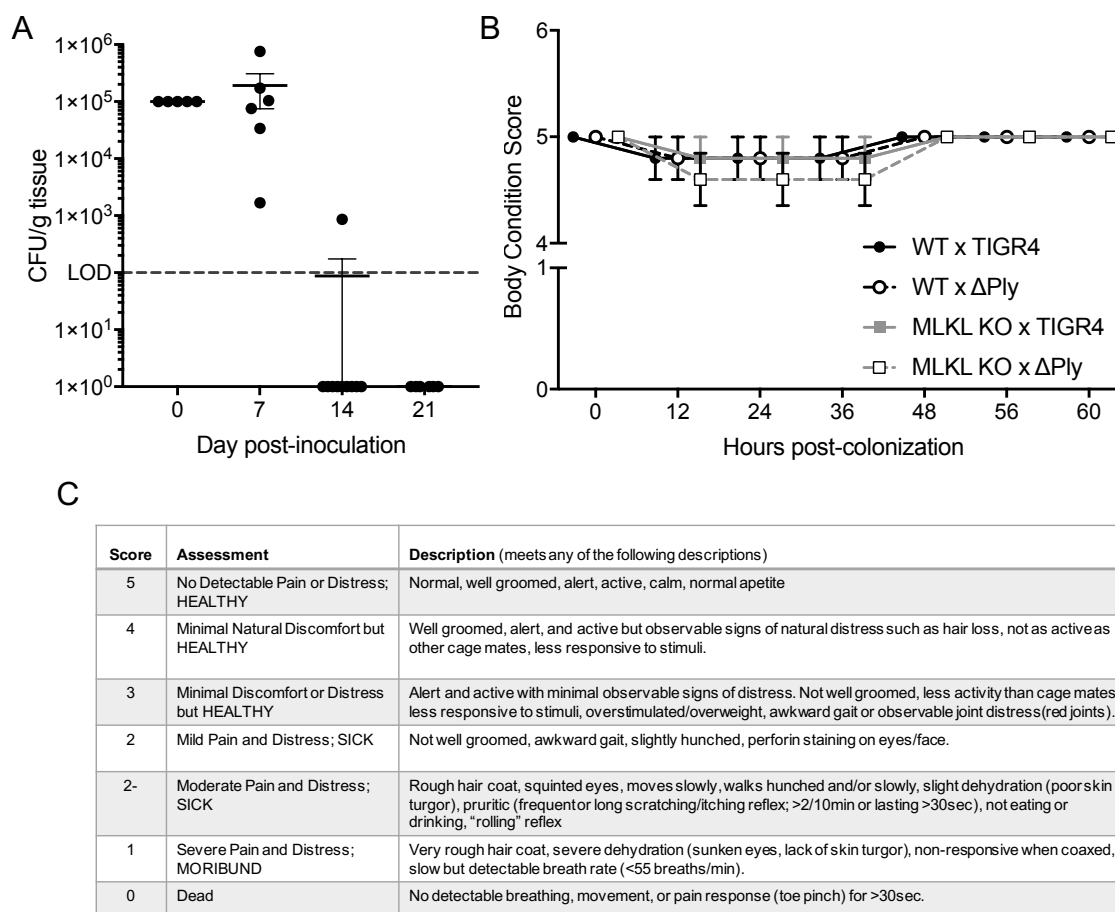
- affect CXCL8 and IL-6 release from cells of the upper and lower respiratory tract. *PLoS One* 9(3), e92355. doi: 10.1371/journal.pone.0092355.
- Land, W.G. (2015). The Role of Damage-Associated Molecular Patterns (DAMPs) in Human Diseases: Part II: DAMPs as diagnostics, prognostics and therapeutics in clinical medicine. *Sultan Qaboos Univ Med J* 15(2), e157-170.
- Lemon, J.K., Miller, M.R., and Weiser, J.N. (2015). Sensing of interleukin-1 cytokines during *Streptococcus pneumoniae* colonization contributes to macrophage recruitment and bacterial clearance. *Infect Immun* 83(8), 3204-3212. doi: 10.1128/IAI.00224-15.
- Linkermann, A., Hackl, M.J., Kunzendorf, U., Walczak, H., Krautwald, S., and Jevnikar, A.M. (2013). Necroptosis in immunity and ischemia-reperfusion injury. *Am J Transplant* 13(11), 2797-2804. doi: 10.1111/ajt.12448.
- Lizcano, A., Chin, T., Sauer, K., Tuomanen, E.I., and Orihuela, C.J. (2010). Early biofilm formation on microtiter plates is not correlated with the invasive disease potential of *Streptococcus pneumoniae*. *Microb Pathog* 48(3-4), 124-130. doi: 10.1016/j.micpath.2010.01.002.
- Marks, L.R., Parameswaran, G.I., and Hakansson, A.P. (2012). Pneumococcal interactions with epithelial cells are crucial for optimal biofilm formation and colonization in vitro and in vivo. *Infect Immun* 80(8), 2744-2760. doi: 10.1128/IAI.00488-12.
- Matthias, K.A., Roche, A.M., Standish, A.J., Shchepetov, M., and Weiser, J.N. (2008). Neutrophil-toxin interactions promote antigen delivery and mucosal clearance of *Streptococcus pneumoniae*. *J Immunol* 180(9), 6246-6254.

- McCool, T.L., Cate, T.R., Moy, G., and Weiser, J.N. (2002). The immune response to pneumococcal proteins during experimental human carriage. *J Exp Med* 195(3), 359-365.
- McDaniel, L.S., Sheffield, J.S., Delucchi, P., and Briles, D.E. (1991). PspA, a surface protein of *Streptococcus pneumoniae*, is capable of eliciting protection against pneumococci of more than one capsular type. *Infect Immun* 59(1), 222-228.
- Murphy, J.M., Czabotar, P.E., Hildebrand, J.M., Lucet, I.S., Zhang, J.G., Alvarez-Diaz, S., et al. (2013). The pseudokinase MLKL mediates necroptosis via a molecular switch mechanism. *Immunity* 39(3), 443-453. doi: 10.1016/j.immuni.2013.06.018.
- Niggli, V. (2003). Signaling to migration in neutrophils: importance of localized pathways. *Int J Biochem Cell Biol* 35(12), 1619-1638.
- Nogusa, S., Thapa, R.J., Dillon, C.P., Liedmann, S., Oguin, T.H., 3rd, Ingram, J.P., et al. (2016). RIPK3 Activates Parallel Pathways of MLKL-Driven Necroptosis and FADD-Mediated Apoptosis to Protect against Influenza A Virus. *Cell Host Microbe* 20(1), 13-24. doi: 10.1016/j.chom.2016.05.011.
- Opferman, J.T., and Korsmeyer, S.J. (2003). Apoptosis in the development and maintenance of the immune system. *Nat Immunol* 4(5), 410-415. doi: 10.1038/ni0503-410.
- Orzalli, M.H., and Kagan, J.C. (2017). Apoptosis and Necroptosis as Host Defense Strategies to Prevent Viral Infection. *Trends Cell Biol* 27(11), 800-809. doi: 10.1016/j.tcb.2017.05.007.

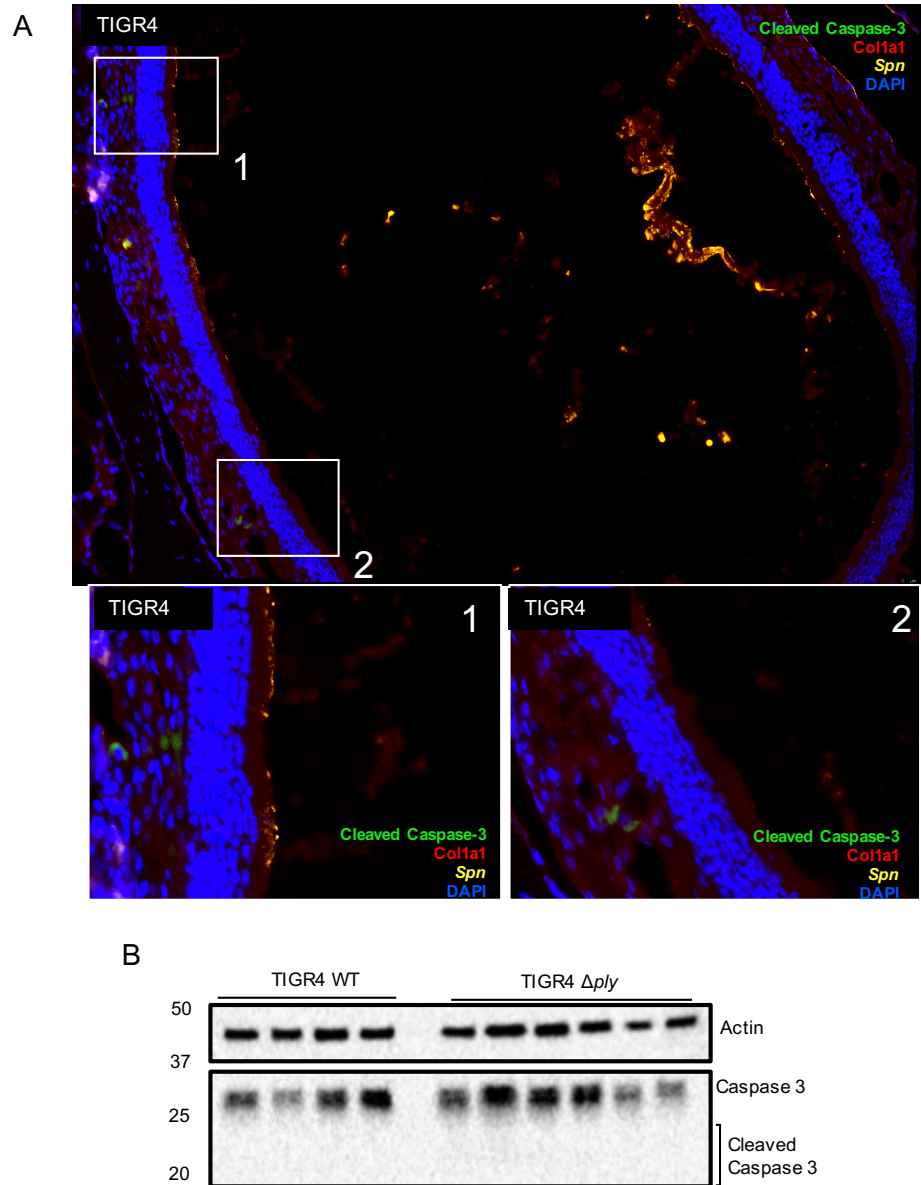
- Pan, T., Wu, S., He, X., Luo, H., Zhang, Y., Fan, M., et al. (2014). Necroptosis takes place in human immunodeficiency virus type-1 (HIV-1)-infected CD4+ T lymphocytes. *PLoS One* 9(4), e93944. doi: 10.1371/journal.pone.0093944.
- Pasparakis, M., and Vandenabeele, P. (2015). Necroptosis and its role in inflammation. *Nature* 517(7534), 311-320. doi: 10.1038/nature14191.
- Ren, B., Szalai, A.J., Thomas, O., Hollingshead, S.K., and Briles, D.E. (2003). Both family 1 and family 2 PspA proteins can inhibit complement deposition and confer virulence to a capsular serotype 3 strain of *Streptococcus pneumoniae*. *Infect Immun* 71(1), 75-85.
- Sanders, M.E., Norcross, E.W., Moore, Q.C., Onwubiko, C., King, L.B., Fratkin, J., et al. (2008). A comparison of pneumolysin activity and concentration in vitro and in vivo in a rabbit endophthalmitis model. *Clin Ophthalmol* 2(4), 793-800.
- Sattar, S.B.A., and Haseer Koya, H. (2018). "Pneumonia, Bacterial," in *StatPearls*. (Treasure Island (FL)).
- Shenoy, A.T., Brissac, T., Gilley, R.P., Kumar, N., Wang, Y., Gonzalez-Juarbe, N., et al. (2017). *Streptococcus pneumoniae* in the heart subvert the host response through biofilm-mediated resident macrophage killing. *PLoS Pathog* 13(8), e1006582. doi: 10.1371/journal.ppat.1006582.
- van Rossum, A.M., Lysenko, E.S., and Weiser, J.N. (2005). Host and bacterial factors contributing to the clearance of colonization by *Streptococcus pneumoniae* in a murine model. *Infect Immun* 73(11), 7718-7726. doi: 10.1128/IAI.73.11.7718-7726.2005.

- Vandenabeele, P., Galluzzi, L., Vanden Berghe, T., and Kroemer, G. (2010). Molecular mechanisms of necroptosis: an ordered cellular explosion. *Nat Rev Mol Cell Biol* 11(10), 700-714. doi: 10.1038/nrm2970.
- Walsh, C.M. (2014). Grand challenges in cell death and survival: apoptosis vs. necroptosis. *Front Cell Dev Biol* 2, 3. doi: 10.3389/fcell.2014.00003.
- WHO (2011). *Immunization, Vaccines and Biologicals: Pneumococcal Disease* [Online]. [Accessed 2011].
- WHO (2016). "Pneumonia Fact Sheet", in: *Fact Sheets*. (ed.) W.H. Organization.).
- Wilson, R., Cohen, J.M., Reglinski, M., Jose, R.J., Chan, W.Y., Marshall, H., et al. (2017). Correction: Naturally Acquired Human Immunity to Pneumococcus Is Dependent on Antibody to Protein Antigens. *PLoS Pathog* 13(3), e1006259. doi: 10.1371/journal.ppat.1006259.
- Zafar, M.A., Wang, Y., Hamaguchi, S., and Weiser, J.N. (2017). Host-to-Host Transmission of *Streptococcus pneumoniae* Is Driven by Its Inflammatory Toxin, Pneumolysin. *Cell Host Microbe* 21(1), 73-83. doi: 10.1016/j.chom.2016.12.005.
- Zhang, Z., Clarke, T.B., and Weiser, J.N. (2009). Cellular effectors mediating Th17-dependent clearance of pneumococcal colonization in mice. *J Clin Invest* 119(7), 1899-1909. doi: 10.1172/JCI36731.
- Zhou, W., and Yuan, J. (2014). Necroptosis in health and diseases. *Semin Cell Dev Biol* 35, 14-23. doi: 10.1016/j.semcdb.2014.07.013.

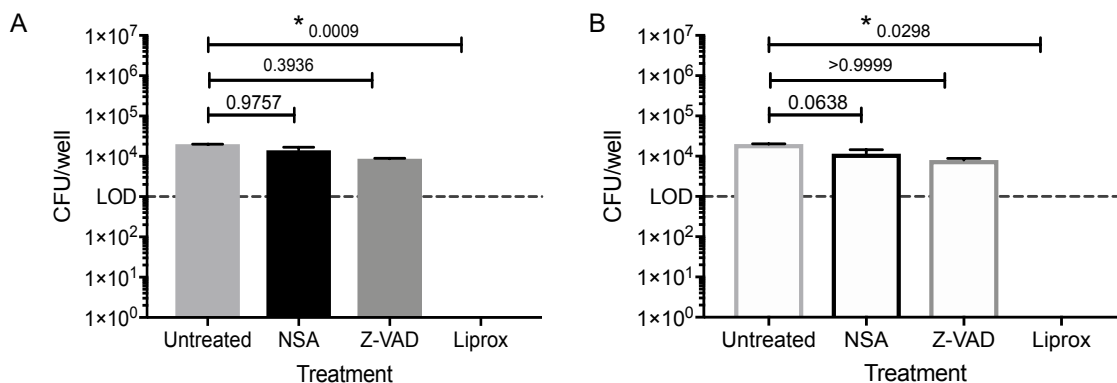
SUPPLEMENTAL FIGURES/TABLES



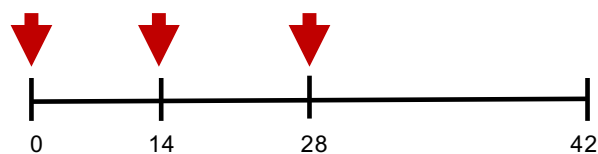
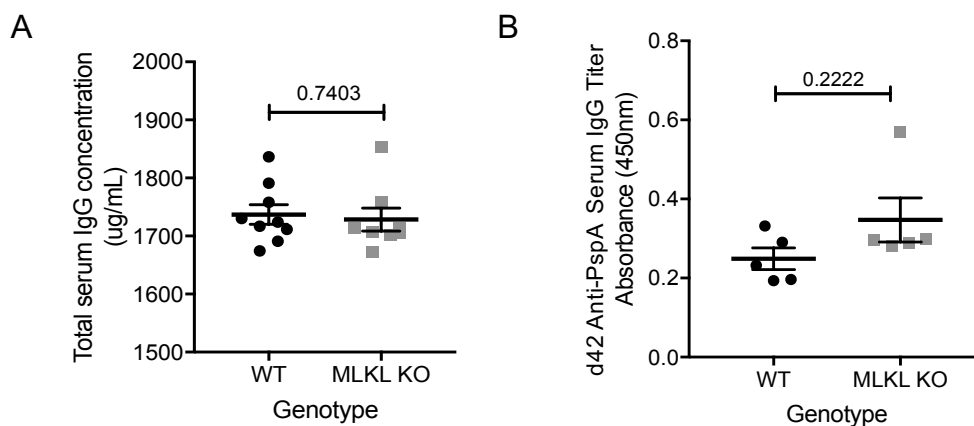
Supplemental Figure 1. Nasopharyngeal colonization model. (A) Nasopharyngeal burden from nasal homogenates at 7-days post-inoculation. (B) Body condition scores of colonized WT and MLKL KO mice for the initial 60 hours' post-inoculation. Note that all colonized mice remained at a healthy score of 4-5 for the duration of colonization. (C) Table defining body condition score assessment criteria.



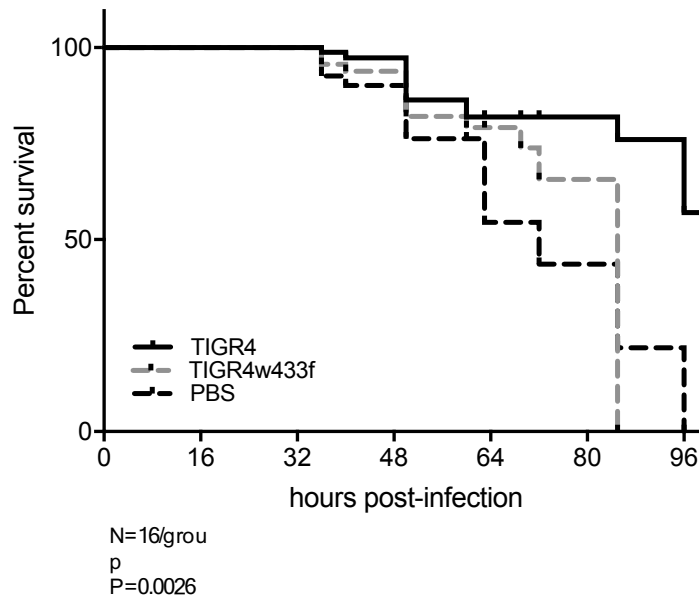
Supplemental Figure 2. Amount of apoptosis during *Spn* colonization is negligible. (A) Nasoturbinate from TIGR4 colonized WT mouse immunofluorescently stained for cleaved caspase-3 (green), collagen1a (red), *Spn* (yellow), and DAPI (blue). Panels 1 and 2 indicating the limited cell number staining positive for active caspase-3. Notably, most sections showed no active caspase-3. (B) Western blot for cytoskeletal actin and pro- and cleaved caspase-3 in nasal homogenates from TIGR4 and TIGR4 Δply colonized mice.



Supplemental Figure 3. Reduction in FaDu cytotoxicity is not due to *Spn* growth differences during treatment. Infectious burden (CFU/well) following 1 hour inhibitor pre-treatment and overnight (15h) challenge with (A) TIGR4 or (B) TIGR4 Δ *ply*. Dashed line indicates limit of detection. One-way analysis of variance used for comparisons and individual p-values shown on graph.



Supplemental Figure 4. Reduction in antibody in MLKL KO mice is not a genotype defect. Total serum IgG at day 21 post inoculation of WT and MLKL KO mice colonized with TIGR4 (n=8-9 mice per genotype). (B) Day 42 serum anti-PspA IgG of mice given 5 μ g rPspA intranasally at days 0, 14, and 28. Mann-Whitney U test for comparison (n= 5 mice per genotype).



Supplemental Figure 5. Protection against secondary lethal challenge is not due to anti-pneumolysin antibody. Survival of WT mice, initially colonized with wildtype TIGR4 (solid), TIGR4w433f (grey dashed), or mock colonized (black dashed), and re-challenged intra-tracheally at day 30 post colonization-inoculation with a lethal infectious dose of D39 (10^6). Mantel-Cox Comparison, N=16 mice/group, $p=0.0026$.

Supplemental Table 1. Reagents and Resources. Details for all key resources used for data collection.

| REAGENT or RESOURCE | SOURCE | Details |
|--|-----------------------------|-----------------|
| Antibodies | | |
| Mouse Anti-Collagen I Antibody | Abcam | Cat#ab90395 |
| Rabbit anti-mouse pMLKL Antibody | Abcam | Cat#ab196436 |
| Rabbit anti-Human, Mouse, Rat, Monkey Caspase-3 Antibody (western) | Cell Signaling Technologies | Cat#9662S |
| Rabbit anti-Mouse pMLKL Antibody (western) | Cell Signaling Technologies | Cat#37333S |
| Rabbit anti-Mouse MLKL Antibody (western) | Cell Signaling Technologies | Cat#37705 |
| Rabbit anti-Human MLKL Antibody (western) | Abcam | Cat#ab184718 |
| Rabbit anti-Human pMLKL Antibody (western) | Cell Signaling Technologies | Cat#91689S |
| Rabbit anti-Cytoskeletal Actin Antibody (western) | Bethyl | Cat#A300-485A |
| Affinipure Goat Anti-Rabbit IgG (Peroxidase) | Jackson Immuno | Cat#111-035-144 |
| Rabbit Anti-Human, Mouse Active Caspase-3 Antibody | R&D Systems | Cat#AF835SP |
| Rabbit anti-serotype 4 Antibody | Statens Serum Institut | Cat#16747 |
| Donkey anti-rabbit IgG (Dylight® 550) | Abcam | Cat#ab96920 |
| Goat anti-rabbit IgG (FITC) | Jackson Immuno | Cat#111-095-003 |
| Donkey anti-rabbit IgG (Rhodamine) | Jackson Immuno | Cat#711-025-152 |
| Hamster anti-mouse CD11c (ALEXA Fluor® 647) | Biologend | Cat#117314 |

| | | |
|--|----------------------|-----------------|
| Rat anti-mouse F4/80 (ALEXA Fluor® 647) | Biologend | Cat#123121 |
| Rat anti-mouse Ly-6G (ALEXA Fluor® 594) | Biologend | Cat#127636 |
| Rabbit anti-human/mouse active caspase-3 | R&D Systems | Cat# AF835SP |
| Affinipure Goat Anti-mouse IgG | Jackson Immuno | Cat#115-000-003 |
| Affinipure Goat Anti-mouse IgM | Jackson Immuno | Cat#115-005-003 |
| Affinipure Goat Anti-mouse IgG (Peroxidase) | Jackson Immuno | Cat#115-035-003 |
| Affinipure Goat Anti-mouse IgM (Peroxidase) | Jackson Immuno | Cat#115-035-020 |
| Bacterial Strains | | |
| <i>Streptococcus pneumoniae</i> : type 4 serotype strain TIGR4 | ATCC | ATCC BAA-334 |
| <i>Streptococcus pneumoniae</i> : type 4 serotype strain TIGR4 Δ ply | Lizcano et al., 2010 | N/A |
| <i>Streptococcus pneumoniae</i> : type 4 serotype strain TIGR4ply _{w433F} | Zafar et al., 2016 | N/A |
| <i>Streptococcus pneumoniae</i> : type 2 serotype strain D39 | NCTC | NTCT 7466 |
| Chemicals, Peptides, and Recombinant Proteins | | |
| NucBlue Live ReadProbes™ Reagent | Invitrogen | Cat#R37605 |
| Recombinant pneumococcal surface protein A, rPspA | Ren et al., 2003 | N/A |
| Recombinant pneumolysin, rPly | Douce et al., 2010 | N/A |
| Necrosulfonamide | Tocris | Cat#5025 |
| Z-VAD-fmk | R&D Systems | Cat#FMK001 |
| Liproxstatin-1 | Sigma-Aldrich | CAS#950455-15-9 |
| HALT™ Protease and Phosphatase Inhibitor Cocktail | Thermo Scientific | Cat#78446 |

| | | |
|--|------------------------------------|---|
| PROTOCOL HEMA 3 Manual Staining System and Stat Pack | Fisher HealthCare | Cat#22-122911 |
| Critical Commercial Assays | | |
| Pierce LDH Cytotoxicity Assay Kit | Thermo Scientific | Cat#88954 |
| Mouse IL-1 Alpha/IL- 1F1 DuoSet ELISA Kit | R&D Systems | Cat#DY400 |
| Mouse/Rat IL-33 Quantikine ELISA Kit | R&D Systems | Cat#M3300 |
| Mouse CXCL2/MIP-2 DuoSet ELISA Kit | R&D Systems | Cat#DY452-05 |
| Mouse IL-6 DuoSet ELISA Kit | R&D Systems | Cat#DY406-05 |
| Mouse IL-17 DuoSet ELISA Kit | R&D Systems | Cat#DY413-05 |
| Bicinchoninic Acid (BCA) Kit for Protein Determination | Sigma-Aldrich | Cat#BCA1 |
| Clarity™ Western ECL Substrate | BIO-RAD | Cat#1705061 |
| APEX™ Alexa Fluor® 488 Antibody Labeling Kit | Molecular Probes | Cat#A10468 |
| RDO Decalcification Solution | Electron Microscopy Sciences | Cat#6414301 |
| Mouse and Cell Lines | | |
| Human: FaDu cells | ATCC | HTB-43 |
| Experimental Models: Organisms/Strains | | |
| Mouse: C57BL/6 | Jackson Laboratory | JAX#0006644 |
| Mouse: Mikl ^{tm1.2Wsa} /Mikl ^{tm1.2Wsa} | Murphy et al., 2013 | RRID#5614466 |
| Recombinant DNA and Proteins | | |
| pUAB099; rPspA expression | Ren et al., 2003 | N/A |
| pET33(+) rPly; rPly expression | Douce et al., 2010 | N/A |
| Software and Algorithms | | |
| GraphPad Prism 8 | GraphPad | https://www.graphpad.com/scientific-software/prism/ |
| Leica Application Suite X; imaging | Leica Microsystems | https://www.leica-microsystems.com/products/microscope-software/details/product/leica-las-x-ls/ |

NECROPTOSIS INHIBITION PREVENTS LONG-TERM CARDIAC DAMAGE
DURING INVASIVE PNEUMOCOCCAL PNEUMONIA AND INVASIVE DISEASE

by

ASHLEIGH N. RIEGLER*, SARAH M. BENO*, RYAN P. GILLEY, TERRY
BRISSAC, YONG WANG, KATHERINE L. KRUCKOW, JEEVAN K. JADAPALLI,
GRIFFIN M. WRIGHT, ANUKUL T. SHENOY, SARA N. STONER, MARCOS I.
RESTREPO, JESSY S. DESHANE, GANESH V. HALADE, NORBERTO
GONZALEZ-JUARBE#, AND CARLOS J. ORIHUELA#

Journal of Infectious Disease

Copyright

2020

by

Ashleigh Riegler and Sarah Beno *et al.*

Used by permission

*co-first authors; #co-senior authors

Format adapted and errata corrected for dissertation

PREFACE

Necroptosis as elicited by *Spn* and its pore-forming toxin, pneumolysin have been shown previously to contribute to the severity of pneumococcal pneumonia and invasive pneumococcal disease. Additionally, it has been shown that individuals who become bacteremic when hospitalized with pneumococcal pneumonia, developing invasive pneumococcal disease (IPD), are at a drastically increased risk for adverse cardiac events up to ten years post-infection. Here we used mouse and tissue culture models to identify whether pneumococcal cardiac invasion during IPD causes long-term cardiac damage *in vivo*, whether this damage was due to *Spn* induced necroptosis, and whether inhibiting this necroptosis reduces severity of disease both in the acute setting (during infection) as well as the long-term damage. This work adds to our understanding of the role of necroptosis in the disease pathology of pneumococcal infections as well as identifies potential modes of intervention to prevent long-term damage from IPD.

ABSTRACT

Rationale: Severe *Streptococcus pneumoniae* (*Spn*) pneumonia can result in bacteremia with devastating consequences including heart damage. Necroptosis is a pro-inflammatory form of cell death instigated by pore-forming toxins, such as *Spn* pneumolysin. Necroptosis-inhibiting drugs may lessen organ damage in individuals with invasive pneumococcal disease (IPD).

Objectives: Determine the form of cell death experienced by cardiomyocytes exposed to *Spn*. Determine if *Spn* is responsible for long-term cardiac damage. Test the potential of Ponatinib, a necroptosis-inhibitor, as therapeutic treatment against organ damage during severe *Spn* infection.

Methods: *In vitro* experiments were carried out with human and mouse cardiomyocytes. Long-term cardiac damage from IPD was assessed in ampicillin-rescued mice previously infected with *Spn*. Heart function was assessed using high-resolution echocardiography. Ponatinib was administered intraperitoneally alongside ampicillin to test its efficacy as an adjunct therapeutic. Histological examination of heart sections included staining with hematoxylin and eosin, immunofluorescence, and Sirius Red Fast Green.

Measurements and Main Results: Cardiomyocyte death and heart damage was due to pneumolysin-mediated necroptosis. IPD leads to long-term cardiac damage as evidenced by echocardiography and histological detection of collagen deposition in mouse hearts 3-months post-infection. Adjunct Ponatinib treatment reduced markers of acute injury including number of *Spn* foci in hearts and serum levels of Troponin. Ponatinib treatment also reduced collagen deposition and protected heart function in convalescence.

Conclusions: Acute and long-term cardiac damage incurred during IPD is due to cardiomyocyte necroptosis. Ponatinib, a necroptosis inhibitor and FDA-approved drug for treatment of lymphocytic leukemia, may be a viable option as an adjunct therapy.

Key Words: *Streptococcus pneumoniae*, heart, Ponatinib, echocardiograph, cell death

INTRODUCTION

Streptococcus pneumoniae (*Spn*, the pneumococcus) is a leading cause of community-acquired pneumonia, responsible for 25-40% of all cases [1]. *Spn* pneumonia has also been directly linked to major adverse cardiac events (MACE), with Musher et al. finding that 20% of individuals hospitalized for *Spn* pneumonia in a Veterans Administration hospital simultaneously experienced cardiac failure, arrhythmia, or infarct, alone or in combination [2]. More recently, Eurich et al. showed that patients who developed bacteremia during hospitalization for pneumococcal pneumonia were specifically at risk for MACE in convalescence (adjusted hazard ratio = 2.4, 1.08-5.3 compared to controls). Moreover, the risk of cardiac complications persisted for up to ten years following the pneumonia episode [3, 4].

In 2014, we showed that pneumococci in the bloodstream were capable of invading the heart. Within the myocardium, *Spn* can replicate to form a focus of infection, disrupt contractility, and kill cardiomyocytes; together contributing to the multifaceted cardiac dysfunction that is known to occur during severe and systemic infections [5-8]. Foci of pneumococci within the myocardium have been termed “cardiac microlesions”, which can vary in their morphology. In some instances, cardiac

microlesions present as densely packed pneumococci surrounded by the remnants of dead host cells, in other instances they contain fewer bacteria in a dispersed state, are associated with dead or dying host cells, and surrounded or infiltrated by immune cells. We have determined that the morphological properties of these microlesions are dependent on the pneumococcal strain responsible for the infection, their maturity at time of sample collection, and the infecting strain's ability to produce the pore-forming toxin (PFT) pneumolysin [6]. Critically, in mice and non-human primates who had been rescued from invasive pneumococcal disease (IPD) with antibiotics, immune cell infiltration and highly disorganized collagen deposition was seen to occur at sites in the heart where microlesions had been present [5, 9]. This cardiac remodeling was reminiscent to that which occurs in humans after infarct [5, 9], and was speculated to be an explanation for the increased incidence of MACE that is observed in convalescent individuals; however, this remained unproven.

Necroptosis is a programmed mode of cell death that leads to the disruption of cellular membranes and increased inflammation through the release of alarmins [10]. This pro-inflammatory cell death program is executed upon activation of the signaling molecules RIPK1 and RIPK3 followed by the effector protein MLKL (mixed lineage kinase domain like pseudokinase). It is now known that PFTs, such as pneumolysin, induce activation of necroptosis as a result of the sustained ion dysregulation and/or catastrophic energy loss that occurs upon pore formation [11]. During *Spn*, *Staphylococcus aureus*, and *Serratia marcescens* pneumonia, PFT-initiated necroptosis was shown to be involved in the killing of lung macrophages, lung epithelial cells, and to directly contribute to pulmonary injury [12, 13]. Further supporting a detrimental role for

PFT-mediated necroptosis, *Spn*-infected mice deficient in MLKL had less severe pathological hallmarks of pneumonia and experienced prolonged survival compared to wild type controls [11]. Thus, pharmacological inhibition of necroptosis may be a therapeutic strategy to protect against the extensive organ injury that occurs during severe *Spn* pneumonia. Importantly, and while pneumolysin-formed pores have been shown to induce calcium dysregulation that impairs cardiomyocyte contractility [10], whether cardiomyocytes died as result of pneumolysin-induced necroptosis during severe pneumococcal infections was not known.

The objectives of this study were to (i) identify the form of cell death experienced by cardiomyocytes exposed to *Spn*, (ii) determine if *Spn* is responsible for long-term cardiac damage, and (iii) test the potential of Ponatinib, a Food and Drug Administration (FDA) approved necroptosis-inhibitor [14], as a therapeutic adjunct treatment for organ damage during IPD. Our results provide compelling evidence that the severity and long-term negative consequences of pneumococcal disease may be ameliorated through inhibition of necroptosis.

RESULTS

Pneumolysin is required for *Spn* cardiac damage. Following *in vitro* challenge, mouse HL-1 cardiomyocytes and human cardiomyocytes immortalized with SV40 T-antigen (HC_{SV40}) were susceptible to killing by two unrelated strains of *Spn*: serotype 4 strain TIGR4 and serotype 2 strain D39 (**Figure 1A**). A requirement for pneumolysin in killing was evidenced by the decreased cytotoxicity observed in HC_{SV40} exposed to an isogenic mutant of TIGR4 lacking pneumolysin (TIGR4 Δply), as well as in HC_{SV40} that were in

media containing neutralizing antibody against the toxin (**Figure 1B**). The contribution of pneumolysin to the pathogenesis of *Spn*-mediated cardiac damage *in vivo* was also re-tested and found to be stark. Mice challenged with TIGR4 Δply had fewer and smaller foci of *Spn* in the myocardium, i.e. cardiac microlesions, than mice challenged with TIGR4 (**Figure 1C-E**). Moreover, and in contrast to TIGR4, cardiac microlesions formed by TIGR4 Δply were characterized by the presence of infiltrated immune cells (**Figure 1E**) as has previously been described [8]. Notably, TIGR4 infection was associated with detection of the pro-inflammatory mediators KC, Interleukin (IL)-1 α , and IL-6, along with a reduction in Interferon (IFN)- γ in heart homogenates (**Supplemental Figure 1**). IL-1 α is released during necrotic forms of cell death [15]. IFN- γ is produced by macrophages [16]; which have previously been shown to be depleted by heart-invaded *Spn* [17]. Together, these results reconfirmed that *Spn* invades the heart, causes cardiac damage, and that pneumolysin is a key factor in the induction of cardiomyocyte death.

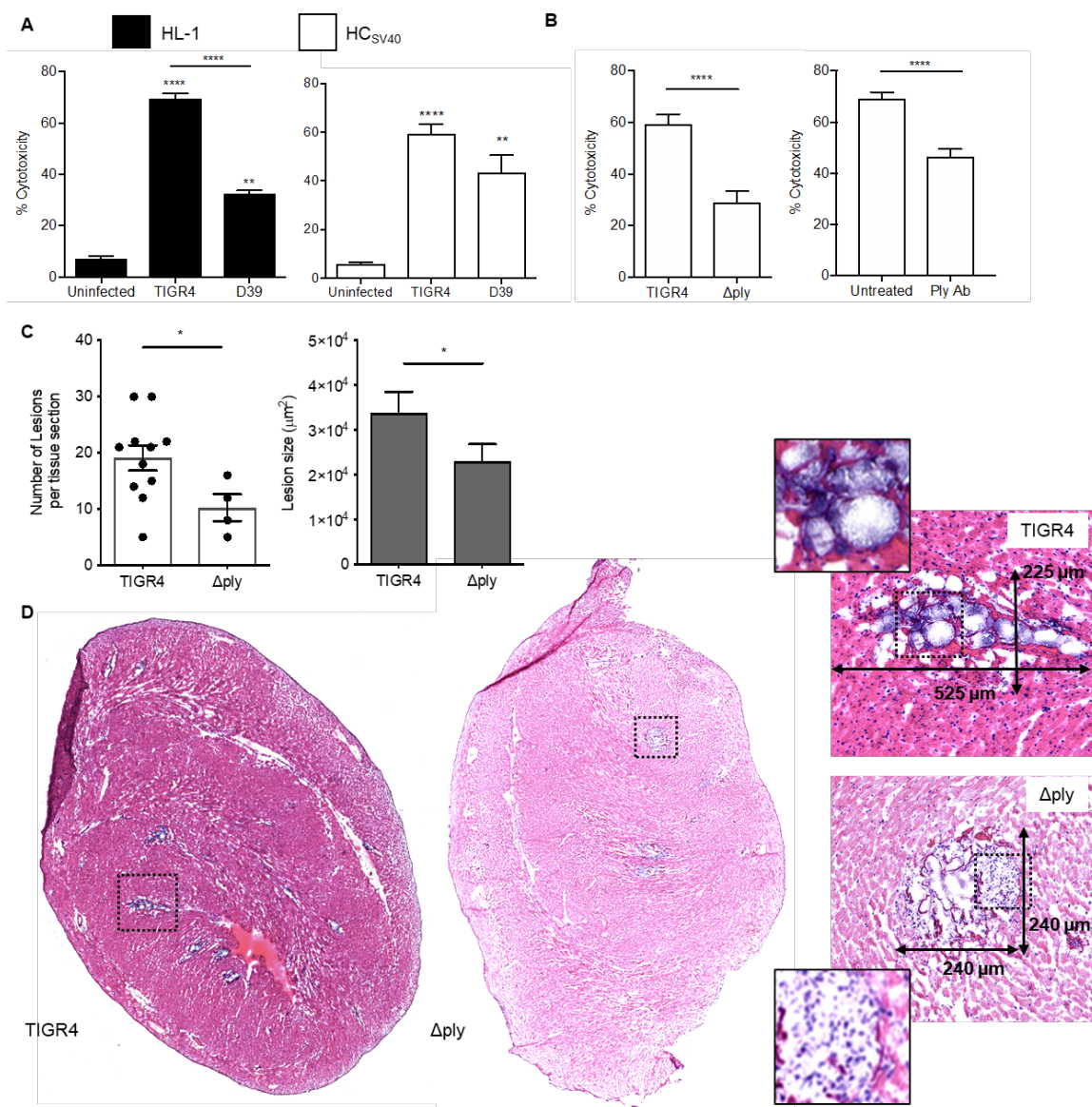


Figure 1: Pneumolysin is required for *Spn* cardiac damage. **A)** Cytotoxicity as assessed by the amount of lactate dehydrogenase released into the supernatant by HL-1 mouse cardiomyocytes (black bars) and HCSV40 human cardiomyocytes (white bars) infected with *Spn* strains TIGR4, D39, or mock infected (uninfected) after 4 hours at MOI of 100. **B)** Cytotoxicity of HCSV40 cardiomyocytes infected with TIGR4 or TIGR4 Δ ply and in presence of neutralizing monoclonal antibody against pneumolysin (Ply Ab) after 4 hours at MOI of 100. **C)** number of cardiac microlesions and their **D)** size in heart sections from mice infected with TIGR4 or Δ ply, quantified from H&E stained cardiac sections. **E)** Representative H&E images and number of lesions in heart sections from mice infected intraperitoneally with TIGR4 or Δ ply. Hearts from infected mice were collected 30 hours after i.p. challenge. Sections tile scan imaged at 40X magnification. * = $P \leq 0.05$, ** = $P \leq 0.01$, **** = $P \leq 0.0001$. (See also Supplemental Figure 1).

Pneumolysin kills cardiomyocytes via necroptosis. PFTs such as pneumolysin trigger necroptosis in pulmonary epithelial cells and macrophages [11-13]. To determine if cardiomyocytes exposed to *Spn* also underwent necroptosis, we tested whether *Spn*-mediated death of HC_{SV40} *in vitro* could be blocked with necroptosis inhibitors. A schematic of the necroptosis pathway and the inhibitors used to block distinct steps in its activation is provided in **Figure 2A**. Pretreatment of cells with Necrostatin-5 (Nec-5), an inhibitor of RIPK1 [24], GSK'872 (GSK), an inhibitor of RIPK3 [18], or necrosulfonamide (NSA), an inhibitor of MLKL [19], all reduced cardiomyocyte cytotoxicity after challenge with *Spn* (**Figure 2B**). Likewise, knockdown of RIPK3 or MLKL using siRNA also reduced *Spn*-mediated cytotoxicity versus control (**Figure 2C**). Within heart tissue of TIGR4-infected mice, phosphorylated MLKL (p-MLKL), the active form of the necroptosis effector, was detected by immunofluorescent microscopy (**Figure 2D, Supplemental Figure 2A**). Following TIGR4 challenge and compared to wildtype mice, RIPK3 KO and MLKL KO mice had lower levels of serum Troponin-I (**Figure 2E**), a marker of cardiac damage that is released by dying cardiomyocytes [20]. Moreover, we detected considerably fewer microlesions in MLKL KO and RIP3 KO mice versus wild type controls (**Figure 2F**). It is noteworthy that KO mice had equivalent bacterial burden in the blood and heart versus wildtype mice (**Supplemental Figure 2B**). Thus, reduced bacterial entry into the heart is not an explanation for differences in cardiac microlesion frequency. Finally, infection of HC_{SV40} with TIGR4 Δply resulted in reduced levels of detectable p-MLKL versus TIGR4 infected cells (**Figure 3**); as previously reported for challenged macrophages [12]. All together, these findings

demonstrate that *Spn*-derived pneumolysin triggers necroptosis of human and murine cardiomyocytes during acute infection.

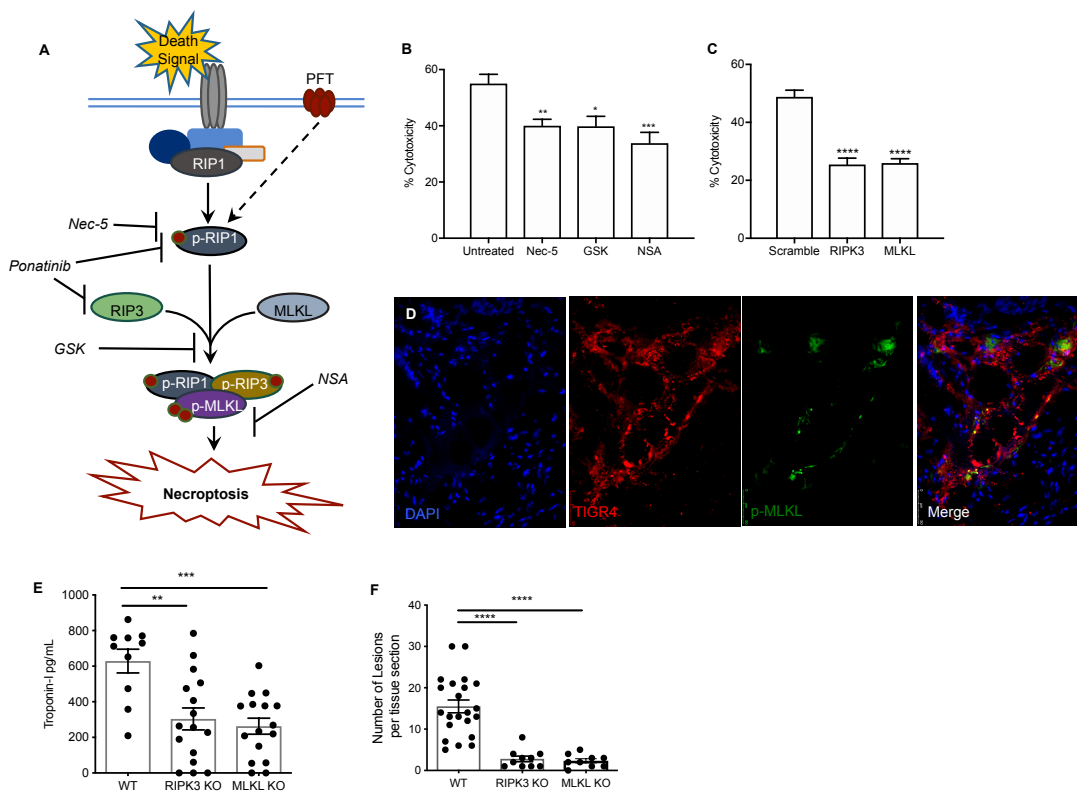


Figure 2: Pneumolysin kills cardiomyocytes via necroptosis. **A)** Illustrative model of the necroptosis pathway and the pharmacological inhibitors used to block activation of the necroptotic machinery. Cytotoxicity as quantified by lactate dehydrogenase release from HC_{SV40} cardiomyocytes infected with TIGR4 following **B)** pretreatment with Necrostatin-5 (Nec-5; 10 μ M), GSK'872 (GSK, 10 μ M), and Necrosulfonamide (NSA, 10 μ M) or **C)** siRNA knockdown of RIPK3 and MLKL. Cells were infected for 4 hours at a MOI of 100. **D)** Representative immunofluorescent stained cardiac microlesion in a cardiac section from a BALBc/J mouse intraperitoneally infected with TIGR4. Nuclei (DAPI; blue), p-MLKL (green), TIGR4 (red), with merged image shown. **E)** Cardiac Troponin-I detected in the serum of wild type C57Bl/6 mice (n=10; Wild Type), mice deficient in RIPK3 (n=16, RIPK3 KO) and MLKL (n=16, MLKL KO) of the same background following infection with TIGR4. **F)** Number of lesions per tissue section from the same mice used in panel E. Lesions were counted using immunofluorescent-stained sections. Hearts from infected mice were collected 30h after i.p. challenge. For multiple group comparisons Dunn's or Tukey's (C) multiple comparison were used: * = $P \leq 0.05$, ** = $P \leq 0.01$, *** = $P \leq 0.001$, **** = $P \leq 0.0001$. (See also Supplemental Figures 2 and 3).

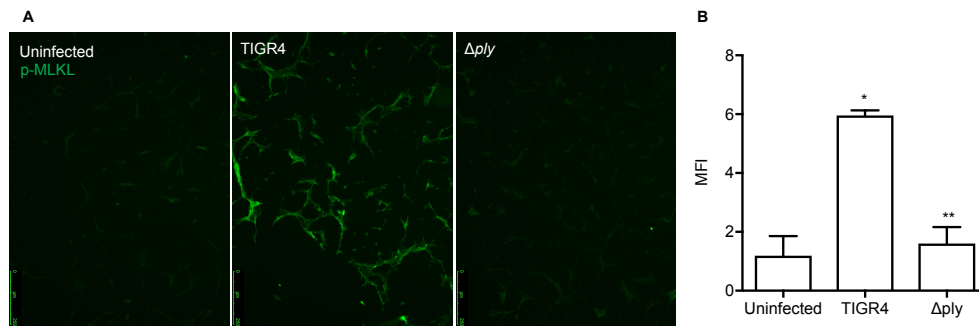


Figure 3: Pneumolysin inhibition reduces necroptosis activation *in vitro*. **A)** Representative immunofluorescent stained images of HC_{SV40} infected with TIGR4 or TIGR4 Δply probed for p-MLKL (green). **B)** Mean Fluorescence Intensity (MFI) of p-MLKL signal quantified with ImageJ. Cells were infected for 4 hours at a MOI of 100. Dunn's multiple-comparison post-test was used: * = $P \leq 0.05$, ** = $P \leq 0.01$.

IPD results in long-term cardiac damage. We have previously reported that extensive cardiac remodeling is observed within a *Spn*-injured heart 7-10 days following antimicrobial intervention for IPD [9]. Yet, it remained unknown if this collagen persisted or if the negative effects of *Spn* on heart function were long-lasting. Using an antimicrobial intervention model of IPD rescue (schema shown in **Figure 4A**), we examined heart sections in TIGR4 infected mice that had been rescued by i.p. ampicillin administration beginning 22 hours after *Spn* challenge and continuing for 3 days (mice were confirmed to have cleared *Spn* by blood culture). Specifically, hearts from mice 2 weeks, 1 month, and 3 months after infection were examined. Semi-quantitation of collagen deposition in cardiac sections using Sirius Red Fast Green stain (**Figure 4B-C**) showed that collagen levels were significantly higher in hearts from mice that had experienced severe disease ($>10^5$ CFU/mL of blood at onset of antibiotic treatment) at all time points, indicating that scar formation happened early and was persistent. Mice that experienced mild bacteremia ($<10^5$ CFU/mL blood at onset of antibiotic treatment) did not have higher levels of collagen in cardiac sections than uninfected mice. In mice with severe disease, collagen deposition was frequently perivascular but also randomly distributed across the myocardium (**Figure 4C**), as has previously been reported for the location of *Spn*-induced cardiac lesions in non-human primates [9]. In several instances, collagen deposition was seen on the heart periphery, suggesting that pericarditis may have also occurred (**Supplemental Figure 3**). Importantly, and regardless of the bacterial burden at time of antimicrobial intervention, echocardiography of mice revealed that post-infection deficiencies in ejection fraction and fractional shortening persisted as a sign of heart dysfunction in all previously infected mice at 3 months (**Figure 4D**).

Detailed echocardiography demonstrated that contraction in some of the infected mice was now characterized by irregular left ventricle longitudinal and circumferential myocardial strain (**Figure 4E**). Thus, IPD had physiological consequence even if long-term remodeling was not evident by stains for collagen.

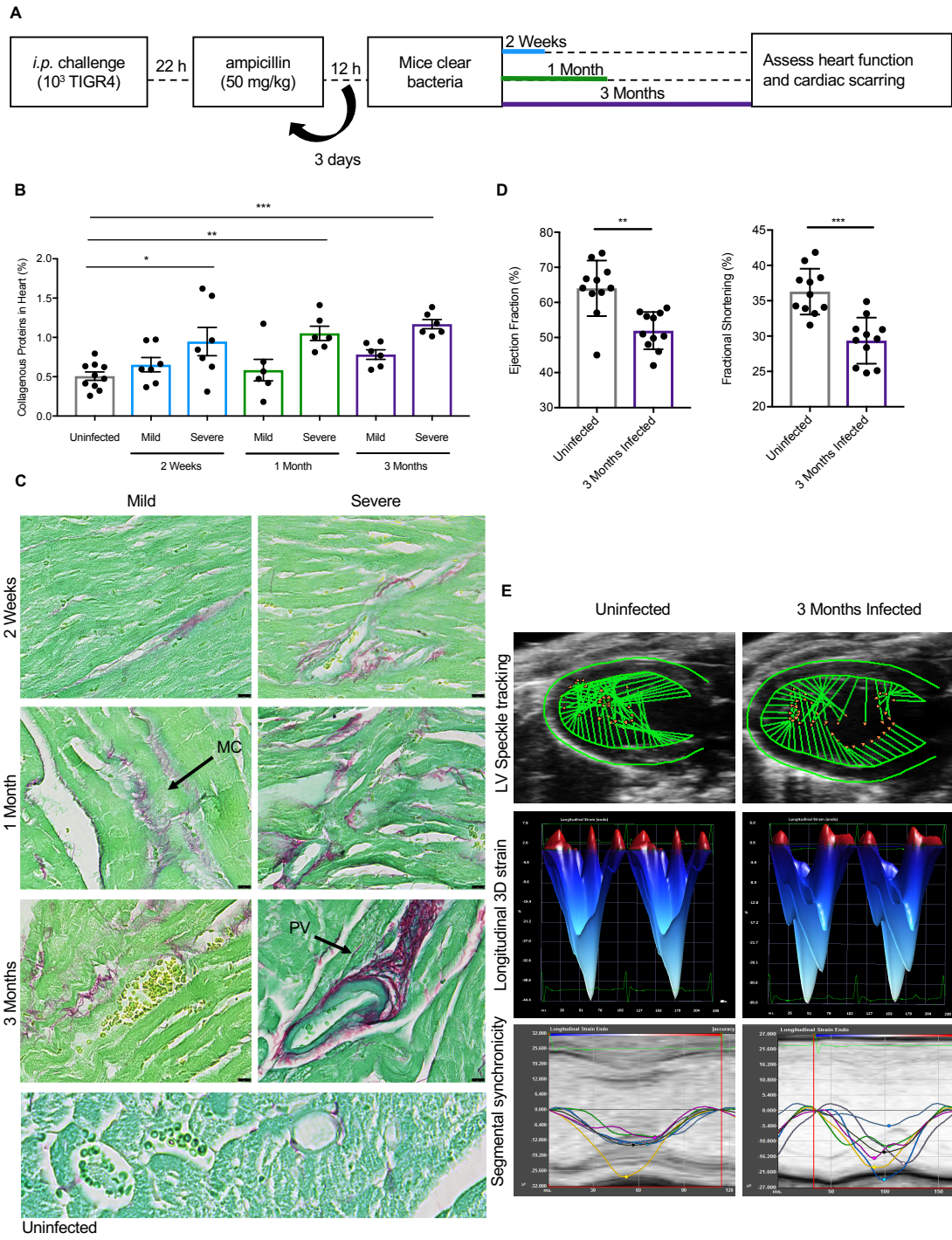


Figure 4: IPD results in long-term cardiac damage. **A)** Schematic of *Spn* challenge and antimicrobial intervention used in this study. **B)** The percentage of collagen in heart sections from uninfected mice, mice recovered from mild *Spn* infections ($<10^5$ CFU/ml blood), and mice that had experienced severe IPD ($>10^5$ CFU/mL blood) at two weeks, one month, and three months post-antimicrobial treatment. **C)** Hearts stained with Sirius Red Fast Green and having median levels of collagen per group and time point are shown as representatives. Areas stained red are collagenous proteins while green stains non-collagenous proteins. Black arrows indicate: MC= myocardial collagen deposition, PV= perivascular collagen deposition **D)** Ejection fraction and fractional shortening in uninfected mice and in mice that had experienced *Spn* infections, both mild and severe, 3 months post-antimicrobial treatment. **E)** Representative images from echocardiography demonstrating changes in left ventricular function between uninfected mice and mice that experienced *Spn* infection and were treated with ampicillin 3 months earlier. For multiple group comparisons, Sidak's post-test was used. Mann-Whitney U tests were applied for two-group comparisons. * = $P \leq 0.05$, ** = $P \leq 0.01$, *** = $P \leq 0.001$. (See also Supplemental Figure 3).

Therapeutic inhibition of necroptosis protects against organ damage during IPD.

We hypothesized that necroptosis inhibition would be beneficial to the host during IPD. Therapeutic treatment of infected mice with the Necrostatin-5 at 5 mg/kg resulted in significantly fewer cardiac microlesions than the mice that received the vehicle control (**Figure 5A**). Similar to our observation with MLKL and RIPK3 KO mice, Necrostatin-5 conferred protection despite the fact that bacteria numbers in the heart were not diminished (**Supplemental Figure 4A**). Notably, cardiac microlesions formed in Necrostatin-5 treated mice also had infiltrating immune cells (**Figure 5B**), similar to those caused by TIGR4 *Δply* (**Figure 1E**). As necrostatins are not approved for use in humans, we explored suitable alternatives. Ponatinib, a tyrosine kinase inhibitor that is FDA approved for the treatment of chronic myeloid leukemia (CML) and Philadelphia-positive acute lymphocytic leukemia, was recently discovered to also block RIPK1 and RIPK3 activation (**Figure 2A**) [21]. Therapeutic treatment of mice at 12 and 24 hours post *Spn* infection with Ponatinib at 1 mg/kg, without antimicrobials, resulted in reduced levels of Troponin-I in sera (**Figure 5C**) and formation of fewer cardiac microlesions (**Figure 5D**). As with Necrostatin-5, Ponatinib had no impact on bacterial titers recovered from the blood or heart of infected mice (**Supplemental Figure 4B**). Finally, Ponatinib was found not to have any direct antimicrobial activity *in vitro* (**Supplemental Figure 4C**).

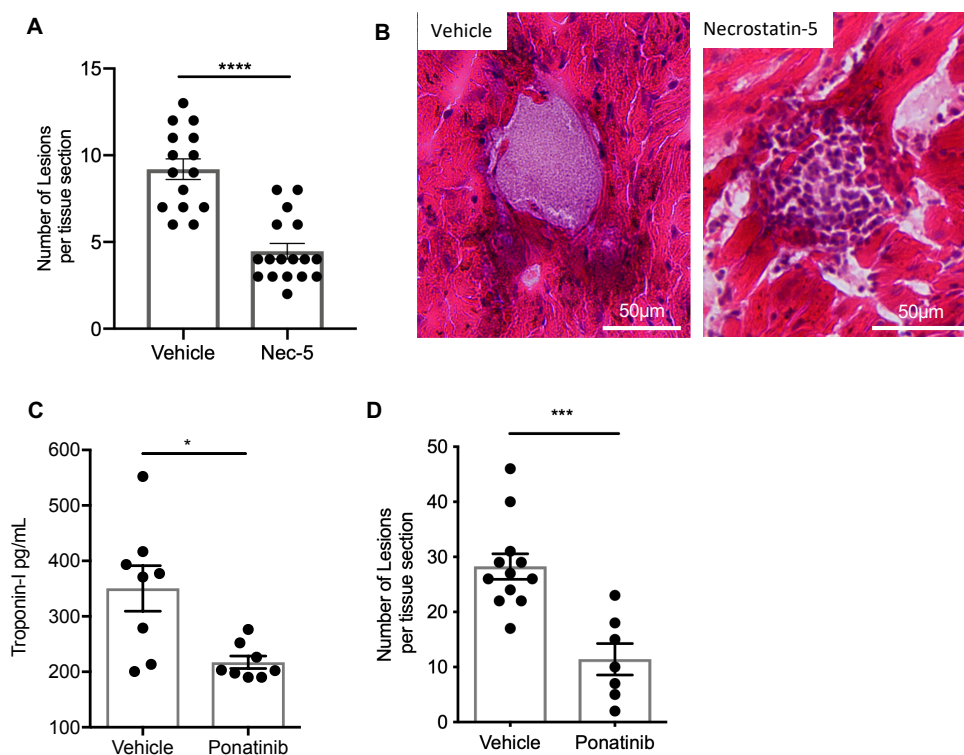


Figure 5: Therapeutic inhibition of necroptosis protect against organ damage during IPD. **A)** Number of lesions per cardiac tissue section from vehicle and Necrostatin-5 (Nec-5) treated mice. **B)** Representative images of microlesions observed in H&E stained cardiac sections from mice treated with a vehicle or Nec-5 starting 12 hours prior to infection and every 12 hours until euthanized at 36 hours post-infection. **C)** Serum cardiac Troponin-I from C57Bl/6 mice infected i.p. with TIGR4 and treated with 100 μ L i.p. injection of vehicle or Ponatinib (1 mg/kg) at 12- and 24-hours post-infection and euthanized at 30 hours post-infection. **D)** Number of cardiac microlesions per tissue section from immunofluorescent stained cardiac sections probed for TIGR4. Mann-Whitney U tests were applied for two-group comparisons: * = $P \leq 0.05$, *** = $P \leq 0.001$, **** = $P \leq 0.0001$, (See also Supplemental Figure 4).

Up to this point, challenge of mice was done by i.p. injection. This challenge route is preferred in the laboratory as infected mice are synchronized in regards to disease onset and severity and the resultant cardiac damage faithfully recapitulates that which is observed to occur in mice that develop IPD after intratracheal challenge [22]. However, this approach does not provide translatable information on events in the lungs. For this reason, we were compelled to determine if Ponatinib also protected against airway damage and the subsequent cardiac injury associated with severe pneumonia that results in bacteremia. Therapeutic treatment with Ponatinib after intratracheal challenge of mice with TIGR4 resulted in starkly decreased pulmonary consolidation, albeit considerable immune cell infiltration still occurred (**Figure 6A-C**). We also observed a significant reduction in frequency of cardiac microlesions (**Figure 6D, Supplemental Figure 5**). Despite some of the mice on Ponatinib clearing pneumococci from the airway, there were not significant differences in bacterial burden across the groups (**Supplemental Figure 6**).

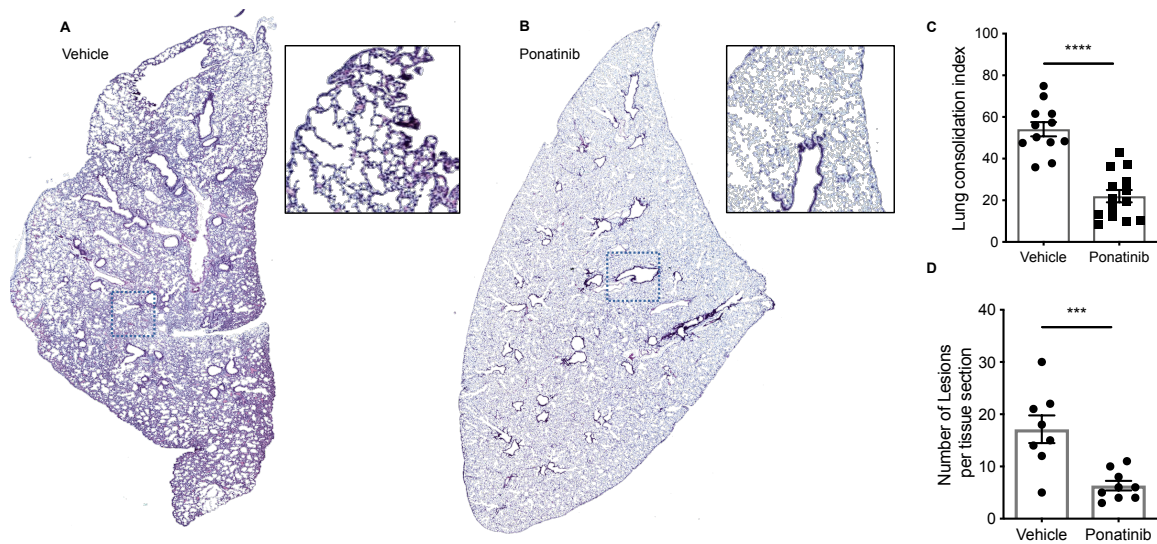


Figure 6: Therapeutic Ponatinib treatment reduces lung and cardiac damage from pneumococcal pneumonia and IPD. Representative H&E stained lung sections from C57Bl/6 mice (n=12-14) infected intratracheally with TIGR4 and treated intraperitoneally with **A**) vehicle (2% DMSO in PBS; 0 mg/kg) or **B**) Ponatinib at 1 mg/kg every 12 hours and euthanized at 48 hours post-infection. **C**) H&E stained lung sections were quantified for detectable biomass using ImageJ as indication of lung consolidation. **D**) Number of cardiac microlesions per cardiac tissue section from these same mice. Mann-Whitney U tests were applied for two-group comparisons: *** = $P \leq 0.001$, **** = $P \leq 0.0001$. (See also Supplemental Figure 5).

Ponatinib protects against long-term cardiac dysfunction. Subsequently, we sought to determine if Ponatinib treatment conferred protection against cardiac dysfunction in convalescence. As before, mice were challenged i.p. with TIGR4, but in this instance received Ponatinib alongside ampicillin beginning at 22 hours post-infection, and then every 12 hours for 3 days. Only mice who had developed severe infection ($>10^5$ CFU/mL blood) were used to assess the protective effects of this drug. Mice were assessed at 2 weeks, 1 month, and 3 months post-infection by high-resolution echocardiography. At these same time points, some mice were sacrificed and their hearts were examined histologically for collagen deposition. Control mice included cohorts that received a vehicle instead of Ponatinib alongside ampicillin. Importantly, and at all measured timepoints, mice that had received adjunct Ponatinib had significantly lower collagen levels than those that received vehicle and ampicillin. Pathological features observed in hearts from infected mice that had not received Ponatinib such as remnants of cardiac microlesions, pericarditis, and diffuse collagen deposition were not present in mice given Ponatinib (**Figure 7A-B**). Further supporting a protective effect for Ponatinib, echocardiography at 3 months post-infection showed that fractional shortening values were preserved in mice that had received Ponatinib versus the vehicle control group (**Figure 7C**). Likewise, aberrations in left ventricular contraction were not seen in Ponatinib treated mice (**Figure 7D**).

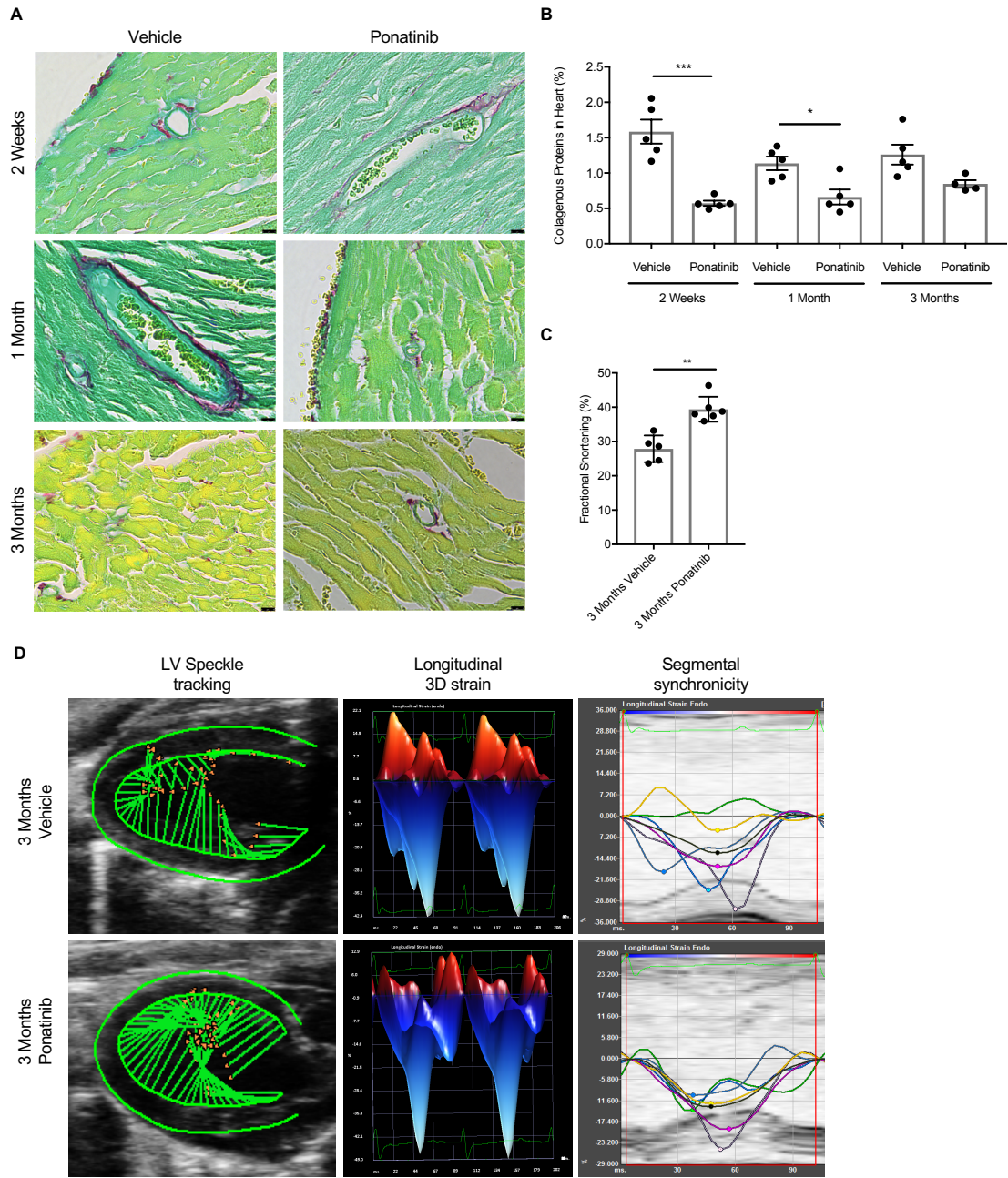


Figure 7: Ponatinib protects against long-term cardiac dysfunction. Mice were infected with TIGR4 and received Ponatinib treatment (1 mg/kg) or vehicle control in adjunct to antimicrobials. Hearts from mice experiencing severe disease ($>10^5$ CFU/ml of blood) at time of intervention were examined. **A)** Hearts stained with Sirius Red Fast Green and having median levels of collagen per group and time point are shown as representatives. Collagenous tissue is stained red while non-collagenous proteins are green. **B)** Collagen levels at 2 weeks and 1 month post-infection were significantly higher in mice that received vehicle treatment versus mice that received Ponatinib. **C)** Fractional shortening was preserved (3 months post onset of antimicrobial treatment) in mice that had received adjunct Ponatinib. **D)** Representative images from echocardiography demonstrating cardiac function recovery shown by mice receiving Ponatinib 3 months earlier. For multiple group comparisons, Sidak's post-test was used. Mann-Whitney U tests were applied for two-group comparisons. * = $P \leq 0.05$, ** = $P \leq 0.01$, *** = $P \leq 0.001$. (See also Supplemental Figure 6).

DISCUSSION

In addition to the physiological stressors imposed by severe systemic infection, considerable clinical, epidemiological, and experimental evidence now supports the notion that *Spn* directly damages the heart and this contributes to MACE within the hospital setting [2-5, 22, 23]. More specifically, our findings here affirm that *Spn* is capable of causing cardiomyocyte death and this is the result of its toxin pneumolysin. Importantly, our results demonstrate that cardiotoxicity is the result of pneumolysin's ability to trigger a form of programmed cell death known as necroptosis. While necroptosis had been previously implicated in exacerbating cardiac damage following sterile injury, such as in an ischemia-reperfusion model of infarct [24], and implicated in the depletion of tissue resident macrophages [12, 17], this is the first report to indicate a role for necroptosis in the death of cardiomyocytes.

The identification of necroptosis as responsible for pneumolysin-instigated cardiomyocyte death raised the possibility that cardiac damage and its associated dysfunction might be preventable. This was demonstrated genetically, using RIPK3 and MLKL KO mice, and pharmacologically, by treatment of infected wildtype mice with Necrostatin-5 or Ponatinib. Notably, Ponatinib is a tyrosine kinase inhibitor approved by the FDA to treat individuals with CML and Philadelphia chromosome–positive acute lymphoblastic leukemia [25]. Thus, it is a potential adjunct therapeutic for IPD. Importantly, MLKL KO mice and wildtype mice treated with Necrostatin-5 or Ponatinib had equivalent bacterial burdens in the airway, bloodstream, and heart, versus control mice following infection. Thus, inhibition of necroptosis does not seem to enhance susceptibility to the infection. The fact that necroptosis inhibition does not affect bacterial

burden in the heart also suggests that the translocation rate of pneumococci into the myocardium is not affected. The latter, previously shown to be mediated by bacterial attachment to laminin receptor and platelet-activating factor receptor on vascular endothelial cells [23]. Importantly, the reduction in cardiac microlesion formation seen in necroptosis-inhibited mice suggests that cardiomyocyte death is an event required for microlesion formation. This aligns well with our published observation that *Spn* can be taken up by cardiomyocytes after entering the myocardium and these host cells are killed [9]. We propose that the reason no differences are seen in recoverable CFU from hearts of necroptosis-inhibited mice versus control despite the absence of microlesions is because pneumococci are continuously invading the heart and many can be found outside these microlesions [17].

It is worth noting that cardiac microlesions formed by mice treated with Necrostatin-5 mirrored the morphology of cardiac microlesions from mice infected with TIGR4 *Δply*. That is, these lesions were characterized by immune cell infiltrates whereas TIGR4 forms microlesions that lack immune cell infiltration [17]. Previously we have shown that pneumolysin depletes the heart of cardiac resident macrophages and this inhibits the recruitment of neutrophils [17]. Thus, our results suggest pneumolysin activity is impaired across a number of cell types, and may be preserving resident macrophages, when using necroptosis inhibitors. Further studies are warranted in regards to how necroptosis inhibition impacts the innate immune response.

Our observation that ejection fraction and fractional shortening were diminished in mice who had experienced severe IPD, and that this was absent in mice that had received Ponatinib, is strong evidence that pneumolysin-mediated cytotoxicity is indeed a direct

contributor to the increased rate of cardiac dysfunction that occurs in convalescent individuals. Furthermore, that therapeutic necroptosis inhibition may have long-term beneficial effects for those who experience IPD. Importantly, Ponatinib has a black box warning due to liver toxicity and its associated risk for thrombosis in patients being treated for leukemia [26]. Its use during IPD, as tested here, would thereby merit considerable caution due to the serious medical complications that are concomitant with IPD as well as the drug's own negative effects. Critically, herein the drug was administered at a considerably truncated timeframe and at a dose significantly lower than those used in murine leukemia models. Our results open the possibility of repurposing anticancer drugs for infectious disease-related tissue injury in the myocardium, an avenue not explored until this report [27]. Also exciting was our observation that Ponatinib-treated mice were protected against acute pulmonary injury and subsequent cardiac damage following intratracheal challenge. A negative role for necroptosis during pneumonia has already been established, principally using KO mice [12]. While Ponatinib is certainly a promising potential therapeutic, there are still many factors requiring consideration. In particular, how early would the Ponatinib treatment need to start in order to provide a protective effect? Does Ponatinib have negative consequences during viral co-infection? We did not observe negative drug interactions between ampicillin and Ponatinib, however, studies are required to ensure Ponatinib does not have negative interactions with other antibiotics. Regardless, the use of Ponatinib in this study reduced pulmonary and cardiac damage during pneumococcal disease.

Collectively, our results reaffirm that cardiomyocyte death and myocardium damage occurs during IPD. They show for the first time that cardiomyocyte death is the result of

pneumolysin-mediated necroptosis. What is more, that cardiac damage is long-lasting and its associated dysfunction is a viable explanation for the increased risk of adverse cardiac events reported in convalescent individuals. Our results also show that pulmonary injury and cardiac damage during severe pneumococcal infections are potentially preventable. Pharmacological inhibition of necroptosis reduced the acute injury observed in the lungs and heart during *Spn* pneumonia and IPD and abrogated the cardiac dysfunction seen in convalescent control animals. We conclude that further studies are warranted to study the viability of necroptosis inhibitors in preventing tissue damage during IPD.

Acknowledgments. We thank Kelley Bradley, Alexis Herrera, and the UAB Pathology Core Lab for their technical assistance. We thank Dr. Luis Reyes for his commentary. We thank Drs. Vishva Dixit (Genentech, San Francisco, CA) and Warren Alexander (Walter and Eliza Hall Institute of Medical Research Parkville, Victoria, Australia) for the gift of RIPK3 KO and MLKL KO mice, respectively.

METHODS

Ethics Statement. Animal experiments were approved by the Institutional Animal Care and Use Committees at UT-Health San Antonio (#13032-34-01C) and the University of Alabama at Birmingham (#20270, #20175, #20479, and #21048).

Bacterial strains and media. *Spn* strain TIGR4, its isogenic pneumolysin deficient mutant, and D39 are described [21, 28, 29]. Pneumococci were grown on blood agar plates or in Todd-Hewitt broth containing 0.5% yeast extract at 37°C and 5% CO₂.

Cell lines and assays. HC_{SV40} were purchased from ABM (Richmond, B.C., Canada). HL-1 atrial cardiomyocytes were a gift from Dr. W. Claycomb (Louisiana State University School of Medicine, New Orleans, LA) [30].

Animal models and disease severity assessments. Male and female 6-week-old BALB/c mice and C57Bl/6 mice were obtained from Jackson Laboratories (Sacramento, California). MLKL KO and RIPK3 KO mice in a C57Bl/6 background were obtained from Drs. Warren Alexander (Walter and Eliza Hall Institute of Medical Research Parkville, Victoria, Australia) and Vishva Dixit (Genentech, San Francisco, CA), respectively [31, 32]. Mice were challenged by intraperitoneal (i.p.) injection with 10³ colony forming units (CFU) of *Spn* suspended in 100 μL PBS or by forced aspiration with 10⁵ CFU of *Spn* in 100 μL PBS. For rescue experiments, mice received ampicillin (50 mg/kg) i.p. in 100 μL PBS every 12 hours for 3 days. When indicated, mice also

received Necrostatin-5 (5 mg/kg) (Sigma, St. Louis, MO) or Ponatinib (1 mg/kg) (Selleckchem, Houston, TX) dissolved in DMSO and diluted with PBS to a total of 100 μ L (final <5% DMSO) by i.p. injection every 6 or 12 hours for up to 3 days. Vehicle controls received saline solution with equivalent amounts of DMSO. Cardiac troponin-I in sera was measured by ELISA (G Biosciences, St. Louis, MO). Cardiac function measurements, i.e. ejection fraction, fractional shortening, and myocardium strain were assessed by echocardiography at the UAB Mouse Cardiovascular Core using the VisualSonics Vevo 3100 imaging system and Vevo Strain software (Fujifilm VisualSonics).

Tissue staining and immunofluorescent microscopy. Methods used for heart and lung processing, hematoxylin/eosin staining, and immunofluorescent staining of sections are detailed in **Supplemental Material**. Note that we used fluorophore-conjugated monoclonal antibodies against p-MLKL; eliminating the need for secondary antibody. Cardiac sections were examined and microlesions enumerated using microscopy. Cardiac sections were H&E stained or examined by immunofluorescence using antibody against type 4 capsular polysaccharide. Sirius Red Fast Green staining (Chondrex 9046, Redmond, WA) was performed for detection of collagen. Collagen was measured semi-quantitatively with ImageJ using threshold analysis of tile-scanned images. Note that thresholds were manually set on the RGB image to visually match the red-stained portions in the color image.

Cell Death Assays. Details on the reagents to block necroptosis and methods used assess cell death are provided as **Supplemental Material** through the Journal of Infectious Diseases website.

Statistical analyses. For multiple group analyses we used one-way ANOVA with Dunn's *post-hoc* analysis, Tukey or Sidak post-tests were used only when stated; grouped analyses were performed using a Two-Way ANOVA. Summary statistics are presented using mean \pm SEM. For non-parametric data sets, we used a Mann-Whitney U test. Statistical analyses were performed using Prism 8 (GraphPad Software, La Jolla, CA).

Funding. This work was supported by National Institutes for Health grants GM088010 (SMB), 2T32A1007051-41 (ANR), DE014318 (RPG), AI007051 (NGJ), AG055144 (CJO), and AI114800 (CJO). CJO also received support from American Heart Association grants 16GRNT30230007 and 18TPA34110195. Research support was also provided by the Comprehensive Cardiovascular Center and Inflammation, Infection & Immunity joint pilot grant program to CJO through The University of Alabama at Birmingham.

REFERENCES

1. Steel HC, Cockeran R, Anderson R, Feldman C. Overview of community-acquired pneumonia and the role of inflammatory mechanisms in the immunopathogenesis of severe pneumococcal disease. *Mediators Inflamm* **2013**; 2013:490346.
2. Musher DM, Rueda AM, Kaka AS, Mapara SM. The association between pneumococcal pneumonia and acute cardiac events. *Clin Infect Dis* **2007**; 45:158-65.

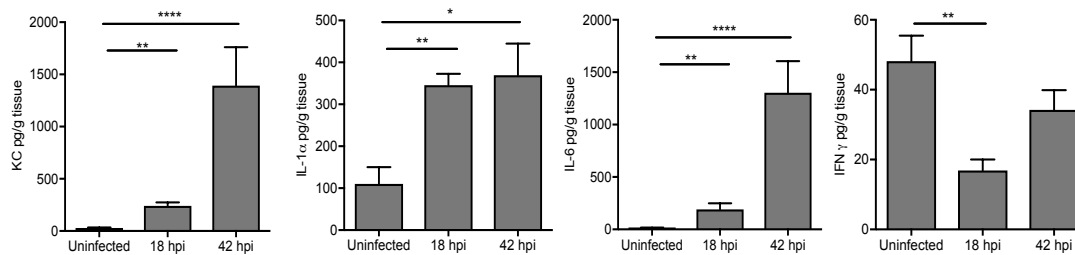
3. Eurich DT, Marrie TJ, Minhas-Sandhu JK, Majumdar SR. Risk of heart failure after community acquired pneumonia: prospective controlled study with 10 years of follow-up. *BMJ* **2017**; 356:j413.
4. Musher DM, Abers MS, Corrales-Medina VF. Acute Infection and Myocardial Infarction. *N Engl J Med* **2019**; 380:171-6.
5. Reyes LF, Restrepo MI, Hinojosa CA, et al. Severe Pneumococcal Pneumonia Causes Acute Cardiac Toxicity and Subsequent Cardiac Remodeling. *Am J Respir Crit Care Med* **2017**.
6. Shenoy AT, Beno SM, Brissac T, Bell JW, Novak L, Orihuela CJ. Severity and properties of cardiac damage caused by *Streptococcus pneumoniae* are strain dependent. *PLoS One* **2018**; 13:e0204032.
7. Brissac T, Shenoy AT, Patterson LA, Orihuela CJ. Cell invasion and pyruvate oxidase derived H₂O₂ are critical for *Streptococcus pneumoniae* mediated cardiomyocyte killing. *Infect Immun* **2017**.
8. Shenoy AT, Brissac T, Gilley RP, et al. *Streptococcus pneumoniae* in the heart subvert the host response through biofilm-mediated resident macrophage killing. *PLoS Pathog* **2017**; 13:e1006582.
9. Brown AO, Mann B, Gao G, et al. *Streptococcus pneumoniae* translocates into the myocardium and forms unique microlesions that disrupt cardiac function. *PLoS Pathog* **2014**; 10:e1004383.
10. Pasparakis M, Vandenabeele P. Necroptosis and its role in inflammation. *Nature* **2015**; 517:311-20.

11. Gonzalez-Juarbe N, Bradley KM, Shenoy AT, et al. Pore-forming toxin-mediated ion dysregulation leads to death receptor-independent necroptosis of lung epithelial cells during bacterial pneumonia. *Cell Death Differ* **2017**.
12. Gonzalez-Juarbe N, Gilley RP, Hinojosa CA, et al. Pore-Forming Toxins Induce Macrophage Necroptosis during Acute Bacterial Pneumonia. *PLoS Pathog* **2015**; 11:e1005337.
13. Gonzalez-Juarbe N, Bradley KM, Riegler AN, et al. Bacterial Pore-Forming Toxins Promote the Activation of Caspases in Parallel to Necroptosis to Enhance Alarmin Release and Inflammation During Pneumonia. *Sci Rep* **2018**; 8:5846.
14. Fauster A, Rebsamen M, Huber KV, et al. A cellular screen identifies ponatinib and pazopanib as inhibitors of necroptosis. *Cell Death Dis* **2015**; 6:e1767.
15. England H, Summersgill HR, Edey ME, Rothwell NJ, Brough D. Release of interleukin-1alpha or interleukin-1beta depends on mechanism of cell death. *J Biol Chem* **2014**; 289:15942-50.
16. Darwich L, Coma G, Pena R, et al. Secretion of interferon-gamma by human macrophages demonstrated at the single-cell level after costimulation with interleukin (IL)-12 plus IL-18. *Immunology* **2009**; 126:386-93.
17. Gilley RP, Gonzalez-Juarbe N, Shenoy AT, et al. Infiltrated Macrophages Die of Pneumolysin-Mediated Necroptosis following Pneumococcal Myocardial Invasion. *Infect Immun* **2016**; 84:1457-69.
18. Geserick P, Wang J, Schilling R, et al. Absence of RIPK3 predicts necroptosis resistance in malignant melanoma. *Cell Death Dis* **2015**; 6:e1884.

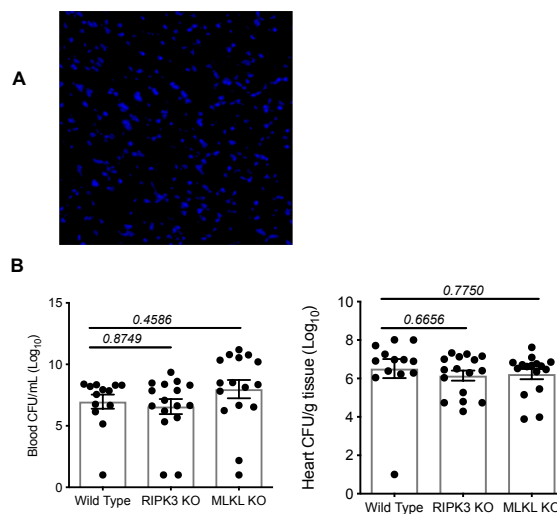
19. Liao D SL, Liu W, He S, Wang X, Lei X. . Necrosulfonamide inhibits necroptosis by selectively targeting the mixed lineage kinase domain-like protein. . *MedChemComm* **2014**:333-7.
20. Adams JE, 3rd, Bodor GS, Davila-Roman VG, et al. Cardiac troponin I. A marker with high specificity for cardiac injury. *Circulation* **1993**; 88:101-6.
21. Lanie JA, Ng WL, Kazmierczak KM, et al. Genome sequence of Avery's virulent serotype 2 strain D39 of *Streptococcus pneumoniae* and comparison with that of unencapsulated laboratory strain R6. *J Bacteriol* **2007**; 189:38-51.
22. Corrales-Medina VF, Suh KN, Rose G, et al. Cardiac complications in patients with community-acquired pneumonia: a systematic review and meta-analysis of observational studies. *PLoS Med* **2011**; 8:e1001048.
23. Brown AO, Millett ER, Quint JK, Orihuela CJ. Cardiotoxicity during invasive pneumococcal disease. *Am J Respir Crit Care Med* **2015**; 191:739-45.
24. Koshinuma S, Miyamae M, Kaneda K, Kotani J, Figueredo VM. Combination of necroptosis and apoptosis inhibition enhances cardioprotection against myocardial ischemia-reperfusion injury. *J Anesth* **2014**; 28:235-41.
25. Cortes JE, Kim DW, Pinilla-Ibarz J, et al. A phase 2 trial of ponatinib in Philadelphia chromosome-positive leukemias. *N Engl J Med* **2013**; 369:1783-96.
26. Gainor JF, Chabner BA. Ponatinib: Accelerated Disapproval. *Oncologist* **2015**; 20:847-8.
27. Fulda S. Regulation of necroptosis signaling and cell death by reactive oxygen species. *Biol Chem* **2016**; 397:657-60.

28. Lizcano A, Chin T, Sauer K, Tuomanen EI, Orihuela CJ. Early biofilm formation on microtiter plates is not correlated with the invasive disease potential of *Streptococcus pneumoniae*. *Microb Pathog* **2010**; 48:124-30.
29. Tettelin H, Nelson KE, Paulsen IT, et al. Complete genome sequence of a virulent isolate of *Streptococcus pneumoniae*. *Science* **2001**; 293:498-506.
30. Claycomb WC, Lanson NA, Jr., Stallworth BS, et al. HL-1 cells: a cardiac muscle cell line that contracts and retains phenotypic characteristics of the adult cardiomyocyte. *Proc Natl Acad Sci U S A* **1998**; 95:2979-84.
31. Murphy JM, Czabotar PE, Hildebrand JM, et al. The pseudokinase MLKL mediates necroptosis via a molecular switch mechanism. *Immunity* **2013**; 39:443-53.
32. Newton K. RIPK1 and RIPK3: critical regulators of inflammation and cell death. *Trends Cell Biol* **2015**; 25:347-53.

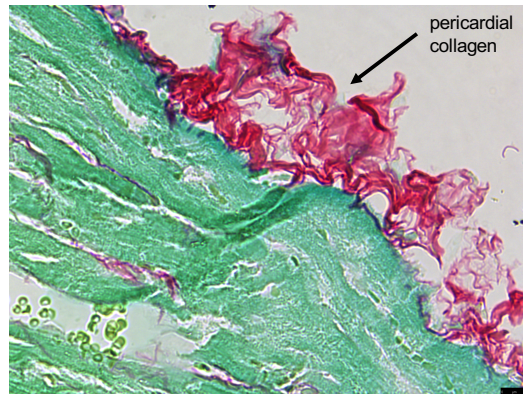
SUPPLEMENTAL FIGURES



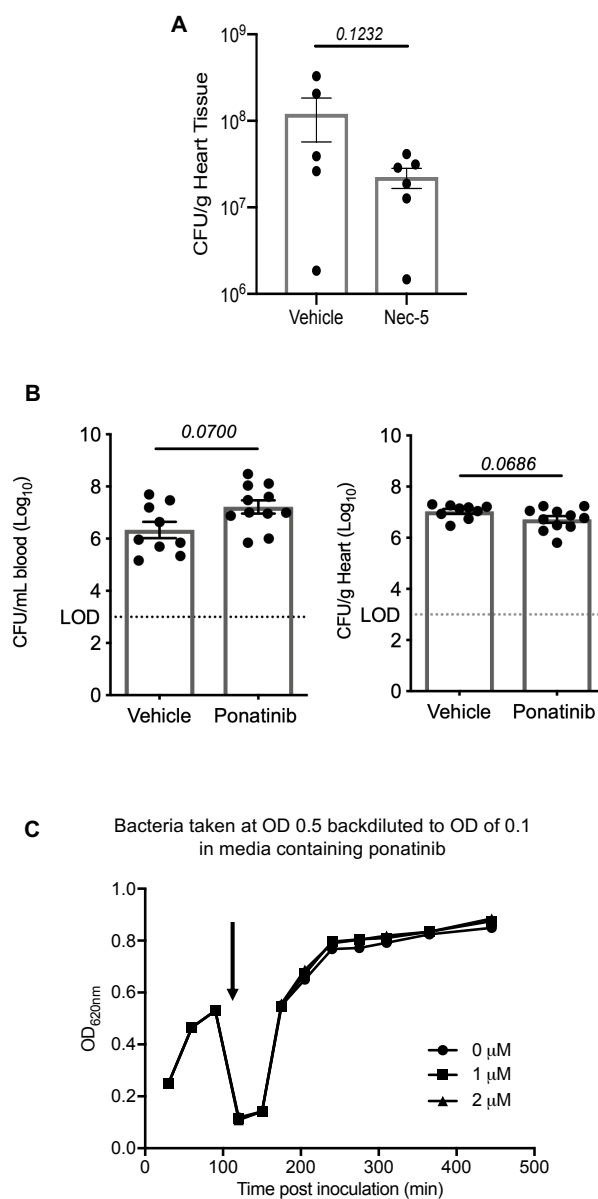
Supplemental Figure 1: Cardiac pro-inflammatory mediators are increased during IPD. Quantification of KC, IL-1 α , IL-6, and IFN γ in cardiac tissue homogenates from mice infected with TIGR4. Samples collected at 18 and 42 hours post intraperitoneal inoculation. * = P \leq 0.05, ** = P \leq 0.01, **** = P \leq 0.0001.



Supplemental Figure 2: Necroptosis is active during pneumococcal cardiac infection but does not influence bacterial burdens. A) Representative immunofluorescent stained cardiac section from a BALBc/J uninfected mouse. Absence of detectable *Spn* (red) or p-MLKL (green) demonstrates specificity of fluorescent labeled antibodies used in Figure 2D. Visible are DAPI (blue) stained nuclei. B) Pneumococcal burdens in blood and heart homogenates from wild type C57Bl/6, RIPK3 KO, and MLKL KO mice intraperitoneally infected with TIGR4.

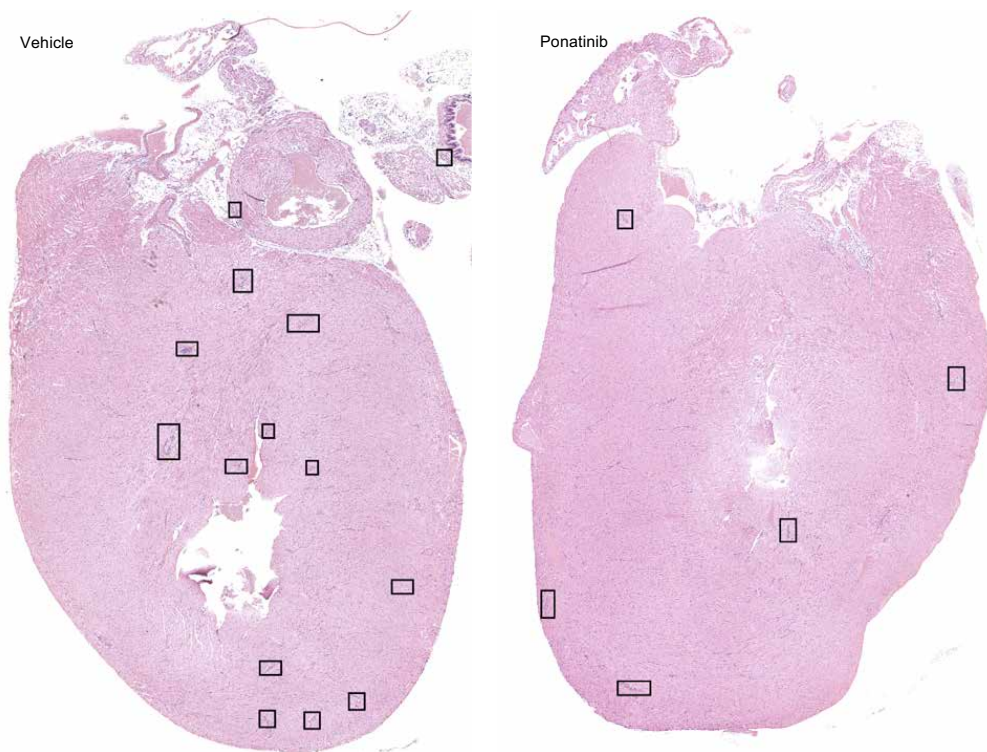


Supplemental Figure 3: TIGR4 infection can lead to pericarditis. Example from a mouse infected with TIGR4, treated with ampicillin, and euthanized two weeks post-treatment. Collagen deposition was observed in the pericardium.

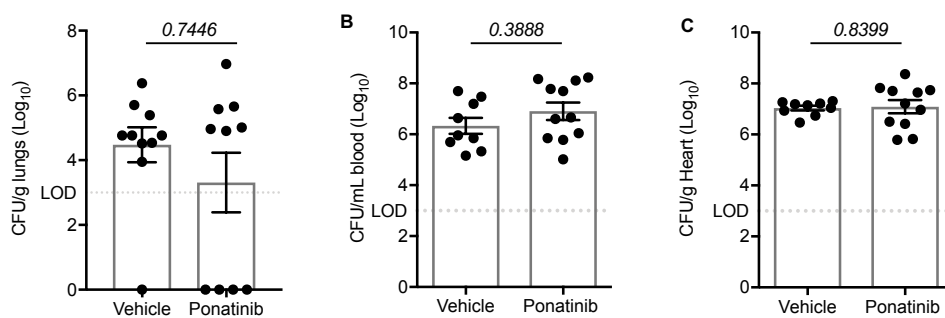


Supplemental Figure 4: Ponatinib treatment does not affect pneumococcal growth.

A) Pneumococcal burdens in heart homogenates at time of sacrifice from C57Bl/6 mice i.p. infected with TIGR4 and therapeutically treated with vehicle or 5 mg/kg of Necrostatin-5 (Nec-5) starting 12 hours prior to infection and every 12 hours until mice were euthanized at 36 hours post-infection. **B)** Pneumococcal burdens in blood and heart homogenates at time of sacrifice from C57Bl/6 mice i.p. infected with TIGR4 and therapeutically treated with 1 mg/kg of Ponatinib at 12 and 24 hours post inoculation and euthanized at 30 hours post-inoculation. **C)** Pneumococcal growth as monitored by optical density of TIGR4 in THY grown to an OD_{620nm} of 0.5 and diluted in media containing Ponatinib to an OD_{620nm} of 0.1. Limit of detection (LOD) denoted by dashed line.



Supplemental Figure 5: Therapeutic Ponatinib treatment reduces cardiac damage from pneumococcal pneumonia and IPD. Representative H&E stained cardiac sections from C57Bl/6 mice infected intratracheally with TIGR4 and treated i.p. with vehicle or Ponatinib at 1 mg/kg every 12 hours and euthanized at 48 hours post-infection. Cardiac microlesions are indicated by black boxes.



Supplemental Figure 6: Necroptosis inhibition by Ponatinib does not influence pneumococcal burdens. Pneumococcal burdens in **A)** lungs, **B)** blood, and **C)** heart homogenates from C57Bl/6 mice intratracheally infected with TIGR4 and therapeutically treated with 1 mg/kg of Ponatinib at 12 and 24 hours post inoculation and euthanized at 48 hours post-inoculation. Limit of detection (LOD) denoted by dashed line.

INFLUENZA-INDUCED OXIDATIVE STRESS SENSITIZES LUNG CELLS TO
BACTERIAL TOXIN-MEDIATED NECROPTOSIS

by

NORBERTO GONZALEZ-JUARBE, ASHLEIGH N. RIEGLER, ALEXANDER S.
JUREKA, RYAN P. GILLEY, JEFFREY BRAND, JOHN E. TROMBLEY, NINECIA
R. SCOTT, PETER H. DUBE, CHAD M. PETIT, KEVIN S. HARROD, AND CARLOS
J. ORIHUELA

Cell Reports

Copyright

2020

by

Gonzalez-Juarbe *et al.*

Used by permission

Format adapted and errata corrected for dissertation

PREFACE

While understanding the role of necroptosis during pneumococcal infection alone is extremely important, it is notable that many deaths associated with *Spn* occur as result of a co- or secondary infection from another airway pathogen. One such pathogen is Influenza A Virus (IAV) which, alone, is capable of causing considerable lung damage, including eliciting necroptosis, but when combined with *Spn* is associated with high mortality. Additionally, 34%-55% of the deaths linked to the 2009 IAV pandemic were associated with bacterial co-infections, with *Spn* the most common bacteria identified (Gill et al., 2010; Louie et al., 2009). In this manuscript we further assessed whether prior IAV infection sensitizes airway cells to necroptotic death elicited by *Spn* (specifically the *Spn* toxin, pneumolysin). We also identify a potential mechanism for this sensitization. This work continues to address the role of necroptosis in the pathology of airway infections and begins the transition to viral infection, specifically IAV.

SUMMARY

Pneumonias caused by influenza A virus (IAV) co- and secondary bacterial infections are characterized by their severity and high mortality rate. Previously, we have shown that bacterial pore-forming toxin (PFT)-mediated necroptosis is a key driver of acute lung injury during bacterial pneumonia. Here, we evaluate the impact of IAV on PFT-induced acute lung injury during co- and secondary *Streptococcus pneumoniae* (*Spn*) infection. We observe that IAV synergistically sensitizes lung epithelial cells for PFT-mediated necroptosis *in vitro* and in murine models of *Spn* co-infection and secondary infection. Pharmacological induction of oxidative stress without virus sensitizes cells for PFT-mediated necroptosis. Antioxidant treatment or inhibition of necroptosis reduces disease severity during secondary bacterial infection. Our results advance our understanding on the molecular basis of co- and secondary bacterial infection to influenza and identify necroptosis inhibition and antioxidant therapy as potential intervention strategies.

KEY WORDS: Pneumonia, Influenza A virus, *Streptococcus pneumoniae*, epithelial cells, necroptosis, cell death, oxidative stress, inflammation

INTRODUCTION

Influenza A virus (IAV) is the most common cause of human influenza (flu) (Morens et al., 2008), infecting 4-8% of the U.S. population annually (Tokars et al., 2018).

Worldwide, the World Health Organization estimates that flu affects approximately 1 billion individuals annually, with 3 to 5 million cases of severe disease and a resulting 300,000 to 500,000 deaths (Clayville, 2011). While IAV alone is capable of considerable morbidity and mortality, clinical and molecular epidemiology have shown that the most serious infections are frequently associated with co-infections or a secondary infection with a bacterial pathogen. *Streptococcus pneumoniae* (*Spn*; the pneumococcus) is the leading cause of community-acquired pneumonia and by far the most common bacterium associated with IAV infections (van der Sluijs et al., 2010). Highlighting the seriousness of IAV/*Spn* co-infections, 34%-55% of the deaths linked to the 2009 IAV pandemic were associated with bacterial infections, with *Spn* the most common bacteria identified (Gill et al., 2010; Louie et al., 2009).

Over the past 20 years a number of seminal discoveries have helped to explain, at the molecular level, the synergy observed during IAV/*Spn* super-infection. Key findings include the observation that IAV neuraminidase cleaves terminal sialic acid on host cell glycoconjugates exposing normally cryptic antigens for bacterial attachment (McCullers and Bartmess, 2003). Viral neuraminidase-cleaved sialic acid serves as a nutrient for *Spn* and promotes bacterial outgrowth (Hentrich et al., 2016). IAV-induced down regulation of ion channels in bronchial epithelial cell results in dysregulated pulmonary fluid homeostasis that favors bacterial replication (Brand et al., 2018). Cytokines, and alarmins released from IAV-infected dying cells elicit a transcriptional response from *Spn* that

causes it to disperse from biofilms and enhances its virulence (Pettigrew et al., 2014). In addition, IAV-induced interferon (IFN) gamma down regulates expression of scavenger receptors on macrophages, such as MARCO, that are required for uptake of *Spn* in absence of capsule specific antibody (Sun and Metzger, 2008). Finally, the immune response induced by IAV is inappropriate for clearance of bacteria and enhances pulmonary injury (Shahangian et al.; van der Sluijs et al., 2006). It is noteworthy, that the majority of this work has not focused on events that occur within lung epithelial cells (LEC), which are the nexus of co-infection.

Necroptosis is a programmed form of cell death that results in host cell membrane failure, i.e. necrosis. It is inflammatory due to the release of cytoplasmic contents that serve as alarmins. Canonically, necroptosis is regulated by receptor-interacting serine-threonine kinase (RIPK)1, that activates RIPK3. Subsequently, RIPK1/RIPK3 activates the necroptosis effector molecule MLKL through phosphorylation, p-MLKL, which targets cell membranes leading to cell rupture and death (Moreno-Gonzalez et al., 2016; Vandenabeele et al., 2010). Importantly, both IAV and bacterial pore-forming toxins (PFT), such as pneumolysin produced by *Spn*, have recently been shown to induce necroptosis of LEC in a death receptor independent manner (Gonzalez-Juarbe et al., 2018; Gonzalez-Juarbe et al., 2017; Nogusa et al., 2016; Thapa et al., 2016; Wang et al., 2019). For IAV, this has been shown to be the result of viral RNA interactions with DAI (also known as Zbp or DLM-1), a sensor for cytoplasmic nucleic acid, which activates RIPK3. Necroptosis of virally infected LEC is thought to be beneficial as RIPK3 KO and MLKL/FADD double KO mice were considerably more susceptible to IAV, the latter showing inhibited death of virus-infected cells. Along such lines, RIPK3 activation is

necessary to establish an efficient response to the virus. (Balachandran and Rall, 2020; Nailwal and Chan, 2019; Nogusa *et al.*, 2016). Our research group has shown that during bacterial pneumonia initiation of necroptosis (i.e. MLKL-activity) is detrimental and exacerbates bacterial outgrowth, pulmonary injury, and loss of alveolar-capillary integrity (Gonzalez-Juarbe *et al.*, 2017; Gonzalez-Juarbe *et al.*, 2015a). Together, these observations suggest that inhibition of MLKL may have a possible protective role for viral and bacterial infections alike and extend to co- and secondary bacterial infections. Critically and up to this point, the role of necroptosis on disease severity during IAV/bacteria co-infection was not known. Here we determined its consequence and identified IAV-induced oxidative stress as a sensitizing agent for PFT-mediated cell death.

EXPERIMENTAL MODEL AND SUBJECT DETAILS

Ethics Statement. Animal experiments were approved by the Institutional Animal Care and Use Committee at The University of Alabama at Birmingham (Protocol # 20358). Human LEC were harvested from whole lung sections obtained from the International Institute for the Advancement of Medicine (Fulcher *et al.*, 2005). The use of primary tissue, obtained in de-identified fashion, does not meet the criteria for human subject research.

IAV and *Spn*. Pandemic H1N1 A/California/7/2009 (pdmH1N1) and H1N1 A/Puerto Rico/8/1934 (PR8) influenza viruses were propagated in MDCK cells. *Spn* serotype 4 strain TIGR4 and its derivatives were used for all studies (Tettelin *et al.*, 2001). TIGR4

mutants deficient in *ply* (Δply), the gene encoding pneumolysin, and *spxB* ($\Delta spxB$), the gene encoding pyruvate oxidase, have been described (Lizcano et al., 2010). We also used mutants provided by Dr. Jeffrey Weiser (New York University, NY). These were matched strains of TIGR4 (TIGR4_{JW}), TIGR4 lacking pneumolysin, TIGR4_{JW} Δply , a TIGR4 point mutant deficient in pore formation (TIGR4_{JW} W433F), and a corrected mutant (TIGR4_{JW} *ply*⁺) (Zafar et al., 2017); these were used as a set. Recombinant pneumolysin (rPly) was purified from *E. coli* (Brown et al., 2014). *Staphylococcus aureus* alpha-toxin was purchased (Sigma-Aldrich, St. Louis, MO).

Animal strains and infections. Male and female 8-week-old C57BL/6 mice were obtained from Taconic Biosciences (Rensselaer, NY). MLKL KO mice were made available by Dr. Warren Alexander (Walter and Eliza Hall Institute of Medical Research Parkville, Victoria, Australia) (Murphy et al., 2013). For IAV/*Spn* co-infection, 8-week-old C57BL/6 mice were intranasally challenged with 250 PFU PR8. Five days post-influenza challenge, mice received by forced aspiration 5×10^5 CFU *Spn* (Gonzalez-Juarbe et al., 2015b). For the co-infection model we use an LD₅₀ of *Spn* to demonstrate bacterial infection was on its own capable of causing disease, yet this was augmented in a co-infection model. For studies involving *Spn* secondary infection, i.e. after viral clearance, mice were challenged with 250 PFU pdmH1N1 and ten days post-influenza, challenged with 10^3 CFU *Spn*. In all the secondary infection mouse models the *Spn* dose chosen was a sublethal (1000 CFU/mL) since the mice were challenged for 10-days with IAV, thus making the mice extremely susceptible to the bacterial infection (Gill et al., 2010; Louie et al., 2009).

Cell Infections. A549 type II alveolar epithelial cells (Fulcher *et al.*, 2005), MH-S mouse alveolar macrophages (Saxena *et al.*, 2008), and primary normal human bronchiolar epithelial cells (Fulcher *et al.*, 2005), were infected with IAV at MOI 2 for 2 hours, and subsequently challenged with *Spn* at an MOI 10 for 4 hours. As our purpose was to characterize the cellular responses to influenza infection in regard to potentiation of bacteria induced cell death without the complication of cell lysis caused by late stage replication we used a high infectious dose and short time period. Other investigators have used the same approach (Hoffmann *et al.*, 2016). The majority of chemical inhibitors were obtained from Sigma-Aldrich. Exceptions include necrosulfonamide (Tocris Bioscience, QL, UK), GSK'872 and Nec1s (BioVision, Milpitas, CA), oseltamivir carboxylate (MCE, Monmouth, NJ), TNFR inhibitor R-7050 and TNF- α inhibitor SPD-304 (Cayman Chemicals, Ann Arbor, MI) and Pimodivir (AdooQ Bioscience, Irvine, CA). Cells receiving inhibitors were treated continuously beginning 1-hour prior to IAV infection and inhibitor was maintained in the media until the end of the experiment. Pimodivir treated cells received the drug 2-hours prior to IAV challenge. A549 cells deficient in MLKL have been previously described (Gonzalez-Juarbe *et al.*, 2018). Cell death was evaluated by detection of lactate dehydrogenase (LDH) in culture supernatants (Gonzalez-Juarbe *et al.*, 2015a). The presence of reactive oxygen species (ROS) was measured with the H₂-DCF assay (Thermo Fisher Scientific, Waltham, MA). Lipid peroxidation was detected with the lipid peroxidation malondialdehyde (MDA) assay (Abcam). Antibodies against 8-hydroxydeoxyguanosine, an oxidative stress-mediated DNA damage marker, and HNE-J, a lipid peroxidation marker, were purchased (Abcam).

METHOD DETAILS

Histology and Microscopy. The methods used for tissue processing, sectioning, and immunofluorescent microscopy are described (Gilley et al., 2016; Gonzalez-Juarbe *et al.*, 2017; Gonzalez-Juarbe *et al.*, 2015b). Briefly, tissue sections were fixed with cold acetone (-20°C), in 70% ethanol (-20°C). then rehydrated in PBS. The sections were then blocked \ in 3% goat serum–3% bovine serum albumin (BSA) for 30min. Each primary antibody used was diluted at 1:500 in the blocking solution and incubated over the tissue for 40 min. After incubation, sections were washed 3 times with PBS–0.05% Tween 20. Then sections were stained with secondary antibody diluted at 1:1000 in blocking solution and incubated over sections for 30 min. Slides were then washed 3 times and mounted with ProLong Gold Antifade reagent containing DAPI (4',6'-diamidino-2-phenylindole) (Life Technologies, Carlsbad CA). For histology, formalin fixed slides were stained with hematoxylin, then washed, subsequently stained with eosin. Tissue was washed again and mounted with Cytoseal (ThermoFisher, Waltham, MA). Images were captured using a Zeiss AxioXam MRm Rev3 and/or MRc cameras attached to a Zeiss AxioImager Z1 epifluorescent microscope (Carl Zeiss, Thornwood, NY) or a Leica LMD6 with DFC3000G-1.3-megapixel monochrome camera (Leica Biosystems, Buffalo Grove, IL). TUNEL (Promega, Madison, WI) and Annexin V (Abcam, Cambridge, UK) staining was done per manufacturer's instruction. Cleaved caspase-3 staining was done using anti-cleaved-caspase-3 antibody (Abcam). Mean fluorescent intensity and densitometry of immunoblots was measured using ImageJ (Schindelin et al., 2015).

Immunoblots and ELISA. Western blots were done as previously described (Riegler et al., 2019). Briefly, 10 μ g of total protein was separated on a 10% polyacrylamide gel (Biorad) before transfer to a nitrocellulose membrane (Biorad). Membranes were blocked in 5% BSA and washed 3 times with TBS-0.1% Tween 20 (TBST). Membranes were incubated with anti -MLKL (1:1000, #37705, Cell Signaling Technologies), -p-MLKL (1:1000, #37333S, Cell Signaling Technologies) and -cytoskeletal actin (1:10000, #A300-485A, Bethyl Laboratories Inc., Montgomery, TX), in 5% BSA overnight. Then, membranes were washed 3 times with TBST and incubated with HRP-conjugated goat antibody at 1:10,000 (ThermoFisher, Waltham, MA). After 3 additional washes, signal was detected using Clarity™ Western ECL and ChemiDoc XRS+ (both from Biorad). ELISA-based measurements for IFN- β , IFN- α and TNF- α were done using kits from PBL Assay Science (Piscataway, NJ) and InvivoGen (San Diego, CA). For each cytokine, 100 μ L of protein standard and supernatants of tissue homogenates were added to wells in a 96-well plate. Manufacturer instructions for washes and duration of detection antibody and HRP conjugate incubations were followed after initial sample incubation. Finally, absorbance or luminisence was read using a BioTek Synergy H4 plate reader (BioTek, Winooski, VT).

QUANTIFICATION AND STATISTICAL ANALYSIS

All results are displayed as standard error of the mean (SEM). In addition, individual data points in all *in vitro* assays represent all technical replicates collected from 3 separate experiments. For *in vivo* experiments, each individual data point represents an individual animal sample. Number of animals for *in vivo* experiments are denoted in the figure

legends. For non-parametric multiple group analyses we used a Kruskal-Wallis H test with Dunn's post-hoc analysis. For parametric grouped analyses we used ANOVA with Sidak's post-hoc analysis. For data with a single independent factor of two groups we used a Mann-Whitney U test. Survival comparisons were assessed using Log-rank (Mantel-Cox) test. Asterisks denote the level of significance observed: * = $P \leq 0.05$; ** = $P \leq 0.01$; *** = $P \leq 0.001$; **** = $P \leq 0.0001$. Statistical analyses were calculated using Prism 8 (GraphPad Software: La Jolla, CA).

RESULTS

Necroptosis is synergistically increased during IAV/*Spn* co-infection. Using an established mouse model of co-infection (McCullers and Hayden, 2012; McCullers and Tuomanen, 2001), we recapitulated the synergy known to occur between IAV and *Spn*. Briefly, we observed a >50-fold increase in the amount of *Spn* present in bronchoalveolar lavage fluid (BALF) and blood (**Fig. 1A, B**), as well as a significant decrease in time to death following IAV/*Spn* challenge versus *Spn* or IAV alone (**Fig. 1C**). Importantly, ongoing IAV infection synergistically enhanced the number of lung cells undergoing necroptosis after *Spn* challenge; necroptosis activity in frozen lung sections was inferred by immunofluorescent detection of phosphorylated MLKL (p-MLKL) (**Fig. 1D, E**).

To validate this *in vivo* observation and begin to dissect the molecular mechanisms underlying IAV-enhanced bacteria-induced necroptosis, we used an established *in vitro* co-infection model (Hoffmann *et al.*, 2016). Briefly, A549 type II alveolar epithelial cells were infected with either pdmH1N1 or PR8 at a MOI of 2 for two hours and then challenged with *Spn* at a MOI of 10 for another four hours. Importantly,

A549 cytotoxicity was synergistic increased in cells challenged with both pathogens (**Fig. 2A, B**). Similar results were also observed with MH-S murine alveolar macrophages (**Fig. 2C**), indicating influenza-mediated sensitization to necroptosis is not restricted to airway epithelial cells. Of note, the enhanced death of A549 co-infected cells occurred without significant differences in bacterial titers versus control (**Fig. S1A**); indicating that the increased levels of necroptosis observed *in vivo* were not solely due to increased bacterial burden. Tumor necrosis factor (TNF) and IFN responses have been shown to promote necroptosis during viral infection (Upton et al., 2017). Along such lines, inhibition of TNF receptor 1 or blocking of TNF- α by pre-treatment of cells with R7050 or SPD304, respectively, did not reduce influenza-induced cell death potentiation in A549 cells *in vitro* (**Fig. S1B**). Moreover, the timeframe of the *in vitro* model did not lead to significant increases in the interferon response (**Fig. S1C**). Altogether, no evidence supporting a role for the synergistic initiation of receptor-mediated apoptosis was found *in vitro* or *in vivo* under the conditions tested (**Fig S2**).

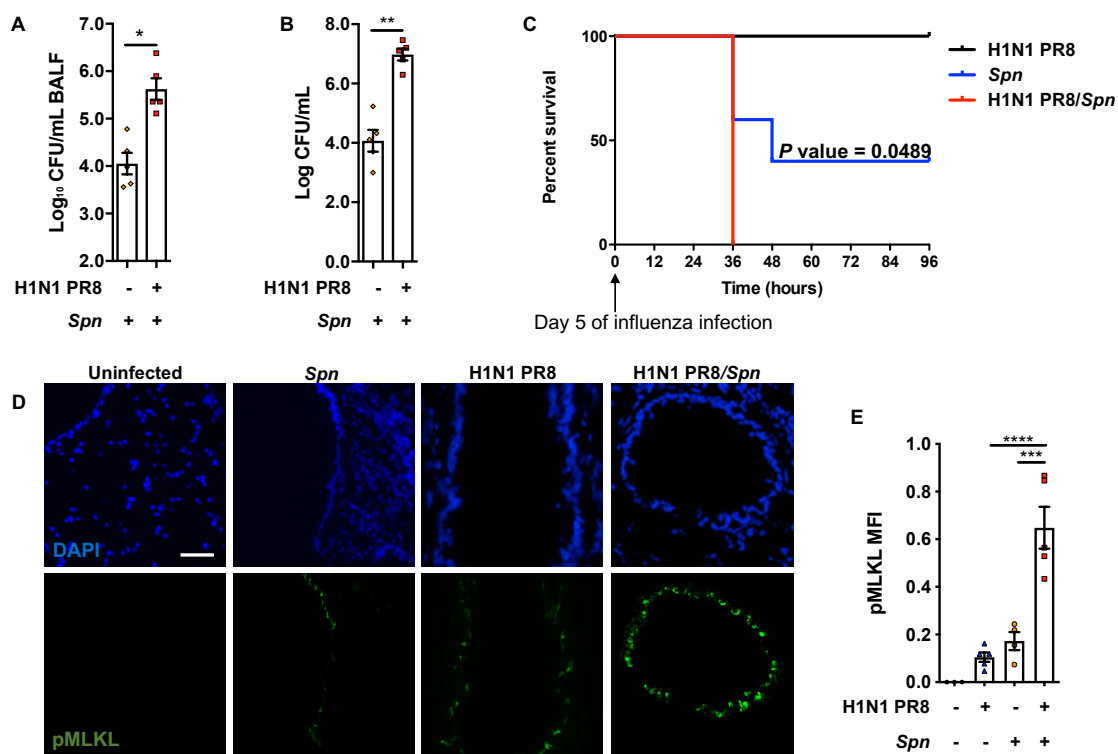


Figure 1: IAV/*Spn* co-infection leads to increased mortality and enhanced tissue necroptosis. 8-week-old C57Bl/6 mice were intranasally infected with H1N1 PR8 (250 PFU) for 5 days and subsequently challenged intratracheally with *Spn* strain TIGR4 at the LD₅₀ dose of 5×10^5 CFU. Mice were euthanized 24-hours post-secondary infection (n=4-5 mice/cohort). Bacterial titers in **A**) bronchoalveolar lavage (BALF) and **B**) blood of mice at time of sacrifice. **C**) Survival of mice challenged with IAV, *Spn*, or co-infected with *Spn* after 5 days of IAV (n=5); **D**) corresponding and representative images of frozen lung sections from infected mice immunofluorescent stained for p-MLKL (green) (n=4-5/cohort). White bar denotes 50 μ m. **E**) Shown is the quantitation of p-MLKL levels in captured images calculated by mean fluorescent intensity. For *in vivo* experiments, each individual data point represents an individual animal sample.

Pore-forming toxin activity is required for *Spn*-induced necroptosis during co-infection. *Spn*-mediated cytotoxicity of LEC was found to require the pore-forming activity of its PFT pneumolysin (**Fig 2A, B**). What is more, when A549 cells were treated with inhibitors of MLKL, necrosulfonamide (NSA) (**Fig 2A**) or RIPK3, GSK' 872 (**Fig. S3A**), the enhanced sensitivity of these cells to *Spn* killing was lost. Challenge of IAV-infected A549 cells with recombinant pneumolysin (rPly) or α -toxin (the PFT of *Staphylococcus aureus*, the second most common isolate during SBI to influenza (Morris et al., 2017)), recapitulated the potentiation of cell cytotoxicity observed with live bacterial infection (**Fig. S3B-C**). Potentiation of necroptosis by IAV was confirmed by immunoblot and immunofluorescent staining both which showed enhanced amounts of p-MLKL in A549 cells (**Fig. S3D-F**). Further supporting a key role for necroptosis was the observation that A549 cells deficient in MLKL were protected against exacerbated PFT-mediated cell death after influenza infection (**Fig. 2C**). Moreover, that the same results were observed with primary normal human bronchiolar epithelial cells (nHBE) *ex vivo* (**Fig. S3G**). Together, our data provides evidence that necroptosis is the main contributor of cell necrosis during co- and secondary infection. Notably, caspase inhibition (**Fig. S2**) did not confer significant protection suggesting a smaller role for TLR and inflammasome signaling (apoptosis and pyroptosis) in the potentiation of cell death. In support of these results, we have previously demonstrated that pneumolysin alone leads to death receptor-independent necroptosis in pulmonary epithelial cells (Gonzalez-Juarbe et al., 2017).

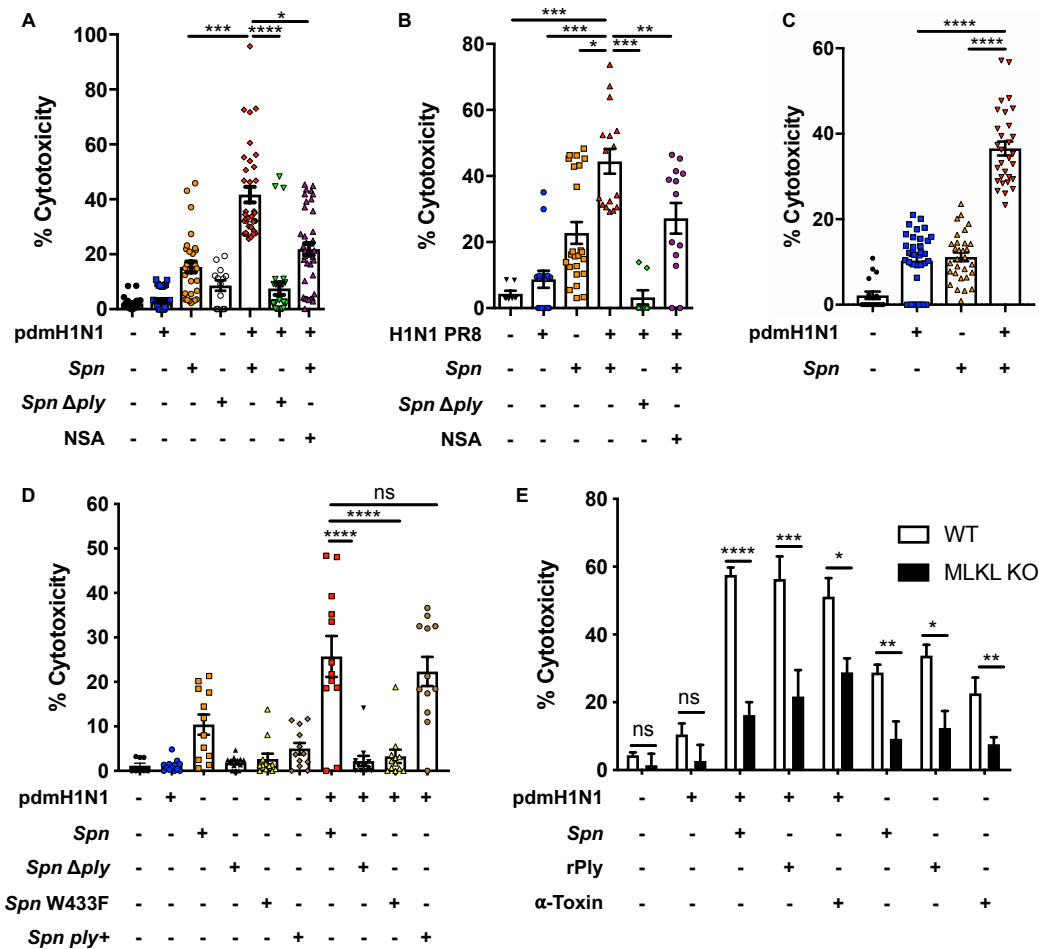


Figure 2: IAV infection promotes PFT-mediated cell death. LDH release was measured from A549 cells following infection with influenza **A**) A/California/7/2009 (pdmH1N1) and **B**) PR8 H1N1 at a MOI of 2 for 2 hours and challenge with wildtype *Spn* (*Spn*, in house strain) or Ply deficient derivative (*Spn* Δ *ply*) at an MOI of 10 for 4 additional hours. Cells were treated with necrosulfonamide (NSA, 10 μ M) when indicated. **C**) LDH release was measured from MH-S alveolar macrophages following infection workflow as in A. **D**) LDH cytotoxicity assay of supernatants from A549 cells was performed following infection with pdmH1N1 at an MOI of 2 for 2 hours and challenge with *Spn* strains and mutants obtained from Dr. Jeffrey Weiser at an MOI of 10 for 4 hours: (Zafar *et al.*, 2017)²⁹ (Zafar *et al.*, 2017) (Zafar *et al.*, 2017) (Zafar *et al.*, 2017) (Zafar *et al.*, 2017) *Spn* TIGR4 WT (*Spn*), Ply deficient mutant (*Spn* Δ *ply*), Ply point mutant deficient in pore formation (*Spn* W433F), and corrected mutant (*Spn* *ply*⁺). **E**) Cytotoxicity of A549 wildtype (white bars) or A549 MLKL deficient cells (dotted bars) was measured following the same challenge model as in panel a using *Spn*, recombinant pneumolysin (rPly), or alpha-toxin (α -Toxin). Individual data points in all *in vitro* assays represent all technical replicates collected from 3 separate experiments.

IAV-induced oxidative stress sensitizes cells *in vitro* for PFT-mediated necroptosis.

IAV-mediated oxidative stress has potent effects on pulmonary epithelial cells and the immune system (Liu et al., 2017). Therefore, it seemed plausible that the oxidative stress induced by the virus may be contributing towards the potentiation of pneumolysin-mediated necroptosis. In support of this notion, we observed that respiratory epithelial cells challenged *in vitro* with pdmH1N1 or PR8 showed increased levels of lipid peroxidation (**Fig. 3A, Fig. S4A**) as measured by MDA and cellular ROS (**Fig. 3B, Fig. S4B**) as measured using H₂-DCF. Importantly, and despite not having an effect on viral titers during the course of infection (**Fig. 3C**), pretreatment of A549 cells with the superoxide dismutase mimetic Tempol (Brissac et al., 2017) prior to viral challenge reduced cell death and MLKL activation in co-infected cells (**Fig. 3D-E**). Directly implicating oxidative stress as a primer for PFT-induced necroptosis, treatment of cells with paraquat (Gonzalez-Juarbe *et al.*, 2015a) enhanced the toxicity of rPly towards LEC and the observed potentiating effect of paraquat was abolished by treatment with Tempol (**Fig. 3F**). Identical results were observed using nHBE *ex vivo* (**Fig. 3G**) and replicated by addition of exogenous H₂O₂ in place of paraquat to A549 epithelial cells prior to rPly challenge (**Fig. S4C**). Note that *Spn* also produces H₂O₂ via its metabolic enzyme SpxB (Brissac *et al.*, 2017). Yet, IAV potentiation of cell death was also observed in A549 cells challenged with *Spn* Δ *spxB* (**Fig. S4D**), indicating that the priming effect of viral-induced ROS was sufficient. Importantly, inhibition of ROS in A549 cells with rotenone + thallium trifluoroacetate (mitochondria-dependent ROS inhibitor), apocynin (ADPH-dependent ROS inhibitor), allopurinol (xanthine oxidase-dependent ROS inhibitor) or mefenamic acid (cyclooxygenase-dependent ROS inhibitor) all conferred protection

against death caused by co-infection (**Fig. 3H**). This results suggested that ROS potentiation of necroptosis may come from multiple cellular sources. Lastly, and to further probe the specificity of oxidative stress as a primer for necroptosis, we tested whether blockage of viral neuraminidase activity with oseltamivir (Takahashi et al., 2003) or treatment of cells with Pimodivir (VX-787) (Byrn et al., 2015), a non-nucleoside polymerase basic protein 2 subunit inhibitor, impacted cell death. Neither of which did (**Fig. S5A-B**), despite the fact that viral titers were decreased by Pimodivir treatment (**Fig. S5C**).

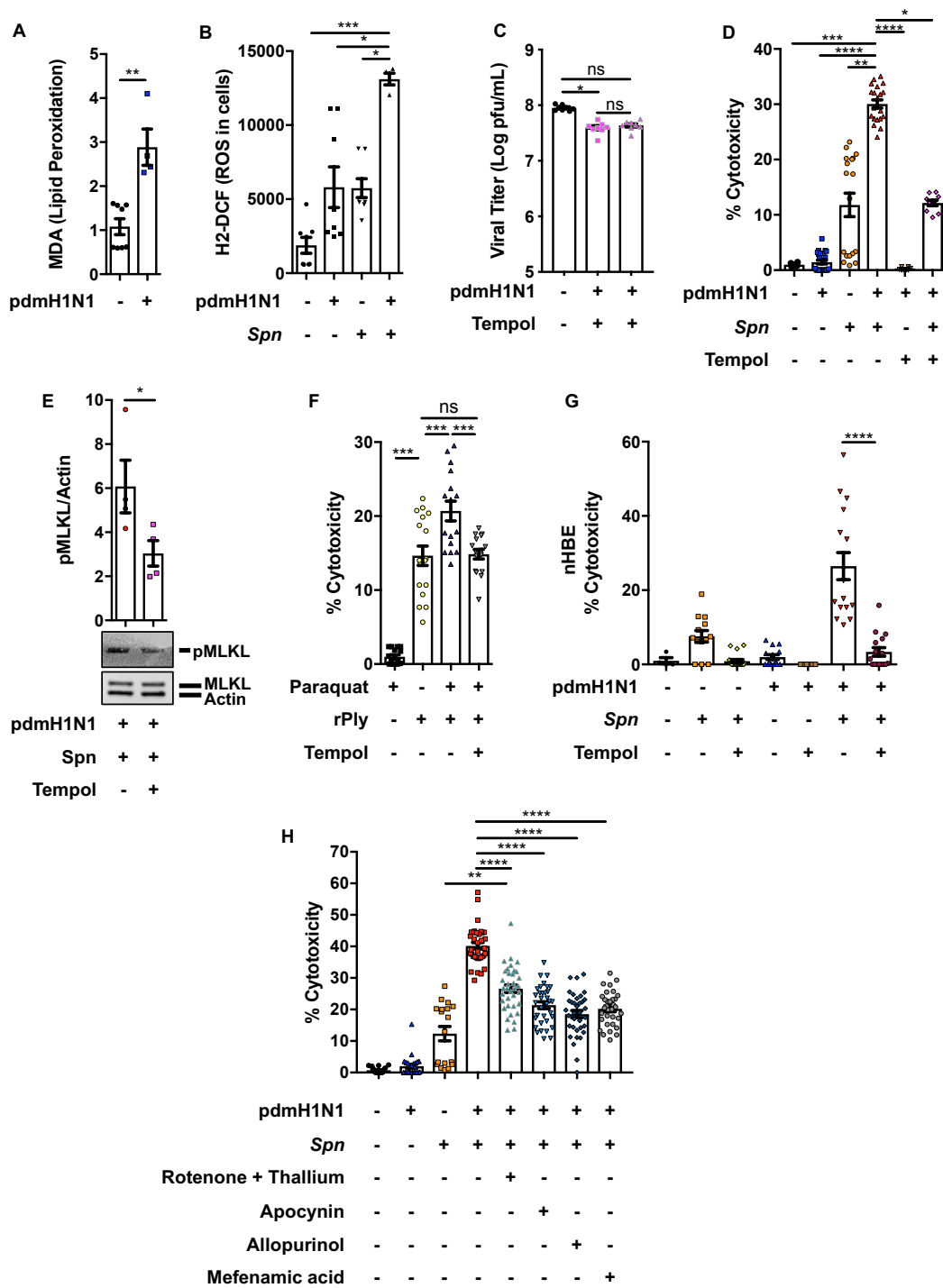


Figure 3: IAV-mediated oxidative stress potentiates pneumolysin-mediated necroptosis. **A)** Lipid peroxidation levels 4-hours after challenge with pdmH1N1 was measured by MDA. **B)** Levels of cellular ROS measured in A549 cells infected with pdmH1N1 at a MOI 2 for 2 hours then challenged with *Spn* at a MOI of 10 for 2 more hours. **C)** Viral titers quantified (Log PFU/mL) in A549 cells treated with Tempol (20 μ M) for 1-hour or 24-hours. **D)** Cytotoxicity and **E)** corresponding p-MLKL levels in A549 cells that were pre-treated with Tempol for 1-hour, infected with pdmH1N1 at a MOI 2 for 2 hours, then challenged with *Spn* at an MOI of 10 for 4 additional hours. **F)** Cytotoxicity was measured in A549 cells pre-treated with Tempol, then treated with Paraquat (10 μ M) for additional 2 hours, followed by challenge with rPly (0.1 μ g) for 2 hours. **G)** Cytotoxicity of *ex vivo* cultured primary normal human bronchial epithelial cells pre-treated with Tempol for 1-hour, infected with pdmH1N1 at a MOI 2 for 2 hours, and challenged with *Spn* at an MOI of 10 for 4 additional hours. **H)** LDH release from A549 cells pretreated with Rotenone + Thallium trifluoroacetate (10 nM/mL/10 nM/mL), a mitochondria-dependent ROS inhibitor; Apocynin (1 μ M/mL), a NADPH-dependent ROS inhibitor; Allopurinol (10nM/mL), a xanthine oxidase-dependent ROS inhibitor; and Mefenamic acid (20nM/mL), a cyclooxygenase-dependent ROS inhibitor following IAV and *Spn*, individually and together. Individual data points in all *in vitro* assays represent all technical replicates collected from 3 separate experiments.

IAV induced oxidative stress remains beyond viral clearance and maintains

susceptibility to bacterial toxin mediated necroptosis. We examined whether residual oxidative stress induced by IAV helped to explain the enhanced susceptibility to bacterial infection that occurs even after IAV is cleared; i.e. in a secondary infection model. Lung sections from pdmH1N1-challenged mice 10 days post-IAV infection showed considerable evidence of oxidative damage to DNA as well as lipid peroxidation (IF 8-Hydroxydeoxyguanosine and 4-Hydroxynonenal staining, respectively (Helbock et al., 1999; Kruman et al., 1997)) in pulmonary tissue (**Fig. 4A-D**). Notably, these mice were confirmed to not have detectable virus (**Fig. 4E**). Similar to co-infection results (see Fig 1), if these mice were challenged with *Spn*, we observed a >100-fold increase in bacterial lung titers 2 days after *Spn* challenge (**Fig. 5A**). This was concomitant with greater lung consolidation, immune cell infiltration (**Fig. S6**), and substantially enhanced levels of lung necroptosis in co-infected mice versus those with *Spn* alone (**Fig. 5B-D**).

Importantly, mice challenged with TIGR4 Δply in our secondary infection model had MLKL activation levels and bacterial titers equivalent to our negative control, i.e. mice infected with wildtype TIGR4 but also receiving the necroptosis inhibitor Nec-1s (**Fig. 5E-G, Fig. S7**). What is more, TIGR4 Δply challenged IAV-infected mice had decreased mortality versus controls (**Fig. 5H**). Interestingly, Tempol treatment at 12 and 24 hours post-*Spn* infection reduced the amount of necroptosis occurring in the airway in our secondary IAV/*Spn* infection model. This was despite not having an observed effect on *in vivo* levels of lipid oxidation (**Fig. 6A-E**). Tempol treatment also reduced bacterial burden within the airway of infected mice (**Fig. 6F**). Thus, necroptosis sensitizing ROS

is primarily due to the virus, persisted beyond detectable IAV infection, and acted directly to sensitize the cell for necroptosis.

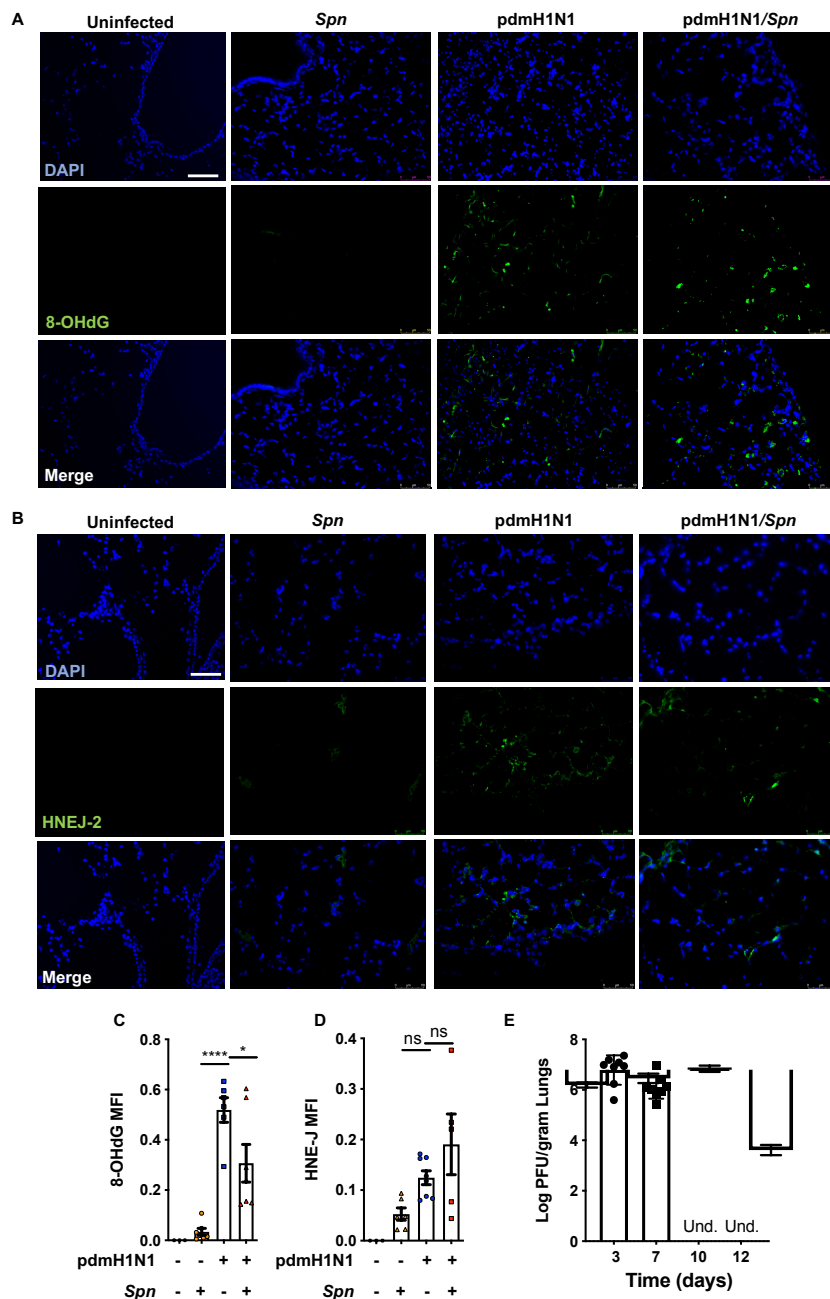


Figure 4: IAV-mediated oxidative stress persists after virus clearance *in vivo*. 8-week-old C57Bl/6 mice were intranasally infected with A/California/7/2009 (pdmH1N1) and 10 days later challenged intratracheally with *S. pneumoniae* (*Spn*). Mice were euthanized 48 hours after secondary infection (n=6-8 mice). Shown are representative immunofluorescent lung sections stained for **A**) 8-Hydroxydeoxyguanosine (8-OHdG) and **B**) 4-Hydroxynonenal (HNE-J). White bar denotes 50 μ m. **C-D**) Quantification of the mean fluorescent intensity (MFI) of 8-OHdG and HNE-J staining's, respectively, was performed. **E**) Viral titers (Log PFU/gram) in lungs at days 3, 7, 10 and 12 post-IAV infection (n=8 mice per group) are indicated. For *in vivo* experiments, each individual data point represents an individual animal sample.

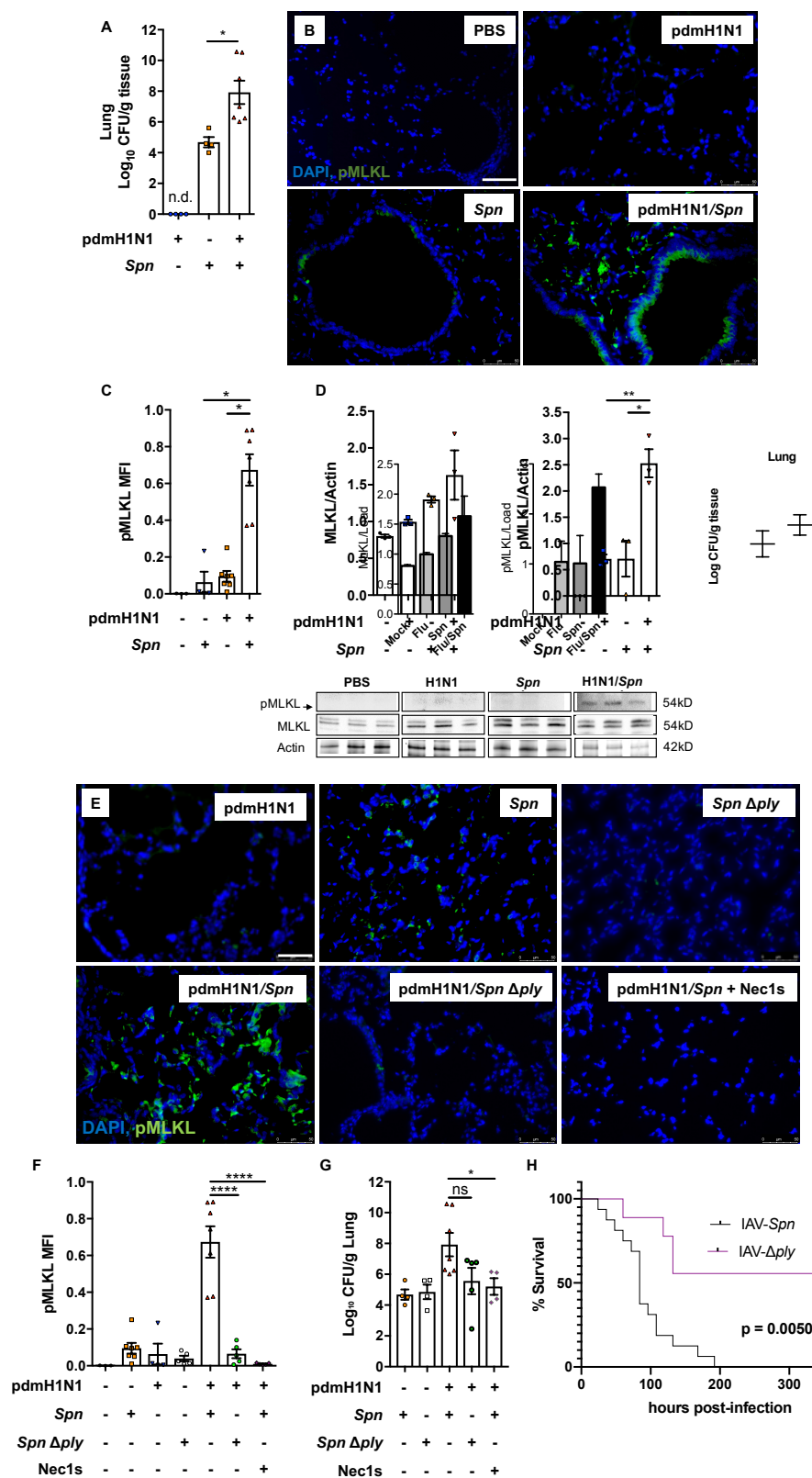


Figure 5: Influenza infection potentiates pneumolysin induced necroptosis activation during secondary *S. pneumoniae* challenge. 8-week-old C57Bl/6 mice were intranasally infected with A/California/7/2009 (pdmH1N1) and 10 days later challenged intratracheally with *S. pneumoniae* (*Spn*). Mice were euthanized 48 hours after secondary infection (n=3-7 mice). Shown are **A**) bacterial titers in homogenized lung samples, as well as **B**) representative images of corresponding lung sections stained for p-MLKL (3 sections stained per mouse). White bar denotes 50 μ m. **C**) Mean fluorescent intensity (MFI) for p-MLKL activity was measured. **D**) Densitometry and western blots for p-MLKL, MLKL and actin from mock, *Spn*, pdmH1N1 and pdmH1N1/*Spn* infected mice (n=3/cohort). **E-G**) 8-week-old C57Bl/6 mice were intranasally infected with A/California/7/2009 (pdmH1N1) and 10 days later challenged intratracheally with *Spn* or *Spn* Δ ply. Mice were euthanized 48 hours after secondary infection (n=4-7 mice). Treatment with Nec1s was done intraperitoneally at 12 and 24 hours following bacterial challenge. **E**) Shown are representative images of lung tissue sections stained for p-MLKL (separate points are average of 3 pictures per mouse) and **F**) mean fluorescent intensity of pMLKL staining. Corresponding **G**) lung bacterial titers (CFU/g tissue) calculated. **H**) Survival of C57Bl/6 mice following intranasal infection with pdmH1N1 for 10 days and subsequent intratracheal challenge with *Spn* or *Spn* Δ ply was monitored. For *in vivo* experiments, each individual data point represents an individual animal sample.

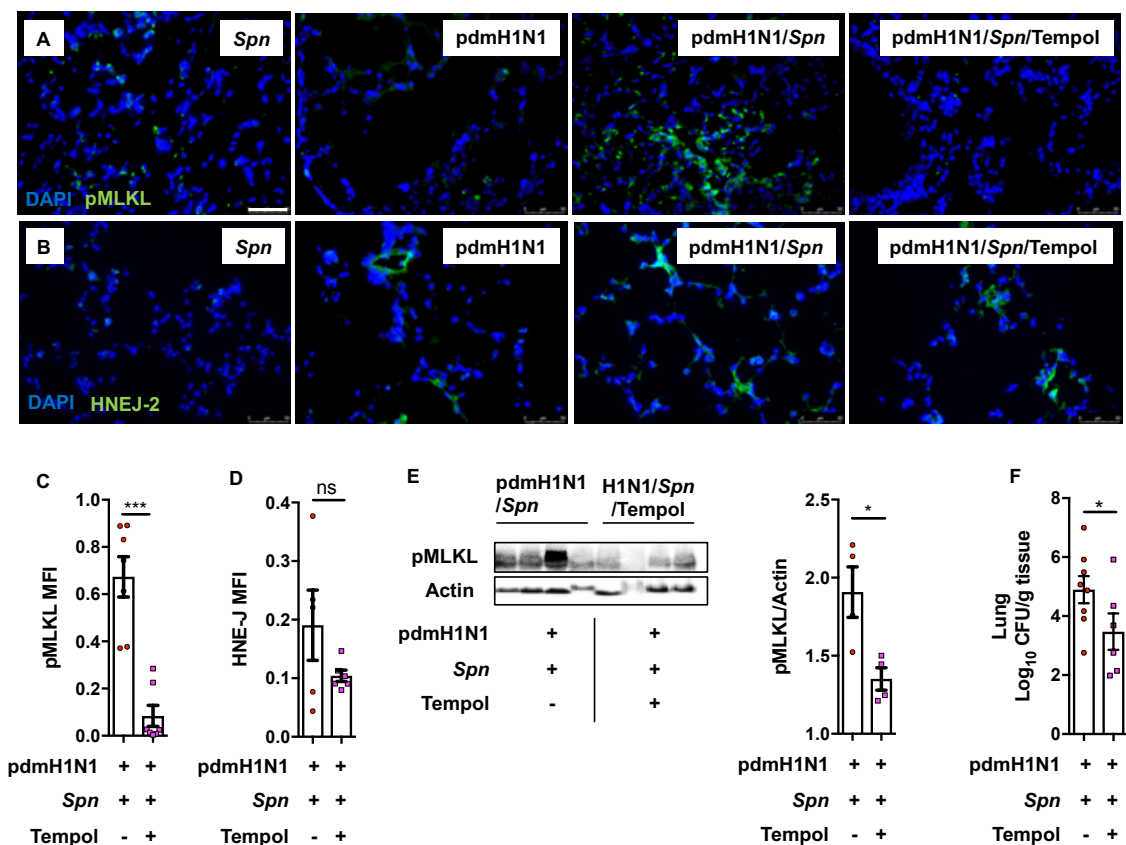


Figure 6: Therapeutic neutralization of ROS reduces necroptosis activation during secondary bacterial pneumonia. 8-week-old C57Bl/6 mice were intranasally infected with A/California/7/2009 (pdmH1N1) and 10 days later challenged intratracheally with *S. pneumoniae* (*Spn*). Mice were euthanized 48 hours after secondary infection (n=5-8 mice). Tempol treatment was done intraperitoneally at 12 and 24 hours post bacterial infection. Representative images of lung sections immunofluorescent stained for **A)** p-MLKL and **B)** 4 Hydroxynonenal (HNE-J). White bar denotes 50 μ m. **C-D)** Quantification of the mean fluorescent intensity (MFI) in corresponding captured images. **E)** Immunoblot for pMLKL and actin of pdmH1N1 infected mice, challenged with *Spn* with subsequent Tempol treatment and its densitometry quantification. **F)** Bacterial titers measured in lungs at time of death. For *in vivo* experiments, each individual data point represents an individual animal sample.

***In vivo* necroptosis inhibition reduces severity of secondary bacterial infection to influenza.** While no changes in oxidative stress induced DNA damage were observed (**Fig. 7A-B**), MLKL deficient mice with secondary *Spn* infection had reduced bacterial titers, reduced lung consolidation, and a reduction in overall TUNEL positive staining in lung sections (a general marker of cell death) (**Fig. 7C-G**). In addition, lungs of MLKL KO Mice showed decreased levels of IFN- α and - β , suggesting a possible role for necroptosis in the IFN response during secondary infections (**Fig. 7H-I**). Most importantly, MLKL KO mice had greater survival versus control in our secondary infection model (**Fig. 7J**). Altogether, our results implicate oxidative-stress enhanced PFT-mediated necroptosis activity as a major driver of disease severity and lung injury during co- and secondary infections to influenza.

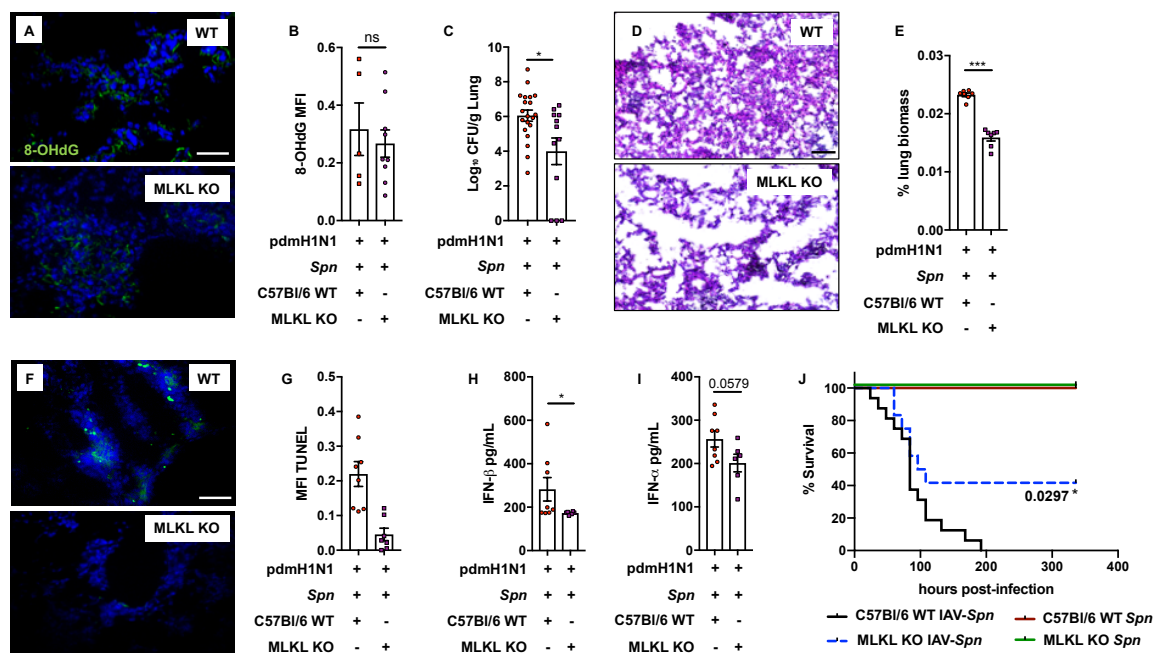


Figure 7: Inhibition of necroptosis reduces disease severity and tissue injury during secondary bacterial pneumonia. 8-week-old C57Bl/6 mice were intranasally infected with A/California/7/2009 (pdmH1N1) and 10 days later challenged intratracheally with *S. pneumoniae* (*Spn*, 1000CFU). Mice were euthanized 48 hours after secondary infection ($n > 12$ mice). **A)** IF of 8-Hydroxydeoxyguanosine (8-OHdG) White bar denotes 50 μ m. **B)** Quantification of the mean fluorescent intensity (MFI) of 8-OHdG staining's. **C)** Measured bacterial titers in homogenized lungs. **D)** Representative H&E staining of corresponding tissue sections. Black bar denotes 100 μ m. **E)** Lung consolidation in tissue sections as measured using ImageJ (white space versus lung area, separate points are the average of 3 pictures per mouse). **F)** TUNEL stain (white bar denotes 50 μ m) and **G)** mean fluorescent intensity of TUNEL stain quantified in lung sections. **H)** IFN- β and **I)** IFN- α levels (pg/mL) in lung homogenates. **J)** Survival of 8-week-old WT and MLKL KO-C57Bl/6 in the secondary *Spn* infection model ($n = 8-12$). For *in vivo* experiments, each individual data point represents an individual animal sample.

DISCUSSION

The molecular mechanisms of IAV subversion of cellular defenses and programmed cell death continues to be investigated (Balachandran and Rall, 2020; Yeganeh et al., 2013). Only recently has it become apparent that necroptosis is essential for control of virus replication during infection (Nogusa *et al.*, 2016). Herein, we demonstrate that oxidative stress triggered by IAV infection plays a role in the potentiation of PFT-induced necroptosis in respiratory cells and thereby worsens injury. What is more, pharmacological blocking of ROS from distinct sources conferred protection against IAV-induced sensitization to PFT-induced necroptosis.

Oxidative stress is pleiotropic and capable of oxidizing proteins and lipid membranes, damaging nucleic acid, and potentially altering cellular energy levels or ion homeostasis of the cell (Sies et al., 2017). The latter were shown to be triggers for non-canonical activation of necroptosis within bacteria-infected cells (Gonzalez-Juarbe *et al.*, 2018; Gonzalez-Juarbe *et al.*, 2017; Gonzalez-Juarbe *et al.*, 2015a). Importantly, in this study, increased susceptibility to PFT-mediated necroptosis was still observed even when IAV replication was blocked with Pimodivir. Moreover, Tempol-mediated protection against priming for PFT killing was applicable to both the co-infection and secondary infection scenario, the latter when virus is no longer present. This suggests the mechanism responsible for IAV-mediated necroptosis potentiation is directly affected by acute intracellular ROS levels and independent of viral replication. Whether and how the latter pathways are sensitized as result of IAV induced ROS or if an independent mechanism is responsible remains unclear, and detailed studies are now warranted to discern key similarities and differences between these events.

Necroptosis is inflammatory and therefore a “dual-edged sword” important towards instigating a robust immune response, but also detrimental under conditions where it is excessive (Balachandran and Rall, 2020; Yeganeh *et al.*, 2013). Along such lines, sensitization to necroptosis most likely contributes to a variety of clinical problems during co- and secondary pneumonia marked by excessive inflammation such as acute respiratory distress syndrome and sepsis; both a direct consequence of the enhanced level of cell death and release of pro-inflammatory alarmins. It is noteworthy that IAV has been specifically demonstrated to drive *Spn* development of otitis media (Tong *et al.*, 2000), which is recognized to be chronic inflammatory state. Critically it is unknown if other viruses enhance permissiveness for PFT-mediated necroptosis and this is an important avenue of future investigation. In support of this notion, a wide variety of viruses have been shown to induce oxidative stress in host cells by a variety of means (Schwarz, 1996). For example, respiratory syncytial virus does so by modulating levels of antioxidant enzymes (Hosakote *et al.*, 2009) and has recently been shown to induce necroptosis in children and in a neonatal mouse model of infection (Simpson *et al.*, 2020). Thus, it is likely that this phenomena is not restricted to IAV. Our prior published work (Gonzalez-Juarbe *et al.*, 2017; Gonzalez-Juarbe *et al.*, 2015a), and that with *S. aureus* α -toxin herein, which showed a wide variety of PFT-producing bacteria can instigate necroptosis of LEC suggests viral-enhanced PFT-mediated necroptosis is not restricted to the pathogen *Spn*. Thus, this synergy may be an important contributor to enhanced disease severity at other anatomical sites where virus and bacteria can co-infect.

Here we demonstrate the critical role of pneumolysin in inducing cell necroptosis during secondary infections to influenza. Interestingly, Wolf et al. have shown that prior exposure of mice to a pneumolysin overexpressing *Spn* strain conferred protection against virus-induced morbidity and lung pathology. The authors concluded that immunity mounted against pneumolysin and its modulation of macrophage activity via arginase-1 reduces severity of infection post re-challenge with pneumococcus and/or influenza infection (Wolf et al., 2014). A recent publication by our group also demonstrated that pneumolysin induction of necroptosis during bacterial colonization initiated low levels of inflammation required for the generation of an antibody-based response against *Spn* (Riegler *et al.*, 2019). These findings suggest that the order which the host is exposed to virus and bacteria has a profound impact on outcomes. Along such lines, McCullers et al showed in 2002 that *Spn* infection preceding IAV conferred protection against secondary bacterial challenge, whereas the reverse order of infection resulted in the dramatic sensitization to *Spn* that is studied herein (McCullers and Rehg, 2002). We now recognize IAV-induced susceptibility to necroptosis via oxidative stress as one contributing factor for this sequence-dependent sensitization.

Of note and during infection, other cells, particularly innate immune cells, also produce copious amounts of ROS (Chen et al., 2018) and these too may contribute to sensitization of LEC. Along such lines, To *et al.* recently showed that influenza infection promotes mitochondrial derived ROS and this in itself is detrimental to the lung epithelium as measured by increased histopathological damage (To et al., 2020). Detailed studies are thereby required to better define the role of the bystander cells into these mechanisms as well as their own sensitivity to PFT-mediated killing during ROS

production. Our results showing no differences in caspase activation suggests the responsible mechanism is also independent of canonical apoptotic and pyroptotic pathways, although it is likely these mechanisms are contributory to overall disease and occurring in parallel during natural infection. This is in agreement with our previous observation that showed pneumolysin is able to initiate necroptosis in a death receptor (TNFr, TLR4) independent manner and that caspase activity may occur in parallel with necroptosis to modulate inflammation (Gonzalez-Juarbe *et al.*, 2018; Gonzalez-Juarbe *et al.*, 2017).

Finally, our results suggest that inhibition of the necroptosis pathway may be a viable therapeutic treatment during IAV mediated co- or secondary infections, although the possibility remains that necroptosis inhibition may promote viral replication during co-infection, an aspect which needs to be studied carefully (unpublished results with primary NHBEs suggest it does not). It is also important to consider inhibition of RIPK1 and RIPK3 will have effects on aspects other than necroptosis as the pathway is linked to apoptosis, NF- κ B signaling, inflammation and responses to ion changes (He and Wang, 2018). For this reason targeting of MLKL alone may be preferable as it will not inhibit the ability of the cell to drive other responses beneficial against infection and reduce necrotic tissue damage and excess inflammation (Moreno-Gonzalez *et al.*, 2016). Altogether, our results provide a molecular explanation for how influenza infection enhances permissiveness for secondary bacterial infection. We demonstrate that PFT-mediated necroptosis is enhanced as result of oxidative stress cause by prior or ongoing viral replications. Increased sensitivity to PFT-mediated necroptosis in turn worsens pulmonary damage and creates an environment that is further permissive for bacterial

replication. The fact that oxidative stress induced by virus and PFT production are common across a wide range of viral and bacterial pathogens, respectively, suggests this is an important aspect of human infectious disease pathogenesis.

Author Contributions: NG-J, KSH and CJO wrote and edited the paper. NG-J, ANR, RPG, ASJ, KSH, PHD, CMP and CJO designed the experiments. NG-J, ANR, RPG, JB, JET, PHD, NRS, MPP and ASJ executed the experiments.

Acknowledgment: NG-J received support from NIH training grant AI007051 and J. Craig Venter Institute start-up funds. ASJ received training support from NIH grant GM008111. ANR received support from training grant AI007051. CMP was supported by NIH AI134693. KSH received support from NIH AI111475. PHD was supported by NIH grants AI070412, CA17286, AI113724 and RP140565 from CPRIT. CJO received support from NIH grants AI114800, AG055144 and AHA grant 16GRNT30230007. MLKL KO mice were made available by Dr. Warren Alexander (Walter and Eliza Hall Institute of Medical Research Parkville, Victoria, Australia) (Murphy *et al.*, 2013).

Declaration of Interest: The authors declare no competing interests.

Lead Contact. Further information and requests for resources and reagents should be directed to and will be fulfilled by the Lead Contact, Dr. Gonzalez-Juarbe

(ngonzale@jcvl.org).

Materials Availability. This study did not generate new unique reagents.

Data and Code Availability Statement. This study did not generate/analyze datasets/code.

EXPERIMENTAL MODEL AND SUBJECT DETAILS

Ethics Statement. Animal experiments were approved by the Institutional Animal Care and Use Committee at The University of Alabama at Birmingham (Protocol # 20358). Human LEC were harvested from whole lung sections obtained from the International Institute for the Advancement of Medicine (Fulcher *et al.*, 2005). The use of primary tissue, obtained in de-identified fashion, does not meet the criteria for human subject research.

IAV and *Spn*. Pandemic H1N1 A/California/7/2009 (pdmH1N1) and H1N1 A/Puerto Rico/8/1934 (PR8) influenza viruses were propagated in MDCK cells. *Spn* serotype 4 strain TIGR4 and its derivatives were used for all studies (Tettelin *et al.*, 2001). TIGR4 mutants deficient in *ply* (Δply), the gene encoding pneumolysin, and *spxB* ($\Delta spxB$), the gene encoding pyruvate oxidase, have been described (Lizcano *et al.*, 2010). We also used mutants provided by Dr. Jeffrey Weiser (New York University, NY). These were matched strains of TIGR4 (TIGR4_{JW}), TIGR4 lacking pneumolysin, TIGR4_{JW} Δply , a TIGR4 point mutant deficient in pore formation (TIGR4_{JW} W433F), and a corrected mutant (TIGR4_{JW} *ply*+) (Zafar *et al.*, 2017); these were used as a set. Recombinant

pneumolysin (rPly) was purified from *E. coli* (Brown *et al.*, 2014). *Staphylococcus aureus* alpha-toxin was purchased (Sigma-Aldrich, St. Louis, MO).

Animal strains and infections. Male and female 8-week-old C57BL/6 mice were obtained from Taconic Biosciences (Rensselaer, NY). MLKL KO mice were made available by Dr. Warren Alexander (Walter and Eliza Hall Institute of Medical Research Parkville, Victoria, Australia) (Murphy *et al.*, 2013). For IAV/*Spn* co-infection, 8-week-old C57BL/6 mice were intranasally challenged with 250 PFU PR8. Five days post-influenza challenge, mice received by forced aspiration 5×10^5 CFU *Spn* (Gonzalez-Juarbe *et al.*, 2015b). For the co-infection model we use an LD₅₀ of *Spn* to demonstrate bacterial infection was on its own capable of causing disease, yet this was augmented in a co-infection model. For studies involving *Spn* secondary infection, i.e. after viral clearance, mice were challenged with 250 PFU pdmH1N1 and ten days post-influenza, challenged with 10^3 CFU *Spn*. In all the secondary infection mouse models the *Spn* dose chosen was a sublethal (1000 CFU/mL) since the mice were challenged for 10-days with IAV, thus making the mice extremely susceptible to the bacterial infection (Gill *et al.*, 2010; Louie *et al.*, 2009).

Cell Infections. A549 type II alveolar epithelial cells (Fulcher *et al.*, 2005), MH-S mouse alveolar macrophages (Saxena *et al.*, 2008), and primary normal human bronchiolar epithelial cells (Fulcher *et al.*, 2005), were infected with IAV at MOI 2 for 2 hours, and subsequently challenged with *Spn* at an MOI 10 for 4 hours. As our purpose was to characterize the cellular responses to influenza infection in regard to potentiation of

bacteria induced cell death without the complication of cell lysis caused by late stage replication we used a high infectious dose and short time period. Other investigators have used the same approach (Hoffmann *et al.*, 2016). The majority of chemical inhibitors were obtained from Sigma-Aldrich. Exceptions include necrosulfonamide (Tocris Bioscience, QL, UK), GSK'872 and Nec1s (BioVision, Milpitas, CA), oseltamivir carboxylate (MCE, Monmouth, NJ), TNFR inhibitor R-7050 and TNF- α inhibitor SPD-304 (Cayman Chemicals, Ann Arbor, MI) and Pimodivir (AdooQ Bioscience, Irvine, CA). Cells receiving inhibitors were treated continuously beginning 1-hour prior to IAV infection and inhibitor was maintained in the media until the end of the experiment. Pimodivir treated cells received the drug 2-hours prior to IAV challenge. A549 cells deficient in MLKL have been previously described (Gonzalez-Juarbe *et al.*, 2018). Cell death was evaluated by detection of lactate dehydrogenase (LDH) in culture supernatants (Gonzalez-Juarbe *et al.*, 2015a). The presence of reactive oxygen species (ROS) was measured with the H₂-DCF assay (Thermo Fisher Scientific, Waltham, MA). Lipid peroxidation was detected with the lipid peroxidation malondialdehyde (MDA) assay (Abcam). Antibodies against 8-hydroxydeoxyguanosine, an oxidative stress-mediated DNA damage marker, and HNE-J, a lipid peroxidation marker, were purchased (Abcam).

METHOD DETAILS

Histology and Microscopy. The methods used for tissue processing, sectioning, and immunofluorescent microscopy are described (Gilley *et al.*, 2016; Gonzalez-Juarbe *et al.*, 2017; Gonzalez-Juarbe *et al.*, 2015b). Briefly, tissue sections were fixed with cold acetone (-20°C), in 70% ethanol (-20°C). then rehydrated in PBS. The sections were

then blocked \ in 3% goat serum–3% bovine serum albumin (BSA) for 30min. Each primary antibody used was diluted at 1:500 in the blocking solution and incubated over the tissue for 40 min. After incubation, sections were washed 3 times with PBS–0.05% Tween 20. Then sections were stained with secondary antibody diluted at 1:1000 in blocking solution and incubated over sections for 30 min. Slides were then washed 3 times and mounted with ProLong Gold Antifade reagent containing DAPI (4',6'-diamidino-2-phenylindole) (Life Technologies, Carlsbad CA). For histology, formalin fixed slides were stained with hematoxylin, then washed, subsequently stained with eosin. Tissue was washed again and mounted with Cytoseal (ThermoFisher, Waltham, MA). Images were captured using a Zeiss AxioXam MRm Rev3 and/or MRc cameras attached to a Zeiss AxioImager Z1 epifluorescent microscope (Carl Zeiss, Thornwood, NY) or a Leica LMD6 with DFC3000G-1.3-megapixel monochrome camera (Leica Biosystems, Buffalo Grove, IL). TUNEL (Promega, Madison, WI) and Annexin V (Abcam, Cambridge, UK) staining was done per manufacturer's instruction. Cleaved caspase-3 staining was done using anti-cleaved-caspase-3 antibody (Abcam). Mean fluorescent intensity and densitometry of immunoblots was measured using ImageJ (Schindelin *et al.*, 2015).

Immunoblots and ELISA. Western blots were done as previously described (Riegler *et al.*, 2019). Briefly, 10 µg of total protein was separated on a 10% polyacrylamide gel (Biorad) before transfer to a nitrocellulose membrane (Biorad). Membranes were blocked in 5% BSA and washed 3 times with TBS-0.1% Tween 20 (TBST). Membranes were incubated with anti -MLKL (1:1000, #37705, Cell Signaling Technologies), -p-MLKL (1:1000, #37333S, Cell Signaling Technologies) and -cytoskeletal actin (1:10000,

#A300-485A, Bethyl Laboratories Inc., Montgomery, TX), in 5% BSA overnight. Then, membranes were washed 3 times with TBST and incubated with HRP-conjugated goat antibody at 1:10,000 (ThermoFisher, Waltham, MA). After 3 additional washes, signal was detected using Clarity™ Western ECL and ChemiDoc XRS+ (both from Biorad). ELISA-based measurements for IFN- β , IFN- α and TNF- α were done using kits from PBL Assay Science (Piscataway, NJ) and InvivoGen (San Diego, CA). For each cytokine, 100 μ L of protein standard and supernatants of tissue homogenates were added to wells in a 96-well plate. Manufacturer instructions for washes and duration of detection antibody and HRP conjugate incubations were followed after initial sample incubation. Finally, absorbance or luminisence was read using a BioTek Synergy H4 plate reader (BioTek, Winooski, VT).

QUANTIFICATION AND STATISTICAL ANALYSIS

All results are displayed as standard error of the mean (SEM). In addition, individual data points in all *in vitro* assays represent all technical replicates collected from 3 separate experiments. For *in vivo* experiments, each individual data point represents an individual animal sample. Number of animals for *in vivo* experiments are denoted in the figure legends. For non-parametric multiple group analyses we used a Kruskal-Wallis H test with Dunn's post-hoc analysis. For parametric grouped analyses we used ANOVA with Sidak's post-hoc analysis. For data with a single independent factor of two groups we used a Mann-Whitney U test. Survival comparisons were assessed using Log-rank (Mantel-Cox) test. Asterisks denote the level of significance observed: * = $P \leq 0.05$; ** =

$P \leq 0.01$; *** = $P \leq 0.001$; **** = $P \leq 0.0001$. Statistical analyses were calculated using Prism 8 (GraphPad Software: La Jolla, CA).

REFERENCES

- Balachandran, S., and Rall, G.F. (2020). Benefits and Perils of Necroptosis in Influenza Virus Infection. *J Virol* 94. 10.1128/JVI.01101-19.
- Brand, J.D., Lazrak, A., Trombley, J.E., Shei, R.J., Adewale, A.T., Tipper, J.L., Yu, Z., Ashtekar, A.R., Rowe, S.M., Matalon, S., and Harrod, K.S. (2018). Influenza-mediated reduction of lung epithelial ion channel activity leads to dysregulated pulmonary fluid homeostasis. *JCI Insight* 3. 10.1172/jci.insight.123467.
- Brissac, T., Shenoy, A.T., Patterson, L.A., and Orihuela, C.J. (2017). Cell invasion and pyruvate oxidase derived H₂O₂ are critical for *Streptococcus pneumoniae* mediated cardiomyocyte killing. *Infect Immun*. 10.1128/IAI.00569-17.
- Brown, A.O., Mann, B., Gao, G., Hankins, J.S., Humann, J., Giardina, J., Faverio, P., Restrepo, M.I., Halade, G.V., Mortensen, E.M., et al. (2014). *Streptococcus pneumoniae* translocates into the myocardium and forms unique microlesions that disrupt cardiac function. *PLoS Pathog* 10, e1004383. 10.1371/journal.ppat.1004383.
- Byrn, R.A., Jones, S.M., Bennett, H.B., Bral, C., Clark, M.P., Jacobs, M.D., Kwong, A.D., Ledebor, M.W., Leeman, J.R., McNeil, C.F., et al. (2015). Preclinical activity of VX-787, a first-in-class, orally bioavailable inhibitor of the influenza virus polymerase PB2 subunit. *Antimicrob Agents Chemother* 59, 1569-1582. 10.1128/AAC.04623-14.
- Chen, Y., Zhou, Z., and Min, W. (2018). Mitochondria, Oxidative Stress and Innate Immunity. *Front Physiol* 9, 1487. 10.3389/fphys.2018.01487.

Clayville, L.R. (2011). Influenza update: a review of currently available vaccines. *P T* 36, 659-684.

Fulcher, M.L., Gabriel, S., Burns, K.A., Yankaskas, J.R., and Randell, S.H. (2005). Well-differentiated human airway epithelial cell cultures. *Methods Mol Med* 107, 183-206.

Gill, J.R., Sheng, Z.M., Ely, S.F., Guinee, D.G., Beasley, M.B., Suh, J., Deshpande, C., Mollura, D.J., Morens, D.M., Bray, M., et al. (2010). Pulmonary pathologic findings of fatal 2009 pandemic influenza A/H1N1 viral infections. *Arch Pathol Lab Med* 134, 235-243. 10.1043/1543-2165-134.2.235.

Gilley, R.P., Gonzalez-Juarbe, N., Shenoy, A.T., Reyes, L.F., Dube, P.H., Restrepo, M.I., and Orihuela, C.J. (2016). Infiltrated Macrophages Die of Pneumolysin-Mediated Necroptosis following Pneumococcal Myocardial Invasion. *Infect Immun* 84, 1457-1469. 10.1128/IAI.00007-16.

Gonzalez-Juarbe, N., Bradley, K.M., Riegler, A.N., Reyes, L.F., Brissac, T., Park, S.S., Restrepo, M.I., and Orihuela, C.J. (2018). Bacterial Pore-Forming Toxins Promote the Activation of Caspases in Parallel to Necroptosis to Enhance Alarmin Release and Inflammation During Pneumonia. *Sci Rep* 8, 5846. 10.1038/s41598-018-24210-8.

Gonzalez-Juarbe, N., Bradley, K.M., Shenoy, A.T., Gilley, R.P., Reyes, L.F., Hinojosa, C.A., Restrepo, M.I., Dube, P.H., Bergman, M.A., and Orihuela, C.J. (2017). Pore-forming toxin-mediated ion dysregulation leads to death receptor-independent necroptosis of lung epithelial cells during bacterial pneumonia. *Cell Death Differ* 24, 917-928. 10.1038/cdd.2017.49.

Gonzalez-Juarbe, N., Gilley, R.P., Hinojosa, C.A., Bradley, K.M., Kamei, A., Gao, G., Dube, P.H., Bergman, M.A., and Orihuela, C.J. (2015a). Pore-Forming Toxins Induce

Macrophage Necroptosis during Acute Bacterial Pneumonia. *PLoS Pathog* *11*, e1005337. 10.1371/journal.ppat.1005337.

Gonzalez-Juarbe, N., Mares, C.A., Hinojosa, C.A., Medina, J.L., Cantwell, A., Dube, P.H., Orihuela, C.J., and Bergman, M.A. (2015b). Requirement for *Serratia marcescens* cytolysin in a murine model of hemorrhagic pneumonia. *Infect Immun* *83*, 614-624. 10.1128/IAI.01822-14.

He, S., and Wang, X. (2018). RIP kinases as modulators of inflammation and immunity. *Nat Immunol* *19*, 912-922. 10.1038/s41590-018-0188-x.

Helbock, H.J., Beckman, K.B., and Ames, B.N. (1999). 8-Hydroxydeoxyguanosine and 8-hydroxyguanine as biomarkers of oxidative DNA damage. *Methods Enzymol* *300*, 156-166. 10.1016/s0076-6879(99)00123-8.

Hentrich, K., Löfling, J., Pathak, A., Nizet, V., Varki, A., and Henriques-Normark, B. (2016). *Streptococcus pneumoniae* Senses a Human-like Sialic Acid Profile via the Response Regulator CiaR. *Cell Host & Microbe* *20*, 307-317. <http://dx.doi.org/10.1016/j.chom.2016.07.019>.

Hoffmann, J., Machado, D., Terrier, O., Pouzol, S., Messaoudi, M., Basualdo, W., Espinola, E.E., Guillen, R.M., Rosa-Calatrava, M., Picot, V., et al. (2016). Viral and bacterial co-infection in severe pneumonia triggers innate immune responses and specifically enhances IP-10: a translational study. *Sci Rep* *6*, 38532. 10.1038/srep38532.

Hosakote, Y.M., Liu, T., Castro, S.M., Garofalo, R.P., and Casola, A. (2009). Respiratory syncytial virus induces oxidative stress by modulating antioxidant enzymes. *Am J Respir Cell Mol Biol* *41*, 348-357. 10.1165/rcmb.2008-0330OC.

Kruman, I., Bruce-Keller, A.J., Bredesen, D., Waeg, G., and Mattson, M.P. (1997).

Evidence that 4-hydroxynonenal mediates oxidative stress-induced neuronal apoptosis. *J Neurosci* *17*, 5089-5100.

Liu, M., Chen, F., Liu, T., Chen, F., Liu, S., and Yang, J. (2017). The role of oxidative stress in influenza virus infection. *Microbes Infect* *19*, 580-586.

10.1016/j.micinf.2017.08.008.

Lizcano, A., Chin, T., Sauer, K., Tuomanen, E.I., and Orihuela, C.J. (2010). Early biofilm formation on microtiter plates is not correlated with the invasive disease potential of *Streptococcus pneumoniae*. *Microb Pathog* *48*, 124-130. 10.1016/j.micpath.2010.01.002.

Louie, J.K., Acosta, M., Winter, K., Jean, C., Gavali, S., Schechter, R., Vugia, D., Harriman, K., Matyas, B., Glaser, C.A., et al. (2009). Factors associated with death or hospitalization due to pandemic 2009 influenza A(H1N1) infection in California. *JAMA* *302*, 1896-1902. 10.1001/jama.2009.1583.

McCullers, J.A., and Bartmess, K.C. (2003). Role of Neuraminidase in Lethal Synergism between Influenza Virus and *Streptococcus pneumoniae*. *Journal of Infectious Diseases* *187*, 1000-1009. 10.1086/368163.

McCullers, J.A., and Hayden, F.G. (2012). Fatal influenza B infections: time to reexamine influenza research priorities. *J Infect Dis* *205*, 870-872. 10.1093/infdis/jir865.

McCullers, J.A., and Rehg, J.E. (2002). Lethal synergism between influenza virus and *Streptococcus pneumoniae*: characterization of a mouse model and the role of platelet-activating factor receptor. *J Infect Dis* *186*, 341-350. 10.1086/341462.

McCullers, J.A., and Tuomanen, E.I. (2001). Molecular pathogenesis of pneumococcal pneumonia. *Front Biosci* *6*, D877-D889.

Moreno-Gonzalez, G., Vandenabeele, P., and Krysko, D.V. (2016). Necroptosis: A Novel Cell Death Modality and Its Potential Relevance for Critical Care Medicine. *Am J Respir Crit Care Med* *194*, 415-428. 10.1164/rccm.201510-2106CI.

Morens, D.M., Taubenberger, J.K., and Fauci, A.S. (2008). Predominant Role of Bacterial Pneumonia as a Cause of Death in Pandemic Influenza: Implications for Pandemic Influenza Preparedness. *Journal of Infectious Diseases* *198*, 962-970. 10.1086/591708.

Morris, D.E., Cleary, D.W., and Clarke, S.C. (2017). Secondary Bacterial Infections Associated with Influenza Pandemics. *Front Microbiol* *8*, 1041-1041. 10.3389/fmicb.2017.01041.

Murphy, J.M., Czabotar, P.E., Hildebrand, J.M., Lucet, I.S., Zhang, J.G., Alvarez-Diaz, S., Lewis, R., Lalaoui, N., Metcalf, D., Webb, A.I., et al. (2013). The pseudokinase MLKL mediates necroptosis via a molecular switch mechanism. *Immunity* *39*, 443-453. 10.1016/j.immuni.2013.06.018.

Nailwal, H., and Chan, F.K. (2019). Necroptosis in anti-viral inflammation. *Cell Death Differ* *26*, 4-13. 10.1038/s41418-018-0172-x.

Nogusa, S., Thapa, R.J., Dillon, C.P., Liedmann, S., Oguin, T.H., 3rd, Ingram, J.P., Rodriguez, D.A., Kosoff, R., Sharma, S., Sturm, O., et al. (2016). RIPK3 Activates Parallel Pathways of MLKL-Driven Necroptosis and FADD-Mediated Apoptosis to Protect against Influenza A Virus. *Cell Host Microbe* *20*, 13-24. 10.1016/j.chom.2016.05.011.

Pettigrew, M.M., Marks, L.R., Kong, Y., Gent, J.F., Roche-Hakansson, H., and Hakansson, A.P. (2014). Dynamic changes in the *Streptococcus pneumoniae*

transcriptome during transition from biofilm formation to invasive disease upon influenza A virus infection. *Infect Immun* 82, 4607-4619. 10.1128/iai.02225-14.

Riegler, A.N., Brissac, T., Gonzalez-Juarbe, N., and Orihuela, C.J. (2019). Necroptotic Cell Death Promotes Adaptive Immunity Against Colonizing Pneumococci. *Front Immunol* 10, 615. 10.3389/fimmu.2019.00615.

Saxena, R.K., Gilmour, M.I., and Hays, M.D. (2008). Isolation and quantitative estimation of diesel exhaust and carbon black particles ingested by lung epithelial cells and alveolar macrophages in vitro. *Biotechniques* 44, 799-805. 10.2144/000112754.

Schindelin, J., Rueden, C.T., Hiner, M.C., and Eliceiri, K.W. (2015). The ImageJ ecosystem: An open platform for biomedical image analysis. *Mol Reprod Dev* 82, 518-529. 10.1002/mrd.22489.

Schwarz, K.B. (1996). Oxidative stress during viral infection: a review. *Free Radic Biol Med* 21, 641-649. 10.1016/0891-5849(96)00131-1.

Shahangian, A., Chow, E.K., Tian, X., Kang, J.R., Ghaffari, A., Liu, S.Y., Belperio, J.A., Cheng, G., and Deng, J.C. Type I IFNs mediate development of postinfluenza bacterial pneumonia in mice. *The Journal of Clinical Investigation* 119, 1910-1920. 10.1172/JCI35412.

Sies, H., Berndt, C., and Jones, D.P. (2017). Oxidative Stress. *Annu Rev Biochem* 86, 715-748. 10.1146/annurev-biochem-061516-045037.

Simpson, J., Loh, Z., Ullah, M.A., Lynch, J.P., Werder, R.B., Collinson, N., Zhang, V., Dondelinger, Y., Bertrand, M.J.M., Everard, M.L., et al. (2020). Respiratory Syncytial Virus Infection Promotes Necroptosis and HMGB1 Release by Airway Epithelial Cells. *Am J Respir Crit Care Med* 201, 1358-1371. 10.1164/rccm.201906-1149OC.

Sun, K., and Metzger, D.W. (2008). Inhibition of pulmonary antibacterial defense by interferon-[gamma] during recovery from influenza infection. *Nat Med* *14*, 558-564.

http://www.nature.com/nm/journal/v14/n5/supinfo/nm1765_S1.html.

Takahashi, K., Furuta, Y., Fukuda, Y., Kuno, M., Kamiyama, T., Kozaki, K., Nomura, N., Egawa, H., Minami, S., and Shiraki, K. (2003). In vitro and in vivo activities of T-705 and oseltamivir against influenza virus. *Antivir Chem Chemother* *14*, 235-241.

10.1177/095632020301400502.

Tettelin, H., Nelson, K.E., Paulsen, I.T., Eisen, J.A., Read, T.D., Peterson, S., Heidelberg, J., DeBoy, R.T., Haft, D.H., Dodson, R.J., et al. (2001). Complete genome sequence of a virulent isolate of *Streptococcus pneumoniae*. *Science* *293*, 498-506.

10.1126/science.1061217.

Thapa, R.J., Ingram, J.P., Ragan, K.B., Nogusa, S., Boyd, D.F., Benitez, A.A., Sridharan, H., Kosoff, R., Shubina, M., Landsteiner, V.J., et al. (2016). DAI Senses Influenza A Virus Genomic RNA and Activates RIPK3-Dependent Cell Death. *Cell Host Microbe* *20*, 674-681. 10.1016/j.chom.2016.09.014.

To, E.E., Erlich, J.R., Liong, F., Luong, R., Liong, S., Easaq, F., Oseghale, O., Anthony, D., McQualter, J., Bozinovski, S., et al. (2020). Mitochondrial Reactive Oxygen Species Contribute to Pathological Inflammation During Influenza A Virus Infection in Mice. *Antioxid Redox Signal* *32*, 929-942. 10.1089/ars.2019.7727.

Tokars, J.I., Olsen, S.J., and Reed, C. (2018). Seasonal Incidence of Symptomatic Influenza in the United States. *Clin Infect Dis* *66*, 1511-1518. 10.1093/cid/cix1060.

Tong, H.H., Fisher, L.M., Kosunick, G.M., and DeMaria, T.F. (2000). Effect of adenovirus type 1 and influenza A virus on *Streptococcus pneumoniae* nasopharyngeal

- colonization and otitis media in the chinchilla. *Ann Otol Rhinol Laryngol* *109*, 1021-1027. 10.1177/000348940010901106.
- Upton, J.W., Shubina, M., and Balachandran, S. (2017). RIPK3-driven cell death during virus infections. *Immunol Rev* *277*, 90-101. 10.1111/imr.12539.
- van der Sluijs, K.F., Nijhuis, M., Levels, J.H., Florquin, S., Mellor, A.L., Jansen, H.M., van der Poll, T., and Lutter, R. (2006). Influenza-induced expression of indoleamine 2,3-dioxygenase enhances interleukin-10 production and bacterial outgrowth during secondary pneumococcal pneumonia. *J Infect Dis* *193*, 214-222. 10.1086/498911.
- van der Sluijs, K.F., van der Poll, T., Lutter, R., Juffermans, N.P., and Schultz, M.J. (2010). Bench-to-bedside review: Bacterial pneumonia with influenza - pathogenesis and clinical implications. *Critical Care* *14*, 1-8. 10.1186/cc8893.
- Vandenabeele, P., Galluzzi, L., Vanden Berghe, T., and Kroemer, G. (2010). Molecular mechanisms of necroptosis: an ordered cellular explosion. *Nat Rev Mol Cell Biol* *11*, 700-714. 10.1038/nrm2970.
- Wang, Y., Hao, Q., Florence, J.M., Jung, B.G., Kurdowska, A.K., Samten, B., Idell, S., and Tang, H. (2019). Influenza Virus Infection Induces ZBP1 Expression and Necroptosis in Mouse Lungs. *Front Cell Infect Microbiol* *9*, 286. 10.3389/fcimb.2019.00286.
- Wolf, A.I., Strauman, M.C., Mozdzanowska, K., Williams, K.L., Osborne, L.C., Shen, H., Liu, Q., Garlick, D., Artis, D., Hensley, S.E., et al. (2014). Pneumolysin expression by streptococcus pneumoniae protects colonized mice from influenza virus-induced disease. *Virology* *462-463*, 254-265. 10.1016/j.virol.2014.06.019.

Yeganeh, B., Rezaei Moghadam, A., Tran, A.T., Rahim, M.N., Ande, S.R., Hashemi, M., Coombs, K.M., and Ghavami, S. (2013). Asthma and influenza virus infection: focusing on cell death and stress pathways in influenza virus replication. *Iran J Allergy Asthma Immunol* 12, 1-17. 012.01/ijaai.117.

Zafar, M.A., Wang, Y., Hamaguchi, S., and Weiser, J.N. (2017). Host-to-Host Transmission of *Streptococcus pneumoniae* Is Driven by Its Inflammatory Toxin, Pneumolysin. *Cell Host Microbe* 21, 73-83. 10.1016/j.chom.2016.12.005.

RIPK3 SUPPRESSES NF κ B ACTIVATION DURING INFLUENZA A VIRUS
INFECTION OF AIRWAY EPITHELIAL CELLS TO REDUCE DISEASE
PATHOLOGY

by

ASHLEIGH N. RIEGLER, MEAGAN M. JENKINS, HANSOL IM, ANDRE
BALLESTEROS-TATO, AND CARLOS J. ORIHUELA

Submitted to *The Journal of Immunology*

Format adapted for dissertation

PREFACE

While we and other have contributed significantly to our understanding of necroptosis during bacterial infection, what was known about necroptosis during viral infection was more complicated. That is, in part, due to the complication of direct inhibition of pathway components which viruses often exhibit, but also in part due to conflicting results from previous studies. Notably, the role which necroptosis plays in the host response to and pathology of IAV infection has come up for debate recently, due to new and conflicting evidence. Briefly, the majority of previous work had indicated necroptotic signaling as a means to abort viral replication, that elimination of necroptosis resulted in increased severity of disease and susceptibility to IAV infection. However, recent work utilizing newly available molecular tools, like the MLKL KO mice and more specific inhibitors, indicates that RIPK3 functions to reduce viral pathology but not MLKL. Here we sought to further identify the role of necroptotic signaling in the host response to IAV infection, and to potentially identify the mechanistic bridge between these previously published data.

ABSTRACT

Necroptosis is a form of programmed necrosis regulated by RIPK1 and RIPK3. Once phosphorylated by various cellular signaling proteins, RIPK1/3 activate the effector MLKL through phosphorylation which subsequently targets cell membranes, forming large pores, ultimately resulting in cell lysis. Prior work examining the role of necroptosis during Influenza A virus (IAV) infection has contradictory conclusions on whether necroptosis is beneficial or detrimental to the host. Here, using mice and in vitro cell models, we dissected the impact and role of RIPK signaling on the severity of IAV pneumonia. We observed that RIPK3 deficient (KO) mice had an increased susceptibility to infection as well as decreased survival rate compared to wildtype mice; whereas mice deficient in MLKL were not different from wildtype. In the airway, RIPK3 deficiency resulted in increased neutrophil infiltration and lung consolidation. Subsequently, we observed that RIPK3 KO mice, gene-edited RIPK3 KO epithelial cells, and cells treated with a RIPK3-targeting inhibitor had increased release of the neutrophilic cytokine/chemokine IL-8 (KC and MIP-2 in mice) as well as increased pro-inflammatory IL-1 α and IL-1 β during IAV infection. Similar results were observed in RIPK3 KO cells challenged with toll-like receptor (TLR) agonists. Upon IAV challenge and in the absence of RIPK3, cells exhibited significantly increased NF κ B but not AP-1 or MK2 associated signaling. We conclude that RIPK3 has a protective anti-inflammatory role during IAV pneumonia that occurs in parallel to MLKL-mediated cell lysis, and that this role is via NF κ B inhibition.

INTRODUCTION

Programmed cell death (PCD) is fundamental toward the development, homeostasis, and survival of metazoans. Since first being formally described in the 1960s, the mechanisms by which mammalian cells undergo regulated death have been characterized into various categories, both by morphological description and biochemical classification. Morphological categorization of PCD includes apoptosis, autophagy, and necrosis (1). The latter which culminates in a loss of cell membrane integrity and cell lysis, which is highly inflammatory due to the release of cytosolic contents, some of which serve as alarmins (2, 3). Multiple forms of programmed necrosis are now recognized to exist, each of which is initiated by distinct cellular triggers and executed via distinct signaling cascades (4). Necroptosis, the PCD that is subject of this study, was accidentally discovered following the observation of necrotic cell death following TNF receptor engagement during caspase-8 inhibition (5). Necroptosis has since been shown to have a vital role in the instigation of the host defense against bacteria which produce a pore-forming toxin, to be part of the initiating response to sterile injury following ischemic episodes, and also, as result of its inflammatory role, to exacerbate acute and chronic inflammatory conditions such as pneumonia, septic shock, and infection-associated adverse cardiac remodeling (6, 7). Importantly, necroptosis is canonically regulated by receptor-interacting serine-threonine kinase(RIPK)-1, which activates RIPK3 forming the necroptosome. Successively, the necroptosome phosphorylates the effector molecule MLKL, activating it; and the p-MLKL then targets phosphatidylserine residues in cell membranes, resulting in cellular rupture and death (8, 9).

Influenza A virus (IAV) is a single-stranded RNA virus belonging to the Orthomyxoviridae family. It is the most common cause of human influenza (flu), infecting an estimated 1 billion individuals annually and resulting in 300,000 to 500,000 deaths in non-pandemic years (10, 11). IAV has been shown to initiate necroptosis of various cell types including epithelial cells, macrophages, and dendritic cells through the interaction of its nucleoprotein (NP) and polymerase B1 (PB1) with cellular DNA-dependent activator of IFN regulatory factors (DAI; also known as Zbp or DLM-1); this complex then initiates the activation of RIPK3 (12-15). Instigation of necroptosis during viral infection has in general been considered to be beneficial; a means for the host to abort replication in apoptosis-inhibited virus infected cells. Supporting this notion, necroptosis deficient mice have been reported as having increased susceptibility to IAV, West Nile, Vaccinia, and Herpes simplex viruses (14, 16-20). It is noteworthy that recent studies suggest oxidative stress induced by IAV infection sensitizes cells for necroptosis as well, although the mechanism responsible for this is unknown (21).

Pertinently, recent findings by Zhang et al and Nogusa et al have brought the consensus that necroptosis is beneficial during viral infection into question. Specifically, Zhang et al reported that nuclear rupture induced as result of necroptosis drives IAV disease severity, and instead that MLKL deficient mice have increased survival following IAV infection (13). Similarly, Nogusa and colleagues showed that MLKL deficiency did not alter susceptibility to IAV infection compared to wildtype (WT) mice (14). Critically, it has been shown that RIPK3 can act as an inhibitor of RIPK1/IKK complex-mediated NF κ B activation, with RIPK3 inhibition resulting in unmitigated NF κ B activation upon chemical stimulus (22). Therefore, one possible explanation for this discrepancy is that

studies which relied on RIPK3 inhibition/deletion to assess the impact of necroptosis on viral infection were convoluted by unappreciated and excessive NF κ B activation.

Here, we sought to dissect the specific consequence of RIPK3 activation on IAV disease. We determined that RIPK3 inhibition results in increased lung pathology and mortality. Pulmonary damage was the result enhanced neutrophil recruitment, which in turn was at least in part, due to an increased production of pro-inflammatory cytokines produced by lung epithelial cells with exacerbated NF κ B activation. Our findings provide clarity on the role of necroptosis during viral infection and refine our understanding of necroptosis is an inflammatory form of cell death that is purposefully curtailed in its scope as result of targeted NF κ B suppression.

MATERIALS AND METHODS:

Ethics Statement. Animal experiments were performed using protocols approved by the Institutional Animal Care and Use Committee at The University of Alabama at Birmingham (UAB) (Protocol # 21231). Animal care and protocols followed the NIH Guide for the Care and Use of Laboratory Animals.

Viruses. Pandemic H1N1 A/California/7/2009 (Cali'09) and H1N1 A/Puerto Rico/8/1934 (PR8) influenza viruses were propagated in Madin-Darby Canine Kidney cells (MDCK) in Eagle's minimal essential media (EMEM) supplemented with 3 μ g/mL L-1-tosylamido-2-phenylethyl chloromethyl ketone (TPCK) treated trypsin (Worthington Biochemical, Lakewood, NJ) grown at 37°C with 5% CO₂. All viral stocks were titered by standard plaque assay in MDCK.

Animal strains and infections. WT C57BL/6 mice were obtained from The Jackson Laboratory (Bar Harbor, Maine, USA) prior to their breeding and maintenance at UAB. MLKL KO mice were supplied by Dr. Douglas Green (St. Jude Children's Research Hospital, Memphis, TN, USA) through a material transfer agreement with Dr. Warren Alexander (Walter and Eliza Hall Institute of Medical Research Parkville, Victoria, Australia) (23). RIPK3 knockout (KO) mice were obtained from Dr. Vishva Dixit (Genentech, Dan Francisco, CA, USA) (24). At all times mice used in this study, including controls, were sustained on acidified water (pH 2.4-3.0). For challenge with IAV, mice were anesthetized with 2-3% vaporized isoflurane then intranasally (i.n.) challenged with 200-250 plaque-forming units (PFU) of PR8 in 50 μ L saline. Mice were euthanized using 5% isoflurane with confirmation by induced pneumothorax at designated time points or if deemed moribund. For Bronchoalveolar lavage (BAL), 2 mL saline was instilled into the lungs in 1 mL increments through a tracheal canula and collected through a three-way stopcock into a sterile syringe.

Viral titration by foci assay. Viral titers from experimental samples were calculated by viral foci assay using MDCK seeded into a 96-well plate (25). Overlay media contained 2.4% Avicel® (Dupont Nutrition and Biosciences, New Century, KS, USA). Rabbit IgG antibody against IAV NP (GTX125989, GeneTex, Irvine, CA USA) diluted 1:1000 in blocking solution was used as primary and horseradish peroxidase (HRP)-conjugated goat IgG against rabbit IgG (32460, Invitrogen, ThermoFisher Scientific, Carlsbad, CA, USA) diluted 1:1000 in blocking solution was used as secondary detection. ImmPACT

DAB (Vector Labs, Burlingame, CA, USA) colorizing reagent was used according to manufacturer's protocol for foci detection and counting.

Cells and CRISPR/cas9 modification. A549 human type II alveolar epithelial cells and FaDu (HTB-43) human pharyngeal cells were obtained from ATCC (Manassas, VA, USA) and cultured according to ATCC methods. Cells were regularly determined to be mycoplasma free by PCR (26, 27). For RIPK3 deficient line, cells were transfected with the gene-corresponding CRISPR/cas9 plasmid system (Sc-401008-KO-2 and Sc-401004-HDR) from Santa Cruz Biotechnology (Dallas, TX, USA) using Lipofectamine 3000 transfection reagent (Thermo Fisher Scientific, Waltham, MA, USA) as described previously (28). Transfected cells were selected using puromycin and single cell clones were grown out and probed by Western blot for mutation (**Supplemental Figure 3**).

Transcription factor reporter transfection. Cells for transfection were seeded onto round glass cover slips positioned in the wells of a 24-well plate to reach ~80-90% confluency at transfection. Previously described reporter plasmids pSIRV-NF- κ B-eGFP (#118093), pSIRV-AP-1-mCherry (#118095), and pPBbsr-mKO-MK2 (#115492) were obtained from Addgene (Watertown, MA, USA) in *E. coli* (29-31). Plasmid containing bacteria were cultured in lysogeny broth (LB) supplemented with ampicillin and plasmid was purified using the QIAGEN Plasmid Plus Midi Kit (#12945, Qiagen, Hilden, Germany) then quantified by nanodrop. Cells were transfected with 1 μ g plasmid DNA for every 10⁵ cells using Lipofectamine 3000 transfection reagent (Thermo Fisher Scientific). Since the NF- κ B and AP-1 plasmids do not contain a eukaryotic cell selection

marker, cells were infected with IAV the day following transfection and fixed with 4% paraformaldehyde at times detailed in the results. Fixed cells were permeabilized for 10 minutes using 0.1% Triton-X100 in phosphate buffered saline (PBS) then blocked with 0.3% bovine serum albumin (BSA) in PBS. Primary antibody targeting the reporter, either mouse anti-eGFP (MAI-952, Invitrogen, Carlsbad, CA, USA), rat anti-mCherry (16D7, Invitrogen), or mouse anti-musabira orange 2 (PM015M, MBL International, Woburn, MA, USA), was diluted according to manufacturer's suggested protocol and added to the cells for 1 hour. Following wash, cells were then stained with a secondary antibody conjugated to a fluorophore and targeting the primary antibody for 1 hour. Nuclear stain was accomplished using NucBlue Fixed Cell Ready Probes Reagent (R37606, Invitrogen). Stained cells on coverslips were mounted onto slides using FluorSave (345789, MilliporeSigma, Burlington, MA, USA). (Antibodies detailed in **Supplemental Table 1**).

Immunoblots and ELISA. To confirm the CRISPR/cas9 modification of the cells, Fadu cells were lysed using RIPA lysis buffer (R#0278, Sigma-Aldrich, St. Louis, MO, USA) containing HALT protease inhibitor (78429, Thermo Scientific). Protein concentrations were measured by BCA assay (Bio-rad, Hercules, CA, USA). Lysates were boiled for 10 min at 95 °C with NuPAGE LDS sample buffer then equal amounts of protein were added to each well and lysates were electrophoresed in 10% Mini-PROTEAN® TGX™ Precast Gels (Bio-rad). Proteins were then transferred to a 0.2µm Nitrocellulose membrane (Bio-rad, Transblot kit #1704158) and blocked with 5% BSA in PBS with 0.1% Tween 20 (PBST) (Sigma-Aldrich). All antibody incubation was done within 3%

BSA in PBST buffer. For the RIPK3 blot primary antibody was applied at a 1:300 ratio. For the glyceraldehyde 3-phosphate dehydrogenase (GAPDH) blot, primary antibody was applied at a 1:10,000 ratio. Primary antibodies were incubated overnight at 4°C. Secondary, HRP-conjugated antibody targeting the primary antibody was applied at a 1:10,000 ratio for each. Chemiluminescence was accomplished using clarity western ECL substrate (Bio-rad) and imaged using Bio-RAD ChemiDoc™ XRS+ (Bio-rad). ELISA for IL-1 α , IL-1 β , IL-8, KC/CXCL-1, myeloperoxidase (MPO), MIP-2, CXCL-2, IL-10, IFN- β , IFN- α , and TNF- α were done using kits manufactured by R&D Systems Inc. (Minneapolis, MN, USA) following manufacturer instructions. (Antibodies and ELISA kits detailed in **Supplemental Table 1**).

Key Reagents. Z-VAD-fmk (Sigma-Aldrich), Necrosulfonamide (NSA; Tocris Bioscience, QL, United Kingdom), and GSK'872 and Nec1s (BioVision, Milpitas, California, USA) were reconstituted and stored following manufacturer's instructions and used as described above for associated experiments.

Cell infection assays. Cells were infected for the indicated times with the IAV strain and challenge dose or MOI described in associated results. Cells that received inhibitors targeting MLKL (necrosulfonamide, NSA), RIPK1 and RIPK3 (Necrostatin-1s; Nec-1s), RIPK3 (GSK' 872), or caspases (Z-VAD-fmk) were pre-treated with the inhibitor for 1h prior to IAV infection. For *in vitro* studies, data from ≥ 3 separate experiments are shown. *In vitro* cell death was evaluated by detection of lactate dehydrogenase (LDH), a normally cytoplasmic enzyme, in the culture supernatants using either the Cytotox 96

Assay kit (Promega, Madison, WI) or Pierce LDH cytotoxicity kit (Thermo Fisher Scientific; Discontinued).

Histology. Methods used for tissue collection, tissue processing, and immunofluorescent staining of frozen tissue sections have been previously described (32, 33). Lungs were surgically excised and mounted in either optimal cutting temperature compound (OCT) for frozen sections or fixed in buffered formalin for paraffin embedding. Frozen sections were used for fluorescent microscopy, whereas paraffin embedded sections were stained with Hematoxylin and Eosin (H&E) by the UAB Pathology Core Research Lab (Birmingham, AL, USA) for histology. Images were captured using a Leica LMD6 with DFC3000G-1.3-megapixel monochrome camera or DFC450C-5-megapixel RGB CCD camera (Leica Biosystems, Buffalo Grove, IL). For cytopsin data, bronchoalveolar lavage (BAL) samples were centrifuged onto slides at 1000 rpm for 7 minutes using the Shandon Cytospin 4 (Thermo Fisher Scientific) then stained using the PROTOCOL Hema 3 staining system (Fisher Healthcare, Thermo Fisher Scientific). The extent of lung consolidation (i.e. lung consolidation index) of infected lungs was quantitated as previously described (7). Whole lung tile stitched images were analyzed using the polygon tool in Image J (National Institutes of Health, Bethesda, MD) to determine the total area of the lung. Within the Image J software, the color threshold was then adjusted to select only for stained tissue, and area of stain was measured. Lung consolidation index was calculated as a percentage of total lung biomass ($[\text{area of stained tissue and infiltrate} / \text{total lung area}] \times 100\%$). Mean fluorescent intensity, and densitometry of immunoblots were measured with ImageJ.

Flow Cytometry. Cell suspensions from the mediastinal lymph nodes (mLN) and lungs were prepared as described previously (34, 35). Lungs and mLN were isolated immediately following euthanasia. Lungs were cut into small fragments and digested for 30 min at 37°C with RPMI medium (Gibco, Thermo Fisher Scientific) containing 0.6 mg/ml collagenase A (Sigma) and 30 µg/ml DNase I. Digested lungs and mLN were mechanically dissociated by passing through a 70µm mesh cell strainer. Red blood cells were lysed with ammonium-chloride-potassium (ACK) lysing buffer (Gibco) according to manufacturer's instruction. Cells were washed and resuspended in saline with 2% calf serum and Fc receptors were blocked with 5 µg/ml FcBlock (anti-CD16/32; BD Biosciences) for 10 min on ice. Cells were prepared for intracellular staining using the mouse T regulatory cell staining kit (eBioscience). Suspensions were then stained with fluorochrome-conjugated antibodies at the following dilutions: anti-CD19 (clone 1D3, BD Biosciences, dilution 1/200), anti-CD138 (clone 281.2, BD Biosciences, dilution 1/500), Anti-Bcl-6 (clone K112.91, BD Biosciences, dilution 1/50), anti-CXCR5 (clone 2G-8, BD Biosciences, dilution 1/50), anti-CD4 (clone RM4-5, BD Biosciences, dilution 1/200), anti-CD69 (clone H1.2F3, BD Biosciences, dilution 1/200), anti-CD25 (clone PC61, BD Biosciences, dilution 1/200), anti-PD-1 (clone J43, eBioscience, dilution 1/100), and anti-Foxp3 (clone FJK-16s, eBioscience, dilution 1/200). The I-Ab NP311-325 MHC class II tetramer was acquired from the NIH Tetramer Core Facility and recombinant IAV nucleoprotein (NP) B-cell tetramers were prepared by the Ballesteros-Tato laboratory as previously described (36). Dead cells were stained for exclusion using

7-aminoactinomycin D (7-AAD; BioLegend). Flow cytometry was performed using an Attune NxT Flow Cytometer (ThermoFischer Scientific).

Statistical analyses. Statistical analyses were performed using Prism 8 (GraphPad Software: La Jolla, CA). Data shown as mean \pm standard error. For *in vitro* studies, data from ≥ 3 separate experiments shown. For data with a single independent factor of two groups, we used a Mann-Whitney U test. For multiple group analyses, we used a Kruskal-Wallis H test with Dunn's *post-hoc* analysis; grouped analyses were performed using a Two-Way ANOVA with legend-specified post-test.

Author Contributions. A.N.R and C.J.O. wrote the manuscript. A.N.R. and C.J.O designed the experiments. A.N.R, M.M.J., and H.I. executed the experiments. A.B-T. assisted with flow cytometry. All authors contributed to manuscript editing.

RESULTS

RIPK3 deficiency increased susceptibility to IAV infection independent of MLKL.

Recent findings from other groups on the impact of necroptosis deficiency on IAV infection are contradictory. To resolve this, we first evaluated the impact of necroptosis signaling deficiency on susceptibility to IAV using WT C57BL/6, RIPK3 deficient (RIPK3 KO), and MLKL deficient (MLKL KO) mice. RIPK3 KO mice administered IAV strain Puerto Rico/8/1934 (PR8) at the LD₅₀ dose for WT mice succumbed to infection earlier than both WT or MLKL KO mice; 50% mortality was reached on day 5 versus day 7 post-infection (**Figure 1A**). When challenged with a sub-lethal infectious

dose of IAV, RIPK3 mice similarly displayed increased susceptibility to IAV as measured by weight loss (**Figure 1B**). Notably, no differences were observed between WT and MLKL KO mice in either experiment. Pathological examination of lungs collected from IAV-infected mice on days 4 and 7 post-infection revealed differences in the progression of pulmonary injury that were in line with observed mortality. In particular, RIPK3 KO mice had significantly greater lung consolidation than WT at day 7. Again, we observed no difference between WT and MLKL KO mice (**Figure 2A,B**). Close examination of small airways and alveolar space revealed greater levels of peribronchial and perivascular immune cell infiltration in RIPK3 KO mice versus WT. No discernible difference was observed between WT and MLKL KO mice. It is noteworthy that viral titers in the lungs of RIPK3 KO and MLKL KO were equivalent to those observed for WT (**Figure 2C**). This indicated that necroptosis did not function to reduce viral burden and that an alternative explanation for why RIPK3 deficient animals fared worse than WT or MLKL KO mice was required.

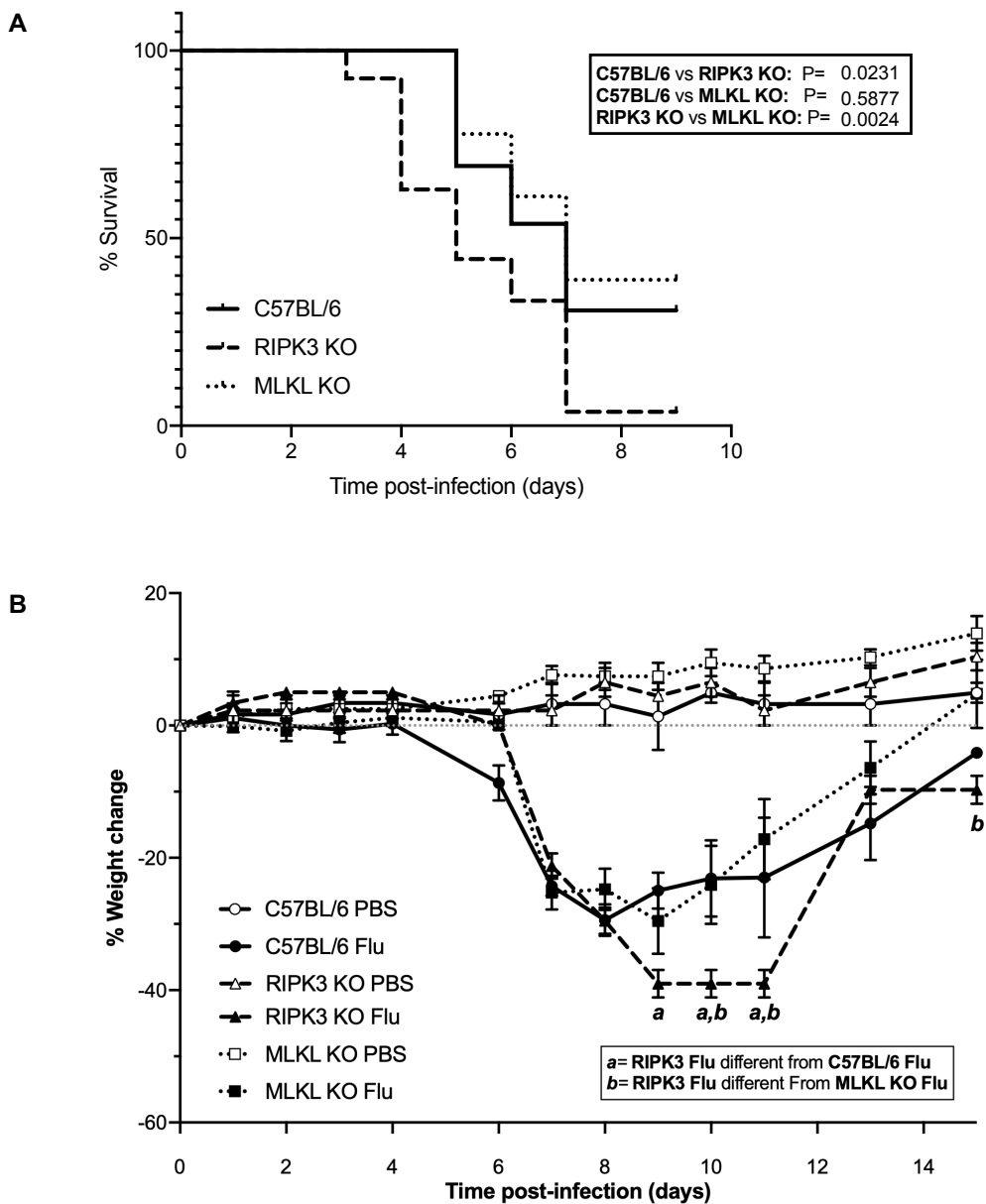


Figure 1: RIPK3 Deficiency but not MLKL Deficiency Increases Susceptibility to IAV Infection. **A)** Percent survival of wildtype C57BL/6 ($n=13$), RIPK3 KO ($n=22$), and MLKL KO ($n=18$) mice infected i.n. with a lethal dose (500 PFU) of Influenza A/Puerto Rico/8/1934 (PR8). Data are combined from duplicate infection experiments and compared by Gehan-Breslow-Wilcoxon survival test. * $P \leq 0.05$ and ** $P \leq 0.01$. **B)** Percent weight change in mice infected i.n. with 250 PFU of PR8 in 50 μL saline or mock challenged with saline only (PBS) ($N= 4-8$ mice per group). Data compared by Two-Way ANOVA with repeated measures and Sidak's post-test. Statistically significant differences ($P \leq 0.05$) between group at each time delineated as follows: $a = \text{RIPK3 Flu}$ is different from C57BL/6 Flu and $b = \text{RIPK3 Flu}$ is different from MLKL KO Flu.

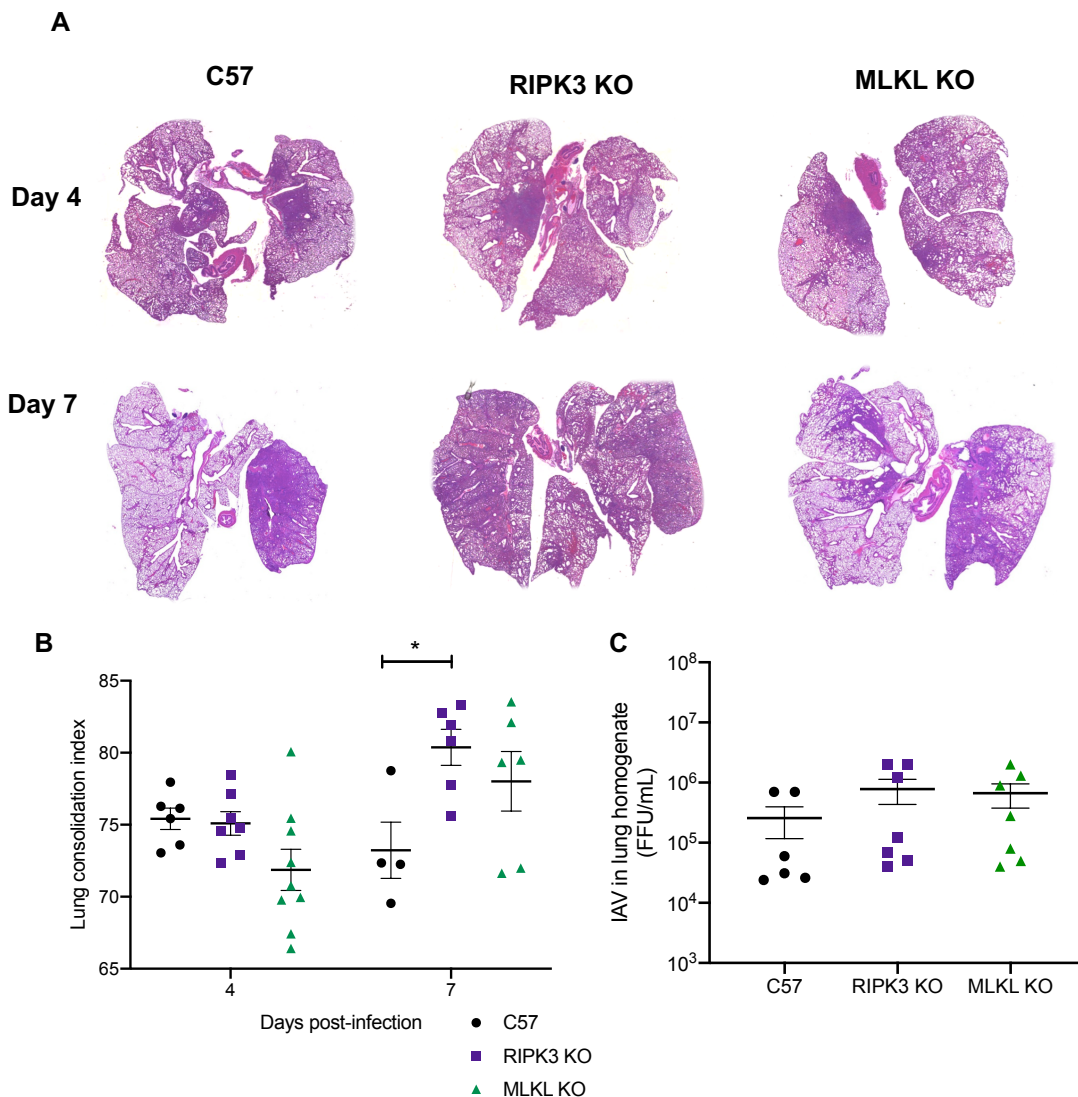


Figure 2: RIPK3 Deficiency but not MLKL Deficiency Increases Disease Pathology During IAV Infection Independent of Viral Titer. C57BL/6, RIPK3 KO, or MLKL KO mice were infected i.n. with 250 PFU of Influenza A/Puerto Rico/8/1934. **A)** Representative images of H&E stained lung sections collected 4- and 7-days post-infection. Tissues were sectioned at 8 μ m and tile-scan imaged at 10X magnification. **B)** Lung consolidation was calculated from corresponding lung H&E images. Data are compared by two-way ANOVA with Sidak's post-test **C)** Viral titers at five days post-infection in lung homogenates. Data in panels C and D are represented as Mean \pm SEM where each data point represents results from one animal. *P \leq 0.05.

RIPK3 deficiency alters immune cellular recruitment during IAV infection. To better understand the impact of RIPK3 deficiency on lung consolidation, we characterized immune cell infiltrates present in the lungs of IAV infected mice. When infected with IAV, RIPK3 KO mice accumulated 50- to 100-fold more cells in the lumen of their airways than WT or MLKL KO mice early during infection (4 days post-infection) (**Figure 3A, B**). While MLKL KO mice showed no significant differences in cell number or cell type present in the lungs compared to WT, RIPK3 deficiency was in particular characterized by a substantial increase in the number of polymorphonuclear cells (PMNs) in the lungs early in IAV infection as well as an increase in percentage of PMN, considering the increased total cell number (**Figure 3C** and **Supplemental Figure 1**). These PMNs were most likely neutrophils as determined by ELISA for myeloperoxidase activity on BAL samples from infected mice (**Figure 3D**) (37).

Higher neutrophil numbers are known to be positively correlated with IAV disease severity (38). It is also understood that the recruitment of adaptive immune cells, chiefly virus-specific CD8⁺ T cells, contributes to pathology of and susceptibility to viral respiratory infection by targeting infected cells and releasing immune-regulating cytokines (39-41). Notably, RIPK3 KO mice also had increased CD8⁺ T cells specific to IAV nucleoprotein (NP) in their lungs compared to WT and MLKL KO counterparts (**Figure 3E**). Further identification of these cells using flow cytometry identified these cells as CD8⁺ effector T cells (CD19⁻CD8⁺CD127⁻CD62L⁻); this observed increase in BAL-associated IAV-specific CD8⁺ T cells did not occur in the lung-draining lymph node (**Supplemental Figure 2**). Finally, and further supporting the notion that RIPK3 deficiency alters the infiltration of immune cells into the airway, we observed that

CXCL-1/KC was increased in BAL from RIPK3 KO mice at 7 days post-infection versus WT and undetectable in MLKL KO mice at any assessed time (**Figure 3F**). Thus, RIPK3 deficiency alters the cytokine response to IAV in the airway such that there are increased numbers of potentially damaging immune cells including neutrophils and virus-specific CD8⁺ effector T cells. The presence of these cells helps to explain the worsened lung pathology seen in RIPK3 KO mice.

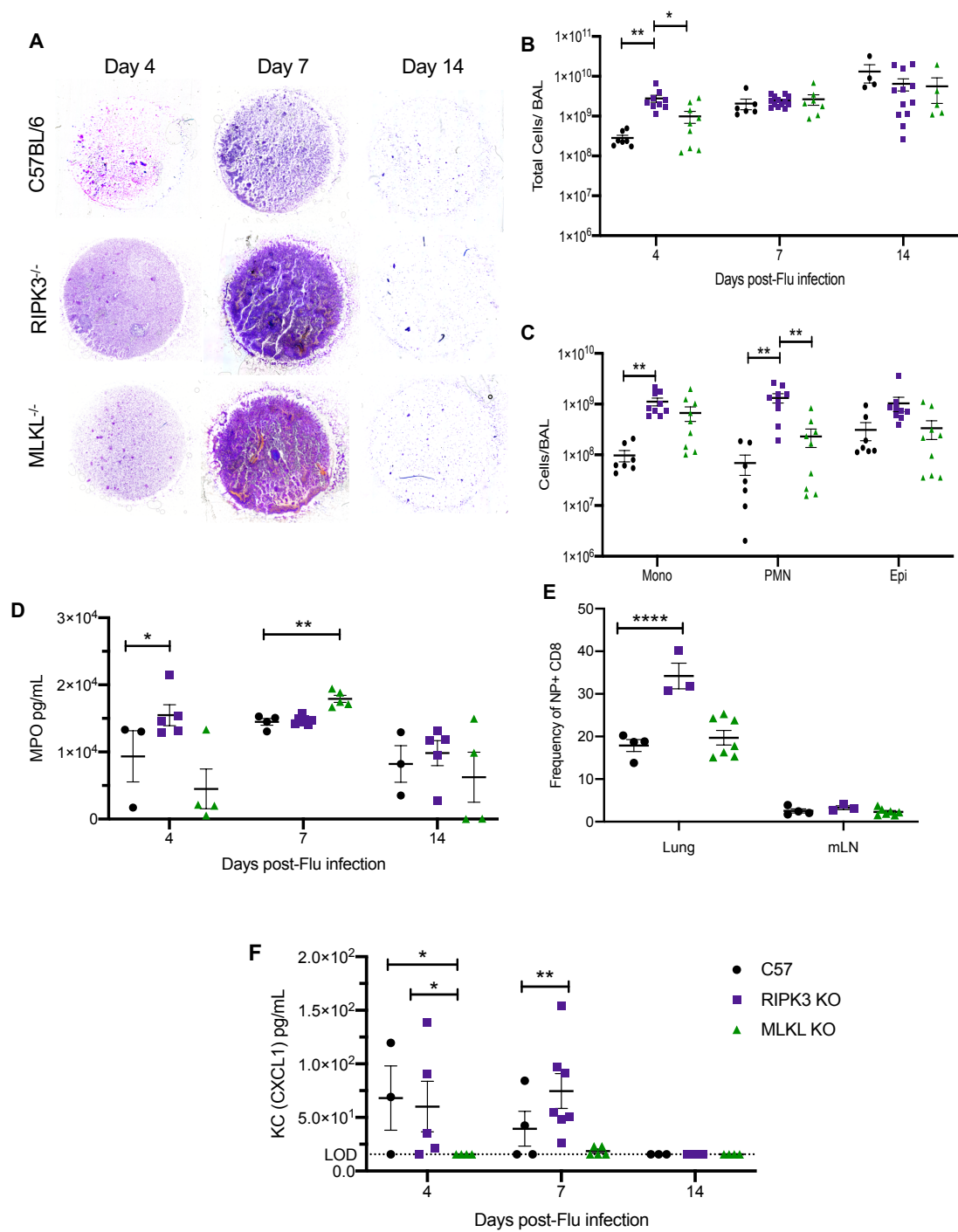


Figure 3: RIPK3 deficiency alters immune cellular recruitment during IAV infection. **A)** Representative HEMA3 stained CytoSpin spots from BAL collected at 4, 7, and 14 days post-infection from wildtype C57BL/6, RIPK3 KO, and MLKL KO mice infected i.n. with 250 PFU of PR8. **B)** Total cells and **C)** different cell types present in BAL were further assessed from CytoSpins through differential stain (HEMA 3). Data are compared by Two- and One-Way ANOVA with Sidak's post-test in B and C, respectively, and each data point represents one animal. **D)** Amount of myeloperoxidase (MPO) was also determined in these BAL samples. **E)** Frequency of NP⁺CD8⁺ T (CD19⁻CD25⁺CD8⁺NP⁺) cells was assessed at two weeks post-infection in the lungs and draining lymph node (i.e. mediastinal lymph node; mLN) of C57BL/6, RIPK3 KO, and MLKL KO mice infected with PR8. **F)** Amount of CXCL-1/KC was measured in BAL samples collected on these designated days following i.n. challenge with PR8. Data are compared by Two-way ANOVA with Sidak's post-test for panels D and F and by One-way ANOVA with Dunn's post-test for panel E. *P ≤ 0.05 and **P ≤ 0.01. (See also **Supplemental Figure 1** and **Supplemental Figure 2**)

RIPK3 Deficiency Alters Cellular Cytokine Response to IAV Infection. To

specifically dissect the impact of RIPK3 deficiency on the airway epithelial cell response to IAV, we created cells deficient in RIPK3 using a CRISPR/cas9 modification system (**Supplemental Figure 3**). Using IAV infected cells at two different MOIs (0.1 and 1), we unexpectedly observed that RIPK3 deficiency increased overall lytic cell death, as measured by lactate dehydrogenase (LDH) release (**Figure 4A**). We also determined that cells deficient in RIPK3 had increased IL-1 α , IL-1 β , and IL-8 released as result of IAV infection compared to WT cells (**Figure 4B**). These results were recapitulated in WT cells treated with GSK'872 to inhibit RIPK3 activation (**Figure 4C**). Subsequent activation of TLR4 and TLR2/6 using LPS and lipoteichoic acid, respectively, in RIPK3 deficient cells also resulted in elevated IL-1 α , IL-1 β , and IL-8 release (**Figure 5A**). Within the timespan examined, this did not result in enhanced lytic death of the challenged cells, with all measured LDH from these cells at the lower limit of detection, independent of cell genotype, suggesting the increased rate of cell death in viral-infected RIPK3 KO cells was due to effects of the virus outside the TLR pathway. We subsequently utilized our gene-edited KO cell lines *in vitro* and further modified them by transfecting them with a plasmid containing a response element for either NF κ B, AP-1, or MK2 then challenged these reporter cells with IAV. We observed that these cells had increased NF κ B activation compared to their negative controls, but no changes in AP-1 or MK2 activation (**Figure 5B-E**). Collectively these data suggest that during IAV infection, RIPK3 acts to suppress inflammatory cytokine signaling and subsequent cellular recruitment by inhibiting NF κ B signaling.

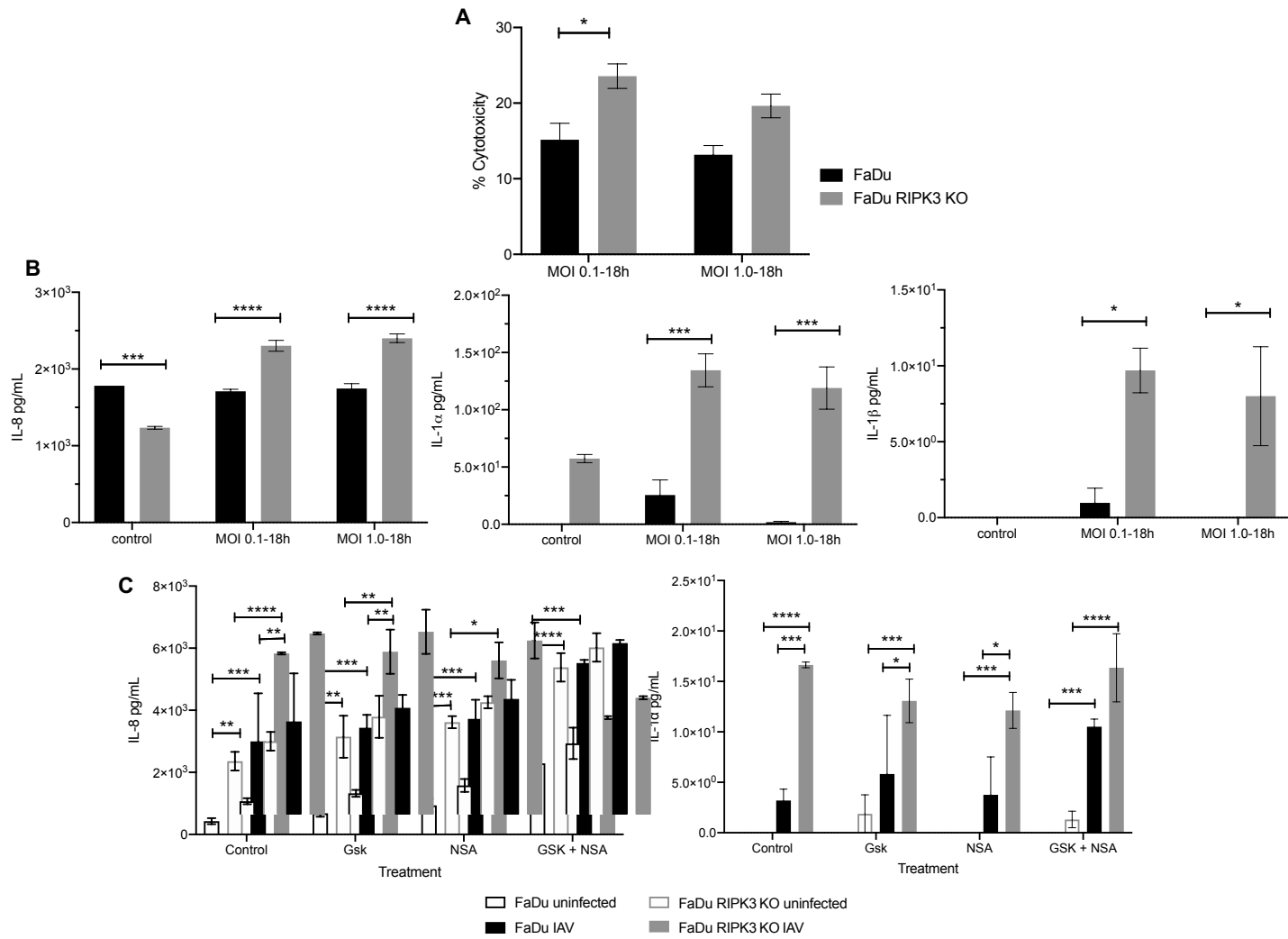


Figure 4: RIPK3 Deficiency Alters Cellular Cytokine Response to IAV Infection. A) Cell death was measured by LDH release to the supernatant from WT and RIPK3 KO gene edited FaDu cells infected with pandemic H1N1 A/California/7/2009 (Cali'09) at a MOI of 0.1 or 1. Note that uninfected controls were used to determine zero percent cytotoxicity and fully lysed cells were used to determine full cytotoxicity range. Levels of IL-8 and IL-1 α following Cali'09 infection were measured by ELISA in supernatants from **B)** WT and RIPK3 KO gene edited FaDu cells or **C)** WT FaDu cells pre-treated with GSK'872 to inhibit RIPK3 or Necrosulfonamide (NSA) to inhibit MLKL activation. Levels of IL-1 β were also measured in WT and gene edited cells (panel B) but were below limit of detection for inhibitor treated cells. For all ELISA data sets, data were compared using One-Way ANOVA with Sidak's post-test. Data are graphed as mean \pm SEM from three biological replicate experiments. *P \leq 0.05, **P \leq 0.01, ***P \leq 0.001, and ****P \leq 0.0001. (See also **Supplemental Figure 3**)

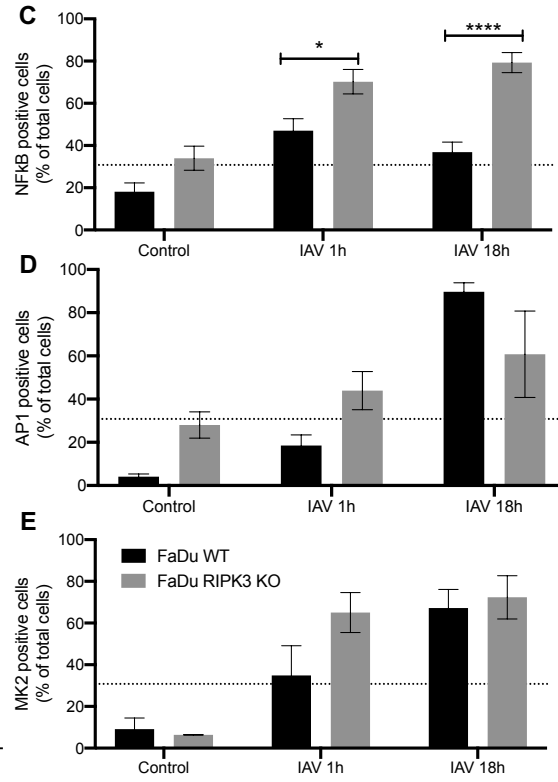
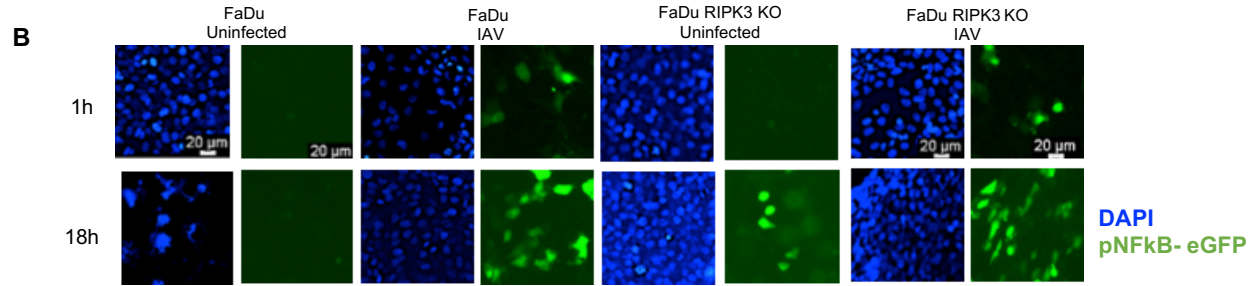
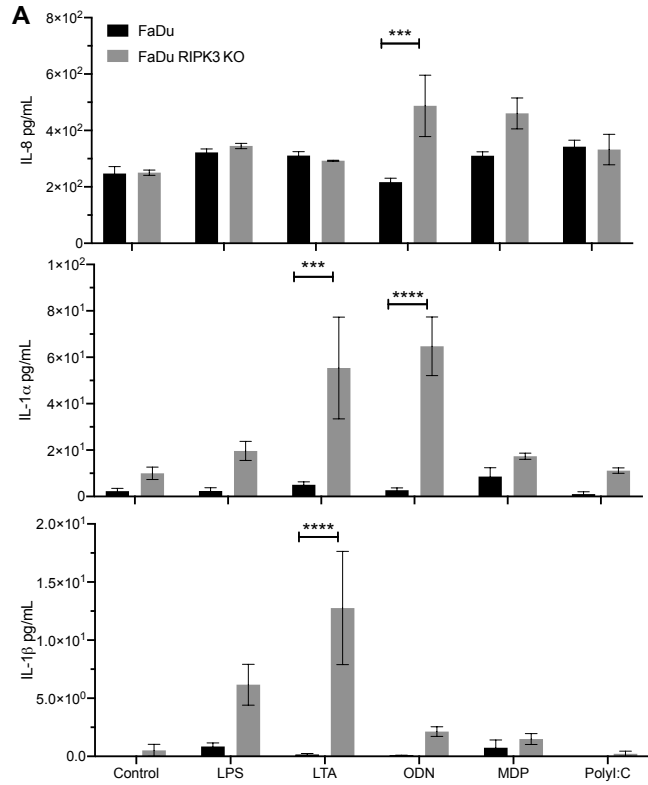


Figure 5: RIPK3 Moderates NF κ B Signaling During IAV Infection. **A)** Amount of IL-8, IL-1 α , and IL-1 β was measured in the supernatant of WT and RIPK3 KO FaDu cells challenged with the TLR ligands lipopolysaccharide (LPS, 1 μ g/mL, TLR4), lipoteichoic acid (LTA, 5 μ g/mL, TLR2/6), CpG oligodeoxynucleotide (ODN, 0.1 μ g/mL, TLR9), Muramyl dipeptide (MDP, 1 μ g/mL, TLR2), or a dsRNA mimetic (Poly I:C, 1 μ g/mL, TLR3 or MDA-5/RIG-I) for 4 hours. Data are plotted as mean \pm SEM and represents three biological replicate experiments. Data are compared by One-Way ANOVA with Sidak's post-test. ***P \leq 0.001 and ****P \leq 0.0001. **B)** Representative images of FaDu cells transfected with a reporter for NF κ B and subsequently infected with pandemic H1N1 A/California/7/2009 (Cali'09) for 1 hour or 18 hours are shown. Images were collected at 10X magnification using Leica LASX imaging software. Quantification of **C)** NF κ B, **D)** AP-1, and **E)** MK2 positive cells was determined from cells transfected with the respective reporter plasmid containing a response element to the respective cellular signal. Percent positive cells was determined by normalization to total cells in each image (nuclear/DAPI signal). Data are compared by One-Way ANOVA with Sidak's post-test. Statistically significant comparisons denoted in graph with asterisks. *P \leq 0.05 and ****P \leq 0.0001.

DISCUSSION:

Though it had been generally concluded that necroptosis during viral infection is beneficial, as means to abort viral replication, and its inhibition results in worsened IAV-associated disease (13, 14, 16), this has of late come into dispute (17). One explanation for this is the increasingly specific molecular tools being used to dissect the role of necroptosis-associated molecules in isolation. Another is our expanded understanding of the diverse roles RIPK3 plays during viral infection. In our own studies, we observed that RIPK3 deficiency increased susceptibility of mice to IAV, whereas MLKL deficiency did not. Moreover, neither RIPK3 or MLKL deficiency affected lung IAV titers following challenge, indicating that necroptosis does not meaningfully reduce viral replication, and instead plays a beneficial role by other means. Using CRISPR/Cas9 gene edited cells this was subsequently determined to be suppression of NF κ B-mediated inflammation and in turn an excessive neutrophilic response in the airway.

PCD is an essential part of the host response to infection. Just as importantly, cell pathways involved in PCD are connected to the activation and pro-inflammatory status of a cell, modulating the effectors released into the milieu and subsequently affecting the response of bystander cells (42). Thus cell death, and the inflammatory mediators released during these processes, have numerous effects on pathogen eradication as well as host pathology during infection and our understanding of their roles in orchestrating immunity to pathogens warrants considerable more attention. Along such lines, the role which necroptosis plays during viral infection is not well understood but has been shown to be very important. Mice deficient in RIPK3 are more susceptible to infection by Vaccinia viruses (19), Herpes simplex viruses (20, 43), and West Nile virus (18), whereas infection with cytomegaloviruses are less affected by RIPK3 presence or absence due to the viral-

encoded inhibitor of RIP activation (44, 45). It is reasonable to postulate that the varying impact of necroptosis on cellular defense against these viruses is most likely reflective of replicative strategies as well as a panel of cell proteins that inhibit cell death to the viruses benefit.

In addition to being involved in the activation of MLKL, RIPK3 functions to signal in a number of other cellular pathways. Under certain stimuli such as TNF α stimulation, RIPK3 functions as a pro-apoptotic adaptor, recruiting RIPK1 and FADD to form a platform with cFLIP which leads to the activation of caspase-8, and subsequent apoptosis, without the requirement of RIP homotypic interaction motif (RHIM)-mediated oligomerization (46, 47). This cFlip and caspase-8 regulation by RIPK1 and RIPK3 has further been shown during mitochondrial damage as well ion dysregulation through the mitochondrial apoptogenic protein Smac (also known as Diablo) which triggers the degradation of cIAP1 and cIAP2, eventually resulting in the formation of cytosolic RIPK-FADD-caspase-8 complex-mediated apoptosis (48, 49). Unexpectedly, we also observed that RIPK3 deficiency results in increased cytotoxicity, as measured by LDH release *in vitro*, indicating that the activation of IAV-infected RIPK3 deficient cells ultimately still results in death, but in a manner other than necroptosis. Previous studies showing that both the sensing of IAV by DAI/ZBP1 and TLR-mediated activation of RIPK1 which complexes to FADD and caspase-8, results in the non-canonical activation of the NLRP3 inflammasome, ultimately resulting in cellular alterations associated pyroptotic cell death (12, 50, 51). Future studies are warranted to determine if this is the case, moreover to determine if the detrimental effect of RIP3 deficiency is abrogated in a pyroptosis deficient cell line.

Pertinently to our study, RIPK3 has been shown to inhibit the RIPK1/IKK-complex mediated activation of NF κ B. These multiple roles for RIPK3 suggests that even in our own studies we cannot rule out a confounding effect of these other functions. Notwithstanding, we show that RIPK3 deficiency results in increased NF κ B activation in response to TLR ligands as well as virus; and this results in subsequent alterations in inflammatory cytokine release, including the pro-inflammatory IL-1 proteins (IL-1 α and IL-1 β) as well as neutrophil chemoattractants (*i.e.* IL-8 or KC), the latter likely contributing to the observed increase in lung PMNs during infection. Interestingly, it has recently been shown that the lethality of IAV infection relies not on the pathogen's ability to kill airway epithelial cells but rather on the inflammatory response which it elicits within the host. In humans infected with IAV, the number of neutrophils in the lower respiratory tract has been correlated with the severity of disease (38, 52). Additionally, recombinant IAV strains which are associated with increased alveolar hemorrhage are also associated with an increased production of chemoattractants (MIP-2/CXCL2) and neutrophil recruitment (52). Neutrophils recruited to the lungs during infection produce a multitude of toxic substances and proinflammatory mediators (*e.g.* ROS, hydrolytic enzymes, peroxidases, defensins, and cytokines) and it has been shown under various conditions that neutralizing these neutrophil-derived signals significantly improves disease outcomes in mice (53-55). The positive association of lung neutrophil numbers with the severity of disease is supported by our observations in RIPK3 KO mice, indicating that RIPK3 may play a role in dampening the signals associated with the recruitment of these cells to the lungs.

Similarly, and despite contributing to viral clearance, increased number of viral-specific CD8⁺ T cells in the lungs also contributes toward disease severity in various models of respiratory viral infection. For example, the presence of lung virus-specific CD8⁺ T cells is positively correlated with increased weight loss in mice following infection with respiratory syncytial virus, decreased survival and increased lung pathology in mice during IAV infection, as well as decreased barrier integrity and increased death of uninfected bystander cells in humans infected with IAV (56-60). The mechanism by which virus-specific CD8⁺ T cells contribute to adverse pathology during respiratory viral infection is complex but is chiefly associated with the effector functions and cytokine (*e.g.* TNF and interferon (IFN)) release from these lung T cells; and during IAV infection, the deleterious impact of these cells on the host seems to be result of an imbalanced activation, associated with increased host age, high-dose infections, or host impairment in lung homeostasis prior to infection (59-64). The increase in NP-specific CD8⁺ T cells we observed in the lungs of RIPK3 KO mice likely contributed to the observed pathology and decreased survival through decreased lung barrier integrity resulting from the dysregulated release of these T-cell associated cytokines, such as TNF and IFN. Notably, the inflammatory response to IAV infection is controlled by a sprawling network of cellular signals which in turn are amplified by autocrine and paracrine mediator cascades and prominent examples include the IFN and TNF pathways, as well as interleukin and cyclooxygenase (COX)-2 pathways; all of which induce NFκB transcription (65, 66). This suggests that the exacerbated NFκB signaling we observed in RIPK3 deficient cells contributed to infection pathology in a feed-forward manner.

The inflammation and immunity elicited by necroptosis-released cytokines versus that elicited by the activation of NF κ B are different. Consequently, the effects that these responses have on overall disease pathology are distinct. The inflammation associated with necroptosis is largely attributed to the release of intracellular damage-associated molecular patterns (DAMPs; *e.g.* IL-33, IL-1 α , histones, and DNA) and is limited by the amount of these DAMPS present in the cell at the time of lysis (67). In contrast, the rapid lysis of cells undergoing necroptosis does suppress inflammation through the termination of transcriptional pro-inflammatory responses (68). Whether the cellular fate of necroptosis is less inflammatory during IAV infection than the alternative de-repression of NF κ B as result of RIPK3 absence cannot yet be concluded, and would require further investigation, particularly with MLKL deficient cells and mice which would have normal RIPK3 activation in absence of necroptosis. This line of investigation falls outside the scope of the present study which is focused on RIPK3.

In summary, our study and various other reports cited above demonstrate a capacity for RIPK3 to reduce damaging inflammation during viral infection, in manner that was independent of necroptosis. We show that much of the damaging inflammation during IAV infection observed in the absence of RIPK3 activation is result of increased NF κ B signaling, which in turn leads to greater recruitment of immune cells with pathological consequence. Cellular signaling pathways like those of the TLRs were also found to be elevated even in uninfected cells suggesting the suppression by RIPK3 is constitutive. This seemed to be the protective mechanism by which RIP3 imparted its effect. Clearly, our understanding of necroptotic signaling during infection has much room for growth.

ACKNOWLEDGEMENTS. We thank Dr. Warren Alexander for the gift of the MLKL KO mice and Dr. Douglas Green for supplying our colony. We also thank Dr. Vishva Dixit for the gift of the RIPK3 KO mice. Finally, we thank all members of the Orihuela lab for technical assistance throughout the conductance of these experiments.

REFERENCES

1. Ziegler, U., and P. Groscurth. 2004. Morphological features of cell death. *News Physiol Sci* 19: 124-128.
2. Wallach, D., T. B. Kang, C. P. Dillon, and D. R. Green. 2016. Programmed necrosis in inflammation: Toward identification of the effector molecules. *Science* 352: aaf2154.
3. Kaczmarek, A., P. Vandenabeele, and D. V. Krysko. 2013. Necroptosis: the release of damage-associated molecular patterns and its physiological relevance. *Immunity* 38: 209-223.
4. Green, D. R., and F. Llambi. 2015. Cell Death Signaling. *Cold Spring Harb Perspect Biol* 7.
5. Degterev, A., Z. Huang, M. Boyce, Y. Li, P. Jagtap, N. Mizushima, G. D. Cuny, T. J. Mitchison, M. A. Moskowitz, and J. Yuan. 2005. Chemical inhibitor of nonapoptotic cell death with therapeutic potential for ischemic brain injury. *Nat Chem Biol* 1: 112-119.
6. Weinlich, R., A. Oberst, H. M. Beere, and D. R. Green. 2017. Necroptosis in development, inflammation and disease. *Nat Rev Mol Cell Biol* 18: 127-136.

7. Beno, S. M., A. N. Riegler, R. P. Gilley, T. Brissac, Y. Wang, K. L. Kruckow, J. K. Jadapalli, G. M. Wright, A. T. Shenoy, S. N. Stoner, M. I. Restrepo, J. S. Deshane, G. V. Halade, N. Gonzalez-Juarbe, and C. J. Orihuela. 2020. Inhibition of Necroptosis to Prevent Long-term Cardiac Damage During Pneumococcal Pneumonia and Invasive Disease. *J Infect Dis* 222: 1882-1893.
8. Vandenabeele, P., L. Galluzzi, T. Vanden Berghe, and G. Kroemer. 2010. Molecular mechanisms of necroptosis: an ordered cellular explosion. *Nat Rev Mol Cell Biol* 11: 700-714.
9. Moreno-Gonzalez, G., P. Vandenabeele, and D. V. Krysko. 2016. Necroptosis: A Novel Cell Death Modality and Its Potential Relevance for Critical Care Medicine. *Am J Respir Crit Care Med* 194: 415-428.
10. Moghadami, M. 2017. A Narrative Review of Influenza: A Seasonal and Pandemic Disease. *Iran J Med Sci* 42: 2-13.
11. Clayville, L. R. 2011. Influenza update: a review of currently available vaccines. *P T* 36: 659-684.
12. Kuriakose, T., S. M. Man, R. K. Malireddi, R. Karki, S. Kesavardhana, D. E. Place, G. Neale, P. Vogel, and T. D. Kanneganti. 2016. ZBP1/DAI is an innate sensor of influenza virus triggering the NLRP3 inflammasome and programmed cell death pathways. *Sci Immunol* 1.
13. Zhang, T., C. Yin, D. F. Boyd, G. Quarato, J. P. Ingram, M. Shubina, K. B. Ragan, T. Ishizuka, J. C. Crawford, B. Tummers, D. A. Rodriguez, J. Xue, S. Peri, W. J. Kaiser, C. B. Lopez, Y. Xu, J. W. Upton, P. G. Thomas, D. R. Green,

- and S. Balachandran. 2020. Influenza Virus Z-RNAs Induce ZBP1-Mediated Necroptosis. *Cell* 180: 1115-1129 e1113.
14. Nogusa, S., R. J. Thapa, C. P. Dillon, S. Liedmann, T. H. Oguin, 3rd, J. P. Ingram, D. A. Rodriguez, R. Kosoff, S. Sharma, O. Sturm, K. Verbist, P. J. Gough, J. Bertin, B. M. Hartmann, S. C. Sealton, W. J. Kaiser, E. S. Mocarski, C. B. Lopez, P. G. Thomas, A. Oberst, D. R. Green, and S. Balachandran. 2016. RIPK3 Activates Parallel Pathways of MLKL-Driven Necroptosis and FADD-Mediated Apoptosis to Protect against Influenza A Virus. *Cell Host Microbe* 20: 13-24.
15. Thapa, R. J., J. P. Ingram, K. B. Ragan, S. Nogusa, D. F. Boyd, A. A. Benitez, H. Sridharan, R. Kosoff, M. Shubina, V. J. Landsteiner, M. Andrade, P. Vogel, L. J. Sigal, B. R. tenOever, P. G. Thomas, J. W. Upton, and S. Balachandran. 2016. DAI Senses Influenza A Virus Genomic RNA and Activates RIPK3-Dependent Cell Death. *Cell Host Microbe* 20: 674-681.
16. Downey, J., E. Pernet, F. Coulombe, B. Allard, I. Meunier, J. Jaworska, S. Qureshi, D. C. Vinh, J. G. Martin, P. Joubert, and M. Divangahi. 2017. RIPK3 interacts with MAVS to regulate type I IFN-mediated immunity to Influenza A virus infection. *PLoS Pathog* 13: e1006326.
17. Shubina, M., B. Tummers, D. F. Boyd, T. Zhang, C. Yin, A. Gautam, X. J. Guo, D. A. Rodriguez, W. J. Kaiser, P. Vogel, D. R. Green, P. G. Thomas, and S. Balachandran. 2020. Necroptosis restricts influenza A virus as a stand-alone cell death mechanism. *J Exp Med* 217.

18. Daniels, B. P., A. G. Snyder, T. M. Olsen, S. Orozco, T. H. Oguin, 3rd, S. W. G. Tait, J. Martinez, M. Gale, Jr., Y. M. Loo, and A. Oberst. 2017. RIPK3 Restricts Viral Pathogenesis via Cell Death-Independent Neuroinflammation. *Cell* 169: 301-313 e311.
19. Cho, Y. S., S. Challa, D. Moquin, R. Genga, T. D. Ray, M. Guildford, and F. K. Chan. 2009. Phosphorylation-driven assembly of the RIP1-RIP3 complex regulates programmed necrosis and virus-induced inflammation. *Cell* 137: 1112-1123.
20. Wang, X., Y. Li, S. Liu, X. Yu, L. Li, C. Shi, W. He, J. Li, L. Xu, Z. Hu, L. Yu, Z. Yang, Q. Chen, L. Ge, Z. Zhang, B. Zhou, X. Jiang, S. Chen, and S. He. 2014. Direct activation of RIP3/MLKL-dependent necrosis by herpes simplex virus 1 (HSV-1) protein ICP6 triggers host antiviral defense. *Proc Natl Acad Sci U S A* 111: 15438-15443.
21. Gonzalez-Juarbe, N., A. N. Riegler, A. S. Jureka, R. P. Gilley, J. D. Brand, J. E. Trombley, N. R. Scott, M. P. Platt, P. H. Dube, C. M. Petit, K. S. Harrod, and C. J. Orihuela. 2020. Influenza-Induced Oxidative Stress Sensitizes Lung Cells to Bacterial-Toxin-Mediated Necroptosis. *Cell Rep* 32: 108062.
22. Meylan, E., K. Burns, K. Hofmann, V. Blancheteau, F. Martinon, M. Kelliher, and J. Tschopp. 2004. RIP1 is an essential mediator of Toll-like receptor 3-induced NF-kappa B activation. *Nat Immunol* 5: 503-507.
23. Murphy, J. M., P. E. Czabotar, J. M. Hildebrand, I. S. Lucet, J. G. Zhang, S. Alvarez-Diaz, R. Lewis, N. Lalaoui, D. Metcalf, A. I. Webb, S. N. Young, L. N. Varghese, G. M. Tannahill, E. C. Hatchell, I. J. Majewski, T. Okamoto, R. C.

- Dobson, D. J. Hilton, J. J. Babon, N. A. Nicola, A. Strasser, J. Silke, and W. S. Alexander. 2013. The pseudokinase MLKL mediates necroptosis via a molecular switch mechanism. *Immunity* 39: 443-453.
24. Newton, K., X. Sun, and V. M. Dixit. 2004. Kinase RIP3 is dispensable for normal NF-kappa Bs, signaling by the B-cell and T-cell receptors, tumor necrosis factor receptor 1, and Toll-like receptors 2 and 4. *Mol Cell Biol* 24: 1464-1469.
25. Plourde, J. R., J. A. Pyles, R. C. Layton, S. E. Vaughan, J. L. Tipper, and K. S. Harrod. 2012. Neurovirulence of H5N1 infection in ferrets is mediated by multifocal replication in distinct permissive neuronal cell regions. *PLoS One* 7: e46605.
26. Uphoff, C. C., and H. G. Drexler. 2002. Comparative PCR analysis for detection of mycoplasma infections in continuous cell lines. *In Vitro Cell Dev Biol Anim* 38: 79-85.
27. Uphoff, C. C., and H. G. Drexler. 2004. Detecting Mycoplasma contamination in cell cultures by polymerase chain reaction. *Methods Mol Med* 88: 319-326.
28. Gonzalez-Juarbe, N., K. M. Bradley, A. N. Riegler, L. F. Reyes, T. Brissac, S.-S. Park, M. I. Restrepo, and C. J. Orihuela. 2018. Bacterial Pore-Forming Toxins Promote the Activation of Caspases in Parallel to Necroptosis to Enhance Alarmin Release and Inflammation During Pneumonia. *Scientific Reports* 8: 5846.
29. Jutz, S., J. Leitner, K. Schmetterer, I. Doel-Perez, O. Majdic, K. Grabmeier-Pfistershammer, W. Paster, J. B. Huppa, and P. Steinberger. 2016. Assessment of costimulation and coinhibition in a triple parameter T cell reporter line:

- Simultaneous measurement of NF-kappaB, NFAT and AP-1. *J Immunol Methods* 430: 10-20.
30. Jutz, S., A. Hennig, W. Paster, O. Asrak, D. Dijanovic, F. Kellner, W. F. Pickl, J. B. Huppa, J. Leitner, and P. Steinberger. 2017. A cellular platform for the evaluation of immune checkpoint molecules. *Oncotarget* 8: 64892-64906.
31. Miura, H., Y. Kondo, M. Matsuda, and K. Aoki. 2018. Cell-to-Cell Heterogeneity in p38-Mediated Cross-Inhibition of JNK Causes Stochastic Cell Death. *Cell Rep* 24: 2658-2668.
32. Gilley, R. P., N. Gonzalez-Juarbe, A. T. Shenoy, L. F. Reyes, P. H. Dube, M. I. Restrepo, and C. J. Orihuela. 2016. Infiltrated Macrophages Die of Pneumolysin-Mediated Necroptosis following Pneumococcal Myocardial Invasion. *Infect Immun* 84: 1457-1469.
33. Gonzalez-Juarbe, N., C. A. Mares, C. A. Hinojosa, J. L. Medina, A. Cantwell, P. H. Dube, C. J. Orihuela, and M. A. Bergman. 2015. Requirement for *Serratia marcescens* cytolysin in a murine model of hemorrhagic pneumonia. *Infect Immun* 83: 614-624.
34. Allie, S. R., J. E. Bradley, U. Mudunuru, M. D. Schultz, B. A. Graf, F. E. Lund, and T. D. Randall. 2019. The establishment of resident memory B cells in the lung requires local antigen encounter. *Nat Immunol* 20: 97-108.
35. Botta, D., M. J. Fuller, T. T. Marquez-Lago, H. Bachus, J. E. Bradley, A. S. Weinmann, A. J. Zajac, T. D. Randall, F. E. Lund, B. Leon, and A. Ballesteros-Tato. 2017. Dynamic regulation of T follicular regulatory cell responses by interleukin 2 during influenza infection. *Nat Immunol* 18: 1249-1260.

36. Ballesteros-Tato, A., B. Leon, B. A. Graf, A. Moquin, P. S. Adams, F. E. Lund, and T. D. Randall. 2012. Interleukin-2 inhibits germinal center formation by limiting T follicular helper cell differentiation. *Immunity* 36: 847-856.
37. Kato, Y. 2016. Neutrophil myeloperoxidase and its substrates: formation of specific markers and reactive compounds during inflammation. *J Clin Biochem Nutr* 58: 99-104.
38. Camp, J. V., and C. B. Jonsson. 2017. A Role for Neutrophils in Viral Respiratory Disease. *Front Immunol* 8: 550.
39. Connors, T. J., T. M. Ravindranath, K. L. Bickham, C. L. Gordon, F. Zhang, B. Levin, J. S. Baird, and D. L. Farber. 2016. Airway CD8(+) T Cells Are Associated with Lung Injury during Infant Viral Respiratory Tract Infection. *Am J Respir Cell Mol Biol* 54: 822-830.
40. Topham, D. J., R. A. Tripp, and P. C. Doherty. 1997. CD8+ T cells clear influenza virus by perforin or Fas-dependent processes. *J Immunol* 159: 5197-5200.
41. Brincks, E. L., A. Katewa, T. A. Kucaba, T. S. Griffith, and K. L. Legge. 2008. CD8 T cells utilize TRAIL to control influenza virus infection. *J Immunol* 181: 4918-4925.
42. Jorgensen, I., M. Rayamajhi, and E. A. Miao. 2017. Programmed cell death as a defence against infection. *Nat Rev Immunol* 17: 151-164.
43. Huang, Z., S. Q. Wu, Y. Liang, X. Zhou, W. Chen, L. Li, J. Wu, Q. Zhuang, C. Chen, J. Li, C. Q. Zhong, W. Xia, R. Zhou, C. Zheng, and J. Han. 2015.

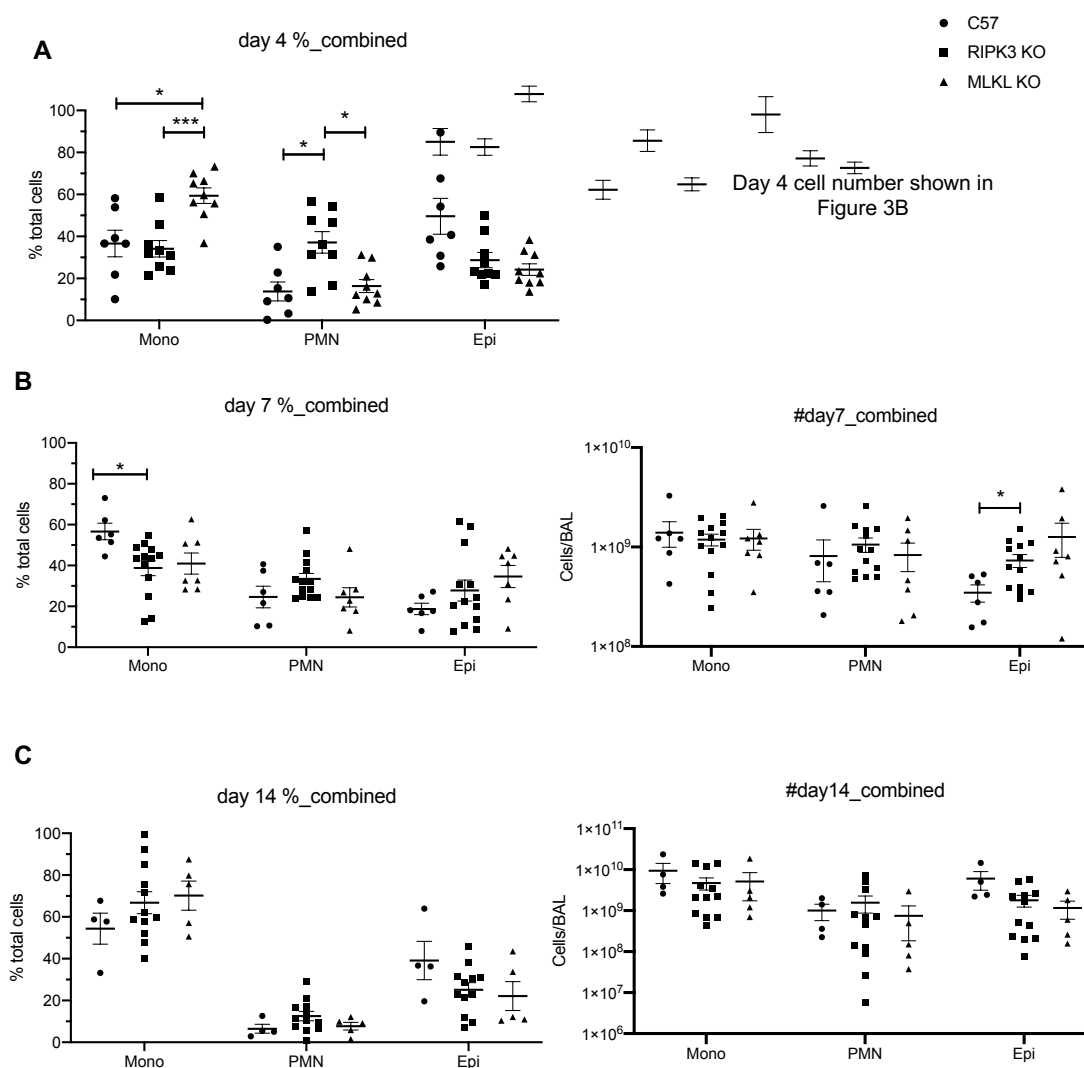
- RIP1/RIP3 binding to HSV-1 ICP6 initiates necroptosis to restrict virus propagation in mice. *Cell Host Microbe* 17: 229-242.
44. Omoto, S., H. Guo, G. R. Talekar, L. Roback, W. J. Kaiser, and E. S. Mocarski. 2015. Suppression of RIP3-dependent necroptosis by human cytomegalovirus. *J Biol Chem* 290: 11635-11648.
 45. Upton, J. W., W. J. Kaiser, and E. S. Mocarski. 2010. Virus inhibition of RIP3-dependent necrosis. *Cell Host Microbe* 7: 302-313.
 46. Newton, K., D. L. Dugger, K. E. Wickliffe, N. Kapoor, M. C. de Almagro, D. Vucic, L. Komuves, R. E. Ferrando, D. M. French, J. Webster, M. Roose-Girma, S. Warming, and V. M. Dixit. 2014. Activity of protein kinase RIPK3 determines whether cells die by necroptosis or apoptosis. *Science* 343: 1357-1360.
 47. Mandal, P., S. B. Berger, S. Pillay, K. Moriwaki, C. Huang, H. Guo, J. D. Lich, J. Finger, V. Kasparcova, B. Votta, M. Ouellette, B. W. King, D. Wisnoski, A. S. Lakdawala, M. P. DeMartino, L. N. Casillas, P. A. Haile, C. A. Schon, R. W. Marquis, J. Upton, L. P. Daley-Bauer, L. Roback, N. Ramia, C. M. Dovey, J. E. Carette, F. K. Chan, J. Bertin, P. J. Gough, E. S. Mocarski, and W. J. Kaiser. 2014. RIP3 induces apoptosis independent of pronecrotic kinase activity. *Mol Cell* 56: 481-495.
 48. He, S., and X. Wang. 2018. RIP kinases as modulators of inflammation and immunity. *Nat Immunol* 19: 912-922.
 49. Gonzalez-Juarbe, N., K. M. Bradley, A. T. Shenoy, R. P. Gilley, L. F. Reyes, C. A. Hinojosa, M. I. Restrepo, P. H. Dube, M. A. Bergman, and C. J. Orihuela. 2017. Pore-forming toxin-mediated ion dysregulation leads to death receptor-

- independent necroptosis of lung epithelial cells during bacterial pneumonia. *Cell Death Differ*.
50. Malireddi, R. K. S., S. Kesavardhana, and T. D. Kanneganti. 2019. ZBP1 and TAK1: Master Regulators of NLRP3 Inflammasome/Pyroptosis, Apoptosis, and Necroptosis (PAN-optosis). *Front Cell Infect Microbiol* 9: 406.
 51. Gaidt, M. M., T. S. Ebert, D. Chauhan, T. Schmidt, J. L. Schmid-Burgk, F. Rapino, A. A. Robertson, M. A. Cooper, T. Graf, and V. Hornung. 2016. Human Monocytes Engage an Alternative Inflammasome Pathway. *Immunity* 44: 833-846.
 52. Brandes, M., F. Klauschen, S. Kuchen, and R. N. Germain. 2013. A systems analysis identifies a feedforward inflammatory circuit leading to lethal influenza infection. *Cell* 154: 197-212.
 53. Abraham, E. 2003. Neutrophils and acute lung injury. *Crit Care Med* 31: S195-199.
 54. Seki, M., S. Kohno, M. W. Newstead, X. Zeng, U. Bhan, N. W. Lukacs, S. L. Kunkel, and T. J. Standiford. 2010. Critical role of IL-1 receptor-associated kinase-M in regulating chemokine-dependent deleterious inflammation in murine influenza pneumonia. *J Immunol* 184: 1410-1418.
 55. Sakai, S., H. Kawamata, N. Mantani, T. Kogure, Y. Shimada, K. Terasawa, T. Sakai, N. Imanishi, and H. Ochiai. 2000. Therapeutic effect of anti-macrophage inflammatory protein 2 antibody on influenza virus-induced pneumonia in mice. *J Virol* 74: 2472-2476.

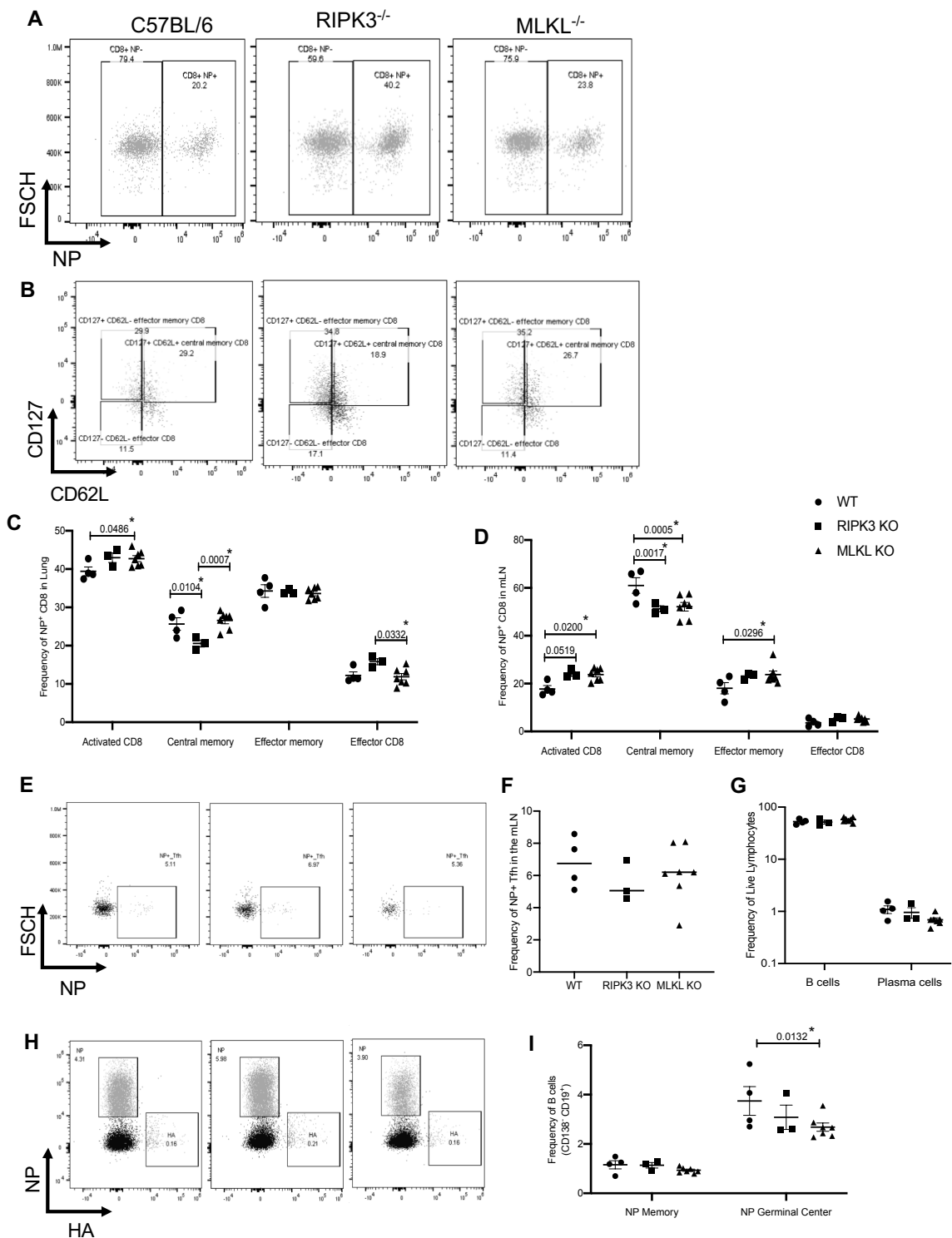
56. Parzych, E. M., L. J. DiMenna, B. P. Latimer, J. C. Small, S. Kannan, B. Manson, M. O. Lasaro, E. J. Wherry, and H. C. Ertl. 2013. Influenza virus specific CD8(+) T cells exacerbate infection following high dose influenza challenge of aged mice. *Biomed Res Int* 2013: 876314.
57. Alwan, W. H., W. J. Kozłowska, and P. J. Openshaw. 1994. Distinct types of lung disease caused by functional subsets of antiviral T cells. *J Exp Med* 179: 81-89.
58. Alwan, W. H., F. M. Record, and P. J. Openshaw. 1992. CD4+ T cells clear virus but augment disease in mice infected with respiratory syncytial virus. Comparison with the effects of CD8+ T cells. *Clin Exp Immunol* 88: 527-536.
59. van de Sandt, C. E., M. Barcena, A. J. Koster, J. Kasper, C. J. Kirkpatrick, D. P. Scott, R. D. de Vries, S. Herold, G. F. Rimmelzwaan, T. Kuiken, and K. R. Short. 2017. Human CD8(+) T Cells Damage Noninfected Epithelial Cells during Influenza Virus Infection In Vitro. *Am J Respir Cell Mol Biol* 57: 536-546.
60. Moskophidis, D., and D. Kioussis. 1998. Contribution of virus-specific CD8+ cytotoxic T cells to virus clearance or pathologic manifestations of influenza virus infection in a T cell receptor transgenic mouse model. *J Exp Med* 188: 223-232.
61. Xu, L., H. Yoon, M. Q. Zhao, J. Liu, C. V. Ramana, and R. I. Enelow. 2004. Cutting edge: pulmonary immunopathology mediated by antigen-specific expression of TNF-alpha by antiviral CD8+ T cells. *J Immunol* 173: 721-725.
62. Rygiel, T. P., E. S. Rijkers, T. de Ruyter, E. H. Stolte, M. van der Valk, G. F. Rimmelzwaan, L. Boon, A. M. van Loon, F. E. Coenjaerts, R. M. Hoek, K. Tesselaar, and L. Meyaard. 2009. Lack of CD200 enhances pathological T cell responses during influenza infection. *J Immunol* 183: 1990-1996.

63. Snelgrove, R. J., J. Goulding, A. M. Didierlaurent, D. Lyonga, S. Vekaria, L. Edwards, E. Gwyer, J. D. Sedgwick, A. N. Barclay, and T. Hussell. 2008. A critical function for CD200 in lung immune homeostasis and the severity of influenza infection. *Nat Immunol* 9: 1074-1083.
64. Quinones-Parra, S., E. Grant, L. Loh, T. H. Nguyen, K. A. Campbell, S. Y. Tong, A. Miller, P. C. Doherty, D. Vijaykrishna, J. Rossjohn, S. Gras, and K. Kedzierska. 2014. Preexisting CD8⁺ T-cell immunity to the H7N9 influenza A virus varies across ethnicities. *Proc Natl Acad Sci U S A* 111: 1049-1054.
65. Tisoncik, J. R., M. J. Korth, C. P. Simmons, J. Farrar, T. R. Martin, and M. G. Katze. 2012. Into the eye of the cytokine storm. *Microbiol Mol Biol Rev* 76: 16-32.
66. Jin, S., Y. Li, R. Pan, and X. Zou. 2014. Characterizing and controlling the inflammatory network during influenza A virus infection. *Sci Rep* 4: 3799.
67. Kearney, C. J., and S. J. Martin. 2017. An Inflammatory Perspective on Necroptosis. *Mol Cell* 65: 965-973.
68. Kearney, C. J., S. P. Cullen, G. A. Tynan, C. M. Henry, D. Clancy, E. C. Lavelle, and S. J. Martin. 2015. Necroptosis suppresses inflammation via termination of TNF- or LPS-induced cytokine and chemokine production. *Cell Death Differ* 22: 1313-1327.

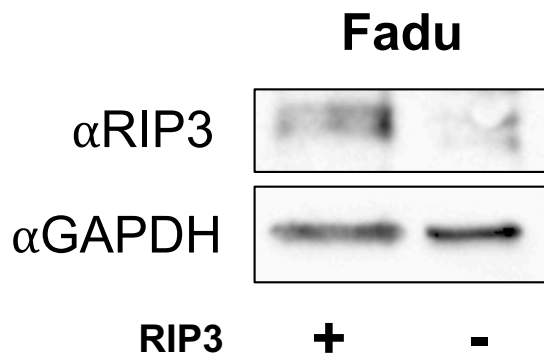
SUPPLEMENTAL FIGURES/TABLES



Supplemental Figure 1: RIPK3 deficiency alters immune cell population dynamics in the lung during IAV infection. Percent cell type distribution and cell type count was determined from HEMA3 stained CytoSpin spots from BAL collected at **A)** 4, **B)** 7, and **C)** 14 days post-infection from wildtype C57BL/6, RIPK3 KO, and MLKL KO mice infected i.n. with 250 PFU of Influenza A/Puerto Rico/8/1934. Data are compared by One-Way ANOVA with Dunn's post-test. * $P \leq 0.05$ and *** $P \leq 0.001$. (See also **Figure 3**)



Supplemental Figure 2: Deficiency in necroptotic signaling proteins alters the adaptive immune response in the lung and draining lymph node during IAV infection. Wildtype C57BL/6, RIPK3 KO, and MLKL KO mice were infected i.n. with 250 PFU of Influenza A/Puerto Rico/8/1934, then lungs and draining lymph node (mediastinal, mLN) were collected for analysis at two weeks post-infection. Representative flow cytometry gates for **A)** IAV NP specific CD8⁺T cells and **B)** NP⁺CD8⁺ T cell subtypes in the lung and mLN are shown. Frequency of NP⁺CD8⁺ T (CD19⁻CD25⁺CD8⁺NP⁺) cell subtypes in the **C)** lung and **D)** mLN at two weeks post-infection of IAV infected mice was determined. Data are compared by One-way ANOVA with Dunn's post-test. *P ≤ 0.05 and P values are shown. Flow cytometry **E)** representative plots and calculated **F)** frequency of IAV NP specific T follicular helper (Tfh, CD19⁻CXCR5⁺PD1⁺Bcl6⁺NP⁺) cells in the mLN of these IAV infected mice are shown. **G)** Frequency of IAV NP specific B cells (CD138⁻CD19⁺) and Plasma cells (CD138⁺CD19^{mid}) in the mLN of IAV infected mice was determined from these same mice. **H)** representative flow cytometry plot and **I)** frequency of memory (CD138⁻CD19⁺CD38^{high}CD95⁻) and germinal center (GC) (CD138⁻CD19⁺CD38^{low}CD95⁺) B cells specific to NP in the mLN of these IAV infected mice are shown. Data are compared by One-Way ANOVA with Sidak's post-test. *P ≤ 0.05 (See also **Figure 3**)



Supplemental Figure 3: Construction of RIPK3 and MLKL deficient cell lines by CRISPR/cas9. Western Blots from wildtype (+) CRISPR/cas9 gene-edited RIPK3 knockout (-) FaDu cell lysates probed for RIPK3 and GAPDH are shown.

| | MANUFACTURER | CAT# / INFORMATION |
|--|----------------------------|--------------------|
| ELISA | | |
| Mouse myeloperoxidase (MPO) | R&D systems | DY3667 |
| Mouse IL-1 β | R&D systems | DY401-05 |
| Mouse CXCL1/KC | R&D systems | DY435-05 |
| Mouse IL-1 α | R&D systems | DY400-05 |
| Human IL-1 α | R&D systems | DY200-05 |
| Human IL-1 β | R&D systems | DY201-05 |
| Human IL-8 | R&D systems | DY208-05 |
| ANTIBODIES | | |
| Mouse anti-RIPK3 | Santa Cruz Biotechnology | Sc-374639 |
| Goat anti-mouse (HRP conjugated) | Jackson ImmunoResearch | 115-035-003 |
| Rabbit anti-GAPDH | Abcam | ab181602 |
| Goat anti-rabbit (HRP conjugated) | Jackson ImmunoResearch | 111-035-144 |
| Mouse anti-eGFP | Invitrogen | 01-647-566 |
| Rat anti-mCherry | Invitrogen | M11217 |
| Mouse anti-Kusabira Orange 2 | MBL International | 50-168-8064 |
| Donkey anti-mouse (Texas Red conjugated) | Invitrogen | PA128626 |
| Rabbit anti-rat (Texas Red conjugated) | Invitrogen | PIPA128571 |
| Donkey anti-rat (Dylight 550 conjugated) | Novus Biologicals | NBP175652 |
| Anti-CD16/32 | BD Biosciences | Clone 2.4G2 |
| Anti-CD19 | BD Biosciences | Clone 1D3 |
| Anti-CD138 | BD Biosciences | Clone 281.2 |
| Anti-Bcl-6 | BD Biosciences | Clone K112.91 |
| Anti-CXCR5 | BD Biosciences | Clone 2G-8 |
| Anti-CD4 | BD Biosciences | Clone RM4-5 |
| Anti-CD69 | BD Biosciences | Clone H1.2F3 |
| Anti-CD25 | BD Biosciences | Clone PC61 |
| Anti-PD-1 | eBioscience | Clone J43 |
| Anti-Foxp3 | eBioscience | Clone FJK-16s |
| SPECIAL REAGENTS | | |
| NucBlue Fixed Cell Reagent (DAPI) | Invitrogen | R37606 |
| Necrosulfonamide | Tocris Bioscience | 5025 |
| Z-VAD-fmk | Sigma-Aldrich | V116 |
| GSK'872 | BioVision | 2673 |
| T Regulatory Cell Staining Kit | eBioscience | 88-8118-40 |
| I-Ab NP311-325 MHC class II tetramer | NIH tetramer Core Facility | N/A |
| NP B-cell tetramer | N/A *see methods | *see methods |
| CytoTox 96 Assay Kit (LDH) | Promega | G1780 |
| Pierce LDH Cytotoxicity Assay Kit | Thermo Scientific | 88954 |

Supplemental Table 1: Key reagents/kits. Table indicates the purpose or target of the kit used, the manufacturer, and the catalog number.

CHAPTER 6

DISCUSSION, CONCLUSIONS, AND FUTURE DIRECTIONS

General Discussion

Respiratory infections are the 3rd leading cause of death worldwide (WHO, 2016) and are among the top three outpatient diagnoses in the United States (Fendrick et al., 2003; Gonzales et al., 1997). Additionally, according to the WHO, pneumonia is the leading cause of infectious death worldwide, in the United States alone resulting in more than 1 million diagnoses and 50,000 deaths annually (Prevention, 2020b). In fact, in 2019, pneumonia is within the top ten causes of death in the United States (Kochanek et al., 2020). These airway infections are associated with various parasites, fungi, bacteria, and viral pathogens. The latter two resulting in the greatest number of respiratory tract infections and hospitalizations, worldwide. Respiratory pathogens, like *Spn* and IAV discussed within this dissertation, possess various mechanisms to interact with host cells and counter the host responses, posing serious risk to human health. Pertinent to this work, prior studies from our laboratory and others showed that both *Spn* and IAV are capable of eliciting necroptosis of host cells during infection, ultimately influencing disease pathology and mortality.

The initiation of necroptosis by *Spn* is accomplished via the expression of ply, its PFT, which binds to cholesterol in host cells, causes ion dysregulation, and ultimately results in the cell dying via necroptosis (Gonzalez-Juarbe et al., 2017a). Our group has

shown that this occurs in macrophages within the lung and heart as well as in lung epithelial cells (Gilley et al., 2016; Gonzalez-Juarbe et al., 2017a; Shenoy et al., 2017). Additional *Spn* virulence factors besides ply, like the polysaccharide capsule and the peroxide produced by the *Spn* pyruvate oxidase encoded within the SpxB gene, also contribute to this activation of necroptosis during infection. Similarly, other bacterial pathogens like *Staphylococcus aureus*, *Salmonella enterica*, *Acinetobacter baumannii*, and *Serratia marcescens* induce necroptosis of host cells during infection (Gonzalez-Juarbe et al., 2017a; Gonzalez-Juarbe et al., 2015; Z. Huang et al., 2015; Kitur et al., 2015; Li et al., 2018; Liang & Qin, 2013; Robinson et al., 2012). This includes within the lower respiratory tract as well as other sites of infection (Bleriot et al., 2015; Wong Fok Lung et al., 2020). A recent study of *Staphylococcal* infections indicated that cell death by necroptosis served to limit pathological inflammation through the avoidance of other even more inflammatory forms of necrosis or mediation of the host immune response (Kitur et al., 2016). Despite this, a multitude of previous work has shown that during bacterial infection necroptosis is largely detrimental to the host pathology and survival, as result of dampened recruitment signal from patrolling resident immune cells, increased release of DAMPS which alter the immune recruitment and subsequent response from neighboring cells, and due to weakened barriers allowing bacteria to disseminate to otherwise sterile areas of the host [reviewed in (Kearney & Martin, 2017; W. Zhou & Yuan, 2014)].

Necroptosis during Spn colonization

When we began this work, whether necroptosis occurred and was beneficial or detrimental to the host pathology during asymptomatic infections by airway bacterial

pathogens was unknown. This is important as many bacterial respiratory pathogens, including *Spn*, first colonize the upper respiratory tract (*e.g.* the nasopharynx) in an asymptomatic fashion, from which the bacteria often disseminate to other bodily sites such as the lungs, blood, brain, and other organs to cause disease. For *Spn*, this colonization is prevalent in the global population and serves as a pre-requisite to symptomatic infection. This colonization is accomplished primarily by the formation of bacterial biofilms which we have previously shown to have increased expression and release of ply (Shenoy et al., 2017). Thus, we hypothesized that this ply resulted in necroptosis of cells in the upper airway during asymptomatic *Spn* colonization; additionally, that this directly influenced the host response to the colonizing pathogen.

Here (Chapter 2) we showed that during *Spn* colonization, necroptosis occurs within the nasopharyngeal epithelial cells. We demonstrated that the regions undergoing necroptosis (*i.e.* positive for pMLKL) are directly associated with submucosal CD11c⁺ cells (likely APCs), whereas these APCs were not observed in the submucosa of regions not undergoing necroptosis, suggesting that PFT-induced necroptosis may be the mechanism which drives APC recruitment. We further identified a significantly impaired ability for mice deficient in necroptosis to release inflammatory cytokines (like IL-1 α , IL-33, and IL-17) when challenged with *Spn*, as well as a delay in nasopharyngeal clearance in these mice compared to those capable of necroptosis. This is notable because the recruitment of APCs and clearance of colonizing *Spn* has previously been shown to be accelerated by these observed cytokines (Cohen et al., 2011; Land, 2015; Lemon, Miller, & Weiser, 2015; Z. Zhang, Clarke, & Weiser, 2009); the absence of their signaling consequently associated with increased neutrophil infiltration (Kafka et al., 2008). Our

observations from mice and cells challenged with *Spn* are consistent with this and the inability to undergo necroptosis severely impaired these key functions. Our results demonstrate that despite the associated tissue damage and unlike during disseminated infections, ply-mediated necroptosis is beneficial to the host pathology and immune response during colonization, serving as a key initiator of innate and adaptive immunity against colonizing *Spn*. Collectively, our observations support the conclusion that ply-mediated necroptosis directly acts in the orchestration of the natural clearance and innate response to colonizing *Spn*.

The impact of these findings may extend further to the various other PFT-producing mucosal colonizers. Given the variety and abundance of these colonizers, our results suggest that necroptosis may be one way by which the host immune system is able to differentiate potential pathogens (*i.e.* those producing PFTs) from other, non-threatening bacteria which colonize the same niche. The recruitment of APCs and the enhanced generation of protective antibody resultant from necroptosis as we report may reduce the severity of disease caused by the same PFT-producing pathogen if subsequently encountered in a disease setting (*e.g.* lower respiratory infection, burns, etc.). Additionally, recent work from Huang et al shows that during *Spn* pneumonia, the absence of RIPK3 results in decreased *Spn* clearance of the lungs (H. R. Huang et al., 2021), suggesting that this dual functionality of necroptosis, in both increasing damaging pathology as well as initiating immunity, applies beyond the setting of asymptomatic colonization. Further, our results suggest that cellular necroptosis during infection by other pathogen types, such as viruses, may also facilitate the recruitment of APCs and the generation of an adaptive immune response.

IPD and necroptosis

Stepping beyond colonization, we and others have extensively examined the detrimental impact of ply-mediated necroptosis of epithelial cells in the lungs as well as immune cells in the lungs and heart during acute infection by *Spn*. However, at the time we began this work, the long-term effects of necroptosis on the host pathology were entirely unknown. Notably, necroptosis had previously been associated with the depletion of tissue resident macrophages in *Spn* infection, during pneumonia as well as IPD (Gilley et al., 2016; Gonzalez-Juarbe et al., 2015). Additionally, and following sterile injury, cardiac damage had been shown to be exacerbated by necroptosis of cardiomyocytes (Koshinuma, Miyamae, Kaneda, Kotani, & Figueredo, 2014). Moreover, patients who develop bacteremia during hospitalization for pneumococcal pneumonia (*i.e.* IPD) have been shown to be at an increased risk of cardiac complications or MACE up to ten years into convalescence (Eurich, Marrie, Minhas-Sandhu, & Majumdar, 2017; Musher, Abers, & Corrales-Medina, 2019). In addition to the various physiological stressors associated with severe systemic bacterial infection (like those experienced during IPD), substantial experimental, clinical, and epidemiological evidence had recently been published suggesting that *Spn* directly damages the heart during IPD, contributing to MACE within the hospital setting (Brown, Millett, Quint, & Orihuela, 2015; Corrales-Medina et al., 2011; Eurich et al., 2017; Musher et al., 2019; Musher, Rueda, Kaka, & Mapara, 2007; Reyes et al., 2017). From this, we hypothesized that cardiomyocytes die by necroptosis during IPD, and that this necroptosis contributes to the observed cardiac dysfunction in convalescence.

Here (Chapter 3) we confirmed that during IPD *Spn* is capable of causing ply-mediated cardiomyocyte death by necroptosis, and showed that this cardiac damage as well as the resulting cardiac dysfunction persists up to 3 months after initial infection; thus, raising the possibility that cardiac damage and its associated dysfunction (*e.g.* MACE) may be preventable. Subsequently, we showed that therapeutic inhibition of necroptosis did, in fact, ameliorate both the acute lung and cardiac damage/dysfunction, as well as the cardiac damage and dysfunction observed in sequelae. Importantly, we show that this inhibition can be accomplished simultaneous to antibiotic therapy by repurposing the FDA-approved drug Ponatinib, typically used to treat leukemia but also capable of inhibiting the activation of RIP kinases (Cortes et al., 2013). We also observed a substantial reduction in cardiac microlesion formation when necroptosis was inhibited, suggesting that cardiomyocyte death by necroptosis directly influences the formation of *Spn* microlesions. This supports our previous work which showed that *Spn* are taken up by cardiomyocytes after entering the myocardium and these host cells die (Brown et al., 2014), and further suggests these cells which take up *Spn* die by ply-mediated necroptosis. Our observation that cardiac dysfunction was absent during acute IPD and sequelae when mice were treated with Ponatinib suggests that ply-mediated necroptosis may also contribute to the increased cardiac dysfunction observed in humans during IPD and in recovery. Our data suggest that therapeutic inhibition of necroptosis may have long-term beneficial effects for individuals with IPD.

The impact of necroptosis on IAV/Spn co-infection

Necroptosis of host cells is not limited in activation to bacterial pathogens and the effects of activation in these settings must also be examined. Notably, our understanding of the consequences of this activation in the disease-relevant co-infection setting of IAV and *Spn* has significant value to treating individuals with respiratory infections.

Activation of necroptosis by viral pathogens, like IAV, is accomplished primarily through direct intracellular sensing of the virus and many viruses, including IAV, have been shown to directly sensitize cells to TNF-mediated necroptosis by encoding proteins which inhibit the activation of caspases and consequently the PCD pathways which rely on caspases (*e.g.* apoptosis and pyroptosis) (Chan et al., 2003; Q. Zhou et al., 1997).

Previous work has also shown that IAV can initiate necroptosis in epithelial cells, macrophages, and dendritic cells through the interaction of viral NP and PB1 with cellular DAI (a.k.a. Zbp or DLM-1), resulting in the activation of RIPK3 (Kuriakose et al., 2016; Nogusa et al., 2016; Thapa et al., 2016; T. Zhang et al., 2020). Generally, the induction of necroptosis during viral infection is considered to be beneficial to the host, aborting viral replication in infected cells (Balachandran & Rall, 2020; Nogusa et al., 2016; W. Zhou & Yuan, 2014). Pertinent to this work, clinical and molecular epidemiology have shown that the most serious IAV infections are typically associated with co- or secondary bacterial infections, with *Spn* by far identified as the most commonly associated bacterium (Gill et al., 2010; Louie et al., 2009; Koenraad F. van der Sluijs et al., 2010). Numerous publications have helped to explain the synergy which contributes to the observed disease severity between IAV and *Spn* during co-infection, including the observations that the NA of IAV cleaves terminal sialic acid on host cell

glycoconjugates, exposing antigens for bacterial attachment (Jonathan A McCullers & Bartmess, 2003); that these cleaved sialic acid residues promote *Spn* outgrowth by serving as a nutrient source for the bacteria (Hentrich et al., 2016); that cytokines and alarmins released during IAV infection from dying cells elicit transcriptional changes in *Spn* that enhance its virulence (Pettigrew et al., 2014); that IAV-induced interferon (IFN) gamma expression results in the down regulation of macrophage surface scavenger receptors required for uptake of *Spn* (K. Sun & Metzger, 2008); that IAV alters the pulmonary fluid homeostasis by down-regulating of ion channels in bronchial epithelial cell, favoring bacterial replication (Brand et al., 2018); and that the immune response induced by viral infection is inappropriate for bacterial clearance, ultimately enhancing pulmonary injury (Shahangian et al.; K. F. van der Sluijs et al., 2006). The potential for necroptosis to influence this synergy and the mechanisms of necroptosis induction during these infections were not yet addressed.

Here (Chapter 4) we determined that IAV-induced cell damage persists in lung epithelial cells, sensitizing the cells to PFT-mediated necroptosis upon subsequent *Spn* infection and worsening disease pathology. We show that this sensitization persists even when IAV replication is blocked by Pimodivir, indicating that the cellular alterations as result of infection are not consequence of viral burden or replication. We show that this damage is instead the result of oxidative stress triggered by IAV. Further, that inhibition of ROS confers protection against IAV-induced sensitization to PFT-mediated necroptosis in both the co-infection and subsequent infection model. Our observations not only suggest the mechanism responsible for IAV-mediated necroptosis sensitization, potentiated by acute intracellular ROS levels and independent of viral replication, but we

have also identified a potential route for therapeutic intervention to reduce the severity of IAV/*Spn* co- and secondary infections.

Here we also provide further support for the critical role of PFTs, using both ply and α -toxin from *S. aureus*, in the induction of necroptosis during secondary infections to influenza. Detailed in Chapter 2 of this dissertation, we showed that necroptosis elicited by ply during *Spn* colonization initiates localized inflammation required for the development of antibodies against *Spn*, directly indicating a link between necroptosis and the subsequent immune response to *Spn* (Riegler, Brissac, Gonzalez-Juarbe, & Orihuela, 2019). Along such lines, it has been shown that mice exposed to *Spn* which over-express ply, prior to IAV/*Spn* dual infection, are more protected against virus-induced lung pathology and mortality; these results then attributed to the modulation of macrophages (Wolf et al., 2014). Similarly, it has been shown that *Spn* infection preceding IAV conferred protection against secondary bacterial challenge, and that IAV infection preceding *Spn* resulted in the dramatic sensitization to the bacteria (J. A. McCullers & Rehg, 2002). Altogether, these findings suggest that the order of exposure to virus and bacteria has a distinct impact on disease outcomes and the overall role of ply, oxidative stress, or necroptosis in this order or how they orchestrate the host response have yet to be fully appreciated.

While the order of sensitization and the individual roles of cellular damage by ply versus ROS require further study, we show that inhibition of the necroptosis pathway may be targeted for therapeutic intervention during IAV co- or secondary *Spn* infections. Notably, directly targeting necroptosis through MLKL is preferable as it is important to consider that inhibition of RIPKs may impact the cell in a non-necroptosis fashion such

as through apoptosis, NF- κ B signaling and resulting inflammation, as well as cellular responses to ion changes (He & Wang, 2018). Additionally, necroptosis inhibition may promote viral replication during co-infection, which may further alter infection pathology and morbidity; however, the effects of necroptosis on viral replication are examined in Chapter 5 and our data suggest this is not a significant concern. Collectively, our results suggest a vital role for necroptosis during IAV/*Spn* co- and secondary infections and provide a molecular explanation for how IAV sensitizes airway cells to undergo necroptosis through long-lasting ROS-mediated cellular alterations. These observations add to our current understanding of how necroptosis serves as both beneficial and detrimental to host outcomes as determined by the overall amount, location, and resultant inflammation (**Figure 1**).

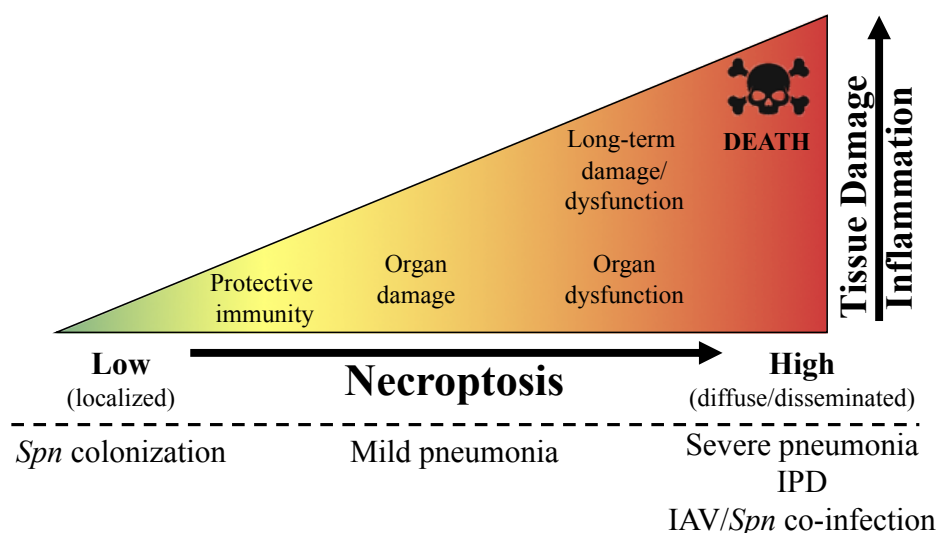


Figure 1. Summary of the impact of necroptosis and associated tissue damage on the host during infection. Diagram of the scale of necroptosis as it relates to tissue damage and host responses during various types of infection.

RIPK3 signaling during IAV pneumonia

The role which necroptosis plays during viral infection alone is not well understood but has been shown to be profoundly important during infection by various viruses. Previous work has shown that mice deficient in RIPK3 are more susceptible to infection by Vaccinia viruses (Cho et al., 2009), Herpes simplex viruses (Z. Huang et al., 2015; Wang et al., 2014), and West Nile virus (Daniels et al., 2017). Likewise, there are data which show that infections by other viruses, like those belonging to the cytomegalovirus genus, are less affected by necroptosis, more specifically the presence or absence of RIPK3, due to viral-encoded inhibitors of RIP activation, supporting the importance of necroptosis during viral infection (Omoto et al., 2015; Upton et al., 2010). During IAV infection, previous studies have shown that necroptosis inhibition results in worsened disease and increased mortality (Downey et al., 2017; Nogusa et al., 2016; T. Zhang et al., 2020). Conversely and more recently, others have shown that necroptosis inhibition results in decreased susceptibility and increased survival following IAV challenge (Shubina et al., 2020). These conflicting conclusions regarding necroptosis during IAV infection were of particular interest to us and we sought out to bridge these data through identification of a potential mechanism.

One consideration regarding our understanding of necroptosis during IAV infection is that recent identification of the diverse roles which RIPK3 plays during viral infection has contributed to the development of more specific molecular targets and tools which were not available during the initial studies. Notably, RIPK3 has recently been shown to signal in a number of other cellular pathways in addition to its canonical role in the activation of MLKL; including as a pro-apoptotic adaptor, recruiting RIPK1, FADD,

and cFLIP to initiate the activation of caspase-8 (Mandal et al., 2014; Newton et al., 2014). This pro-apoptotic function has further been shown as result of ion dysregulation and mitochondrial damage (Gonzalez-Juarbe et al., 2017a; He & Wang, 2018). As detailed in chapter 5 of this dissertation, we examined the specific molecular function of RIPK3 during IAV infection, both in associated with and independent of necroptosis, to better understand the conflicting data which have been previously published and to further characterize the role of this important signaling molecule in the host response to IAV.

Notably, we observed that RIPK3 deficiency increased susceptibility of mice to IAV, whereas MLKL deficiency did not. Further, that deficiency in RIPK3 or MLKL did not affect lung viral titers following IAV challenge, indicating that necroptosis did not reduce viral replication and that RIPK3 plays a beneficial role during IAV infection by means besides MLKL-orchestrated necroptosis. Surprisingly, we also observed that deficiency in RIPK3 was also associated with cytotoxicity (LDH release) *in vitro*, indicating that the activation of IAV-infected RIPK3 deficient cells ultimately still results in death, but in a manner other than necroptosis. These observations provide promising support for necroptosis inhibition as a therapeutic avenue to treat IAV/*Spn* co-infections as discussed above and were consistent with previously published works, further identifying the need for understanding this role of RIPK3 during IAV infection.

Building from previous molecular studies which showed that RIPK3 is capable of inhibiting the activation of NF κ B by preventing the formation of the RIPK1/IKK complex, we sought to determine if the observed pathological results in the absence of RIPK3 during IAV infection were in fact due to unmitigated NF κ B signaling. We show

that RIPK3 deficiency does result in increased NF κ B activation in response to IAV infection as well as TLR stimulation, subsequently resulting in increased release of the pro-inflammatory IL-1 cytokines (IL-1 α and IL-1 β) as well as chemoattractants (*i.e.* IL-8 or KC) associated with neutrophil recruitment. These data were further supported by a marked increase in PMNs in the lungs following IAV infection of mice deficient in RIPK3 and provide significant support for the observed susceptibility in these mice to lethal challenge, as the number of lung neutrophils following IAV infection are positively correlated to the severity of disease in humans (Brandes, Klauschen, Kuchen, & Germain, 2013; Camp & Jonsson, 2017). Additionally, it has been shown that neutralizing neutrophil-derived signals during IAV infection improves survival and pathology in mice (Abraham, 2003; Sakai et al., 2000; Seki et al., 2010). Our observations following IAV indicate that, when present, RIPK3 activation is associated with canonical necroptosis; whereas in the absence of RIPK3, IAV infected cells exhibit increased NF κ B signaling through RIPK1 (**Figure 2**). Thus, RIPK3 may be key in dampening the signals associated with neutrophil recruitment to the lungs; and consequently, RIPK3 may serve to reduce damaging inflammation following IAV infection.

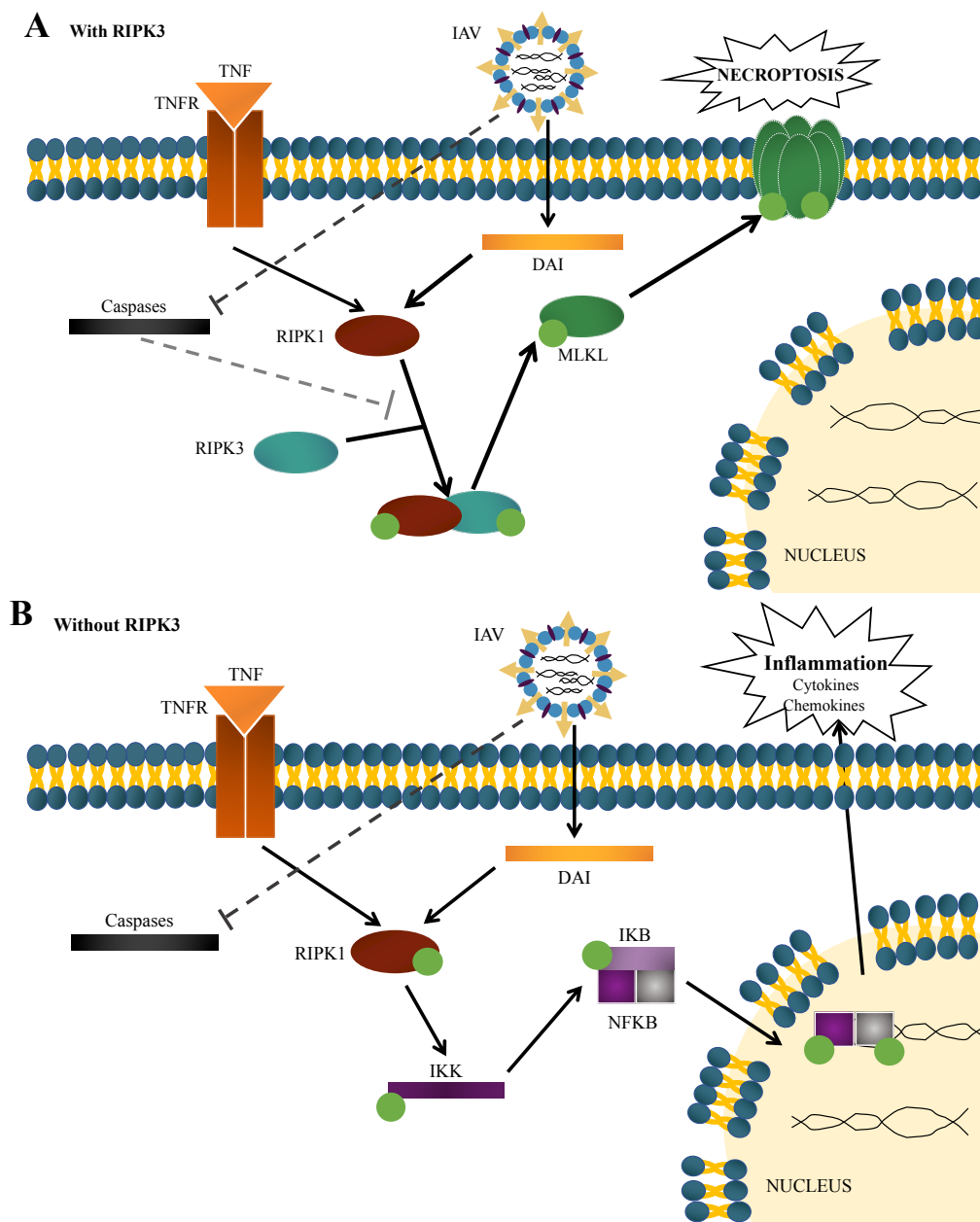


Figure 2. General depiction of RIPK3 during IAV infection. Diagram of the cellular response to IAV infection when A) RIPK3 is present and B) RIPK3 is absent. Phosphorylation is indicated by green circles.

Our observations of immune cell population alterations following IAV infection and in the absence of RIPK3 were further present in examination of viral-specific CD8⁺ T cells in the lungs, which we showed to be considerably increased in RIPK3 KO mice

compared to WT or MLKL KO mice following infection. This observation is notable because despite contributing to the clearance of virus, lung CD8⁺ T cells have also been shown to contribute to the severity of disease not only during IAV infection (Moskophidis & Kioussis, 1998; Parzych et al., 2013; van de Sandt et al., 2017), but also during infection by other respiratory viruses (Alwan, Kozłowska, & Openshaw, 1994; Alwan, Record, & Openshaw, 1992). Thus, the increased number of lung IAV-specific CD8⁺ T cells observed in the absence of RIPK3 likely contributed to the observed pathology and decreased survival by similar mechanisms, through decreased lung barrier integrity resulting from the dysregulated release of T-cell associated cytokines (*e.g.* TNF and IFN).

The inflammation and immunity which result from the cytokines associated with increased NFκB activation are distinct from those which would be released as result of cellular necroptosis, and the effects these responses have on pathology are different. Necroptosis is largely associated with the release of DAMPS (*e.g.* IL-33, IL-1α, histones, and DNA) and is limited by the amount of these DAMPS existing in the cell at the time of lysis (Kearney & Martin, 2017). Notably, the rapid lysis associated with necroptosis does terminate the transcription of various other pro-inflammatory cellular responses (Kearney et al., 2015). So, whether the inflammation triggered as result of necroptosis is less damaging to the host during IAV infection than that elicited by the unmitigated activation of NFκB in the absence of RIPK3 warrants further study. Collectively and in addition to other reports cited above, we have demonstrated that RIPK3 may serve to dampen damaging inflammation through the suppression of RIPK1/IKK-mediated NFκB activation. We have also shown that this suppression by RIPK3, independently of

MLKL-mediated necroptosis, serves to reduce damaging inflammation during IAV infection. While there are many unanswered questions, such as whether this suppression by RIPK3 functions during cellular stimulation by other viruses or non-viral signals, we have further shown that the role of necroptotic signaling during airway infection is multifaceted.

Future Directions

A beneficial role for necroptosis during colonization, like that which we observed in Chapter 2, is in stark contrast to the roles identified for necroptosis during severe bacterial diseases, reflecting the duality of inflammation. Questions remaining from our observations include determining the specific role of alarmins, such as the newly identified IL-1 α and IL-33, in the orchestration of immunity. Additionally, how the host utilizes necroptosis to stimulate immunity in response to asymptomatic infection by other pathogens (*e.g.* *S. aureus* and IAV) as well as in response to co- or polymicrobial infections have yet to be fully characterized. It is likely that the immune-stimulating effects of necroptosis during infection are not limited to *Spn* or to the nasopharynx. Recent work by Huang et al supports this, indicating that RIPK3 is vital in the induction of an adaptive immune response to and clearance of *Spn* during pneumonia (H. R. Huang et al., 2021). Various other mucosal pathobionts are capable of eliciting this cell death pathway in host cells and so the observations made in Chapter 2 of this dissertation have important implications on our understanding of mucosal immunity as well as the co-evolution of the immune system with mucosal pathogens which utilize the host mucosa as an obligate niche, like *Spn*. Similarly, whether we can utilize this localized necroptosis

to initiate adaptive immunity to select antigens, much like a natural adjuvant, present valuable potential for future vaccine development.

Likewise, necroptosis inhibition as a potential therapeutic shows much promise yet there are still many future considerations. Importantly, while our data indicate that the FDA-approved drug Ponatinib is a promising adjunct therapeutic to antibiotics in treating IPD and the associated long-term damage, Ponatinib has a “black box warning” in patients being treated for leukemia (Gainor & Chabner, 2015). The dose of Ponatinib used in our studies was significantly less and for a much shorter time period than those used in treatment for leukemia, and thereby merits considerable caution and future analyses. Further analyses on how early treatment would need to be administered provide a protective effect, whether necroptosis inhibition would have negative consequences during viral co-infection, and whether necroptosis inhibitors, like Ponatinib, would have negative interactions with other drugs must be completed before this treatment avenue could be further considered for clinical trials. Nevertheless, in our study Ponatinib reduced both acute pulmonary and cardiac damage as well as long-term cardiac dysfunction following pneumococcal disease, opening the possibility of repurposing other already FDA-approved drugs to treat or prevent tissue injury which results from infectious disease.

In the context of *Spn*/IAV co-infections, we have shown that necroptosis inhibition reduces the damaging lung pathology which results from this cell death. We also show that the initiation of necroptosis in this setting is influenced by the production of ROS by viral infection and inhibiting this ROS, reduces the amount of necroptosis and consequently the damaging pathology. It is still unknown how the cellular modifications

which result from this IAV-induced ROS are sensed by the cell or sensitize the cell to further PFT-mediated necroptosis. Notably, there is substantial work showing that oxidative stress has pleiotropic effects on the cell, and that intracellular ROS can target cellular proteins, lipid membranes, nucleic acids, and even alter ion homeostasis or cellular energy levels (Sies, Berndt, & Jones, 2017). The latter two we have previously been shown to trigger necroptosis during bacterial infection (Gonzalez-Juarbe et al., 2018; Gonzalez-Juarbe et al., 2017b). Importantly, it is unknown whether other viruses potentiate PFT-mediated necroptosis in a similar way to IAV. Of note, many viruses have previously been shown to induce oxidative stress/ROS in host cells (Hosakote, Liu, Castro, Garofalo, & Casola, 2009; Schwarz, 1996), as well as induce necroptosis of host cells during infection (Nailwal & Chan, 2019; Orzalli & Kagan, 2017; Simpson et al., 2020). Thus, it is likely that this mechanism is not restricted to IAV.

Additionally, it is worth investigating the potential for this ROS-potentiated-necroptosis-mediated IAV/*Spn* synergy in other disease settings. Notably, IAV has been shown to orchestrate the development of *Spn* otitis media (Tong, Fisher, Kosunick, & DeMaria, 2000), and it is reasonable to think that viral-induced ROS may also predispose cells to *Spn*-mediated necroptosis. What is more, whether this synergy extends to other bacterial pathogens which induce necroptosis is unknown. Our preliminary work including the α -toxin of *S. aureus*, detailed in Chapter 4 of this dissertation, would suggest that this synergy is not restricted to *Spn*; additionally, that this synergy may contribute to the severity of at other anatomical sites of co-infection.

Finally, in the context of IAV pneumonia, the role of necroptotic signaling independent of necroptotic cell death is yet to be fully characterized. Our work

identifying the MLKL-independent role of RIPK3 in dampening NFκB activation, consequently mediating the lung immune response and pathology opens various paths of future study. Whether RIPK3 serves to mediate NFκB activation during infection by other pathogens which initiate the necroptotic signaling pathway, remains to be identified. Notably, our data show that TLR stimulation can also stimulate the NFκB alterations in gene-edited cells, independent of virus, indicates that this response may be the case for various pathogens which trigger RIPK activation. Additionally, previous work in non-infectious disease indicates that RIPK3 may serve an anti-inflammatory role, independent of necroptosis (Roychowdhury et al., 2016). Thus, indicating that the RIPK3/NFκB axis regarding immune modulation may extend beyond infection to other inflammatory or organ damaging disease settings. Further investigation into the function of RIPK3 in these additional settings is warranted.

Summary

The work included in this dissertation collectively provides a further understanding for the complicated role of necroptosis in the pathology and immune response to infections (by *Spn* and IAV), during bacterial or viral pneumonia, bacterial/viral co-infection, as well as IPD (the cellular mechanisms of the necroptosis pathway examined herein are summarized in **Figure 3**). This work builds on the foundation of previous work by our group and others examining the role of necroptosis in the pathology of these diseases.

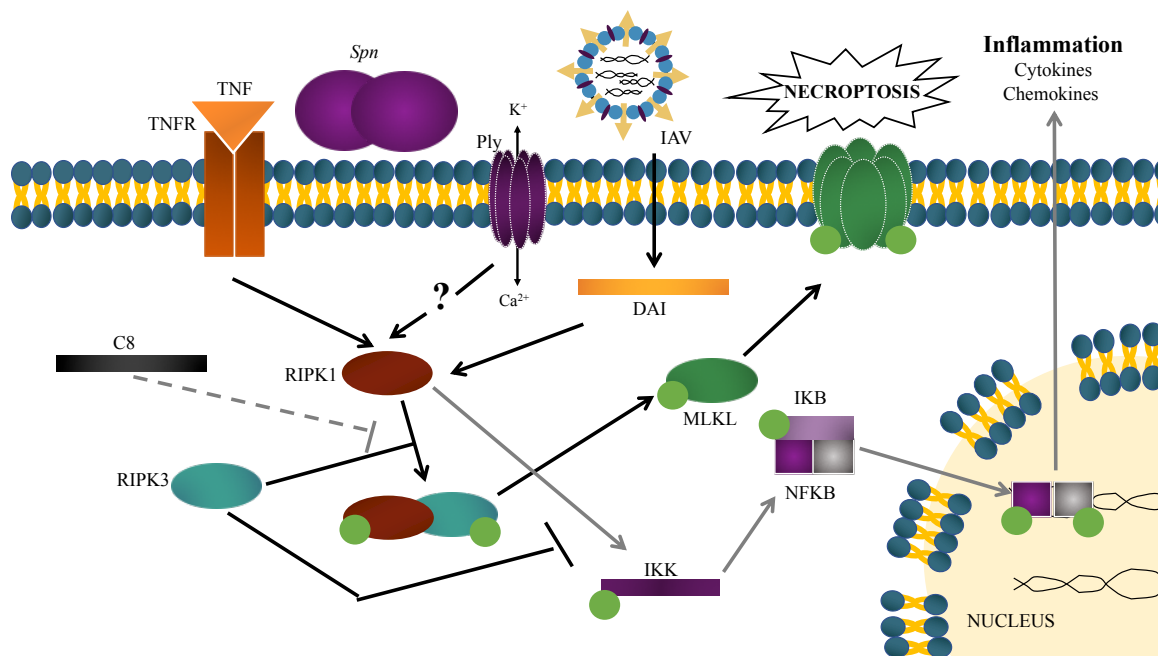


Figure 3. The Initiation and outcomes of necroptosis during infection by airway pathogens.

Diagram depicting the general necroptosis pathway as initiated by TNF receptor, Ply, and detection of IAV infection. Phosphorylation indicated by green circles. Inhibition indicated by flat-capped lines versus positive cascade signaling indicated by arrows. The RIPK1/IKK pathway which is carried out in the absence of RIPK3 is indicated with gray arrows.

We showed that necroptosis occurs during asymptomatic bacterial infection (Chapter 2); that this serves to amplify the immune response to the pathogen; and without necroptosis *Spn* persist within the upper respiratory tract longer and the host's ability to establish protective immunity against subsequent infection is significantly impaired. We demonstrated that during IPD, cardiomyocytes die of necroptosis resulting in long-term cardiac scarring and dysfunction (Chapter 3); that inhibiting necroptosis therapeutically during *Spn* pneumonia and IPD with a re-purposed cancer drug (Ponatinib), can reduce and even prevent acute lung and cardiac damage; and that therapeutic inhibition of necroptosis during IPD can reduce or eliminate long-term cardiac dysfunction and scarring. We demonstrated that prior infection with IAV sensitizes lung epithelial cells to *Spn*-induced

necroptosis (Chapter 4); that this necroptosis increases severity of secondary bacterial infection; that this increased sensitivity is associated with intracellular ROS during infection; and that inhibition of ROS or necroptosis reduces disease severity of secondary *Spn* infection. Finally, we showed that part of the necroptosis cellular machinery (*i.e.* RIPK3) acts to reduce disease pathology and increase survival during IAV infection (Chapter 5); that the absence of RIPK3 results in uncontrolled inflammation; that this inflammation is mediated by NF κ B signaling; and that RIPK3 serves to reduce this NF κ B signaling in response to various TLR stimuli, independent of IAV.

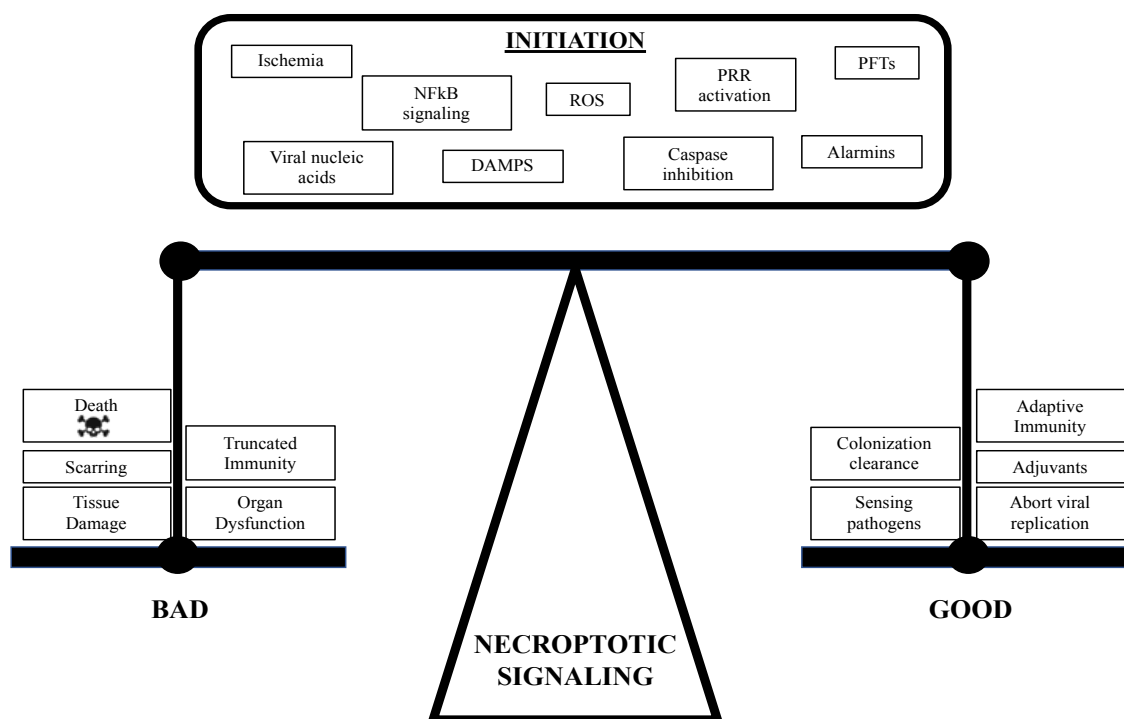


Figure 4. The balance of necroptotic signaling on host outcome. Depiction of the various initiation signals and host outcomes related to necroptotic signaling.

The balance of functions which result from initiating necroptosis during infection, is precarious and ultimately serves as either beneficial or deleterious to the host (**Figure 4**). Understanding the natural mechanisms by which these functions orchestrate different

pathological and immunologic responses can provide a foundation upon which we may further our development of therapeutics and prevention mechanisms for diseases caused by respiratory pathogens.

LIST OF GENERAL REFERENCES

- Abraham, E. (2003). Neutrophils and acute lung injury. *Crit Care Med*, 31(4 Suppl), S195-199. doi:10.1097/01.CCM.0000057843.47705.E8
- Alwan, W. H., Kozłowska, W. J., & Openshaw, P. J. (1994). Distinct types of lung disease caused by functional subsets of antiviral T cells. *J Exp Med*, 179(1), 81-89. doi:10.1084/jem.179.1.81
- Alwan, W. H., Record, F. M., & Openshaw, P. J. (1992). CD4+ T cells clear virus but augment disease in mice infected with respiratory syncytial virus. Comparison with the effects of CD8+ T cells. *Clin Exp Immunol*, 88(3), 527-536. doi:10.1111/j.1365-2249.1992.tb06482.x
- Amarante-Mendes, G. P., Adjemian, S., Branco, L. M., Zanetti, L. C., Weinlich, R., & Bortoluci, K. R. (2018). Pattern Recognition Receptors and the Host Cell Death Molecular Machinery. *Front Immunol*, 9, 2379. doi:10.3389/fimmu.2018.02379
- Arya, R., & White, K. (2015). Cell death in development: Signaling pathways and core mechanisms. *Semin Cell Dev Biol*, 39, 12-19. doi:10.1016/j.semedb.2015.02.001
- Austrian, R. (1981). Pneumococcus: the first one hundred years. *Rev Infect Dis*, 3(2), 183-189. Retrieved from <https://www.ncbi.nlm.nih.gov/pubmed/7020040>
- Balachandran, S., & Rall, G. F. (2020). Benefits and Perils of Necroptosis in Influenza Virus Infection. *J Virol*, 94(9). doi:10.1128/JVI.01101-19

- Bleriot, C., Dupuis, T., Jouvion, G., Eberl, G., Disson, O., & Lecuit, M. (2015). Liver-resident macrophage necroptosis orchestrates type 1 microbicidal inflammation and type-2-mediated tissue repair during bacterial infection. *Immunity*, *42*(1), 145-158. doi:10.1016/j.immuni.2014.12.020
- Brand, J. D., Lazrak, A., Trombley, J. E., Shei, R. J., Adewale, A. T., Tipper, J. L., . . . Harrod, K. S. (2018). Influenza-mediated reduction of lung epithelial ion channel activity leads to dysregulated pulmonary fluid homeostasis. *JCI Insight*, *3*(20). doi:10.1172/jci.insight.123467
- Brandes, M., Klauschen, F., Kuchen, S., & Germain, R. N. (2013). A systems analysis identifies a feedforward inflammatory circuit leading to lethal influenza infection. *Cell*, *154*(1), 197-212. doi:10.1016/j.cell.2013.06.013
- Brown, A. O., Mann, B., Gao, G., Hankins, J. S., Humann, J., Giardina, J., . . . Orihuela, C. J. (2014). *Streptococcus pneumoniae* translocates into the myocardium and forms unique microlesions that disrupt cardiac function. *PLoS Pathog*, *10*(9), e1004383. doi:10.1371/journal.ppat.1004383
- Brown, A. O., Millett, E. R., Quint, J. K., & Orihuela, C. J. (2015). Cardiotoxicity during invasive pneumococcal disease. *Am J Respir Crit Care Med*, *191*(7), 739-745. doi:10.1164/rccm.201411-1951PP
- Burk, M., El-Kersh, K., Saad, M., Wiemken, T., Ramirez, J., & Cavallazzi, R. (2016). Viral infection in community-acquired pneumonia: a systematic review and meta-analysis. *Eur Respir Rev*, *25*(140), 178-188. doi:10.1183/16000617.0076-2015
- Camp, J. V., & Jonsson, C. B. (2017). A Role for Neutrophils in Viral Respiratory Disease. *Front Immunol*, *8*, 550. doi:10.3389/fimmu.2017.00550

- CDC. (2019). NCHS National Vital Statistics System (National Vital Statistics System Data). Retrieved from <https://www.cdc.gov/nchs/products/nvsr.htm>. Retrieved April 01, 2021, from National Center for Health Statistics <https://www.cdc.gov/nchs/products/nvsr.htm>
- Chan, F. K., Shisler, J., Bixby, J. G., Felices, M., Zheng, L., Appel, M., . . . Lenardo, M. J. (2003). A role for tumor necrosis factor receptor-2 and receptor-interacting protein in programmed necrosis and antiviral responses. *J Biol Chem*, *278*(51), 51613-51621. doi:10.1074/jbc.M305633200
- Cho, Y. S., Challa, S., Moquin, D., Genga, R., Ray, T. D., Guildford, M., & Chan, F. K. (2009). Phosphorylation-driven assembly of the RIP1-RIP3 complex regulates programmed necrosis and virus-induced inflammation. *Cell*, *137*(6), 1112-1123. doi:10.1016/j.cell.2009.05.037
- Clayville, L. R. (2011). Influenza update: a review of currently available vaccines. *P T*, *36*(10), 659-684. Retrieved from <https://www.ncbi.nlm.nih.gov/pubmed/22346299>
- Cohen, J. M., Khandavilli, S., Camberlein, E., Hyams, C., Baxendale, H. E., & Brown, J. S. (2011). Protective contributions against invasive *Streptococcus pneumoniae* pneumonia of antibody and Th17-cell responses to nasopharyngeal colonisation. *PLoS One*, *6*(10), e25558. doi:10.1371/journal.pone.0025558
- Collaborators, G. B. D. L. R. I. (2018). Estimates of the global, regional, and national morbidity, mortality, and aetiologies of lower respiratory infections in 195 countries, 1990-2016: a systematic analysis for the Global Burden of Disease Study 2016. *Lancet Infect Dis*, *18*(11), 1191-1210. doi:10.1016/S1473-3099(18)30310-4

- Control, C. f. D. (2020). *Antibiotic Resistance Threats in the United States, 2019*. Retrieved from Atlanta, GA: <https://www.cdc.gov/drugresistance/pdf/threats-report/2019-ar-threats-report-508.pdf>
- Corrales-Medina, V. F., Suh, K. N., Rose, G., Chirinos, J. A., Doucette, S., Cameron, D. W., & Fergusson, D. A. (2011). Cardiac complications in patients with community-acquired pneumonia: a systematic review and meta-analysis of observational studies. *PLoS Med*, *8*(6), e1001048. doi:10.1371/journal.pmed.1001048
- Cortes, J. E., Kim, D. W., Pinilla-Ibarz, J., le Coutre, P., Paquette, R., Chuah, C., . . . Investigators, P. (2013). A phase 2 trial of ponatinib in Philadelphia chromosome-positive leukemias. *N Engl J Med*, *369*(19), 1783-1796. doi:10.1056/NEJMoal306494
- Daniels, B. P., Snyder, A. G., Olsen, T. M., Orozco, S., Oguin, T. H., 3rd, Tait, S. W. G., . . . Oberst, A. (2017). RIPK3 Restricts Viral Pathogenesis via Cell Death-Independent Neuroinflammation. *Cell*, *169*(2), 301-313 e311. doi:10.1016/j.cell.2017.03.011
- Dasaraju, P. V., & Liu, C. (1996). Infections of the Respiratory System. In th & S. Baron (Eds.), *Medical Microbiology*. Galveston (TX).
- Degterev, A., Hitomi, J., Gemscheid, M., Ch'en, I. L., Korkina, O., Teng, X., . . . Yuan, J. (2008). Identification of RIP1 kinase as a specific cellular target of necrostatins. *Nat Chem Biol*, *4*(5), 313-321. doi:10.1038/nchembio.83
- Dondelinger, Y., Hulpiau, P., Saeys, Y., Bertrand, M. J. M., & Vandenabeele, P. (2016). An evolutionary perspective on the necroptotic pathway. *Trends Cell Biol*, *26*(10), 721-732. doi:10.1016/j.tcb.2016.06.004

- Downey, J., Pernet, E., Coulombe, F., Allard, B., Meunier, I., Jaworska, J., . . . Divangahi, M. (2017). RIPK3 interacts with MAVS to regulate type I IFN-mediated immunity to Influenza A virus infection. *PLoS Pathog*, *13*(4), e1006326. doi:10.1371/journal.ppat.1006326
- Elmore, S. (2007). Apoptosis: a review of programmed cell death. *Toxicol Pathol*, *35*(4), 495-516. doi:10.1080/01926230701320337
- Eurich, D. T., Marrie, T. J., Minhas-Sandhu, J. K., & Majumdar, S. R. (2017). Risk of heart failure after community acquired pneumonia: prospective controlled study with 10 years of follow-up. *BMJ*, *356*, j413. doi:10.1136/bmj.j413
- Fendrick, A. M., Monto, A. S., Nightengale, B., & Sarnes, M. (2003). The economic burden of non-influenza-related viral respiratory tract infection in the United States. *Arch Intern Med*, *163*(4), 487-494. doi:10.1001/archinte.163.4.487
- Gainor, J. F., & Chabner, B. A. (2015). Ponatinib: Accelerated Disapproval. *Oncologist*, *20*(8), 847-848. doi:10.1634/theoncologist.2015-0253
- Ganaie, F., Saad, J. S., McGee, L., van Tonder, A. J., Bentley, S. D., Lo, S. W., . . . Nahm, M. H. (2020). A New Pneumococcal Capsule Type, 10D, is the 100th Serotype and Has a Large cps Fragment from an Oral Streptococcus. *mBio*, *11*(3). doi:10.1128/mBio.00937-20
- Gill, J. R., Sheng, Z. M., Ely, S. F., Guinee, D. G., Beasley, M. B., Suh, J., . . . Taubenberger, J. K. (2010). Pulmonary pathologic findings of fatal 2009 pandemic influenza A/H1N1 viral infections. *Arch Pathol Lab Med*, *134*(2), 235-243. doi:10.1043/1543-2165-134.2.235

- Gilley, R. P., Gonzalez-Juarbe, N., Shenoy, A. T., Reyes, L. F., Dube, P. H., Restrepo, M. I., & Orihuela, C. J. (2016). Infiltrated Macrophages Die of Pneumolysin-Mediated Necroptosis following Pneumococcal Myocardial Invasion. *Infect Immun*, *84*(5), 1457-1469. doi:10.1128/IAI.00007-16
- Goldblatt, D., & O'Brien, K. L. (2018). Pneumococcal Infections. In J. L. Jameson, A. S. Fauci, D. L. Kasper, S. L. Hauser, D. L. Longo, & J. Loscalzo (Eds.), *Harrison's Principles of Internal Medicine, 20e*. New York, NY: McGraw-Hill Education.
- Gonzales, R., Steiner, J. F., & Sande, M. A. (1997). Antibiotic prescribing for adults with colds, upper respiratory tract infections, and bronchitis by ambulatory care physicians. *JAMA*, *278*(11), 901-904. Retrieved from <https://www.ncbi.nlm.nih.gov/pubmed/9302241>
- Gonzalez-Juarbe, N., Bradley, K. M., Riegler, A. N., Reyes, L. F., Brissac, T., Park, S. S., . . . Orihuela, C. J. (2018). Bacterial Pore-Forming Toxins Promote the Activation of Caspases in Parallel to Necroptosis to Enhance Alarmin Release and Inflammation During Pneumonia. *Sci Rep*, *8*(1), 5846. doi:10.1038/s41598-018-24210-8
- Gonzalez-Juarbe, N., Bradley, K. M., Shenoy, A. T., Gilley, R. P., Reyes, L. F., Hinojosa, C. A., . . . Orihuela, C. J. (2017a). Pore-forming toxin-mediated ion dysregulation leads to death receptor-independent necroptosis of lung epithelial cells during bacterial pneumonia. *Cell Death Differ*. doi:10.1038/cdd.2017.49
- Gonzalez-Juarbe, N., Bradley, K. M., Shenoy, A. T., Gilley, R. P., Reyes, L. F., Hinojosa, C. A., . . . Orihuela, C. J. (2017b). Pore-forming toxin-mediated ion dysregulation

- leads to death receptor-independent necroptosis of lung epithelial cells during bacterial pneumonia. *Cell Death Differ*, 24(5), 917-928. doi:10.1038/cdd.2017.49
- Gonzalez-Juarbe, N., Gilley, R. P., Hinojosa, C. A., Bradley, K. M., Kamei, A., Gao, G., . . . Orihuela, C. J. (2015). Pore-Forming Toxins Induce Macrophage Necroptosis during Acute Bacterial Pneumonia. *PLoS Pathog*, 11(12), e1005337. doi:10.1371/journal.ppat.1005337
- Grief, S. N., & Loza, J. K. (2018). Guidelines for the Evaluation and Treatment of Pneumonia. *Prim Care*, 45(3), 485-503. doi:10.1016/j.pop.2018.04.001
- He, S., & Wang, X. (2018). RIP kinases as modulators of inflammation and immunity. *Nat Immunol*, 19(9), 912-922. doi:10.1038/s41590-018-0188-x
- Hentrich, K., Löfling, J., Pathak, A., Nizet, V., Varki, A., & Henriques-Normark, B. (2016). *Streptococcus pneumoniae* Senses a Human-like Sialic Acid Profile via the Response Regulator CiaR. *Cell Host & Microbe*, 20(3), 307-317. doi:http://dx.doi.org/10.1016/j.chom.2016.07.019
- Hosakote, Y. M., Liu, T., Castro, S. M., Garofalo, R. P., & Casola, A. (2009). Respiratory syncytial virus induces oxidative stress by modulating antioxidant enzymes. *Am J Respir Cell Mol Biol*, 41(3), 348-357. doi:10.1165/rcmb.2008-0330OC
- Huang, H. R., Cho, S. J., Harris, R. M., Yang, J., Bermejo, S., Sharma, L., . . . Stout-Delgado, H. W. (2021). RIPK3 Activates MLKL-mediated Necroptosis and Inflammasome Signaling during *Streptococcus* Infection. *Am J Respir Cell Mol Biol*, 64(5), 579-591. doi:10.1165/rcmb.2020-0312OC

- Huang, Z., Wu, S. Q., Liang, Y., Zhou, X., Chen, W., Li, L., . . . Han, J. (2015). RIP1/RIP3 binding to HSV-1 ICP6 initiates necroptosis to restrict virus propagation in mice. *Cell Host Microbe*, *17*(2), 229-242. doi:10.1016/j.chom.2015.01.002
- Hussell, T., & Bell, T. J. (2014). Alveolar macrophages: plasticity in a tissue-specific context. *Nat Rev Immunol*, *14*(2), 81-93. doi:10.1038/nri3600
- Kafka, D., Ling, E., Feldman, G., Benharroch, D., Voronov, E., Givon-Lavi, N., . . . Mizrahi-Nebenzahl, Y. (2008). Contribution of IL-1 to resistance to Streptococcus pneumoniae infection. *Int Immunol*, *20*(9), 1139-1146. doi:10.1093/intimm/dxn071
- Kawasaki, T., & Kawai, T. (2014). Toll-like receptor signaling pathways. *Front Immunol*, *5*, 461. doi:10.3389/fimmu.2014.00461
- Kearney, C. J., Cullen, S. P., Tynan, G. A., Henry, C. M., Clancy, D., Lavelle, E. C., & Martin, S. J. (2015). Necroptosis suppresses inflammation via termination of TNF- or LPS-induced cytokine and chemokine production. *Cell Death Differ*, *22*(8), 1313-1327. doi:10.1038/cdd.2014.222
- Kearney, C. J., & Martin, S. J. (2017). An Inflammatory Perspective on Necroptosis. *Mol Cell*, *65*(6), 965-973. doi:10.1016/j.molcel.2017.02.024
- Kell, D. B., Heyden, E. L., & Pretorius, E. (2020). The Biology of Lactoferrin, an Iron-Binding Protein That Can Help Defend Against Viruses and Bacteria. *Front Immunol*, *11*, 1221. doi:10.3389/fimmu.2020.01221
- Kitur, K., Parker, D., Nieto, P., Ahn, D. S., Cohen, T. S., Chung, S., . . . Prince, A. (2015). Toxin-induced necroptosis is a major mechanism of Staphylococcus aureus lung damage. *PLoS Pathog*, *11*(4), e1004820. doi:10.1371/journal.ppat.1004820

- Kitur, K., Wachtel, S., Brown, A., Wickersham, M., Paulino, F., Penaloza, H. F., . . . Prince, A. (2016). Necroptosis Promotes *Staphylococcus aureus* Clearance by Inhibiting Excessive Inflammatory Signaling. *Cell Rep*, *16*(8), 2219-2230. doi:10.1016/j.celrep.2016.07.039
- Kochanek, K. D., Murphy, S. L., Xu, J., & Arias, E. (2019). Deaths: Final Data for 2017. *Natl Vital Stat Rep*, *68*(9), 1-77. Retrieved from <https://www.ncbi.nlm.nih.gov/pubmed/32501199>
- Kochanek, K. D., Xu, J., & Arias, E. (2020). Mortality in the United States, 2019. *NCHS Data Brief*(395), 1-8. Retrieved from <https://www.ncbi.nlm.nih.gov/pubmed/33395387>
- Koshinuma, S., Miyamae, M., Kaneda, K., Kotani, J., & Figueredo, V. M. (2014). Combination of necroptosis and apoptosis inhibition enhances cardioprotection against myocardial ischemia-reperfusion injury. *J Anesth*, *28*(2), 235-241. doi:10.1007/s00540-013-1716-3
- Kuriakose, T., Man, S. M., Malireddi, R. K., Karki, R., Kesavardhana, S., Place, D. E., . . . Kanneganti, T. D. (2016). ZBP1/DAI is an innate sensor of influenza virus triggering the NLRP3 inflammasome and programmed cell death pathways. *Sci Immunol*, *1*(2). doi:10.1126/sciimmunol.aag2045
- Land, W. G. (2015). The Role of Damage-Associated Molecular Patterns (DAMPs) in Human Diseases: Part II: DAMPs as diagnostics, prognostics and therapeutics in clinical medicine. *Sultan Qaboos Univ Med J*, *15*(2), e157-170. Retrieved from <https://www.ncbi.nlm.nih.gov/pubmed/26052447>

- Lemon, J. K., Miller, M. R., & Weiser, J. N. (2015). Sensing of interleukin-1 cytokines during *Streptococcus pneumoniae* colonization contributes to macrophage recruitment and bacterial clearance. *Infect Immun*, 83(8), 3204-3212. doi:10.1128/IAI.00224-15
- Li, Y., Guo, X., Hu, C., Du, Y., Guo, C., Di, W., . . . Qi, X. (2018). Type I IFN operates pyroptosis and necroptosis during multidrug-resistant *A. baumannii* infection. *Cell Death Differ*, 25(7), 1304-1318. doi:10.1038/s41418-017-0041-z
- Liang, S., & Qin, X. (2013). Critical role of type I interferon-induced macrophage necroptosis during infection with *Salmonella enterica* serovar Typhimurium. *Cell Mol Immunol*, 10(2), 99-100. doi:10.1038/cmi.2012.68
- Louie, J. K., Acosta, M., Winter, K., Jean, C., Gavali, S., Schechter, R., . . . California Pandemic Working, G. (2009). Factors associated with death or hospitalization due to pandemic 2009 influenza A(H1N1) infection in California. *JAMA*, 302(17), 1896-1902. doi:10.1001/jama.2009.1583
- Lynch, J. P., 3rd, & Zhanel, G. G. (2010). *Streptococcus pneumoniae*: epidemiology and risk factors, evolution of antimicrobial resistance, and impact of vaccines. *Curr Opin Pulm Med*, 16(3), 217-225. doi:10.1097/MCP.0b013e3283385653
- Mandal, P., Berger, S. B., Pillay, S., Moriwaki, K., Huang, C., Guo, H., . . . Kaiser, W. J. (2014). RIP3 induces apoptosis independent of pronecrotic kinase activity. *Mol Cell*, 56(4), 481-495. doi:10.1016/j.molcel.2014.10.021
- McCullers, J. A., & Bartmess, K. C. (2003). Role of Neuraminidase in Lethal Synergism between Influenza Virus and *Streptococcus pneumoniae*. *Journal of Infectious Diseases*, 187(6), 1000-1009. doi:10.1086/368163

- McCullers, J. A., & Rehg, J. E. (2002). Lethal synergism between influenza virus and *Streptococcus pneumoniae*: characterization of a mouse model and the role of platelet-activating factor receptor. *J Infect Dis*, *186*(3), 341-350. doi:10.1086/341462
- Meier, P., Finch, A., & Evan, G. (2000). Apoptosis in development. *Nature*, *407*(6805), 796-801. doi:10.1038/35037734
- Mitchell, T. J., & Dalziel, C. E. (2014). The biology of pneumolysin. *Subcell Biochem*, *80*, 145-160. doi:10.1007/978-94-017-8881-6_8
- Mogensen, T. H. (2009). Pathogen recognition and inflammatory signaling in innate immune defenses. *Clin Microbiol Rev*, *22*(2), 240-273, Table of Contents. doi:10.1128/CMR.00046-08
- Moskophidis, D., & Kioussis, D. (1998). Contribution of virus-specific CD8⁺ cytotoxic T cells to virus clearance or pathologic manifestations of influenza virus infection in a T cell receptor transgenic mouse model. *J Exp Med*, *188*(2), 223-232. doi:10.1084/jem.188.2.223
- Musher, D. M., Abers, M. S., & Corrales-Medina, V. F. (2019). Acute Infection and Myocardial Infarction. *N Engl J Med*, *380*(2), 171-176. doi:10.1056/NEJMra1808137
- Musher, D. M., Rueda, A. M., Kaka, A. S., & Mapara, S. M. (2007). The association between pneumococcal pneumonia and acute cardiac events. *Clin Infect Dis*, *45*(2), 158-165. doi:10.1086/518849
- Nailwal, H., & Chan, F. K. (2019). Necroptosis in anti-viral inflammation. *Cell Death Differ*, *26*(1), 4-13. doi:10.1038/s41418-018-0172-x

- Newton, K., Dugger, D. L., Wickliffe, K. E., Kapoor, N., de Almagro, M. C., Vucic, D., . . . Dixit, V. M. (2014). Activity of protein kinase RIPK3 determines whether cells die by necroptosis or apoptosis. *Science*, *343*(6177), 1357-1360. doi:10.1126/science.1249361
- Nogusa, S., Thapa, R. J., Dillon, C. P., Liedmann, S., Oguin, T. H., 3rd, Ingram, J. P., . . . Balachandran, S. (2016). RIPK3 Activates Parallel Pathways of MLKL-Driven Necroptosis and FADD-Mediated Apoptosis to Protect against Influenza A Virus. *Cell Host Microbe*, *20*(1), 13-24. doi:10.1016/j.chom.2016.05.011
- Omoto, S., Guo, H., Talekar, G. R., Roback, L., Kaiser, W. J., & Mocarski, E. S. (2015). Suppression of RIP3-dependent necroptosis by human cytomegalovirus. *J Biol Chem*, *290*(18), 11635-11648. doi:10.1074/jbc.M115.646042
- Orzalli, M. H., & Kagan, J. C. (2017). Apoptosis and Necroptosis as Host Defense Strategies to Prevent Viral Infection. *Trends Cell Biol*, *27*(11), 800-809. doi:10.1016/j.tcb.2017.05.007
- Parzych, E. M., DiMenna, L. J., Latimer, B. P., Small, J. C., Kannan, S., Manson, B., . . . Ertl, H. C. (2013). Influenza virus specific CD8(+) T cells exacerbate infection following high dose influenza challenge of aged mice. *Biomed Res Int*, *2013*, 876314. doi:10.1155/2013/876314
- Paton, J. C., & Trappetti, C. (2019). Streptococcus pneumoniae Capsular Polysaccharide. *Microbiol Spectr*, *7*(2). doi:10.1128/microbiolspec.GPP3-0019-2018
- Pettigrew, M. M., Marks, L. R., Kong, Y., Gent, J. F., Roche-Hakansson, H., & Hakansson, A. P. (2014). Dynamic changes in the Streptococcus pneumoniae transcriptome

- during transition from biofilm formation to invasive disease upon influenza A virus infection. *Infect Immun*, 82(11), 4607-4619. doi:10.1128/iai.02225-14
- Prevention, C. f. D. C. a. (2020a, October 05, 2020). Disease Burden of Influenza. *Influenza*. Retrieved from <https://www.cdc.gov/flu/about/burden/index.html>
- Prevention, C. f. D. C. a. (2020b, October, 28 2020). Pneumonia fact sheet. Retrieved from <https://www.cdc.gov/dotw/pneumonia/index.html>
- Reyes, L. F., Restrepo, M. I., Hinojosa, C. A., Soni, N. J., Anzueto, A., Babu, B. L., . . . Orihuela, C. J. (2017). Severe Pneumococcal Pneumonia Causes Acute Cardiac Toxicity and Subsequent Cardiac Remodeling. *Am J Respir Crit Care Med*. doi:10.1164/rccm.201701-0104OC
- Riegler, A. N., Brissac, T., Gonzalez-Juarbe, N., & Orihuela, C. J. (2019). Necroptotic Cell Death Promotes Adaptive Immunity Against Colonizing Pneumococci. *Front Immunol*, 10, 615. doi:10.3389/fimmu.2019.00615
- Robinson, N., McComb, S., Mulligan, R., Dudani, R., Krishnan, L., & Sad, S. (2012). Type I interferon induces necroptosis in macrophages during infection with *Salmonella enterica* serovar Typhimurium. *Nat Immunol*, 13(10), 954-962. doi:10.1038/ni.2397
- Roychowdhury, S., McCullough, R. L., Sanz-Garcia, C., Saikia, P., Alkhouri, N., Matloob, A., . . . Nagy, L. E. (2016). Receptor interacting protein 3 protects mice from high-fat diet-induced liver injury. *Hepatology*, 64(5), 1518-1533. doi:10.1002/hep.28676
- Sakai, S., Kawamata, H., Mantani, N., Kogure, T., Shimada, Y., Terasawa, K., . . . Ochiai, H. (2000). Therapeutic effect of anti-macrophage inflammatory protein 2 antibody

- on influenza virus-induced pneumonia in mice. *J Virol*, 74(5), 2472-2476. doi:10.1128/jvi.74.5.2472-2476.2000
- Schwarz, K. B. (1996). Oxidative stress during viral infection: a review. *Free Radic Biol Med*, 21(5), 641-649. doi:10.1016/0891-5849(96)00131-1
- Seki, M., Kohno, S., Newstead, M. W., Zeng, X., Bhan, U., Lukacs, N. W., . . . Standiford, T. J. (2010). Critical role of IL-1 receptor-associated kinase-M in regulating chemokine-dependent deleterious inflammation in murine influenza pneumonia. *J Immunol*, 184(3), 1410-1418. doi:10.4049/jimmunol.0901709
- Shahangian, A., Chow, E. K., Tian, X., Kang, J. R., Ghaffari, A., Liu, S. Y., . . . Deng, J. C. Type I IFNs mediate development of postinfluenza bacterial pneumonia in mice. *The Journal of Clinical Investigation*, 119(7), 1910-1920. doi:10.1172/JCI35412
- Shenoy, A. T., Brissac, T., Gilley, R. P., Kumar, N., Wang, Y., Gonzalez-Juarbe, N., . . . Orihuela, C. J. (2017). Streptococcus pneumoniae in the heart subvert the host response through biofilm-mediated resident macrophage killing. *PLoS Pathog*, 13(8), e1006582. doi:10.1371/journal.ppat.1006582
- Shubina, M., Tummers, B., Boyd, D. F., Zhang, T., Yin, C., Gautam, A., . . . Balachandran, S. (2020). Necroptosis restricts influenza A virus as a stand-alone cell death mechanism. *J Exp Med*, 217(11). doi:10.1084/jem.20191259
- Sies, H., Berndt, C., & Jones, D. P. (2017). Oxidative Stress. *Annu Rev Biochem*, 86, 715-748. doi:10.1146/annurev-biochem-061516-045037
- Simpson, J., Loh, Z., Ullah, M. A., Lynch, J. P., Werder, R. B., Collinson, N., . . . Phipps, S. (2020). Respiratory Syncytial Virus Infection Promotes Necroptosis and

- HMGB1 Release by Airway Epithelial Cells. *Am J Respir Crit Care Med*, 201(11), 1358-1371. doi:10.1164/rccm.201906-1149OC
- Smith, E. L., Wheeler, I., Adler, H., Ferreira, D. M., Sa-Leao, R., Abdullahi, O., . . . Rylance, J. (2020). Upper airways colonisation of *Streptococcus pneumoniae* in adults aged 60 years and older: A systematic review of prevalence and individual participant data meta-analysis of risk factors. *J Infect*, 81(4), 540-548. doi:10.1016/j.jinf.2020.06.028
- Smith, H. C., German, E., Ferreira, D. M., & Rylance, J. (2019). Nasopharyngeal colonisation with *Streptococcus pneumoniae* in malnourished children: a systematic review and meta-analysis of prevalence. *Trans R Soc Trop Med Hyg*, 113(5), 227-233. doi:10.1093/trstmh/try139
- Sun, K., & Metzger, D. W. (2008). Inhibition of pulmonary antibacterial defense by interferon-[gamma] during recovery from influenza infection. *Nat Med*, 14(5), 558-564. doi:http://www.nature.com/nm/journal/v14/n5/supinfo/nm1765_S1.html
- Sun, X., Lee, J., Navas, T., Baldwin, D. T., Stewart, T. A., & Dixit, V. M. (1999). RIP3, a novel apoptosis-inducing kinase. *J Biol Chem*, 274(24), 16871-16875. doi:10.1074/jbc.274.24.16871
- Thapa, R. J., Ingram, J. P., Ragan, K. B., Nogusa, S., Boyd, D. F., Benitez, A. A., . . . Balachandran, S. (2016). DAI Senses Influenza A Virus Genomic RNA and Activates RIPK3-Dependent Cell Death. *Cell Host Microbe*, 20(5), 674-681. doi:10.1016/j.chom.2016.09.014
- Tokars, J. I., Olsen, S. J., & Reed, C. (2018). Seasonal Incidence of Symptomatic Influenza in the United States. *Clin Infect Dis*, 66(10), 1511-1518. doi:10.1093/cid/cix1060

- Tong, H. H., Fisher, L. M., Kosunick, G. M., & DeMaria, T. F. (2000). Effect of adenovirus type 1 and influenza A virus on *Streptococcus pneumoniae* nasopharyngeal colonization and otitis media in the chinchilla. *Ann Otol Rhinol Laryngol*, *109*(11), 1021-1027. doi:10.1177/000348940010901106
- Trotter, C. L., Stuart, J. M., George, R., & Miller, E. (2008). Increasing hospital admissions for pneumonia, England. *Emerg Infect Dis*, *14*(5), 727-733. doi:10.3201/eid1405.071011
- Upton, J. W., Kaiser, W. J., & Mocarski, E. S. (2010). Virus inhibition of RIP3-dependent necrosis. *Cell Host Microbe*, *7*(4), 302-313. doi:10.1016/j.chom.2010.03.006
- van de Sandt, C. E., Barcena, M., Koster, A. J., Kasper, J., Kirkpatrick, C. J., Scott, D. P., . . . Short, K. R. (2017). Human CD8(+) T Cells Damage Noninfected Epithelial Cells during Influenza Virus Infection In Vitro. *Am J Respir Cell Mol Biol*, *57*(5), 536-546. doi:10.1165/rcmb.2016-0377OC
- van der Sluijs, K. F., Nijhuis, M., Levels, J. H., Florquin, S., Mellor, A. L., Jansen, H. M., . . . Lutter, R. (2006). Influenza-induced expression of indoleamine 2,3-dioxygenase enhances interleukin-10 production and bacterial outgrowth during secondary pneumococcal pneumonia. *J Infect Dis*, *193*(2), 214-222. doi:10.1086/498911
- van der Sluijs, K. F., van der Poll, T., Lutter, R., Juffermans, N. P., & Schultz, M. J. (2010). Bench-to-bedside review: Bacterial pneumonia with influenza - pathogenesis and clinical implications. *Critical Care*, *14*(2), 1-8. doi:10.1186/cc8893

- Vandenabeele, P., Galluzzi, L., Vanden Berghe, T., & Kroemer, G. (2010). Molecular mechanisms of necroptosis: an ordered cellular explosion. *Nat Rev Mol Cell Biol*, *11*(10), 700-714. doi:10.1038/nrm2970
- Wang, X., Li, Y., Liu, S., Yu, X., Li, L., Shi, C., . . . He, S. (2014). Direct activation of RIP3/MLKL-dependent necrosis by herpes simplex virus 1 (HSV-1) protein ICP6 triggers host antiviral defense. *Proc Natl Acad Sci U S A*, *111*(43), 15438-15443. doi:10.1073/pnas.1412767111
- Whitsett, J. A., & Alenghat, T. (2015). Respiratory epithelial cells orchestrate pulmonary innate immunity. *Nat Immunol*, *16*(1), 27-35. doi:10.1038/ni.3045
- WHO. (2016). *Pneumonia Fact Sheet*. Retrieved from <http://www.who.int/mediacentre/factsheets/fs331/en/>
- Wolf, A. I., Strauman, M. C., Mozdzanowska, K., Williams, K. L., Osborne, L. C., Shen, H., . . . Erikson, J. (2014). Pneumolysin expression by streptococcus pneumoniae protects colonized mice from influenza virus-induced disease. *Virology*, *462-463*, 254-265. doi:10.1016/j.virol.2014.06.019
- Wong Fok Lung, T., Monk, I. R., Acker, K. P., Mu, A., Wang, N., Riquelme, S. A., . . . Prince, A. (2020). Staphylococcus aureus small colony variants impair host immunity by activating host cell glycolysis and inducing necroptosis. *Nat Microbiol*, *5*(1), 141-153. doi:10.1038/s41564-019-0597-0
- Yu, H. R. v. D. a. H. (2020). Viral Respiratory Infections. In D. R. H. Edward T. Ryan, Tom Solomon, Naomi E. Aronson, Timothy P. Endy (Ed.), *Hunter's Tropical Medicine and Emerging Infectious Diseases* (10 ed., pp. 284-288): Elsevier.

- Zhang, T., Yin, C., Boyd, D. F., Quarato, G., Ingram, J. P., Shubina, M., . . . Balachandran, S. (2020). Influenza Virus Z-RNAs Induce ZBP1-Mediated Necroptosis. *Cell*, *180*(6), 1115-1129 e1113. doi:10.1016/j.cell.2020.02.050
- Zhang, Z., Clarke, T. B., & Weiser, J. N. (2009). Cellular effectors mediating Th17-dependent clearance of pneumococcal colonization in mice. *J Clin Invest*, *119*(7), 1899-1909. doi:10.1172/JCI36731
- Zhou, Q., Snipas, S., Orth, K., Muzio, M., Dixit, V. M., & Salvesen, G. S. (1997). Target protease specificity of the viral serpin CrmA. Analysis of five caspases. *J Biol Chem*, *272*(12), 7797-7800. doi:10.1074/jbc.272.12.7797
- Zhou, W., & Yuan, J. (2014). Necroptosis in health and diseases. *Semin Cell Dev Biol*, *35*, 14-23. doi:10.1016/j.semcdb.2014.07.013

APPENDIX
ANIMAL RESEARCH APPROVAL

APN 20175: Cardiac Microlesion Formation During Invasive Pneumococcal Disease

Record Number
IACUC-20175

Done Save

Cardiac Microlesion Formation During Invasive Pneumococcal Disease
Carlos J. Orihuela - Microbiology (National Institute of Allergy and Infectious Diseases/NIH/DHHS)

Submissions (20) Linkages (1) Species (1) Summaries

Home > Summaries > Personnel

Summary
Personnel

Research Personnel
All Certifications and Training

| PI | Name | COI | Start Date | |
|----------------------------------|---|-----|-------------|--------|
| <input checked="" type="radio"/> | Carlos Orihuela - Microbiology Role: [PI] | | 29-Jun-2015 | Retire |
| | Certifications and Training | | | Email |
| <input type="radio"/> | Sarah Beno - Microbiology Role: [] | | 03-Aug-2018 | Retire |
| | Certifications and Training | | | Email |
| <input type="radio"/> | Terry Brisac - Microbiology Role: [] | | 07-Mar-2016 | Retire |
| | Certifications and Training | | | Email |
| <input type="radio"/> | Katherine Kruckow - Grad Sch - Biomed Sciences Role: [] | | 03-Aug-2018 | Retire |
| | Certifications and Training | | | Email |
| | Ashleigh Riegler - Grad Sch - Biomed Sciences Role: [] | | 14-Jun-2017 | Retire |
| | Certifications and Training | | | Email |

Past Research Personnel

| Name | Department | Start Date | End Date |
|-----------------------------------|---|-------------|-------------|
| Kelley Bradley Email | Microbiology Certifications and Training | 24-Aug-2015 | 01-Sep-2018 |
| Alex Dalecki Email | Grad Sch - Biomed Sciences Certifications and Training | 21-Nov-2017 | 01-Sep-2018 |
| Norberto Gonzalez-Juarbe Email | Microbiology Certifications and Training | 18-Sep-2015 | 01-Sep-2018 |
| Anukul Shency Email | Grad Sch - Biomed Sciences Certifications and Training | 24-Aug-2015 | 01-Sep-2018 |

Contacts

Office/Lab Contacts

| Name |
|-------------|
| Beno, Sarah |

APN 20479: Caspase-associated Necroptosis of Cardiomyocytes

Record Number
IACUC-20479

Done Save

Caspase-associated necroptosis of cardiomyocytes
Carlos J. Orihuela - Microbiology (American Heart Association)

Submissions (8) Linkages (1) Species (1) Summaries

Home > Summaries > Personnel

Summary
Personnel

Research Personnel
All Certifications and Training 

| PI | Name | COI | Start Date | |
|----------------------------------|---|-----|-------------|--------|
| <input checked="" type="radio"/> | Carlos Orihuela - Microbiology Role: <input type="text" value="PI"/> | | 26-May-2016 | Retire |
| <input type="radio"/> | Sarah Beno - Microbiology Role: <input type="text" value=""/> | | 30-Oct-2017 | Retire |
| <input type="radio"/> | Terry Brissac - Microbiology Role: <input type="text" value=""/> | | 01-Jun-2016 | Retire |
| <input type="radio"/> | Katherine Kruckow - Grad Sch - Biomed Sciences Role: <input type="text" value=""/> | | 03-Aug-2018 | Retire |
| <input type="radio"/> | Asleigh Riegler - Grad Sch - Biomed Sciences Role: <input type="text" value=""/> | | 30-Oct-2017 | Retire |

Past Research Personnel

| Name | Department | Start Date | End Date |
|---|--|-------------|-------------|
| Kelley Bradley Email | Microbiology Certifications and Training | 01-Jun-2016 | 01-Sep-2018 |
| Sarah Connelly Email | Graduate School Dean's Office Certifications and Training | 29-Nov-2016 | 30-Jun-2017 |
| Norberto Gonzalez-Juarbe Email | Microbiology Certifications and Training | 01-Jun-2016 | 01-Sep-2018 |
| LaDonna Patterson Email | Microbiology Certifications and Training | 17-Aug-2016 | 30-Aug-2017 |
| Anukul Shenoy Email | Grad Sch - Biomed Sciences Certifications and Training | 01-Jun-2016 | 01-Sep-2018 |

Contacts

Office/Lab Contacts

Name

[Bradley, Kelley](#)
[Brissac, Terry](#)
[Shenoy, Anukul](#)
[Gonzalez-Juarbe, Norberto](#)

APN 21231: Pneumolysin-induced Necroptosis Drives Adaptive Immunity Against Colonizing Pneumococci

Record Number
IACUC-21231

Pneumolysin-induced necroptosis drives adaptive immunity against colonizing pneumococci
Carlos J. Orihuela - Microbiology (UAB DEPARTMENT)

Done Save

Submissions (12) Linkages Species (1) Summaries

Home > Summaries > Personnel

Summary

Personnel

Research Personnel

All Certifications and Training

| PI | Name | COI | Start Date | |
|----------------------------------|--|-----|-------------|-----------------|
| <input checked="" type="radio"/> | Carlos Orihuela - Microbiology Role: <input type="text" value="PI"/> | | 08-Feb-2018 | Retire Email |
| <input type="radio"/> | Katherine Kruckow - Grad Sch - Biomed Sciences Role: <input type="text"/> | | 09-Feb-2018 | Retire Email |
| <input checked="" type="radio"/> | Ashleigh Riegler - Grad Sch - Biomed Sciences Role: <input type="text"/> | | 09-Feb-2018 | Retire Email |
| <input type="radio"/> | Xuhong Song - Microbiology Role: <input type="text"/> | | 27-Feb-2020 | Retire Email |

Past Research Personnel

| Name | Department | Start Date | End Date |
|---|---|-------------|-------------|
| Sarah Beno Email | Microbiology Certifications and Training | 09-Feb-2018 | 04-Mar-2019 |
| Kelley Bradley Email | Microbiology Certifications and Training | 09-Feb-2018 | 01-Sep-2018 |
| Terry Brisac Email | Microbiology Certifications and Training | 09-Feb-2018 | 01-Jan-2020 |

Contacts

Office/Lab Contacts

Name

[Riegler, Ashleigh](#)



APN 21419: Resident Cardiac Macrophage Dysfunction and Pneumonia-Associated Adverse Cardiac Events

Record Number
IACUC-21419

[Done](#) [Save](#)

Resident cardiac macrophage dysfunction and pneumonia-associated adverse cardiac events

Carlos J. Orihuela - Microbiology (American Heart Association)

Submissions (12)
Linkages (1)
Species (1)
Summaries

[Home](#) > [Summaries](#) > [Personnel](#)

Summary

Personnel

Research Personnel

All Certifications and Training

| PI | Name | COI | Start Date | |
|-----------------------|--|-----|-------------|--------|
| <input type="radio"/> | Carlos Orihuela - Microbiology Role: <input type="text" value="PI"/> | | 23-Jul-2018 | Retire |
| | Certifications and Training | | | Email |
| <input type="radio"/> | Christy Carter - Med-Gerontology/Geriatrics/Palliative Care Role: <input type="text" value=""/> | | 15-Oct-2018 | Retire |
| | Certifications and Training | | | Email |
| <input type="radio"/> | Katelynn Corder-Grier - Biology Role: <input type="text" value=""/> | | 15-Oct-2018 | Retire |
| | Certifications and Training | | | Email |
| <input type="radio"/> | Drew Freeman - Biology Role: <input type="text" value=""/> | | 15-Oct-2018 | Retire |
| | Certifications and Training | | | Email |
| <input type="radio"/> | Katherine Kruckow - Grad Sch - Biomed Sciences Role: <input type="text" value=""/> | | 23-Jul-2018 | Retire |
| | Certifications and Training | | | Email |
| <input type="radio"/> | Ashleigh Riegler - Grad Sch - Biomed Sciences Role: <input type="text" value=""/> | | 30-Jul-2018 | Retire |
| | Certifications and Training | | | Email |
| <input type="radio"/> | Ana Sogorovic - Biology Role: <input type="text" value=""/> | | 15-Oct-2018 | Retire |
| | Certifications and Training | | | Email |
| <input type="radio"/> | Xihong Song - Microbiology Role: <input type="text" value=""/> | | 27-Feb-2020 | Retire |
| | Certifications and Training | | | Email |

Past Research Personnel

| Name | Department | Start Date | End Date |
|--------------------------------|-----------------------------|-------------|-------------|
| Sarah Beno | Microbiology | 30-Jul-2018 | 01-Jan-2020 |
| Email | Certifications and Training | | |
| Kelley Bradley | Microbiology | 23-Jul-2018 | 01-Oct-2018 |
| Email | Certifications and Training | | |
| Terry Brisac | Microbiology | 30-Jul-2018 | 01-Jan-2020 |
| Email | Certifications and Training | | |

Contacts

Office/Lab Contacts

Name

[Kruckow, Katherine](#)

[Bradley, Kelley](#)

APN 21757: Pathogenic Mechanisms of Influenza-Mediated Secondary Bacterial Infection

Record Number
IACUC-21757

Pathogenic mechanisms of influenza-mediated secondary bacterial infection
Carlos J. Orihuela - Microbiology (UAB DEPARTMENT)

Submissions (11)
Linkages
Species (1)
Summaries

Home > Summaries > Personnel

Summary

Personnel

Research Personnel

All Certifications and Training

| | PI | Name | COI | Start Date | |
|---|-------------------|---|-----|-------------|--------|
| <input checked="" type="radio"/> | Carlos Orihuela | Microbiology Role: <input type="text" value="PI"/> | | 09-May-2019 | Retire |
| Certifications and Training | | | | | |
| <input type="radio"/> | Katherine Kruckow | Grad Sch - Biomed Sciences Role: <input type="text" value=""/> | | 13-May-2019 | Retire |
| Certifications and Training | | | | | |
| <input type="radio"/> | Ashleigh Riegler | Grad Sch - Biomed Sciences Role: <input type="text" value=""/> | | 13-May-2019 | Retire |
| Certifications and Training | | | | | |
| <input type="radio"/> | Ninecia Scott | Microbiology Role: <input type="text" value=""/> | | 11-Oct-2019 | Retire |
| Certifications and Training | | | | | |
| <input type="radio"/> | Xuhong Song | Microbiology Role: <input type="text" value=""/> | | 27-Feb-2020 | Retire |
| Certifications and Training | | | | | |

Past Research Personnel

Contacts

Office/Lab Contacts

Name

[Riegler, Ashleigh](#)

[Scott, Ninecia](#)

